

Supplementary Materials for  
**Key role of *Desulfobacteraceae* in C/S cycles of marine sediments is based on  
congeneric catabolic-regulatory networks**

Lars Wöhlbrand *et al.*

Corresponding author: Lars Wöhlbrand, [lars.woehlbrand@uol.de](mailto:lars.woehlbrand@uol.de); Ralf Rabus, [rabus@icbm.de](mailto:rabus@icbm.de)

*Sci. Adv.* **11**, eads5631 (2025)  
DOI: 10.1126/sciadv.ads5631

**The PDF file includes:**

Supplementary Text  
Figs. S1 to S120  
Tables S1 to S10  
Legends for data S1 and S2  
Legend for auxiliary reference list

**Other Supplementary Material for this manuscript includes the following:**

Data S1 and S2  
Auxiliary Reference List

## Supplementary Text

### Desulfobacteraceae contain distinct Qrc and Rnf complexes

Besides the essential Qmo and Dsr redox-complexes, the quinone-reductase complex (QrcABCD) is part of the core genome of *Desulfobacteraceae* as well as the constitutive proteome being abundantly formed. This complex is related to alternative complex III, transferring electrons from reduced TplC<sub>3</sub> (formed by periplasmic hydrogen or formate oxidation) via QrcABCD to the menaquinone pool in *Desulfovibrio* species, with interaction of TplC<sub>3</sub> and QrcA (101, 102). Indeed, the Qrc complex was predicted to form a redox loop with the Qmo complex, coupling periplasmic hydrogen (or formate) oxidation to cytoplasmic sulfate reduction (20, 103). While *Ds. variabilis* 3be13 apparently constitutively forms periplasmic hydrogenase HynAB, *Db. toluolica* Tol2 does not and *Dn. limicola* as well as *Dc. multivorans* completely lack hydrogenase genes, though abundantly forming QrcABCD during chemoorganotrophic growth (27-29). Hence, in case of *Desulfobacteraceae* a different and/or additional electron source has to be present. Notably, phylogenetic analyses revealed that QrcA and QrcB sequences of *Desulfobacteraceae* form distinct branches in the trees, which is more pronounced for QrcB (only 32% sequence identity of *Ds. variabilis* 3be13 as compared to *Dv. vulgaris*), while QrcCD subunits are rather similar between SRB (e.g. 53 % identity for QrcD Supplementary Information Fig. S17). *Desulfobacteraceae* QrcA sequences are ~20 residues longer as compare to *Dv. vulgaris*, containing an expanded cytochrome *c*<sub>3</sub> domain, that is also related to cytochrome *c*<sub>7</sub> (*c*<sub>551</sub>), which was supposed to act as terminal reductase (104). QrcB contains an N-terminal 4Fe-4S domain, a central molybdopterin oxidoreductase and a C-terminal molybdopterin dinucleotide-binding domain (though no molybdenum is present), but its function is unknown at present and was suggested to possibly be only structural (101, 103). The different structure of *Desulfobacteraceae* QrcAB may indicate interaction with electron donors other than TplC<sub>3</sub>.

A second, abundantly formed redox complex in *Desulfobacteraceae*, is a distinct version of RnfABCDEG ferredoxin:NAD<sup>+</sup>-oxidoreductase complex. This complex was shown to reversibly couple oxidation of reduced ferredoxin (RnfB subunit) to reduction of NAD<sup>+</sup> (RnfC subunit) with concomitant generation of a Na<sup>+</sup>-gradient across the cytoplasmic membrane (involving RnfEDAG) in *Acetobacterium woodii* (105). In SRB a second version of Rnf is present, comprising a markedly larger RnfB subunit (~700 aa vs. ~300 aa), that is encoded in all *Desulfobacteraceae* genomes (and also in *Da. baarsii* and *Dv. salexigens*). The RnfB and RnfC subunits of the latter comprise a different domain structure as compared to the *Ac. woodii* types and respective sequences form distinct branches in the phylogenetic tree (Supplementary Information Fig. S18), all other subunits (RnfCDEG) are very similar (106). The N-terminus of the large RnfB variant (i.e. residues 1-200) is highly similar to the small one (40 % identity, 53 % positives), containing 4Fe-4S and ferredoxin domains. The remaining 500 specific residues (absent in Rnf1) accommodate a pyridine nucleotide-disulfide oxidoreductase, NAD-binding domain, indicating interaction with NAD<sup>+</sup>/NADH + H<sup>+</sup> in addition to ferredoxin. In case of RnfC, the central NADH-ubiquinone oxidoreductase, FMN-binding as well as the N-terminal RnfC barrel sandwich domain (sometimes only the first) are absent in the Rnf2 type, challenging a function in NAD<sup>+</sup> reduction as known from *A. woodii*. Notably, some SRB genomes contain genes for both versions and form respective proteins, e.g. *Dt. autotrophicum* HRM2 and *Ds. variabilis* 3be13 (Rnf2 and Rnf3, respectively, in case of the latter). Independent of the type of Rnf complex, respective gene clusters of SRB encode a cytochrome *c*<sub>3</sub> (e.g. Dvar\_58310 in case of *Ds. variabilis* 3be13), that is not present in *Ac. woodii* or *Rhodobacter capsulatus*, which may represent an additional electron entry or exit point (107). In case of SRB harbouring both, the Rnf1 and Rnf2 type gene cluster, only the *Desulfobacteraceae* Rnf2 type clusters encode this cytochrome.

Taken together, it seems feasible that oxidation of ferredoxin (and maybe also NADH + H<sup>+</sup>) by the Rnf complex may not only contribute to Na<sup>+</sup>-gradient formation as described for *Ac. woodii* (105), but additionally reduce the associated cytochrome *c*<sub>3</sub>. The latter may act as electron shuttle to the Qrc complex, contributing to reducing the menaquinone pool and, hence, sulfate reduction via QmoABC. Non-detection of these cytochromes in the proteomic studies of *Desulfobacteraceae* is most likely due to their small size and hydrophobicity, rendering such proteins hardly detectable by LC-MS. In addition to the abundant formation of Qrc and Rnf2 in *Desulfobacteraceae*, this hypothesis is supported by experimental evidence obtained

with mutants of *Desulfovibrio* sp.: (i) TplC<sub>3</sub> transposon mutants of *Dv. alaskensis* G20 were unable to grow with hydrogen or formate, but growth with lactate was not effected (102, 108), (ii) a *qrcA* mutant did only grow poorly with pyruvate and sulfate while pyruvate fermentation was not effected (109), (iii) mutants of the Qrc and Rnf complexes revealed significant deficits during respiratory growth (110), and (iv) mutants in Rnf-subunits grew barely or not with sulfate and substrates that do not allow for substrate-level phosphorylation (e.g. malate or fumarate)(109).

#### Details on the transporter complement of *Desulfobacteraceae*

The genomic transport potential (transportome) of the studied six SRB was inferred by the Transporter Classification Database (TCDB)(32) that applies a five-tier system based on structure and functions of the transport systems. Five well-defined categories (1) channels/pores, (2) electrochemical potential-driven transporters (secondary carriers), (3) primary active transporters (energy-driven, e.g. by ATP hydrolysis), (4) group translocators (substrate-modifying) and (5) transmembrane electron carriers (transferring electrons from one side of a membrane to the other) are complemented by two less-well defined ones: (8) auxiliary transport proteins and (9) putative or incompletely characterized transport systems. Transporter systematics allow for classification from subclass to the actual transport system.

The genome of *Ds. variabilis* 3be13 encodes 979 transport systems, the others pronouncedly less (445 – 712; Fig. 5a, Supplementary Information Fig. S20 and Table S9). In all cases, the most abundant classes are secondary carriers and active transporters, accounting for 58.9% – 73.2% of all transport proteins. In general, the relative share of the different transporter subclasses is rather similar in the studied SRB. In *Ds. variabilis* 3be13, 45.5% of the encoded transport proteins were detected in this study, similar to the other SRB (35.5% - 45.7%), only *Dc. multivorans* 1be1 exceeding this range with 66.2% (Fig 5a, Supplementary Information Fig 20). Notably, subclass-distribution of formed proteins mostly reflects the genomic potential, only a slightly increased share of active transporters and channels, and a bit reduced share of secondary carriers is observed (Fig. 5a). Globally comparing the six SRB, the major sub groups (i.e. 1B, 2A, 3A and 3D) reveal only slight differences in the respective relative share, while more pronounced variation is evident in groups encompassing only a low number of proteins. The different transporter types may be involved in transport of similar substrates. Considering the substrate spectrum of the transport proteins of *Ds. variabilis* 3be13, the majority is involved in transport of amino acids, drugs (mainly antibiotics), inorganic cations (mainly electron, sulfate and phosphate), inorganic anions (mainly protons and sodium), and unknown substrates (Fig. 5b). Similar to transporter subclasses, distribution of formed proteins resembles the genomic potential. While transporters of more general substrates show rather stable abundance profiles (e.g. sulfate-importing Dvar\_38430), specific transporters revealed a more substrate-dependent formation, e.g. DctPQM4 involved in 4-hydroxy-/phenylacetate uptake, reflecting the regulatory pattern observed for cytoplasmic proteins involved in general metabolism and specific catabolic routes, respectively.

## Supplementary Figures

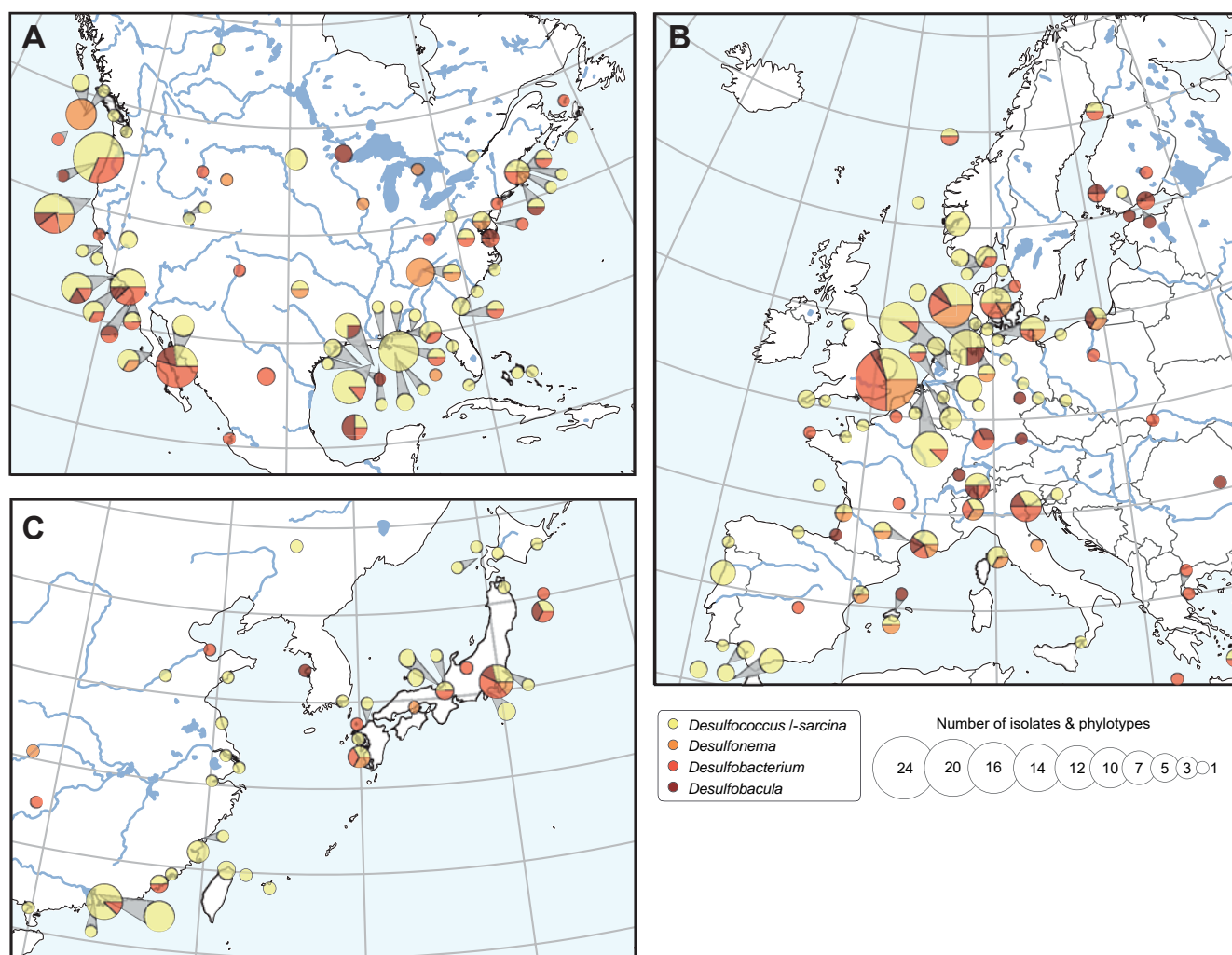


**Fig. S1: Occurrence of *Desulfobacteraceae* species isolates and/or phylotypes.** Densely spaced sites are aggregated into clusters and represented as circles. The circle area indicates the number of occurrences/sites in a cluster and the pie sector area indicates the abundance of a given genus in a cluster. **A**, North America; **B**, Europe; **C**, Asia. Color code: *Desulfococcus/-sarcina* (yellow), *Desulfonema* (orange), *Desulfobacterium* (red), and *Desulfobacula* (dark red).



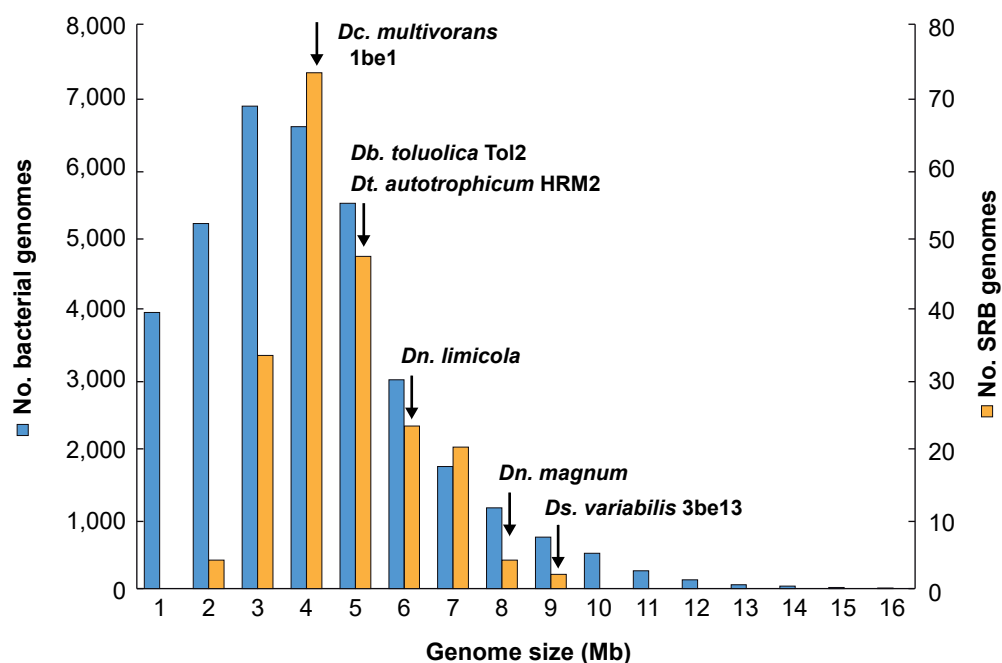


**Fig. S2:** Compilation of genome sizes of currently sequenced bacteria (blue) and sulfate-reducing bacteria (orange) according to NCBI genomes (Mai 2023). Names of proteogenomically studied *Desulfobacteraceae* spp. are indicated at their respective genome size.

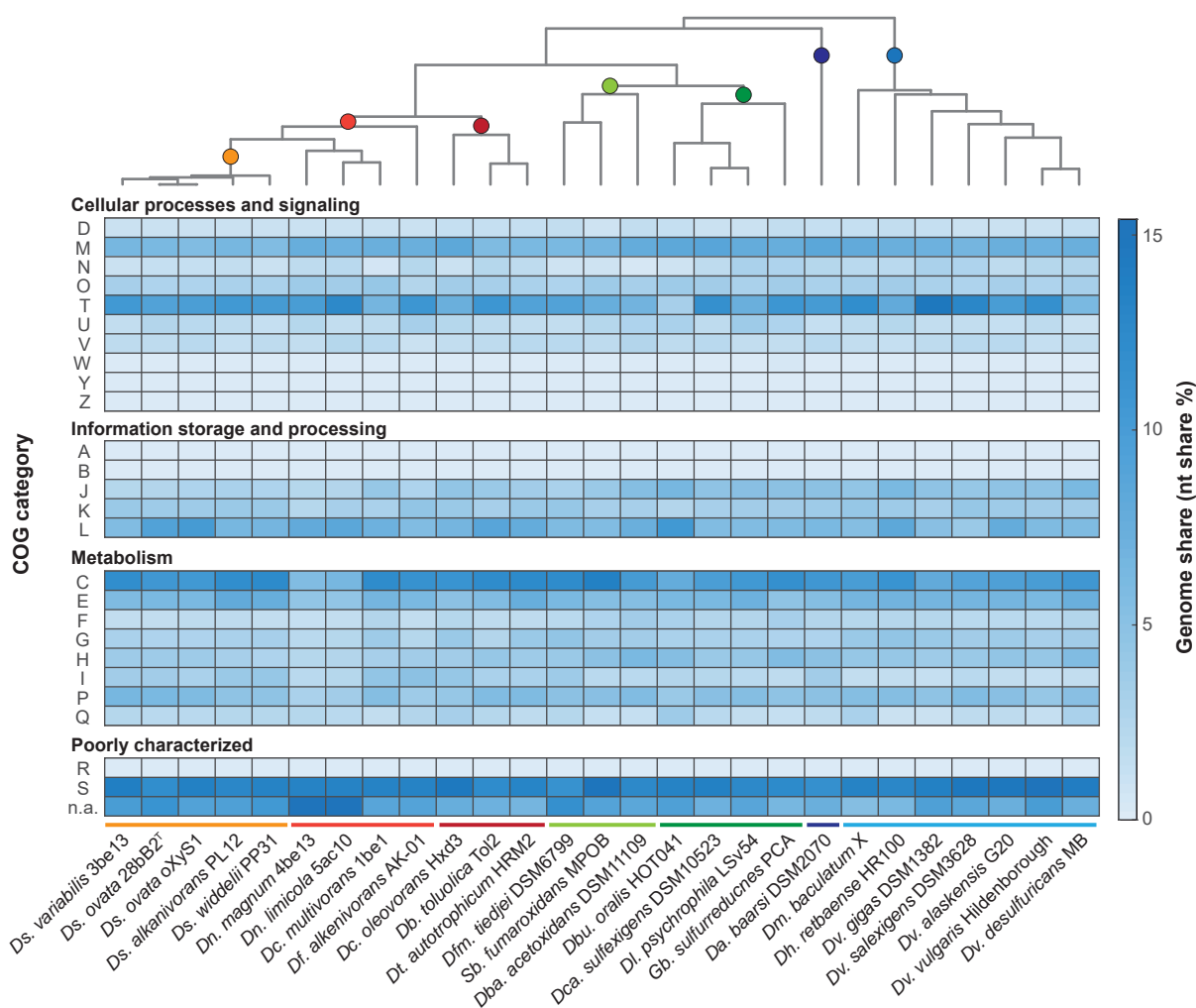


**Fig. S3: Relative genome share of coding sequence (CDS) across the cluster of orthologous groups (COG) for completely sequenced *Desulfobacteraceae* genomes and selected other sulfate-reducing bacteria.** Color-code is based on the indicated 16S rRNA-based phylogeny of the selected SRB (top). Genus abbreviations are as given in legend to Fig. 2.

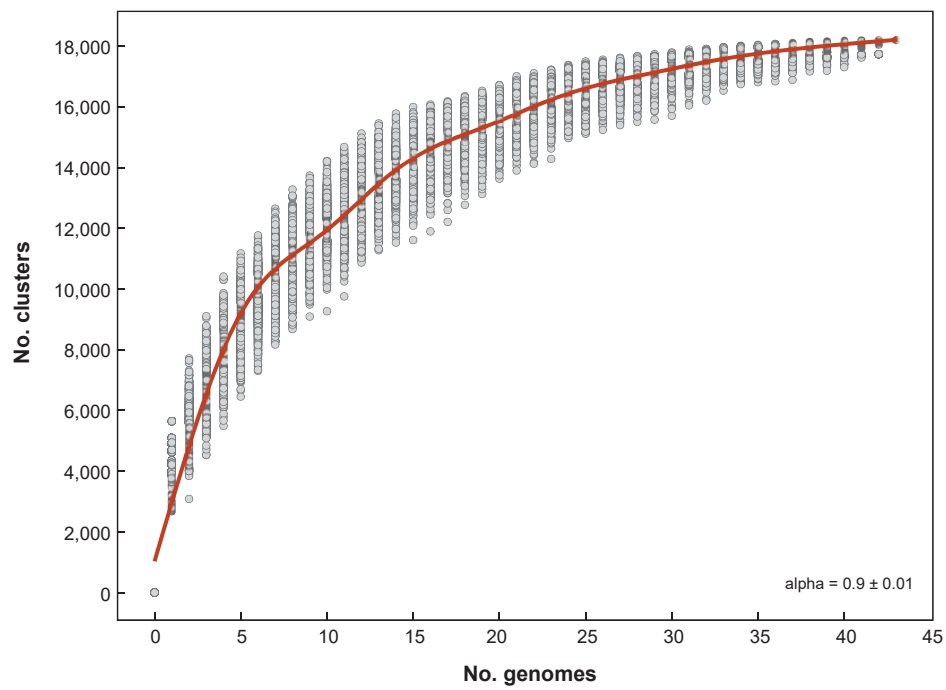


**Fig. S4: Rarefaction curve showing the cumulative number of clusters of orthologous genes for every new genome added.** To prevent influence from the order of inclusion, 1,000 permutations were conducted. The flattening of the curve shows the saturation of the pangenome, with the inclusion of more genomes returning diminishing numbers of new clusters. The "openness" of the pangenome predicts that novel genes will be discovered by increasing the number of genomes included. However, the saturation of the curve suggests that the collection is representative of the vast majority of *Desulfobacteraceae* gene repertoire.

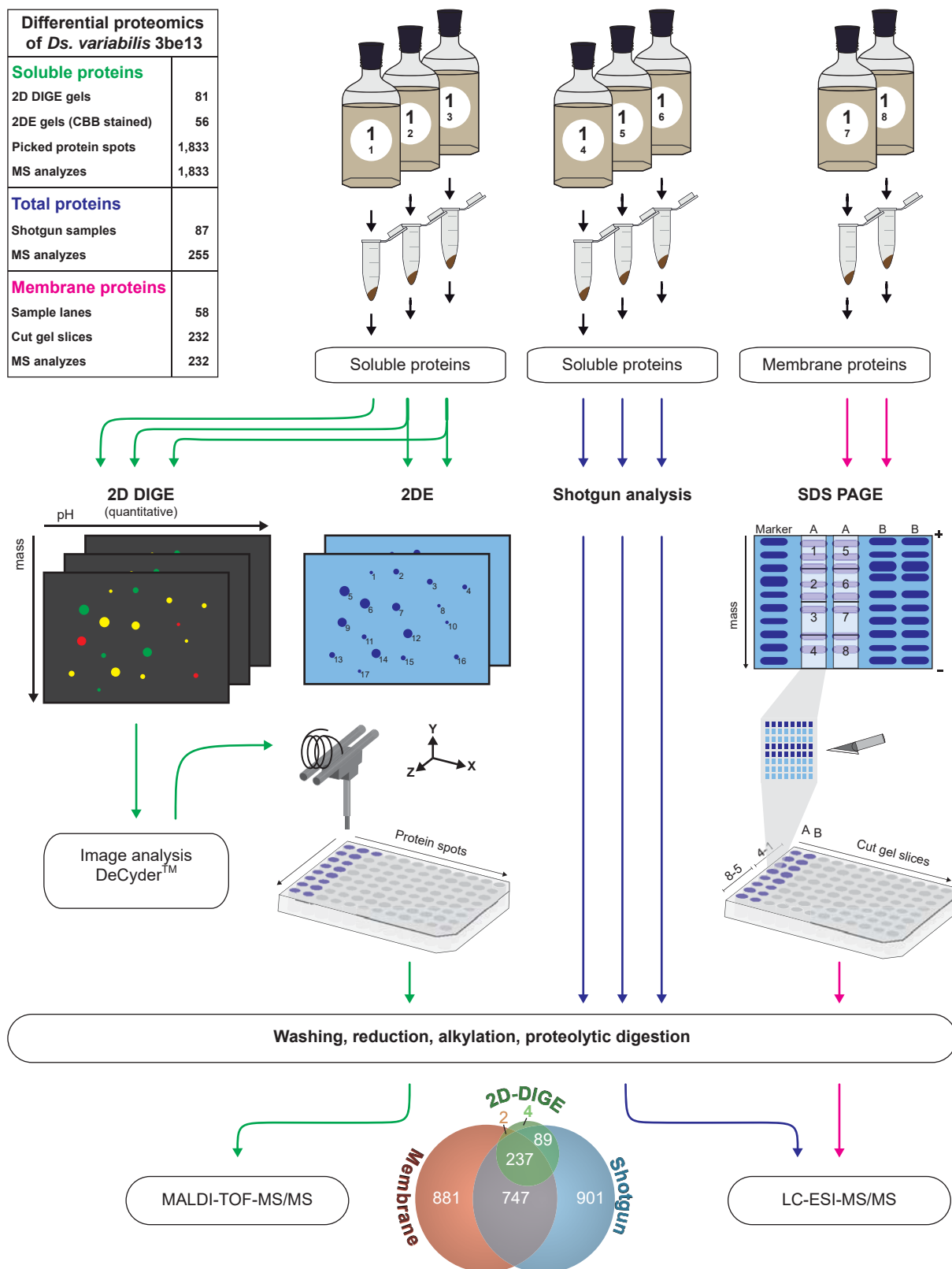


**Fig. S5: Scheme of proteomic analyses workflow of *Desulfosarcina variabilis* 3be13 samples that is also representative for the other 5 studied *Desulfobacteraceae*.** Replicate cultures of substrate-adapted cells were harvested and subjected to appropriate protein extraction procedures to prepare soluble and membrane protein fractions, respectively, for gel-based or gel-free analysis of the respective protein complements coupled to MS-based protein identification. The Venn diagram illustrates complementarity of the applied methods and the inset summarizes sample quanta per analysis method.

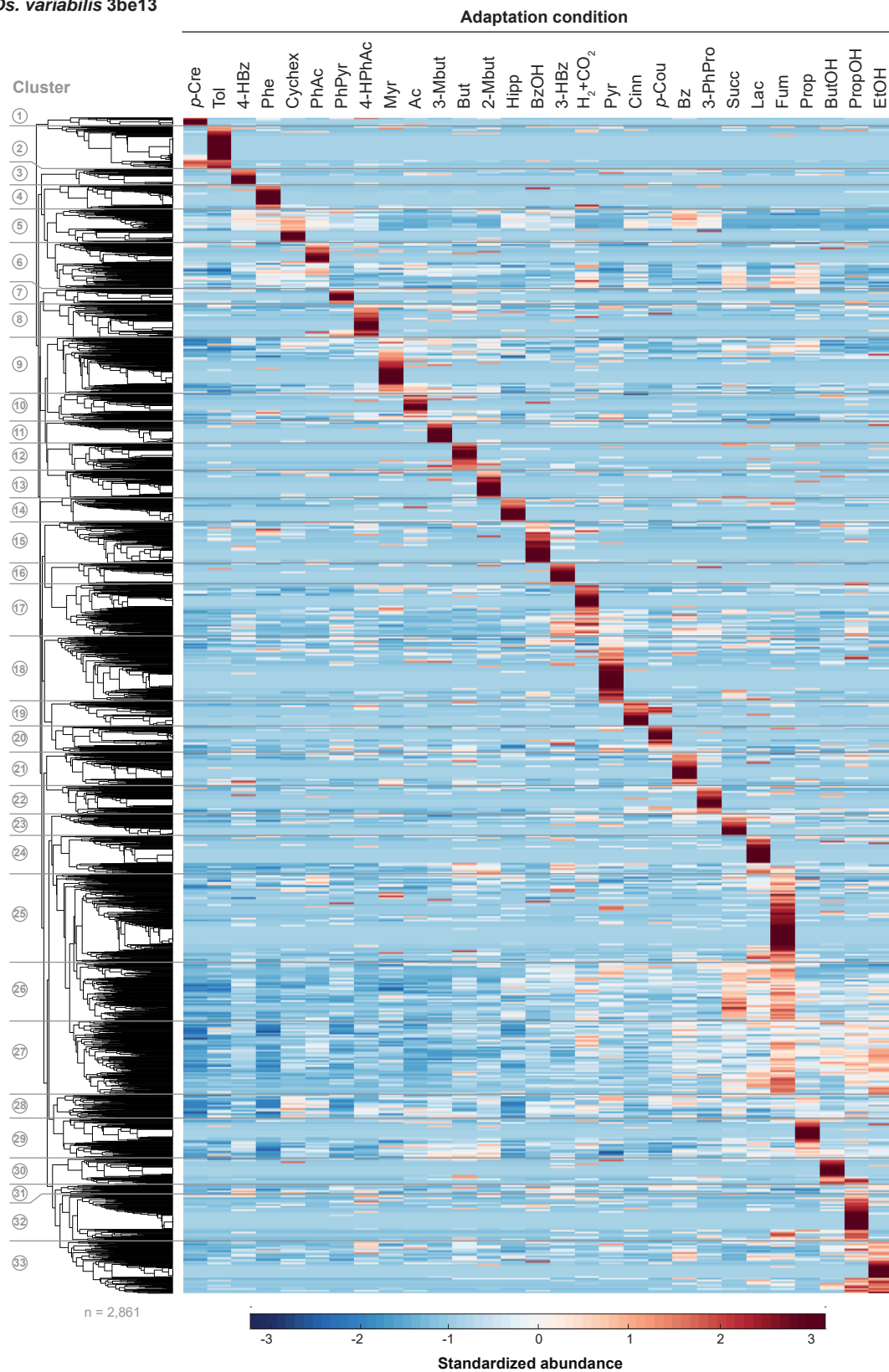


**Fig. S6: Clustering of standardized protein abundances of all detected proteins of *Ds. variabilis* 3be13 across the 29 studied adaptation conditions.** Detailed representations of the 33 clusters are provided in Supporting Information Figs. 26-58. Substrate abbreviations: Ac, acetate; But, butanoate; ButOH, *n*-butanol; Bz, benzoate; BzOH, benzyl alcohol; Cinn, cinnamate; *p*-Cou, *p*-coumarate; *p*-Cre, *p*-cresol; Cychex, cyclohexane carboxylate; EtOH, ethanol; Fum, fumarate;  $H_2 + CO_2$ , lithoautotrophic growth; 3-HBz, 3-hydroxybenzoate; 4-HBz, 4-hydroxybenzoate; Hipp, hippurate; 4-HPhAc, 4-hydroxyphenylacetate; Lac, lactate; 2-Mbut, 2-methylbutanoate; 3-Mbut, 3-methylbutanoate; Myr, myristinate; PhAc, phenylacetate; Phe, phenol; 3-PhPro, 3-phenylpropanoate; PhPyr, phenylpyruvate; Prop, propanoate; PropOH, *n*-propanol; Pyr, pyruvate; Succ, succinate; Tol, toluene.

*Dn. magnum*

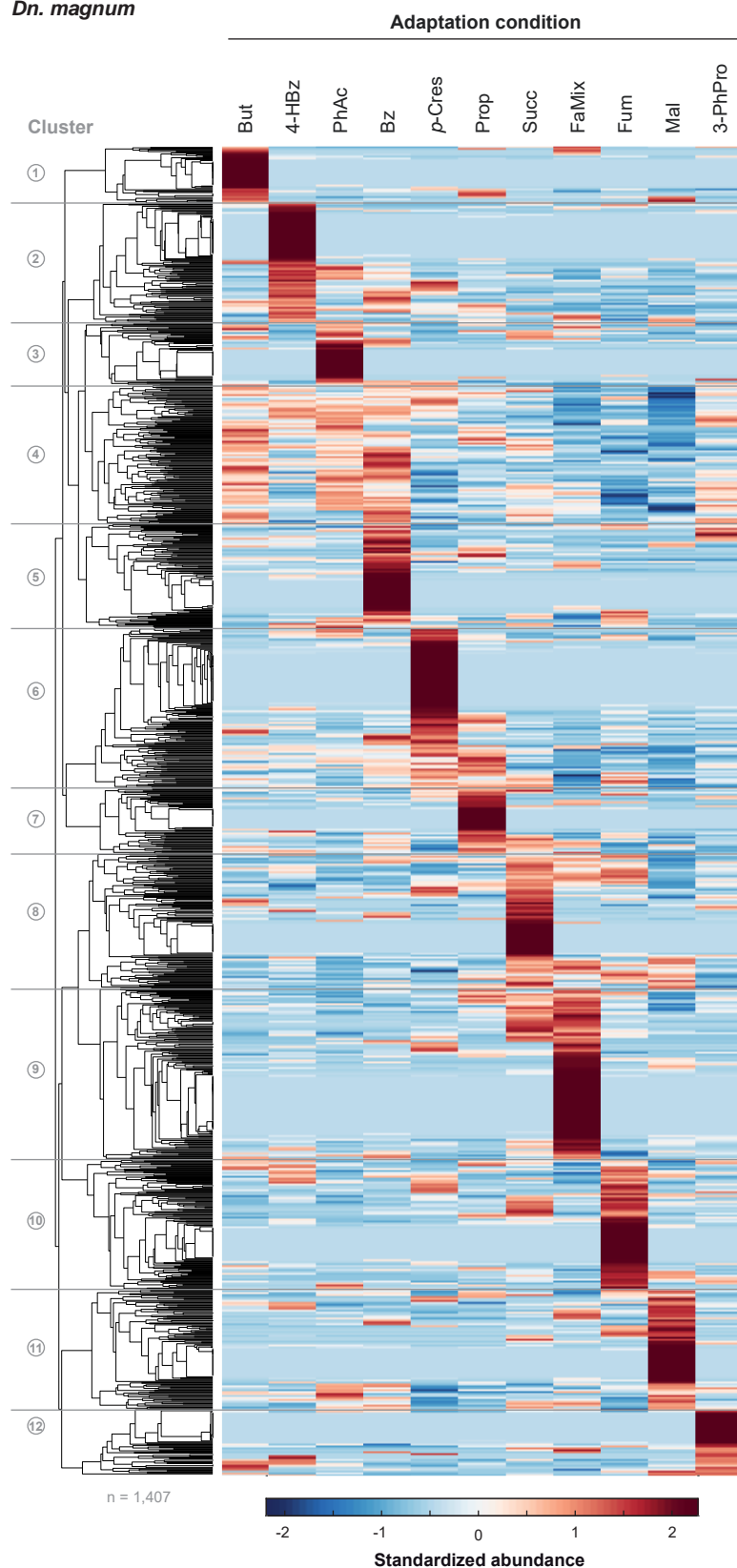


**Fig. S7: Clustering of standardized protein abundances of all detected proteins of *Desulfonema magnum* across the 11 studied substrate adaptation conditions.** Detailed representations of the 12 clusters are provided in Supplementary Figs. S59-S71. Substrate abbreviations: But, butanoate; Bz, benzoate; *p*-Cres, *p*-cresol; FaMix, fatty acid mix; Fum, fumarate; 4-HBz, 4-hydroxybenzoate; Mal, malate; PhAc, phenylacetate; 3-PhPro, 3-phenylpropanoate; Prop, propanoate; Succ, succinate.

*Dn. limicola*

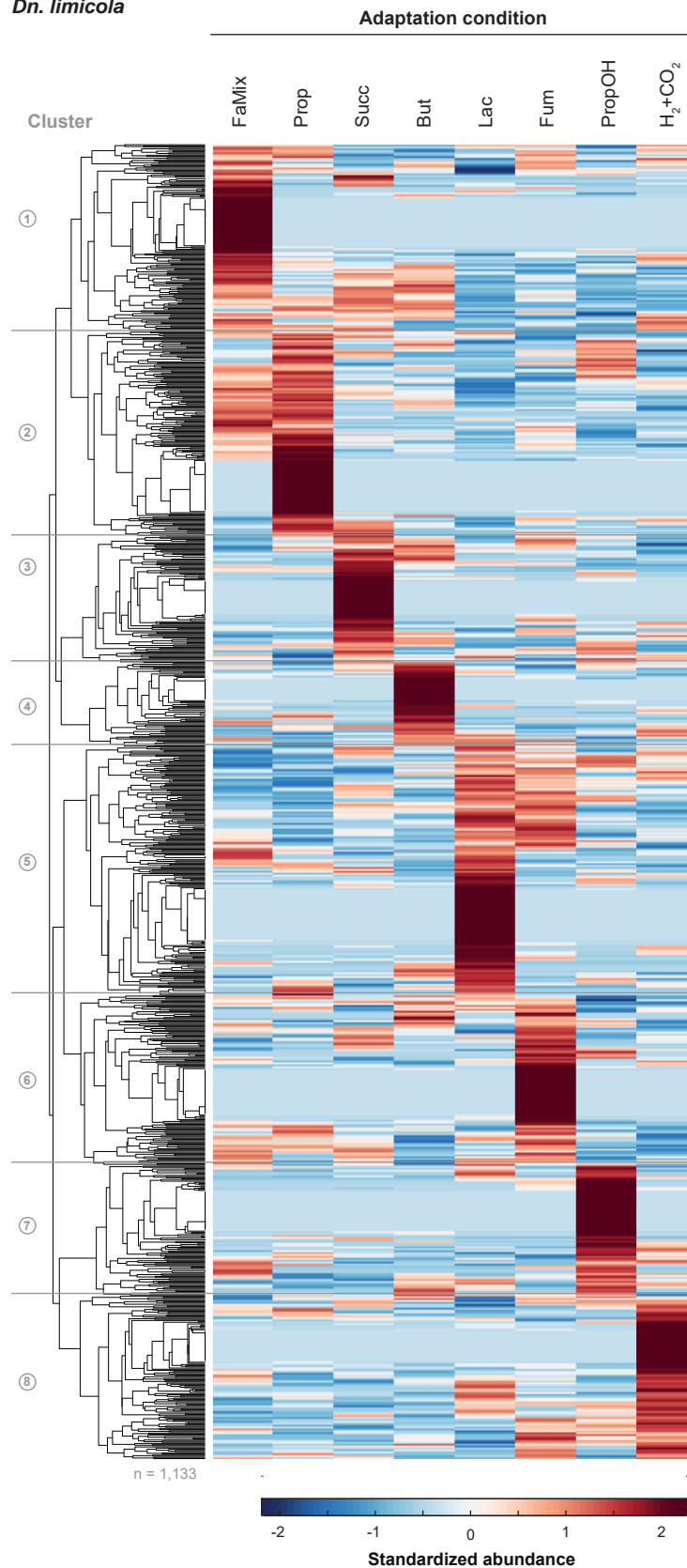


**Fig. S8: Clustering of standardized protein abundances of all detected proteins of *Desulfonema limicola* across the 11 studied substrate adaptation conditions.** Detailed representations of the 8 clusters are provided in Supplementary Figs. S72-S80. Substrate abbreviations: But, butanoate; FaMix, fatty acid mix; Fum, fumarate; H<sub>2</sub> + CO<sub>2</sub>, lithoautotrophic growth; Lac, lactate; Prop, propanoate; PropOH, *n*-propanol; Succ, succinate.

*Dc. multivorans* 1be1

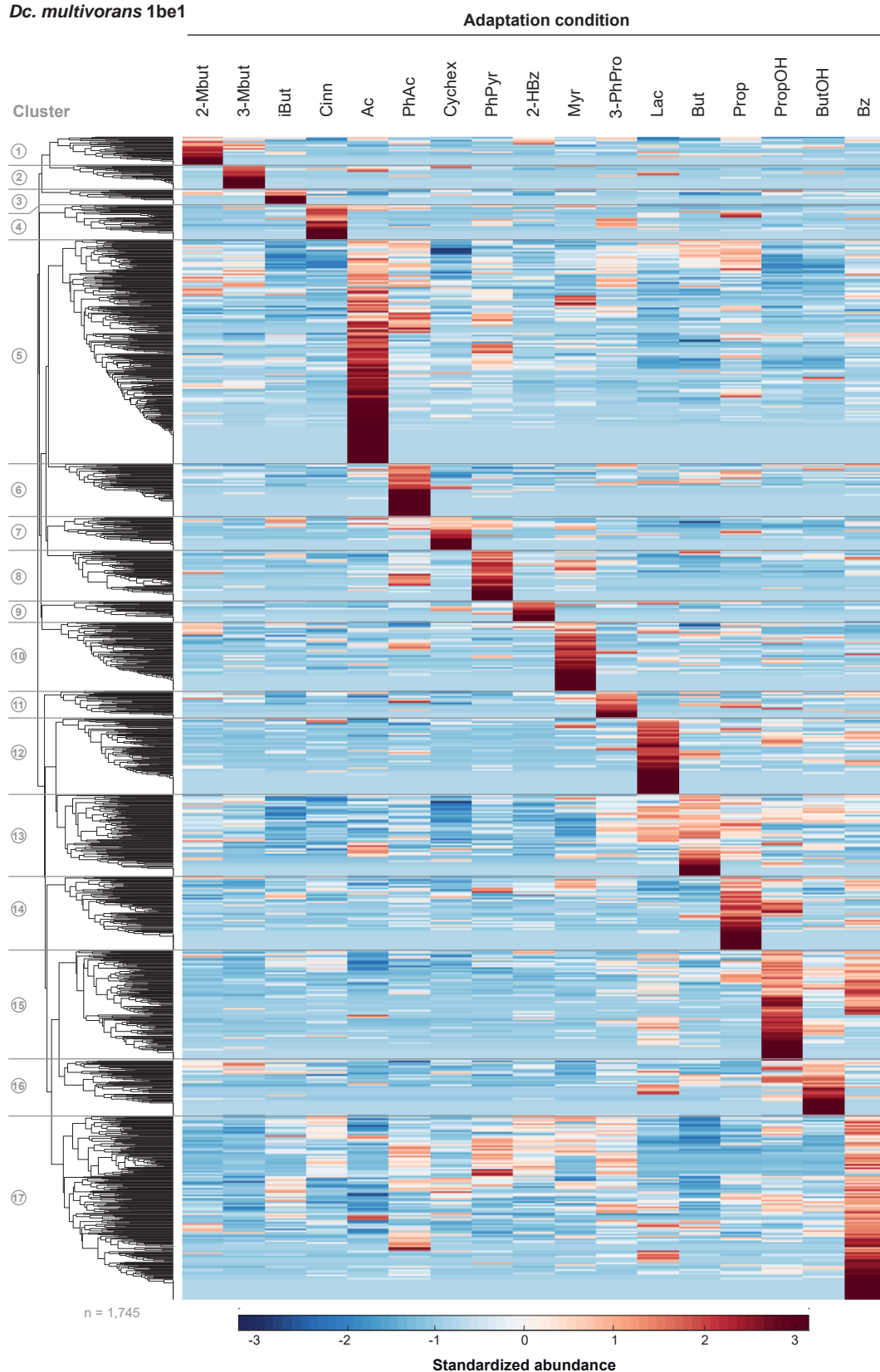


**Fig. S9: Clustering of standardized protein abundances of all detected proteins of *Desulfococcus multivorans* 1be1 across the 17 studied substrate adaptation conditions.** Detailed representations of the 17 clusters are provided in Supplementary Figs. S81-S99. Substrate abbreviations: Ac, acetate; But, butanoate; ButOH, *n*-butanol; iBut, iso-butanol; Bz, benzoate; Cinn, cinnamate; Cyhex, cyclohexane carboxylate; 2-HBz, 2-hydroxybenzoate; Lac, lactate; 2-Mbut, 2-methylbutanoate; 3-Mbut, 3-methylbutanoate; Myr, myristinate; PhAc, phenylacetate; 3-PhPro, 3-phenylpropanoate; PhPyr, phenylpyruvate; Prop, propanoate; PropOH, *n*-propanol; .



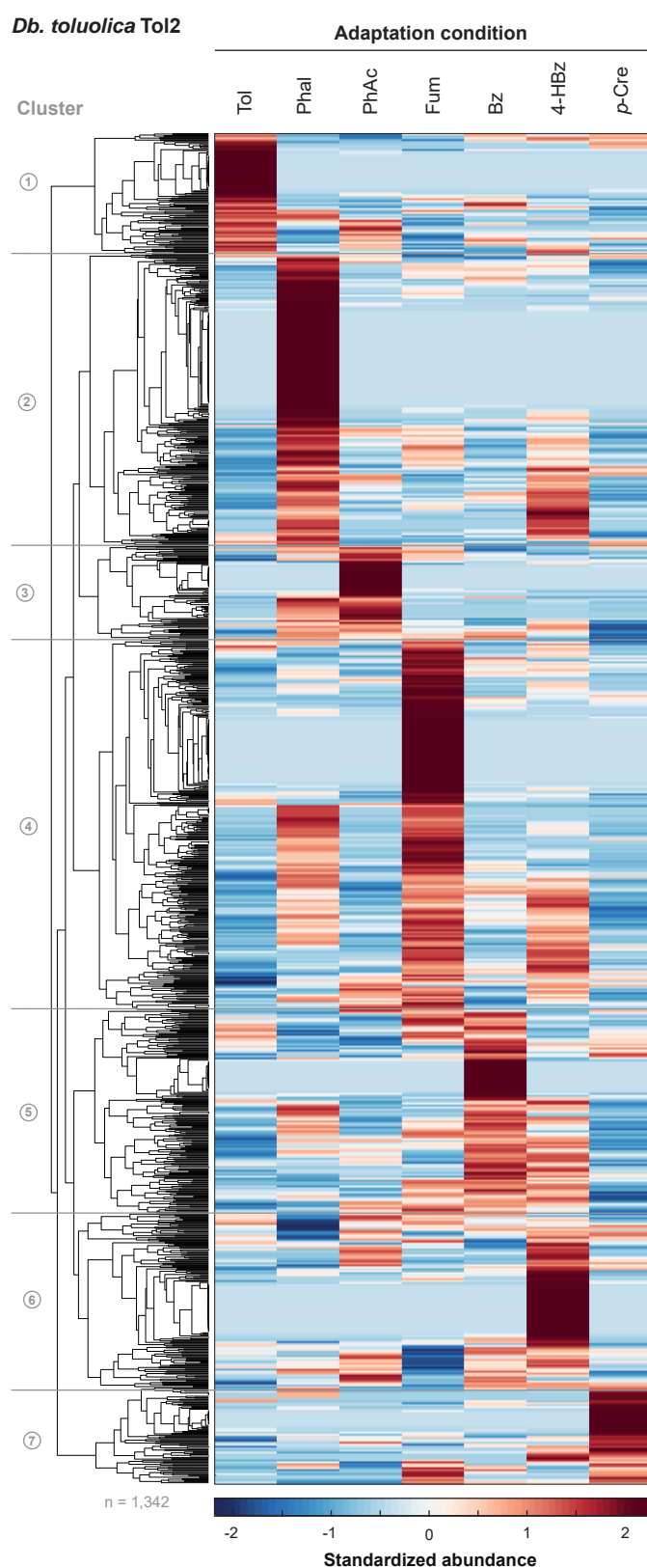


**Fig. S10: Clustering of standardized protein abundances of all detected proteins of *Desulfobacula toluolica* Tol2 across the 7 studied substrate adaptation conditions.** Detailed representations of the 7 clusters are provided in Supplementary Figs. S100-S109. Substrate abbreviations: Bz, benzoate; *p*-Cre, *p*-cresol; Fum, fumarate; 4-HBz, 4-hydroxybenzoate; PhAc, phenylacetate; Phal, phenylalanine; Tol, toluene.

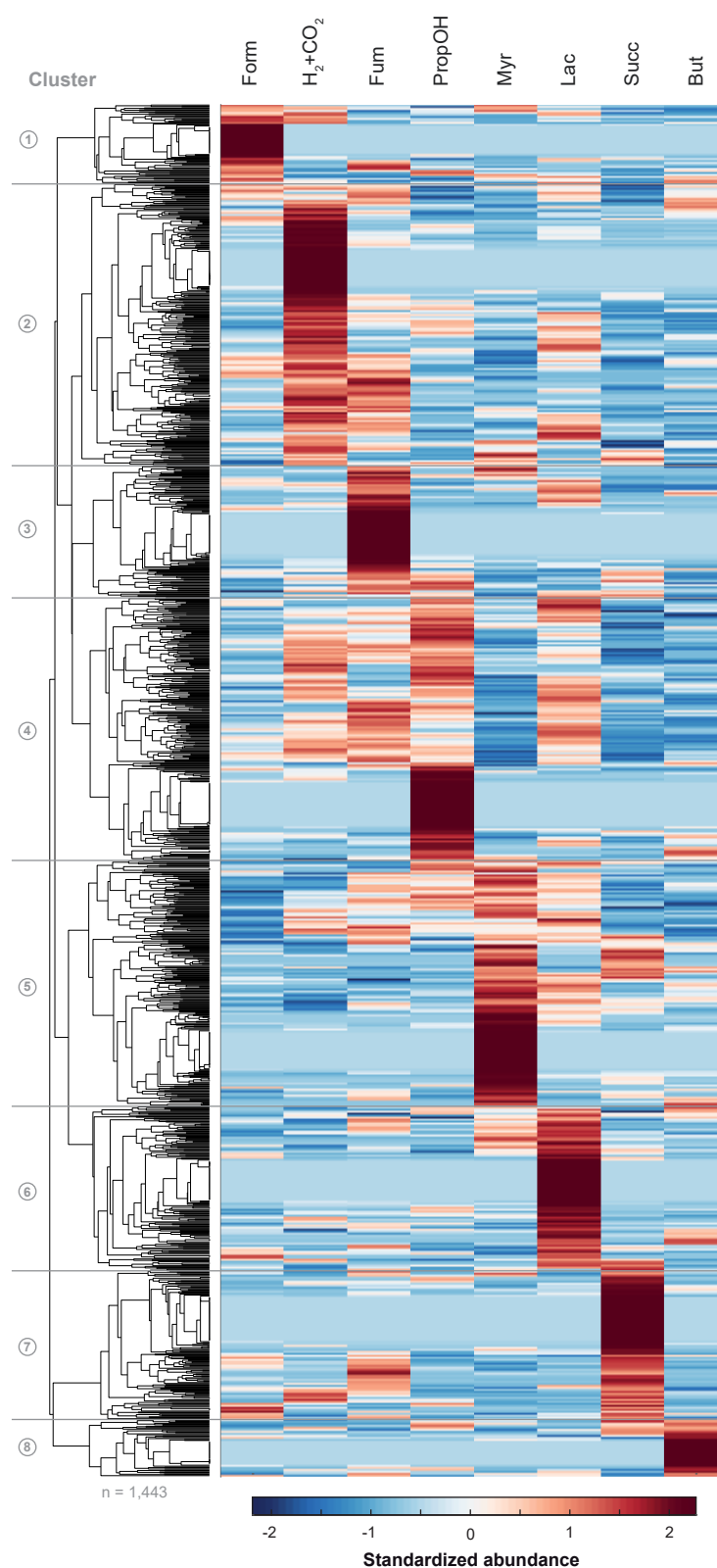


**Fig. S11: Clustering of standardized protein abundances of all detected proteins of *Desulfobacterium autotrophicum* HRM2 across the 8 studied substrate adaptation conditions.** Detailed representations of the 8 clusters are provided in Supplementary Figs. S110-S120. Substrate abbreviations: But, butanoate; Form, formate; Fum, fumarate;  $H_2 + CO_2$ , lithoautotrophic growth; Lac, lactate; Myr, myristinate; PropOH, *n*-propanol; Succ, succinate.

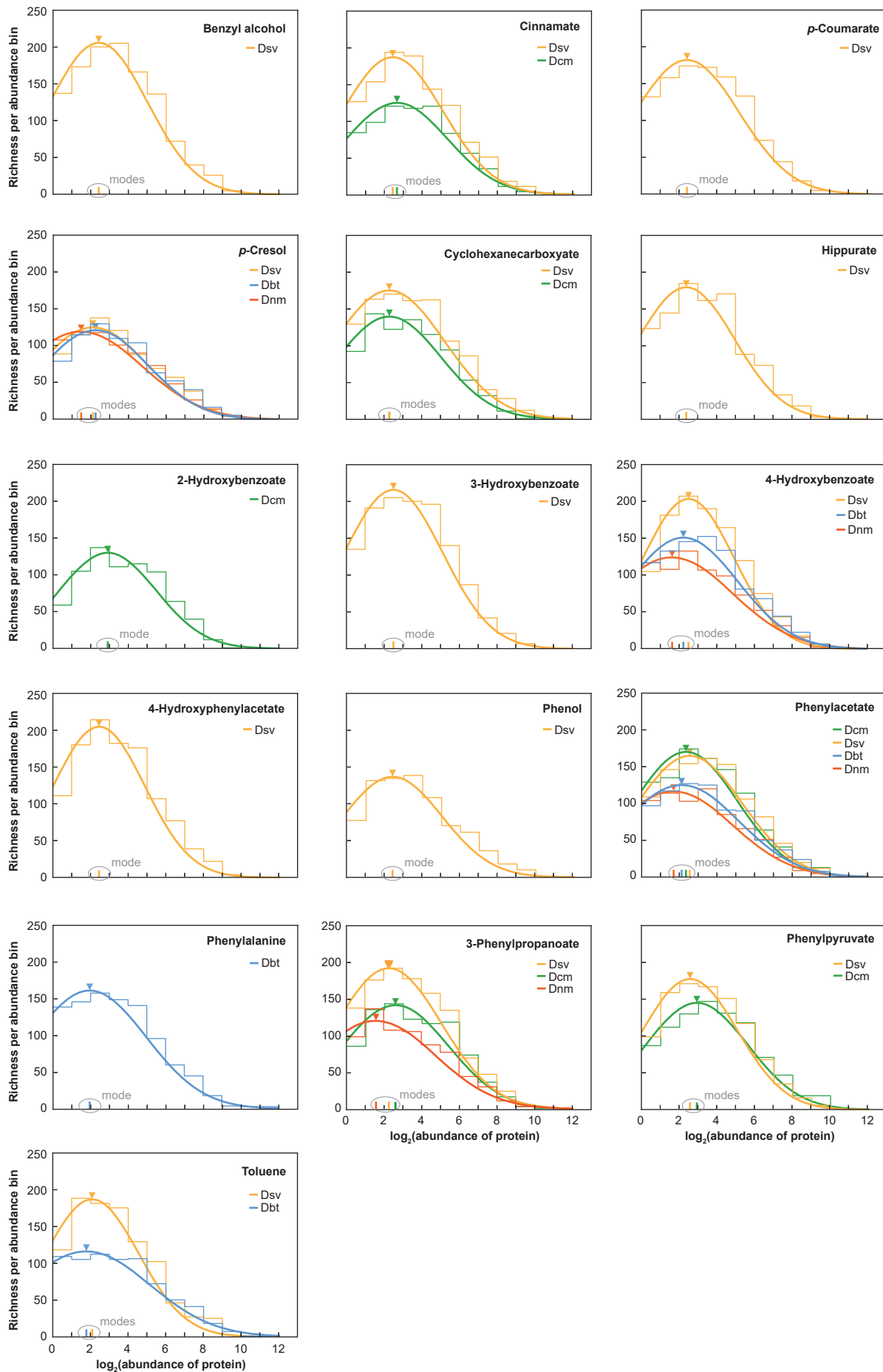


**Fig. S12: Histograms (stairs; log bin size 1) of protein abundance for aromatic growth substrates per strain (in alphabetical order).** All abundance distributions are log normally distributed (fitted smooth lines); *Ds. variabilis* 3be13 (Dsv), *Dc. multivorans* 1be1 (Dcm), *Dn. limicola* (Dnl), *Dn. magnum* (Dnm), *Db. toluolica* Tol2 (Dbt) and *Dt. autotrophicum* HRM2 (Dta). The peak of the distribution (triangles) determines the abundance mode (vertical bars on abscissa), i.e. the abundance value shared by the largest number of different proteins.

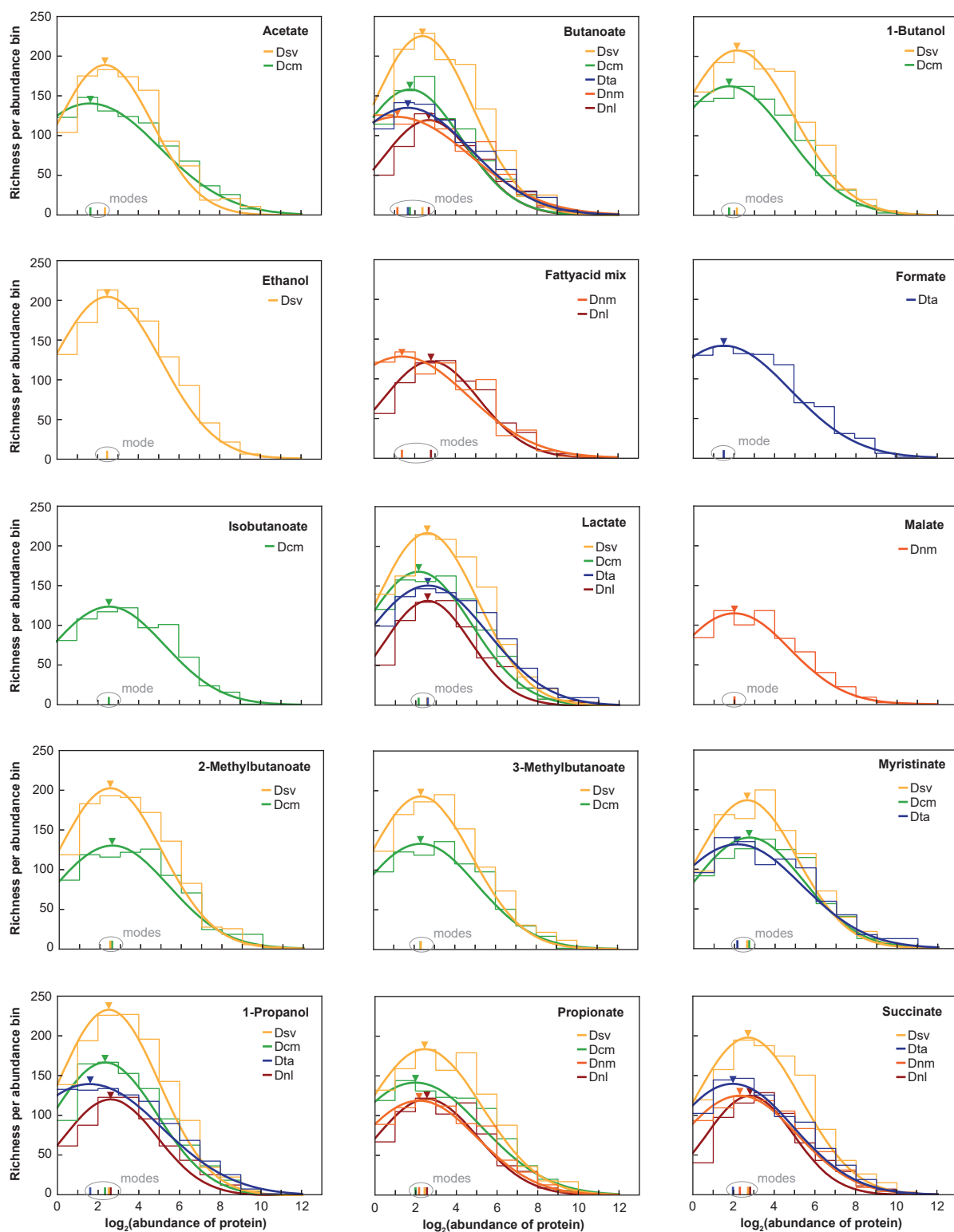
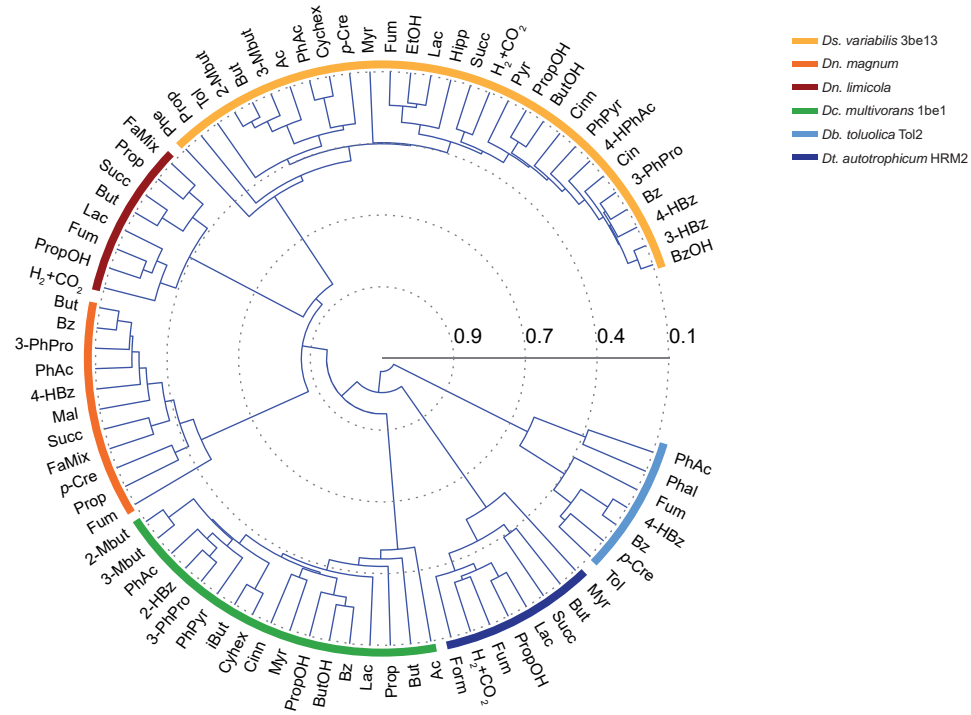


**Fig. S13: Histograms (stairs; log bin size 1) of protein abundance for aliphatic growth substrates per strain (in alphabetical order).** All abundance distributions are log normally distributed (fitted smooth lines); *Ds. variabilis* 3be13 (Dsv), *Dc. multivorans* 1be1 (Dcm), *Dn. limicola* (Dnl), *Dn. magnum* (Dnm), *Db. toluolica* Tol2 (Dbt) and *Dt. autotrophicum* HRM2 (Dta). The peak of the distribution (triangles) determines the abundance mode (vertical bars on abscissa), i.e. the abundance value shared by the largest number of different proteins.

**A**



**B**

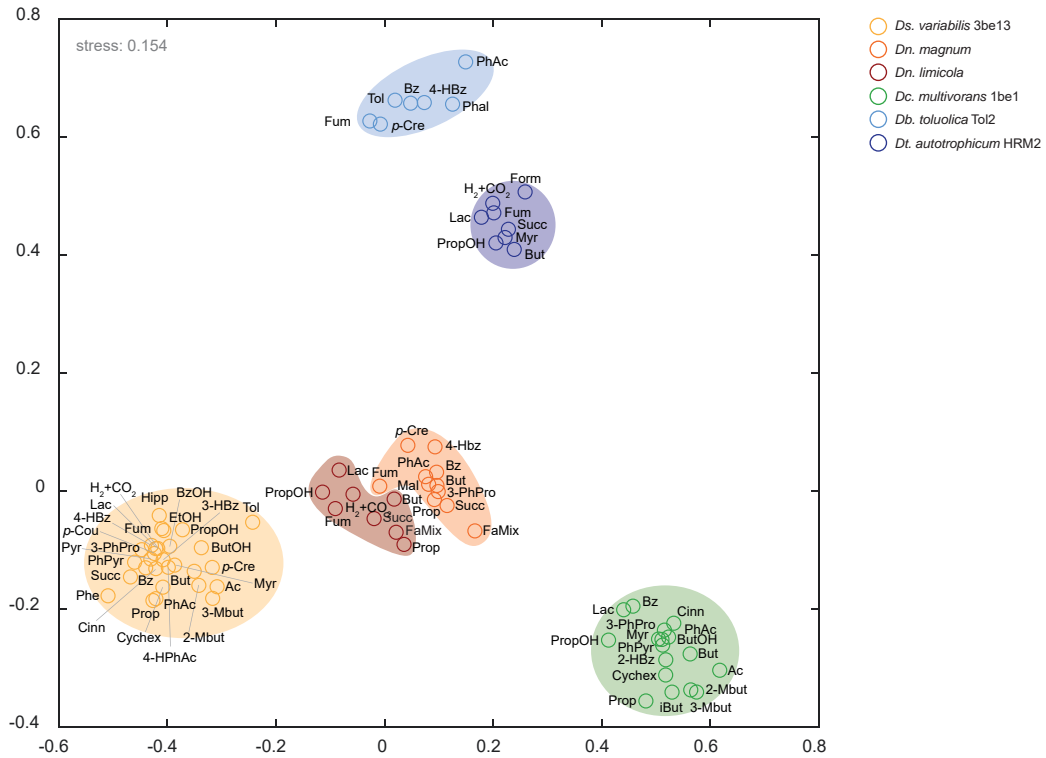


**Fig. S14: Interspecies comparison of condition-specific proteomes based on KEGG orthology and pathways.** We used the relative abundance of proteins per strain and substrate condition to account for the differently sized datasets. Only proteins with assigned KEGG category and present in all conditions per strain were included in the analysis. **A**, Clustering tree (euclidean distance metric, linkage average) covering 80 different conditions of the six proteomically studied SRB strains. **B**, Classical multidimensional scaling plot (cityblock distance metric). Substrate conditions are indicated, and organisms are color coded. The corresponding Shepard plot is provided in fig. S15.

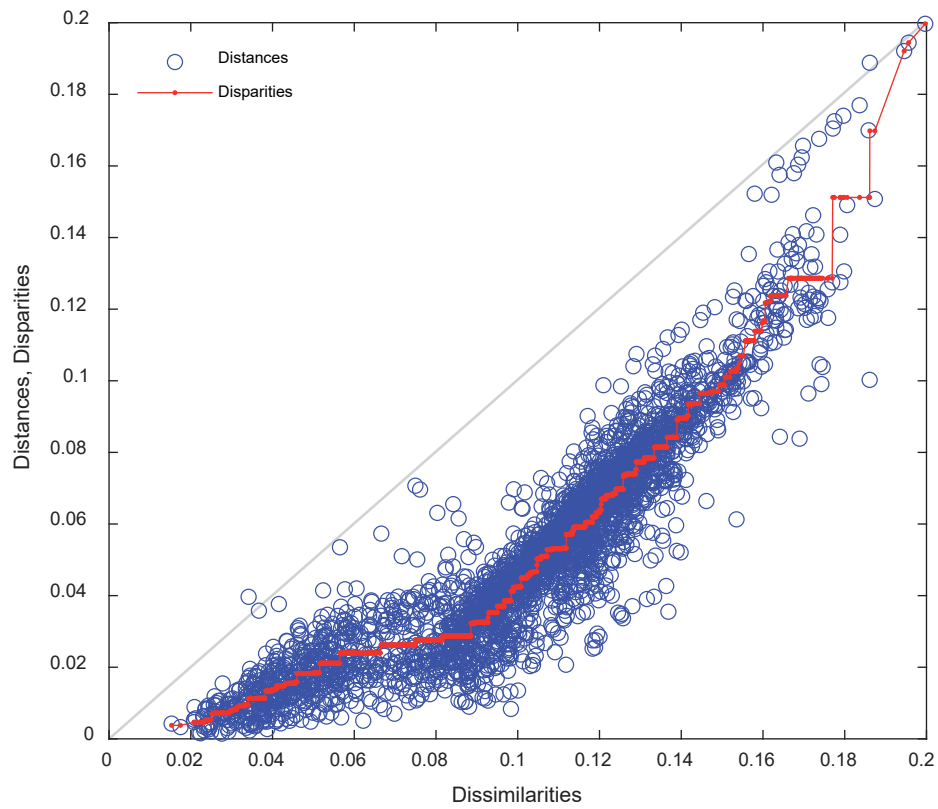
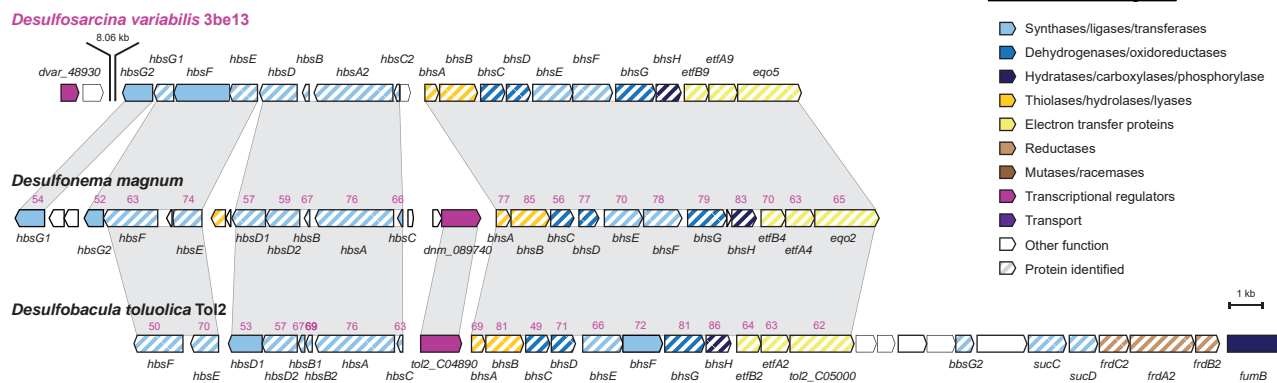
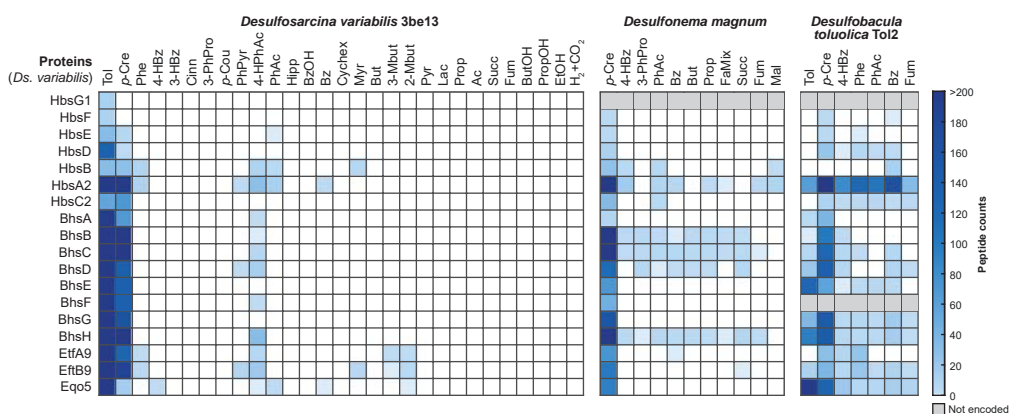


**Fig. S15:** Shepard diagram of data presented in Fig. S14B, relating dissimilarities with distances (blue circles) and disparities (red dots and line), respectively. Dissimilarities and distances show a piecewise linear dependency with high correlation (e.g. for dissimilarities in interval  $[0.02, 0.06]$ ,  $[0.06, 0.09]$ , and  $[0.09, 0.17]$ ).

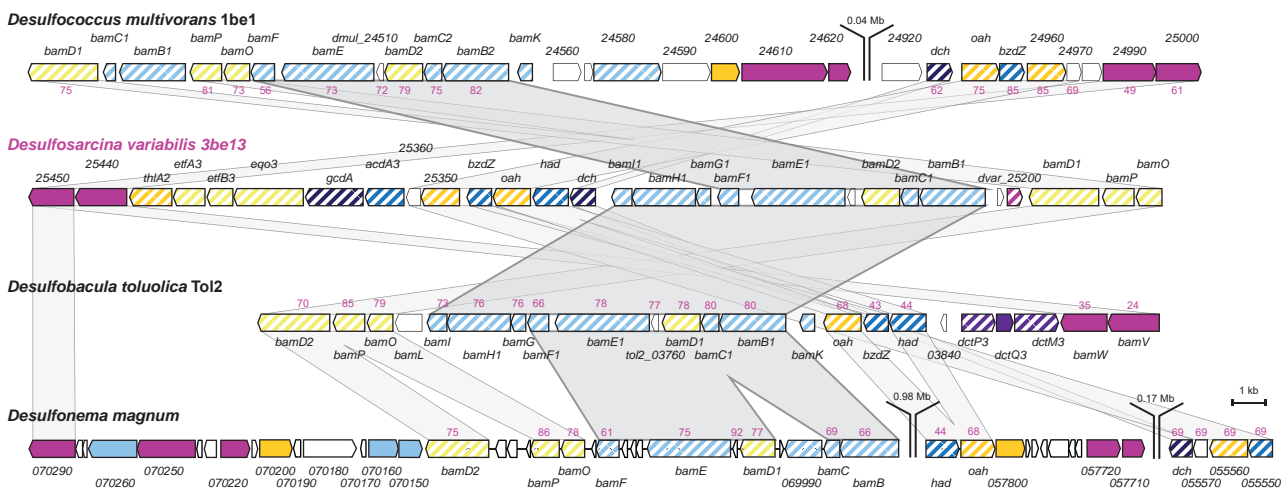
## A *p*-Cresol pathway – *hbs/bhs* gene cluster



## B



## C Central benzoyl-CoA pathway – *bam* gene cluster



## D

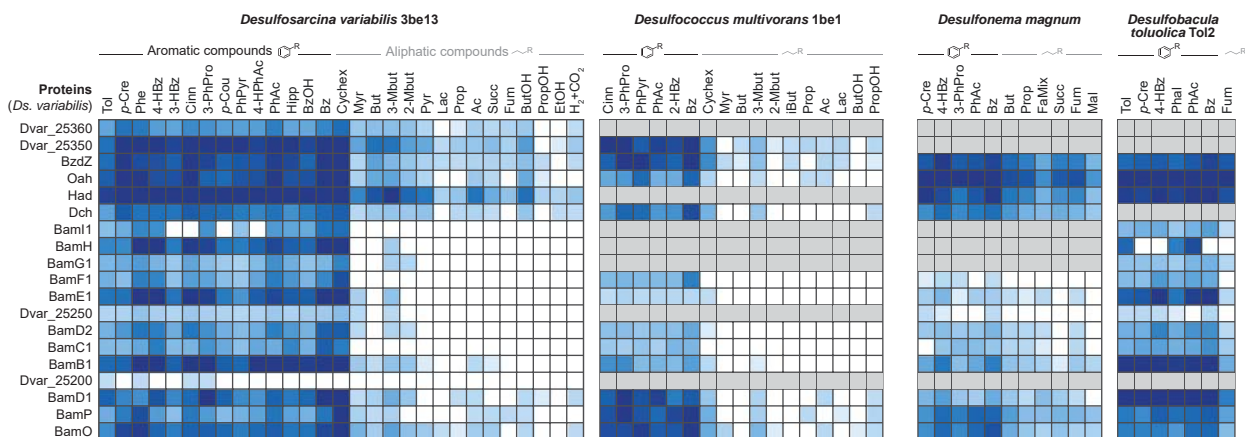
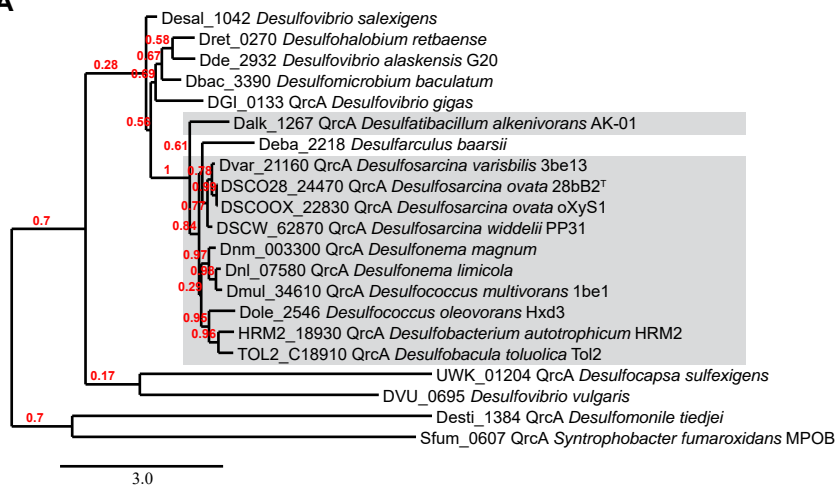
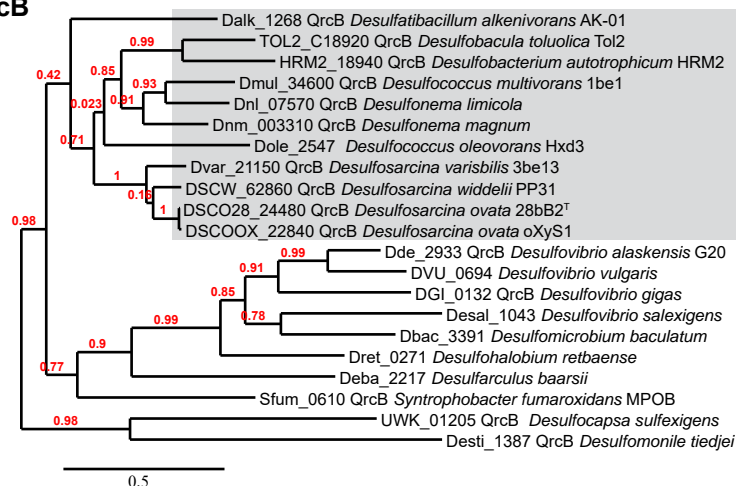


**Fig. S16: Catabolic gene modules of *Desulfobacteraceae*.** **A**, Gene clusters encoding proteins involved in anaerobic *p*-cresol degradation of *Ds. variabilis* 3be13, *Dn. magnum*, and *Db. toluolica* Tol2. Amino acid sequence identities as compared to *Ds. variabilis* 3be13 are given in violet. Protein functions are color coded. **B**, Heatmap of abundance of identified proteins related to the *p*-cresol pathway across respective substrate adaptation conditions per strain. **C**, Gene clusters encoding proteins involved in central anaerobic benzoyl-CoA pathway of *Ds. variabilis* 3be13, *Dc. multivorans* 1be1, *Dn. magnum*, and *Db. toluolica* Tol2. Amino acid sequence identities, as compared to *Ds. variabilis* 3be13, are shown in violet. **D**, Heatmap of abundances of identified proteins of the benzoyl-CoA pathway across respective substrate adaptation conditions per strain.

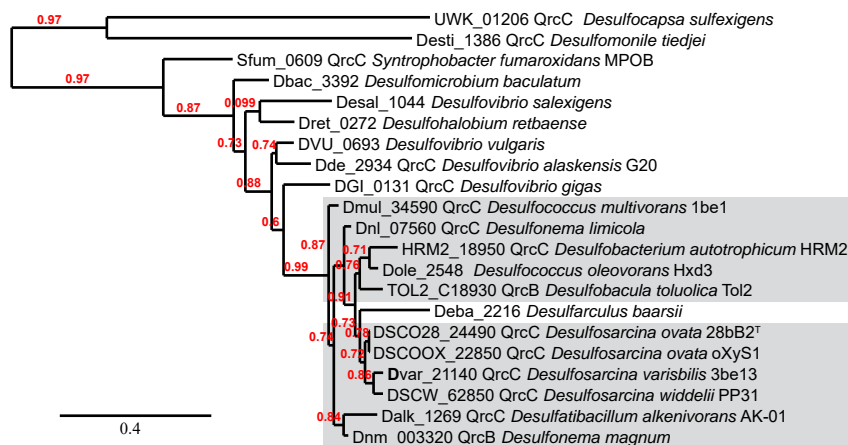
## A QrcA



## B QrcB



## C QrcC



## D QrcD

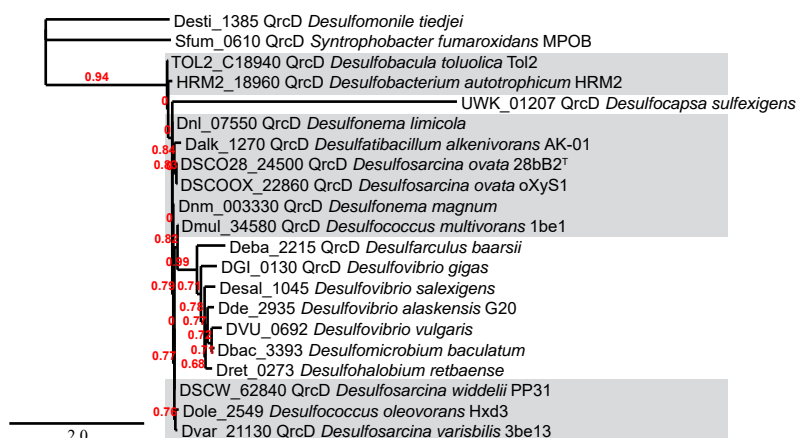


**Fig. S17: Phylogenetic tree of Qrc complex subunits (A-D) of selected SRB.** Qrc sequences of *Desulfobacteraceae* members are highlighted by grey boxes. Branch support values are indicated in red. The tree was constructed using phylogeny.fr (111).



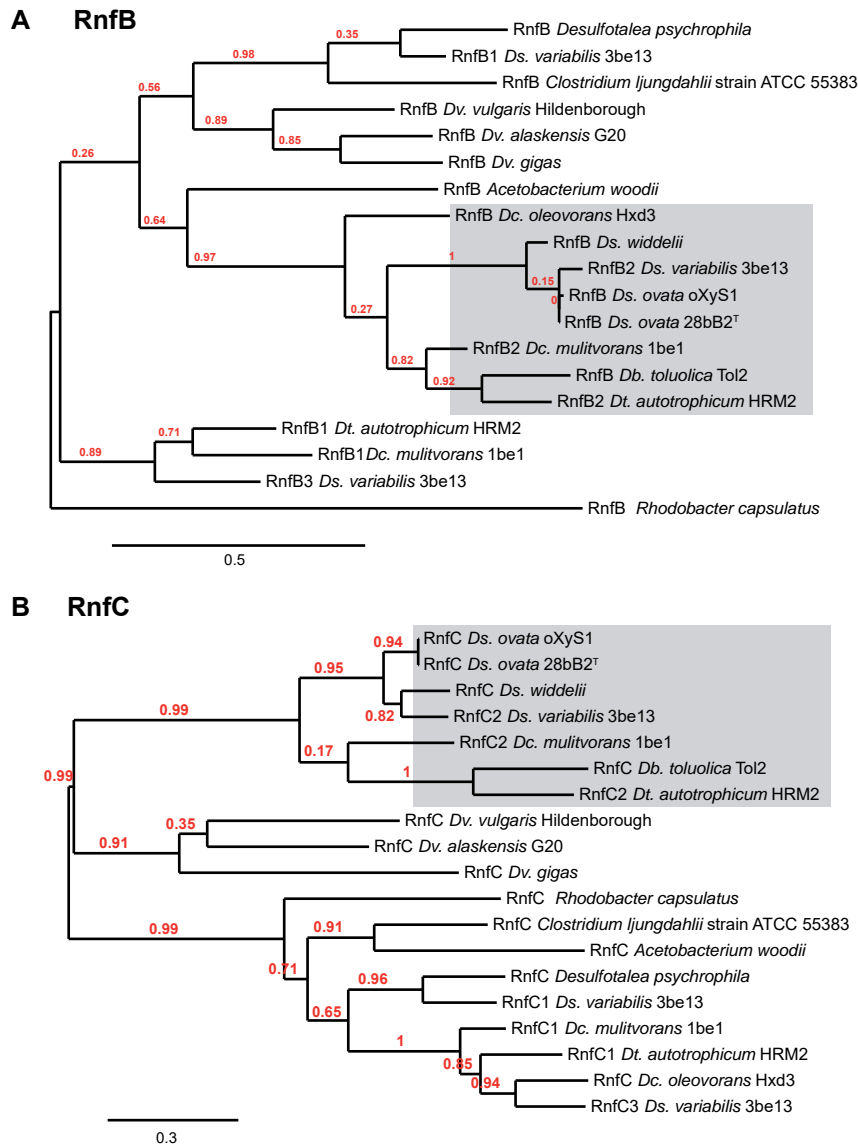
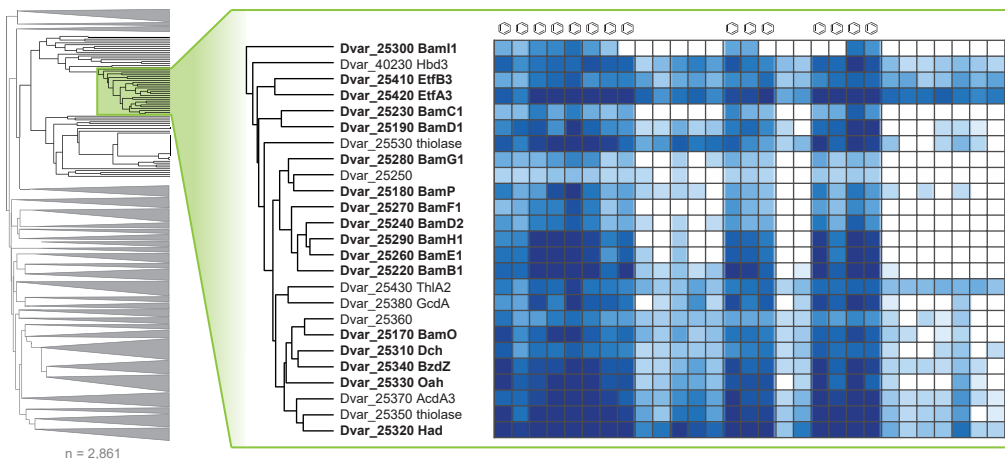
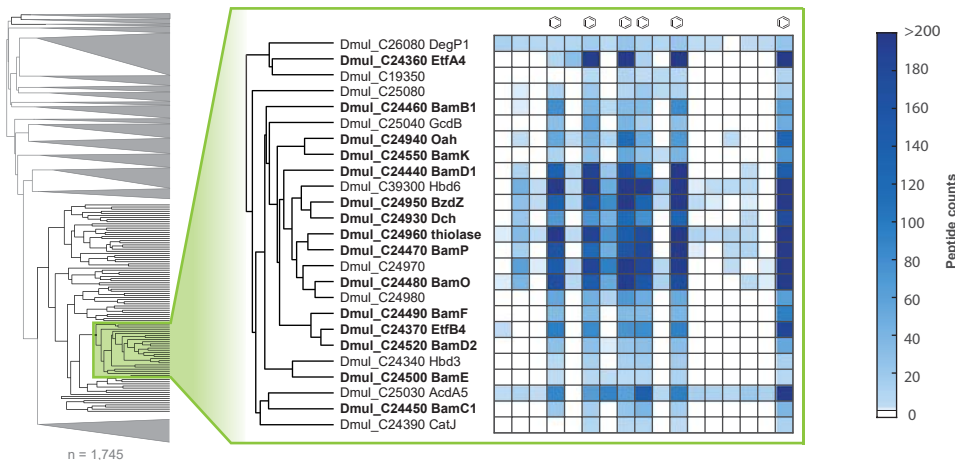


**Fig. S18: Phylogenetic tree of Rnf complex subunits RnfB and RnfC of selected SRB.** Sequences belonging to Rnf2-type complexes of *Desulfobacteraceae* members are highlighted by grey boxes. Branch support values are indicated in red. The tree was constructed using phylogeny.fr (111).

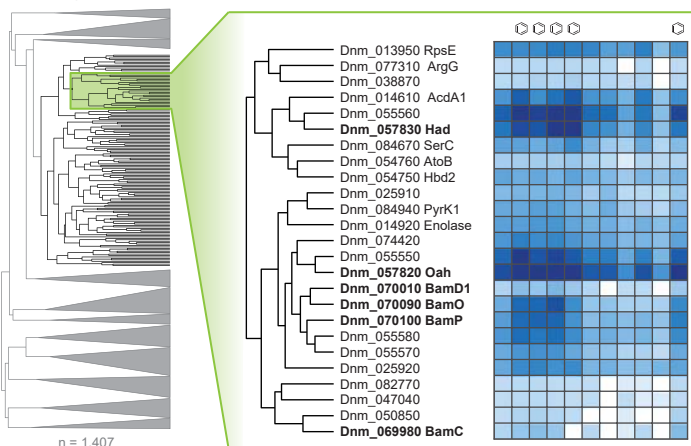
### *Ds. variabilis* 3be13



### *Dc. multivorans* 1be1



### *Dn. magnum*



### *Db. toluolica* Tol2

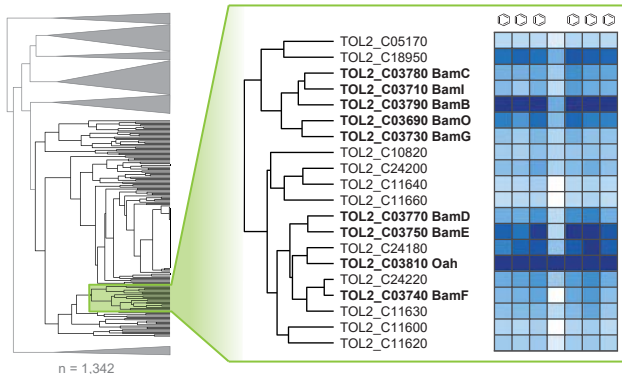
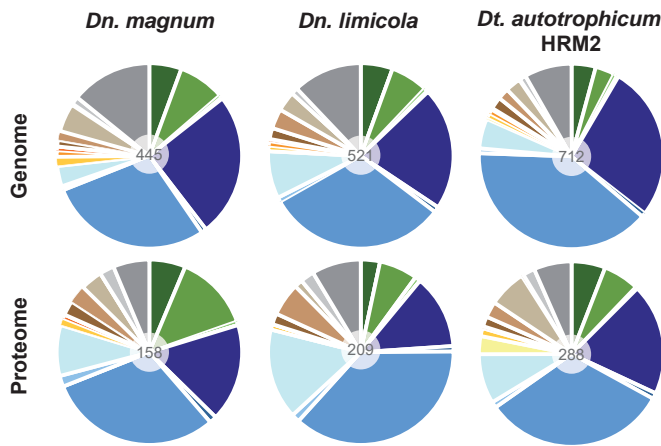


**Fig. S19: Clustering of *bam* gene pathway module products according to protein abundance across tested substrate conditions.** Sub-clusters containing proteins involved in reductive dearomatization of aromatic growth substrates for *Ds. variabilis* 3be13, *Dc. multivorans* 1be1, *Dn. magnum*, and *Db. toluolica* Tol2. Aromatic substrate conditions are indicated by the aromatic ring (growth conditions are as given in Figs. S6, S7, S9 and S10). Localization of respective clusters in the complete clustering tree per strain is indicated by the green box.

**A**



**B**

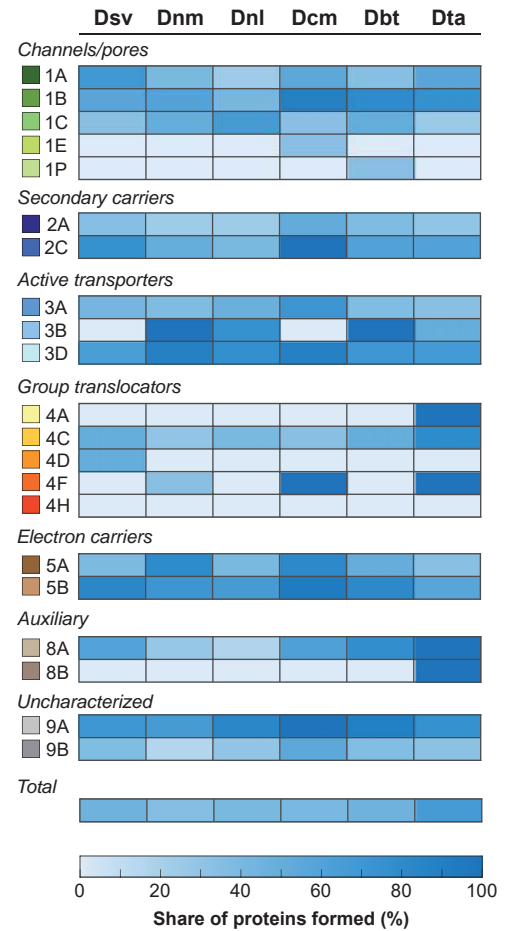


**Fig. S20: Transporter capacities of *Dn. magnum*, *Dn. limicola* and *Dt. autotrophicum* HRM2.** **A**, Share of predicted transport proteins according to TCDB in the respective genomes and proteomes. **B**, Share of proteins formed relative to genome encoded proteins per transporter subclass. Subclass codes: 1A,  $\alpha$ -type channels; 1B,  $\beta$ -barrel porins; 1C, pore-forming toxins; 1E, holins; 1P, non-envelope virus penetration complex; 2A, uniporters/symporters/antiporters; 2C, ion-gradient-driven energizers; 3A, P-P-bond-hydrolysis-driven transporters; 3B, decarboxylation-driven transporters; 3D, oxidoreduction-driven transporters; 4A, phosphotransfer-driven group translocators; 4C, acyl CoA ligase-coupled transporters; 4D, polysaccharide synthase/exporters; 4F, choline/ethanolamine phosphotransferase 1; 4H, lysylphosphatidylglycerol synthase/flippases; 5A, transmembrane 2-electron transfer carriers; 5B, transmembrane 1-electron transfer carriers; 8A, auxiliary transport proteins; 8B, ribosomally synthesized protein/peptide toxins/agonists that target channels and carriers; 9A, recognized transporters of unknown biochemical mechanism; 9B, putative transport proteins.

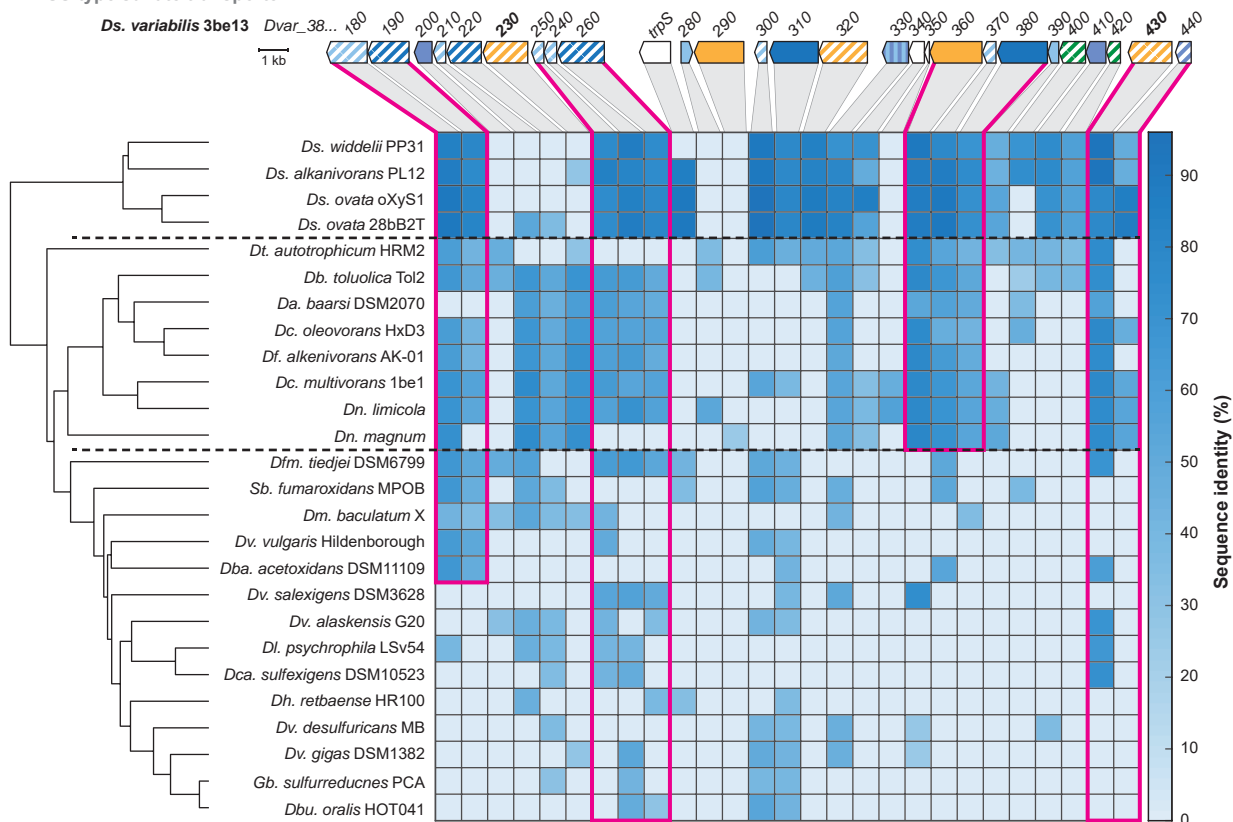
**Encoded protein function:**

- Sulfate transporter, DASS type
- TCS sensor histidine kinase
- TCS response regulator
- Universal stress protein
- CBS domain protein
- TCS response regulator with CBS domain
- Protein identified

**Fig. S21: Scale model of the DASS-type sulfate transporter encoding gene cluster of *Ds. variabilis* 3be13 compared to other selected SRB.** Homologous genes are connected by grey shading and amino acid sequence identity to genes of *Ds. variabilis* 3be13 is given in violet. Locus-tags (or gene names) are presented in black and hatching highlights genes with identified encoded proteins. Functions are color coded (bottom right).

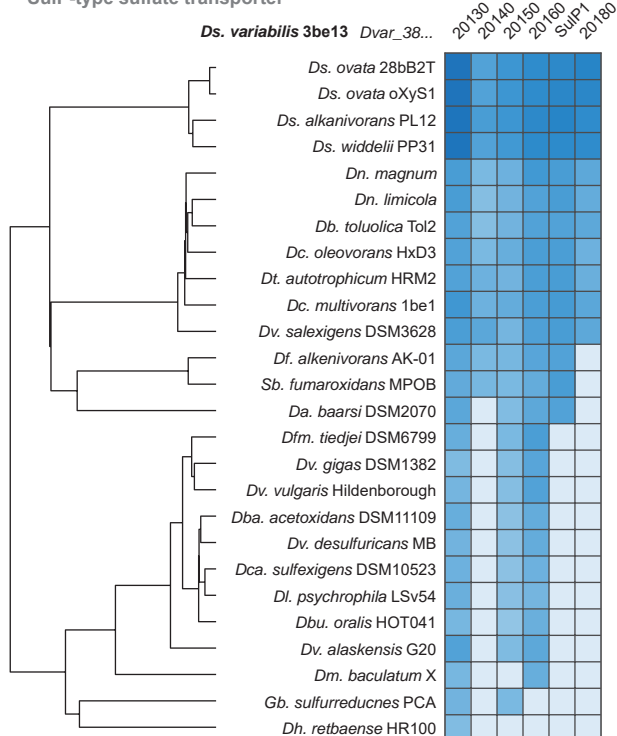
A

## DASS-type sulfate transporter



B

## SulP-type sulfate transporter



C

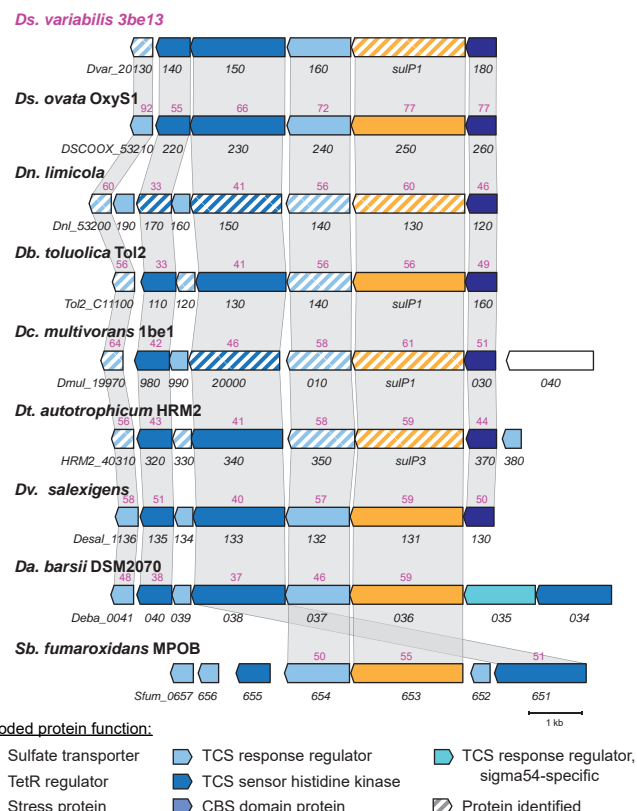


**Fig. S22: Sulfate uptake by DASS- and SulP-type transporters in selected SRB.** A, Scale model of the DASS-type sulfate transporter encoding gene cluster of *Ds. variabilis* 3be13 and heatmap of amino acid sequence identity between homologs of *Ds. variabilis* 3be13 and other SRB. Hierarchical clustering (Euclidian distance) was applied to identify the relationship among the respective gene repertoires (correlation coefficient 0.91). The cutting points for cluster definition are indicated by the dashed line. B, Amino acid sequence identity-based clustering heatmap of predicted SulP-type transporter gene cluster components relative to *Ds. variabilis* 3be3. Hierarchical clustering was applied to identify relationships among the respective gene repertoires of the different SRB (correlation coefficient 0.83). C, Scale model of the SulP-type sulfate transporter encoding gene cluster of *Ds. variabilis* 3be3 compared to other selected SRB. Homologous genes are connected by grey shading and amino acid sequence identity to genes of *Ds. variabilis* 3be13 is given in violet. Locus-tags (or gene names) are presented in black and hatching highlights genes with identified encoded proteins. Functions are color coded (bottom right).

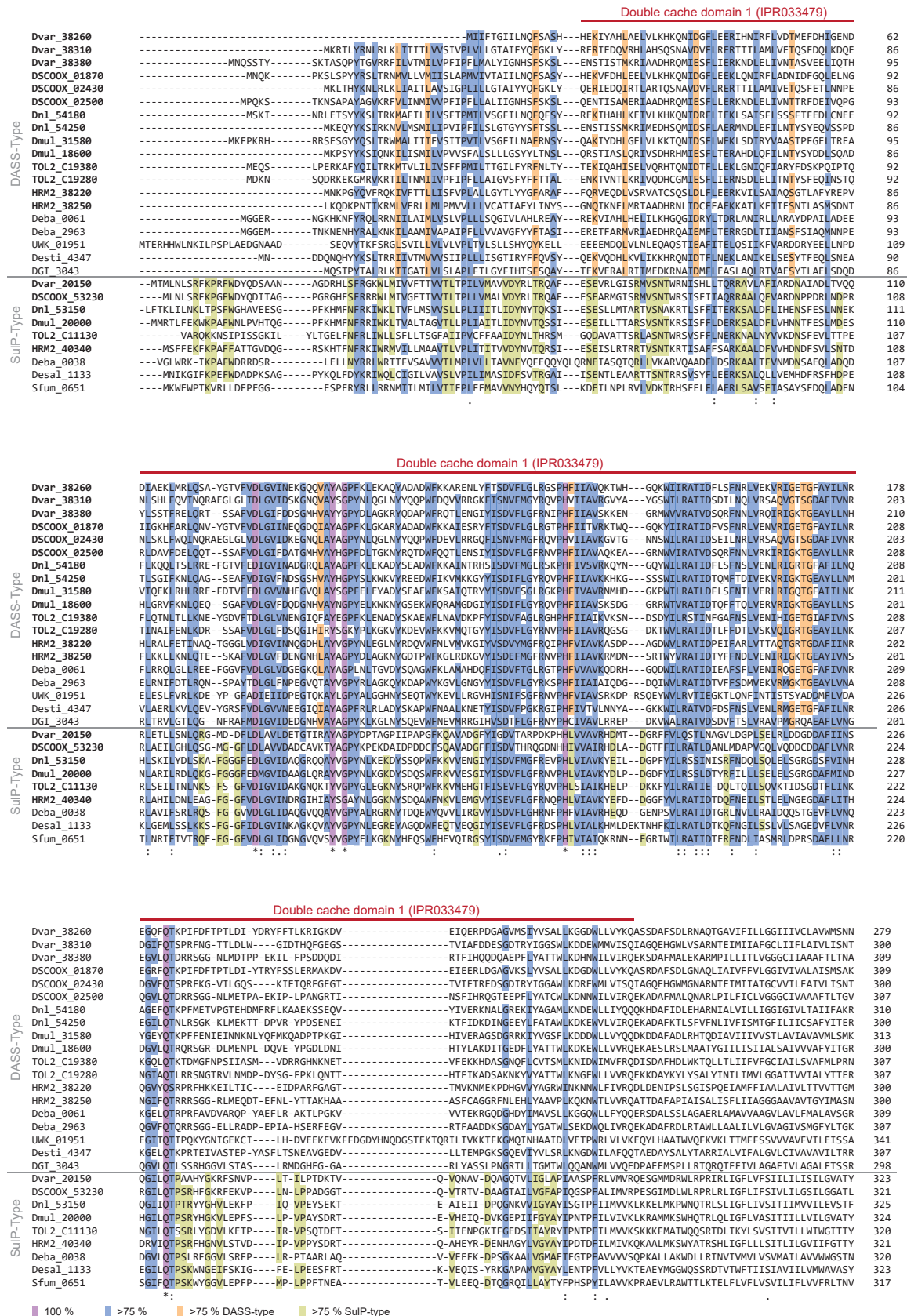
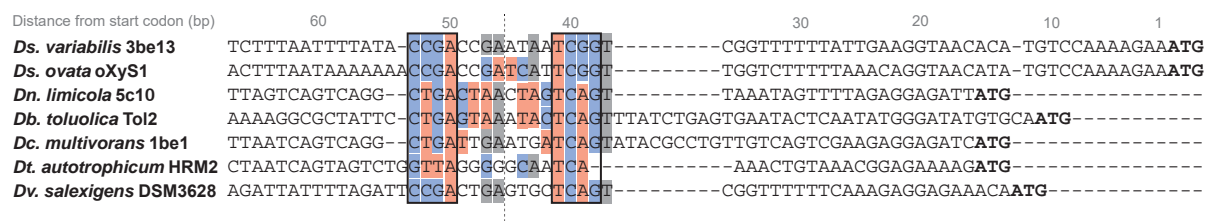
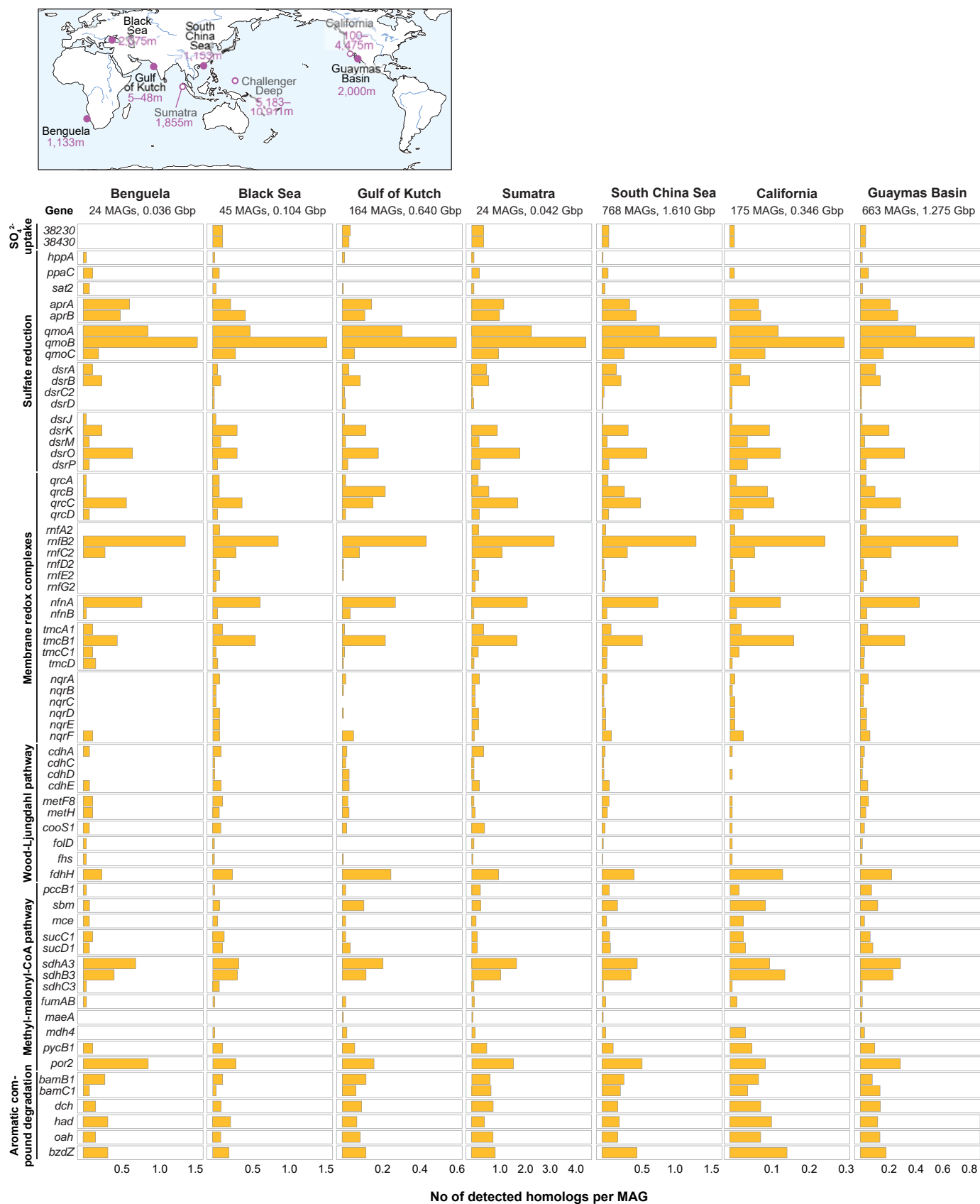


Fig. S23: Protein multiple sequence alignment of sensor histidine kinases predicted to be involved in regulation of sulfate uptake by DASS- and SulP-type transporters (separated by a gray line). Conserved regions among all sequences (blue or purple) or transporter class specific (orange or green for DASS- or SulP-type, respectively) are indicated. The region delineating the location of the effector recognizing double cache domain 1 is given. Numbers to the right of the alignments indicate amino acid positions per protein.





**Fig. S24: Nucleic acid sequence alignment of the upstream region of SulP-type transporter encoding gene clusters of selected SRB.** The start codon of the corresponding TetR-type regulator gene is indicated in bold font and nucleotide positions indicated for *Ds. variabilis* 3be13. Conserved, palindromic sequences are highlighted in blue (C and G) and red (A and T), respectively.



**Fig. S25: Characteristic *Desulfobacteraceae* "catabolic" genes are prevalent in marine sediments.** Location of queried metagenome samples and corresponding depth below sea surface (top). Distribution patterns of detected homologs in MAGs from indicated sites. Diversity profiles are summarized in table S10 and detailed data is available in Data S2. Gene names and locustags refer to *Ds. variabilis* 3be13. Number of MAGs and corresponding size of all assembled genomes is indicated below the station names.



Cluster 1

*Ds. variabilis* 3be13

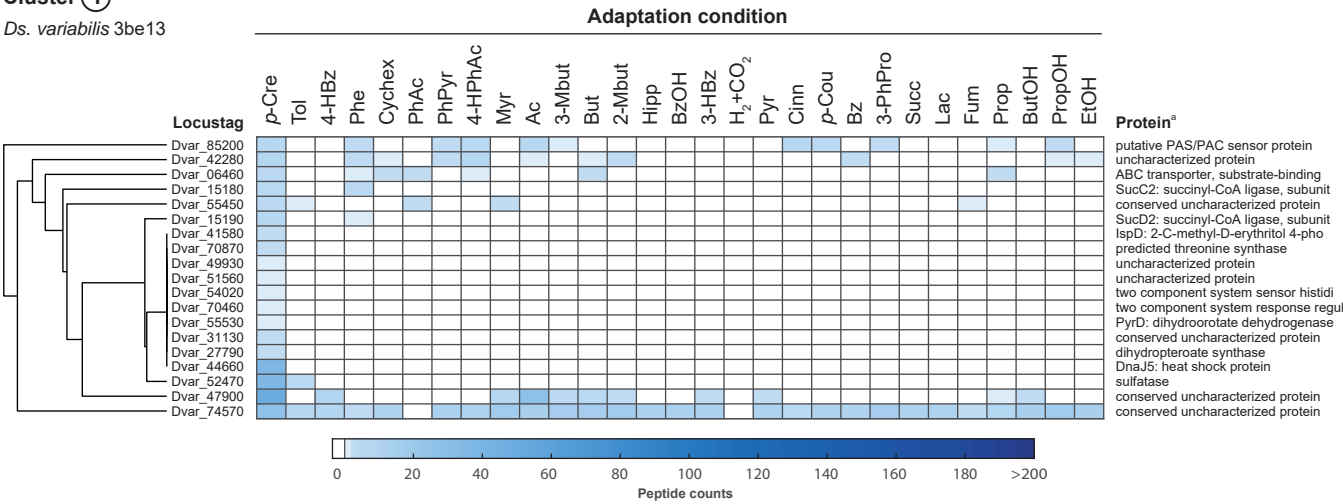


**Fig. S26: Detailed view on abundances of proteins forming a sub-cluster in the global clustering depicted in Fig. S6.** The global clustering is based on standardized protein abundances of all detected proteins of *Ds. variabilis* 3be13 across the 29 studied substrate adaptation conditions.

<sup>a</sup> Full description of protein functions are available in the genome annotation under accession CP159846.

### Cluster ②

*Ds. variabilis* 3be13

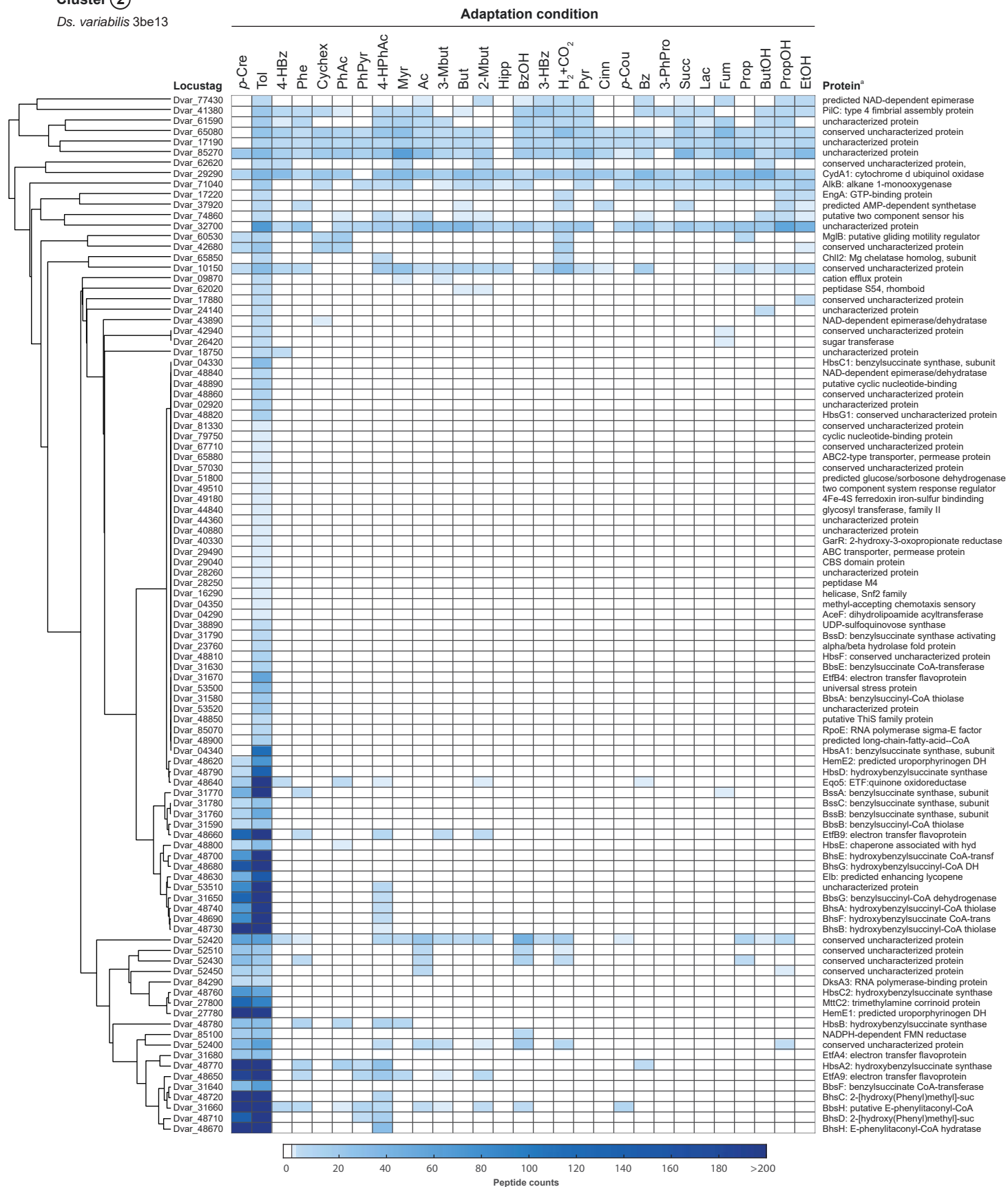


**Fig. S27: Detailed view on abundances of proteins forming a sub-cluster in the global clustering depicted in Fig. S6.** The global clustering is based on standardized protein abundances of all detected proteins of *Ds. variabilis* 3be13 across the 29 studied substrate adaptation conditions.

<sup>a</sup> Full description of protein functions are available in the genome annotation under accession CP159846.

Cluster 3

*Ds. variabilis* 3be13

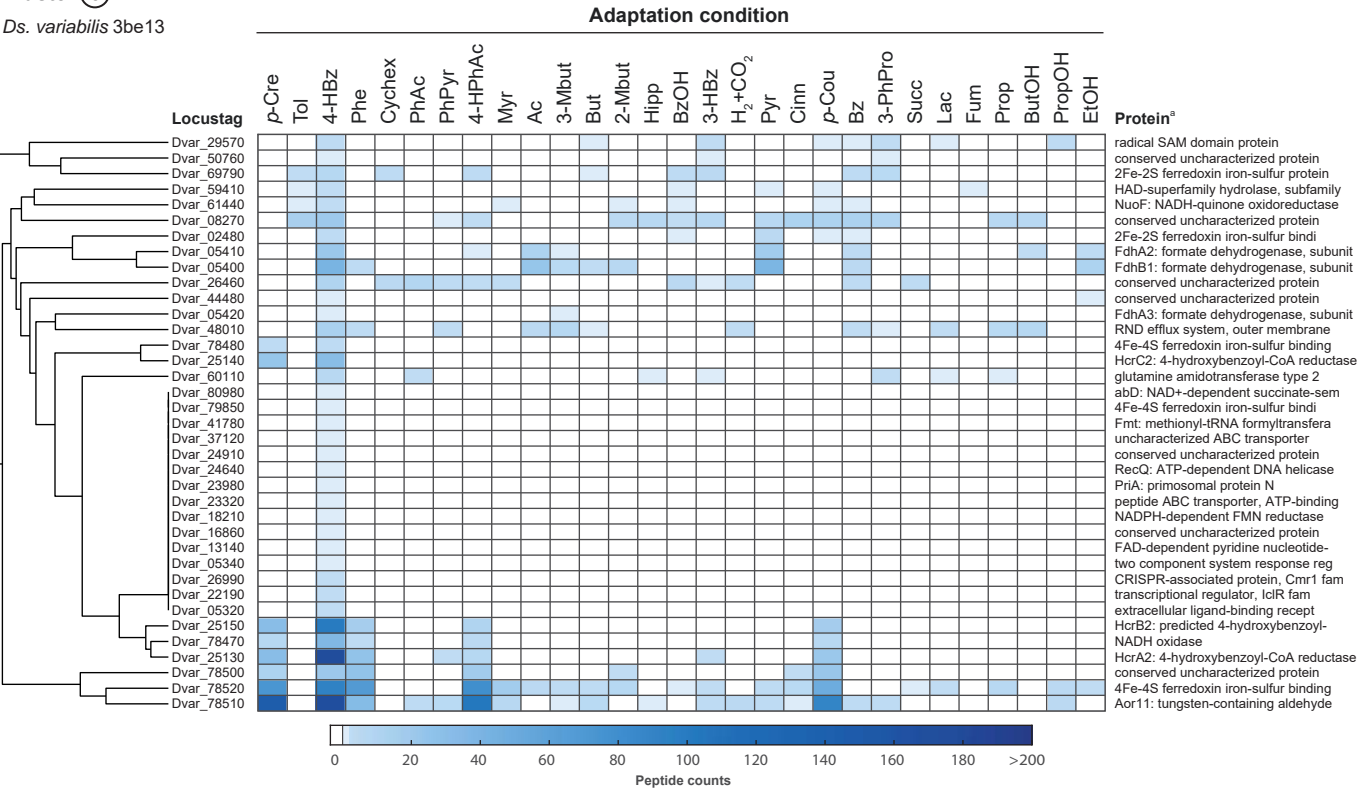
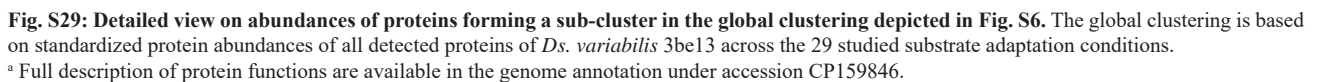


**Fig. S28: Detailed view on abundances of proteins forming a sub-cluster in the global clustering depicted in Fig. S6.** The global clustering is based on standardized protein abundances of all detected proteins of *Ds. variabilis* 3be13 across the 29 studied substrate adaptation conditions.

<sup>a</sup> Full description of protein functions are available in the genome annotation under accession CP159846.

*Ds. variabilis* 3be13



<sup>a</sup> Full description of protein functions are available in the genome annotation under accession CP159846.

Cluster 5

*Ds. variabilis* 3be13

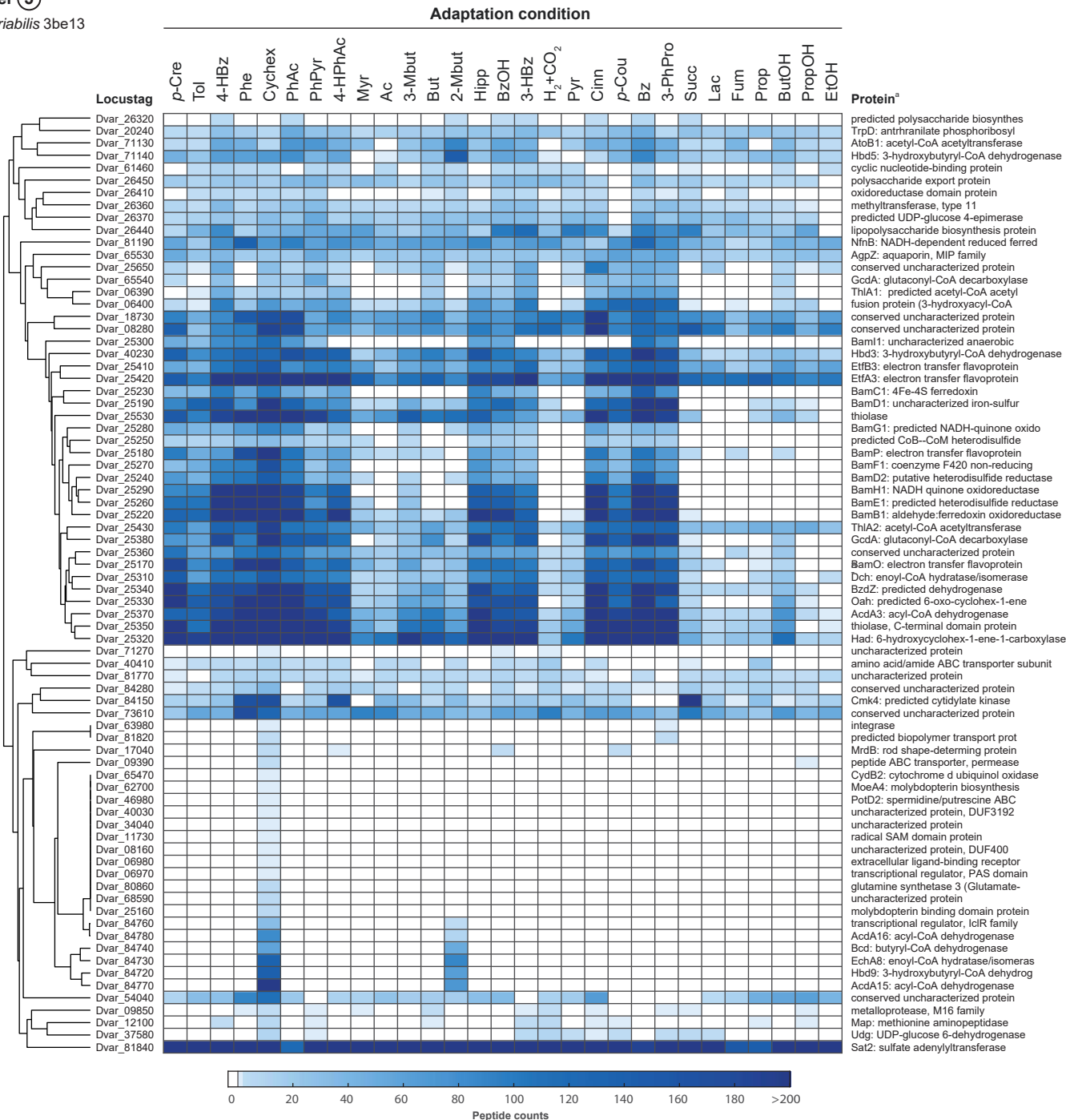


**Fig. S30: Detailed view on abundances of proteins forming a sub-cluster in the global clustering depicted in Fig. S6.** The global clustering is based on standardized protein abundances of all detected proteins of *Ds. variabilis* 3be13 across the 29 studied substrate adaptation conditions.

<sup>a</sup> Full description of protein functions are available in the genome annotation under accession CP159846.

# Cluster 6

*Ds. variabilis* 3be13

## Adaptation condition

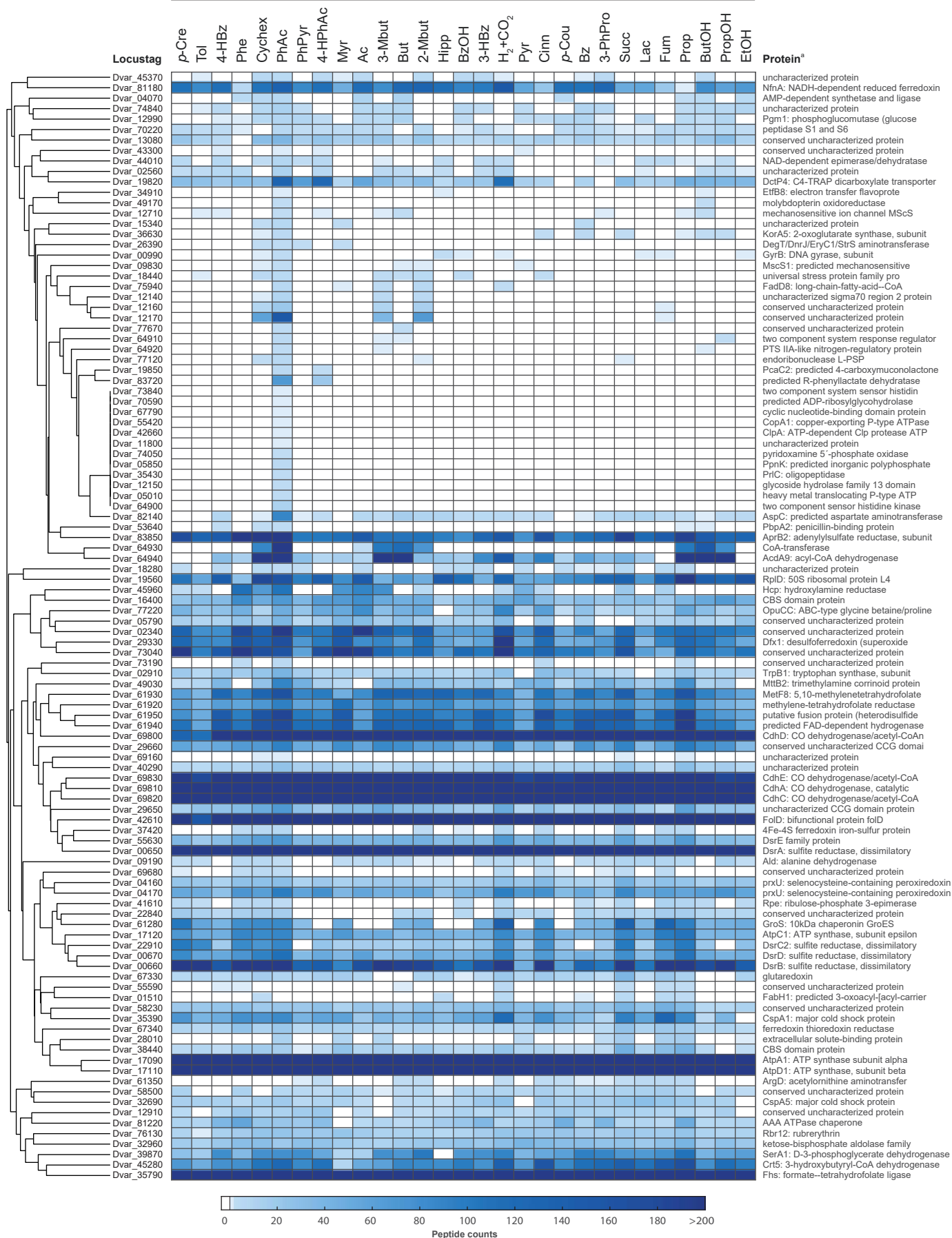


**Fig. S31: Detailed view on abundances of proteins forming a sub-cluster in the global clustering depicted in Fig. S6.** The global clustering is based on standardized protein abundances of all detected proteins of *Ds. variabilis* 3be13 across the 29 studied substrate adaptation conditions.

<sup>a</sup> Full description of protein functions are available in the genome annotation under accession CP159846.

Cluster 7  
*Ds. variabilis* 3be13

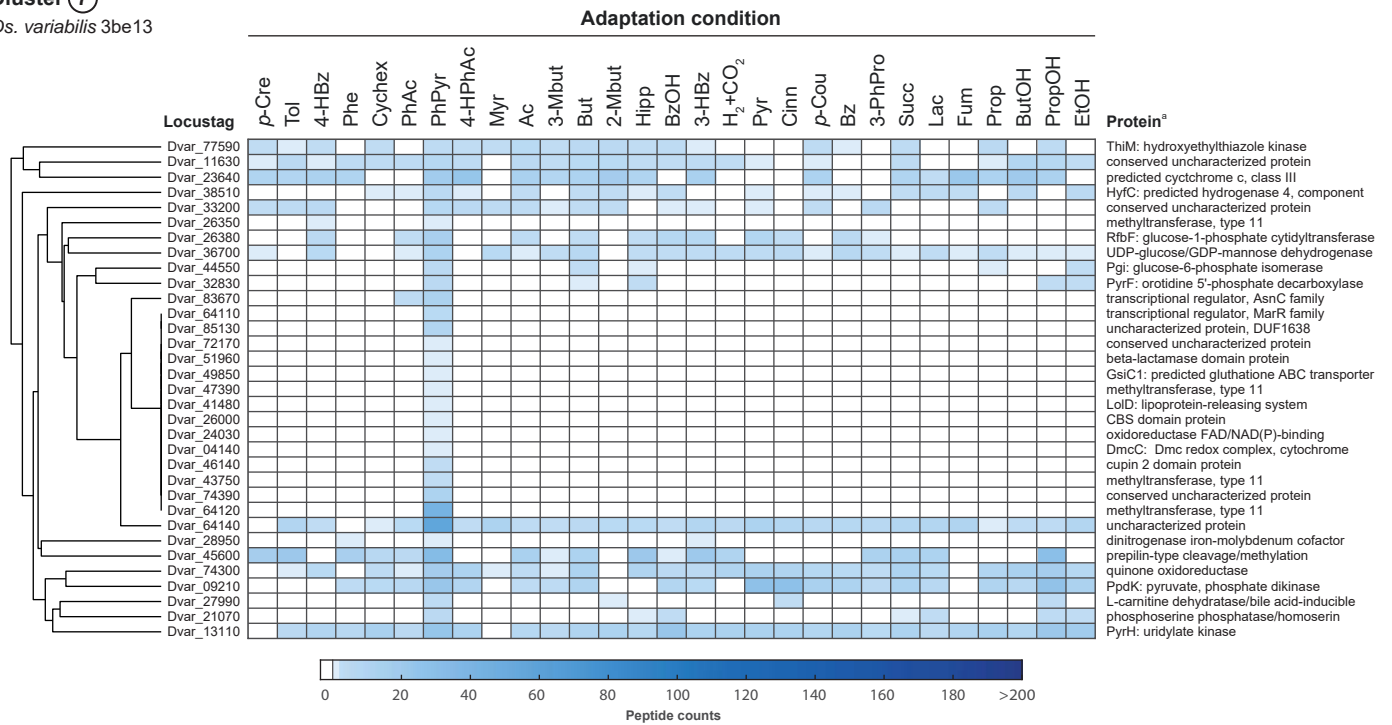


**Fig. S32: Detailed view on abundances of proteins forming a sub-cluster in the global clustering depicted in Fig. S6.** The global clustering is based on standardized protein abundances of all detected proteins of *Ds. variabilis* 3be13 across the 29 studied substrate adaptation conditions.

<sup>a</sup> Full description of protein functions are available in the genome annotation under accession CP159846.



Cluster 8

*Ds. variabilis* 3be13

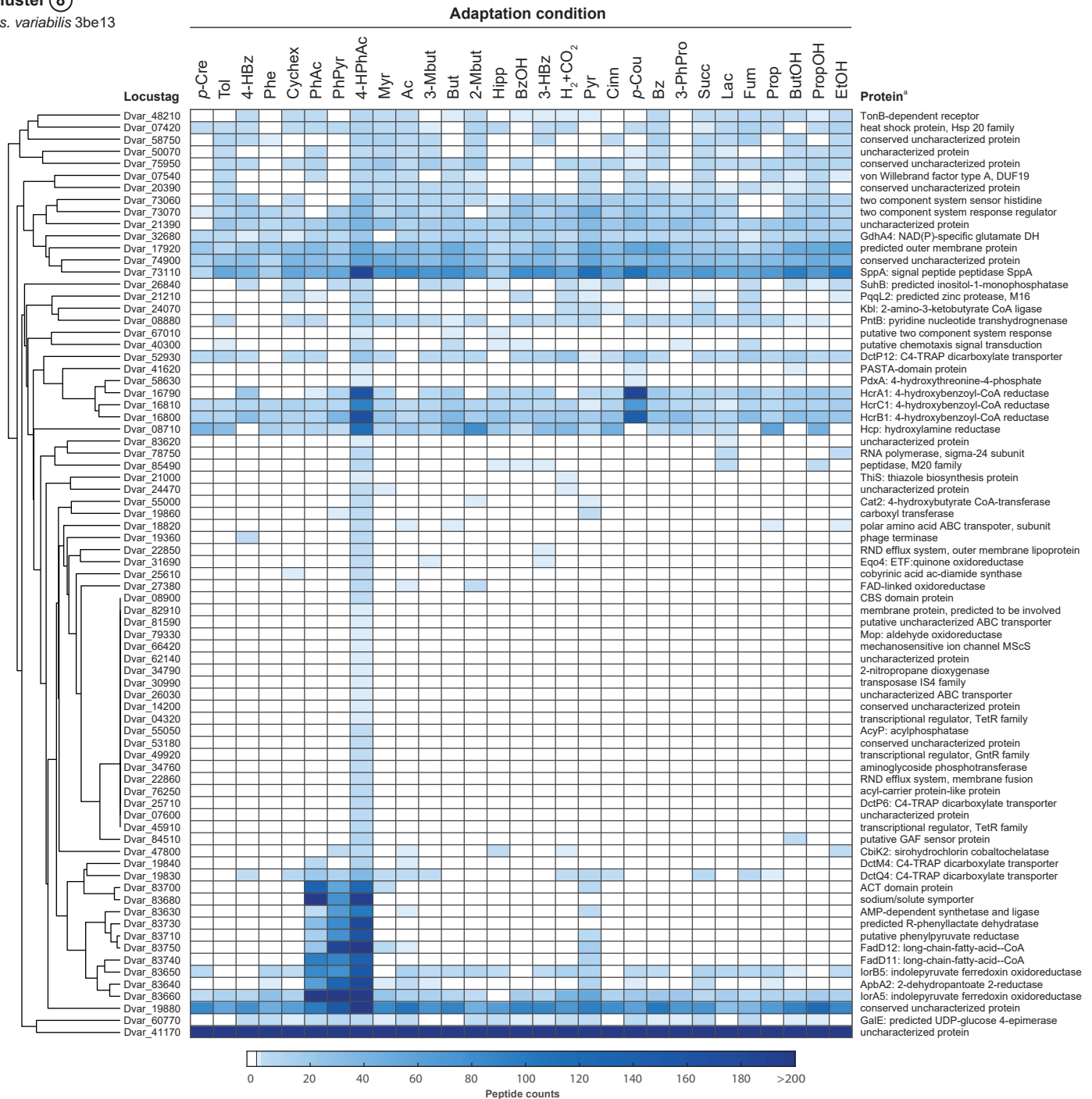


**Fig. S33: Detailed view on abundances of proteins forming a sub-cluster in the global clustering depicted in Fig. S6.** The global clustering is based on standardized protein abundances of all detected proteins of *Ds. variabilis* 3be13 across the 29 studied substrate adaptation conditions.

<sup>a</sup> Full description of protein functions are available in the genome annotation under accession CP159846.



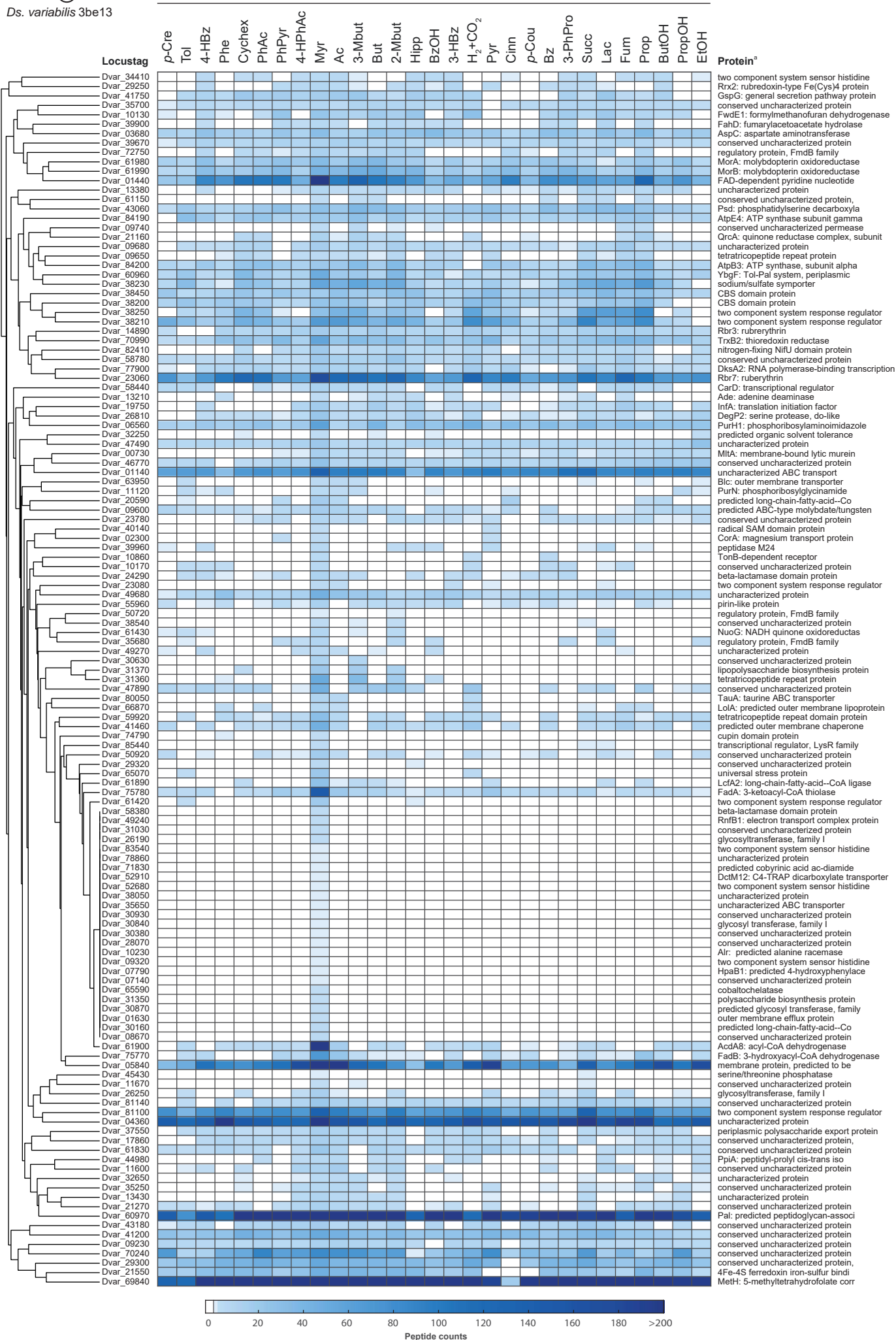


**Fig. S34: Detailed view on abundances of proteins forming a sub-cluster in the global clustering depicted in Fig. S6.** The global clustering is based on standardized protein abundances of all detected proteins of *Ds. variabilis* 3be13 across the 29 studied substrate adaptation conditions.

<sup>a</sup> Full description of protein functions are available in the genome annotation under accession CP159846.

Cluster 10

*Ds. variabilis* 3be13

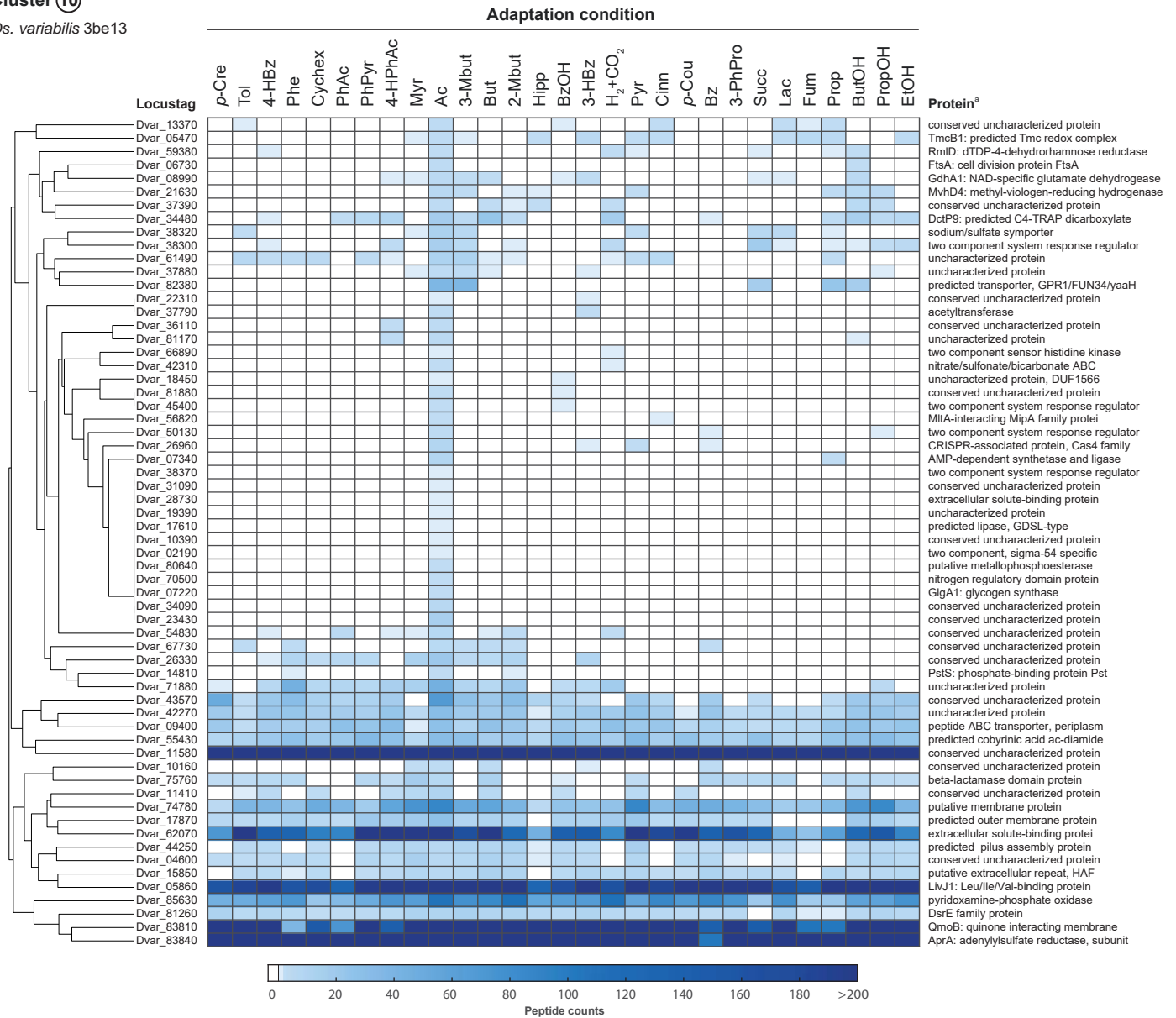
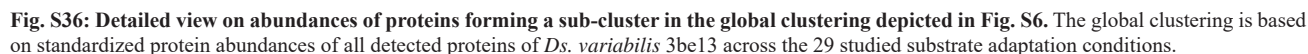


**Fig. S35: Detailed view on abundances of proteins forming a sub-cluster in the global clustering depicted in Fig. S6.** The global clustering is based on standardized protein abundances of all detected proteins of *Ds. variabilis* 3be13 across the 29 studied substrate adaptation conditions.

<sup>a</sup> Full description of protein functions are available in the genome annotation under accession CP159846.

*Ds. variabilis* 3be13



<sup>a</sup> Full description of protein functions are available in the genome annotation under accession CP159846.

Cluster 12

*Ds. variabilis* 3be13

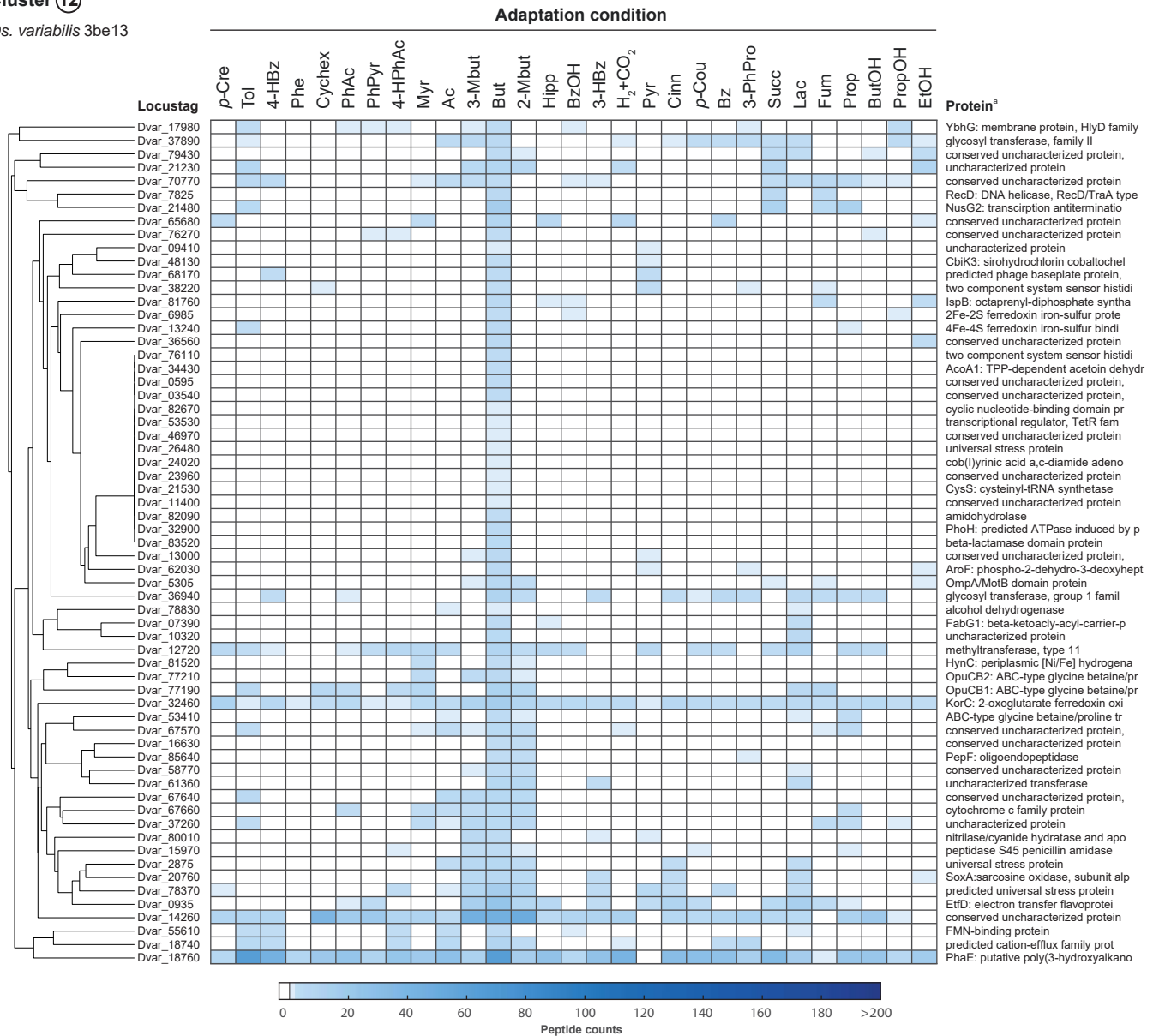


**Fig. S37:** Detailed view on abundances of proteins forming a sub-cluster in the global clustering depicted in Fig. S6. The global clustering is based on standardized protein abundances of all detected proteins of *Ds. variabilis* 3be13 across the 29 studied substrate adaptation conditions.

<sup>a</sup> Full description of protein functions are available in the genome annotation under accession CP159846.

Cluster 13

*Ds. variabilis* 3be13

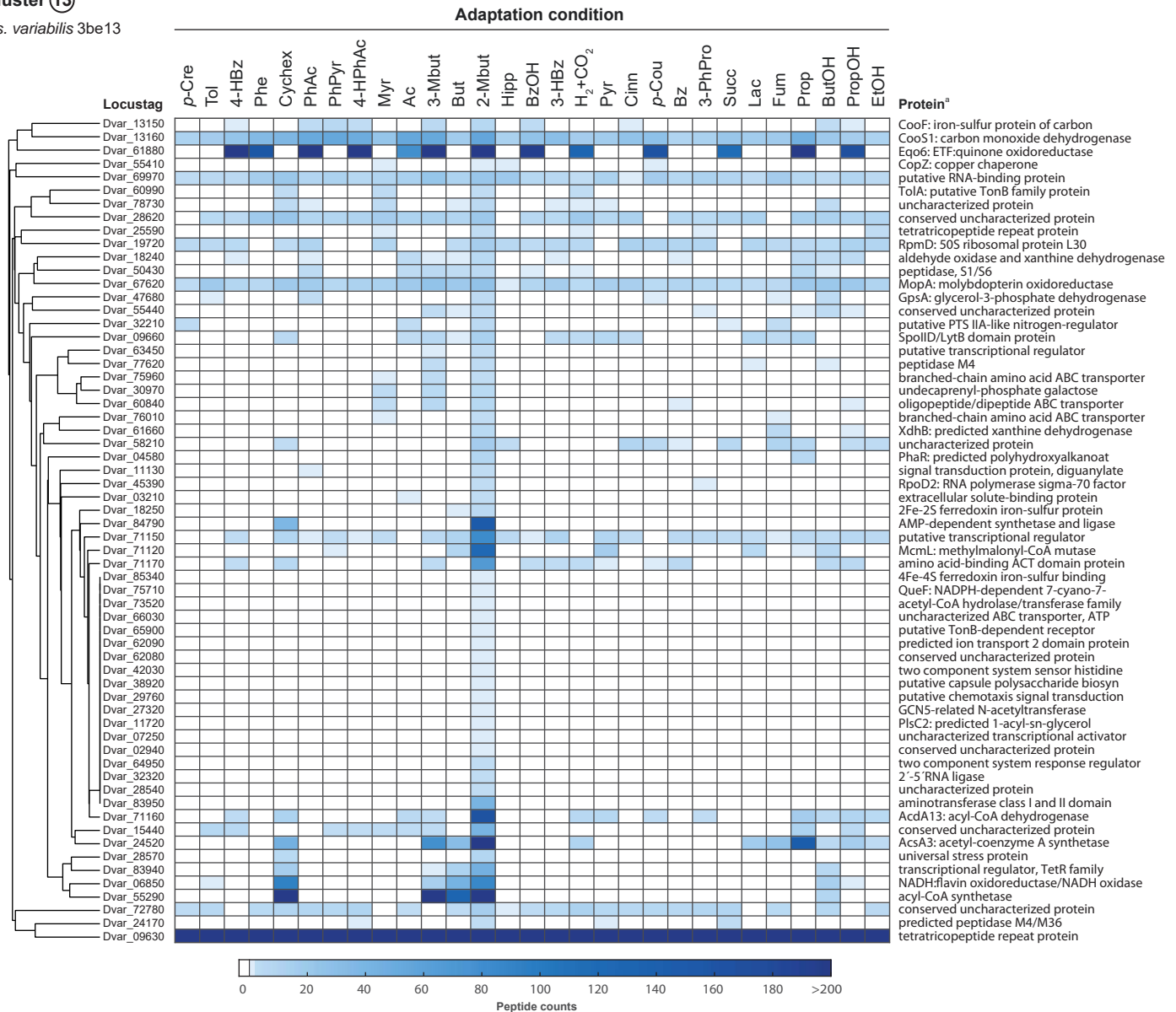


**Fig. S38: Detailed view on abundances of proteins forming a sub-cluster in the global clustering depicted in Fig. S6.** The global clustering is based on standardized protein abundances of all detected proteins of *Ds. variabilis* 3be13 across the 29 studied substrate adaptation conditions.

<sup>a</sup> Full description of protein functions are available in the genome annotation under accession CP159846.

Cluster 14

*Ds. variabilis* 3be13

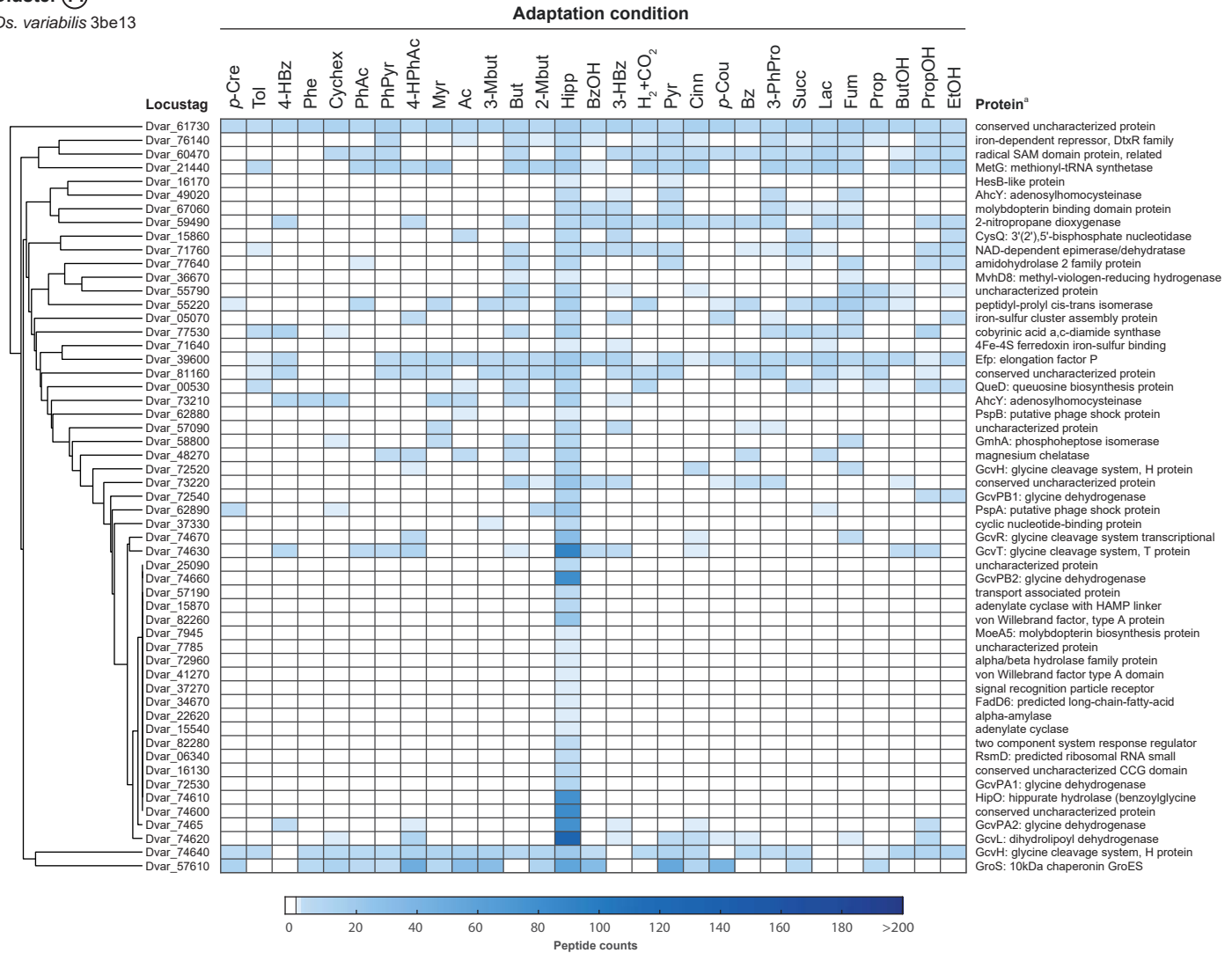


**Fig. S39: Detailed view on abundances of proteins forming a sub-cluster in the global clustering depicted in Fig. S6.** The global clustering is based on standardized protein abundances of all detected proteins of *Ds. variabilis* 3be13 across the 29 studied substrate adaptation conditions.

<sup>a</sup> Full description of protein functions are available in the genome annotation under accession CP159846.

# Cluster 15

*Ds. variabilis* 3be13

## Adaptation condition

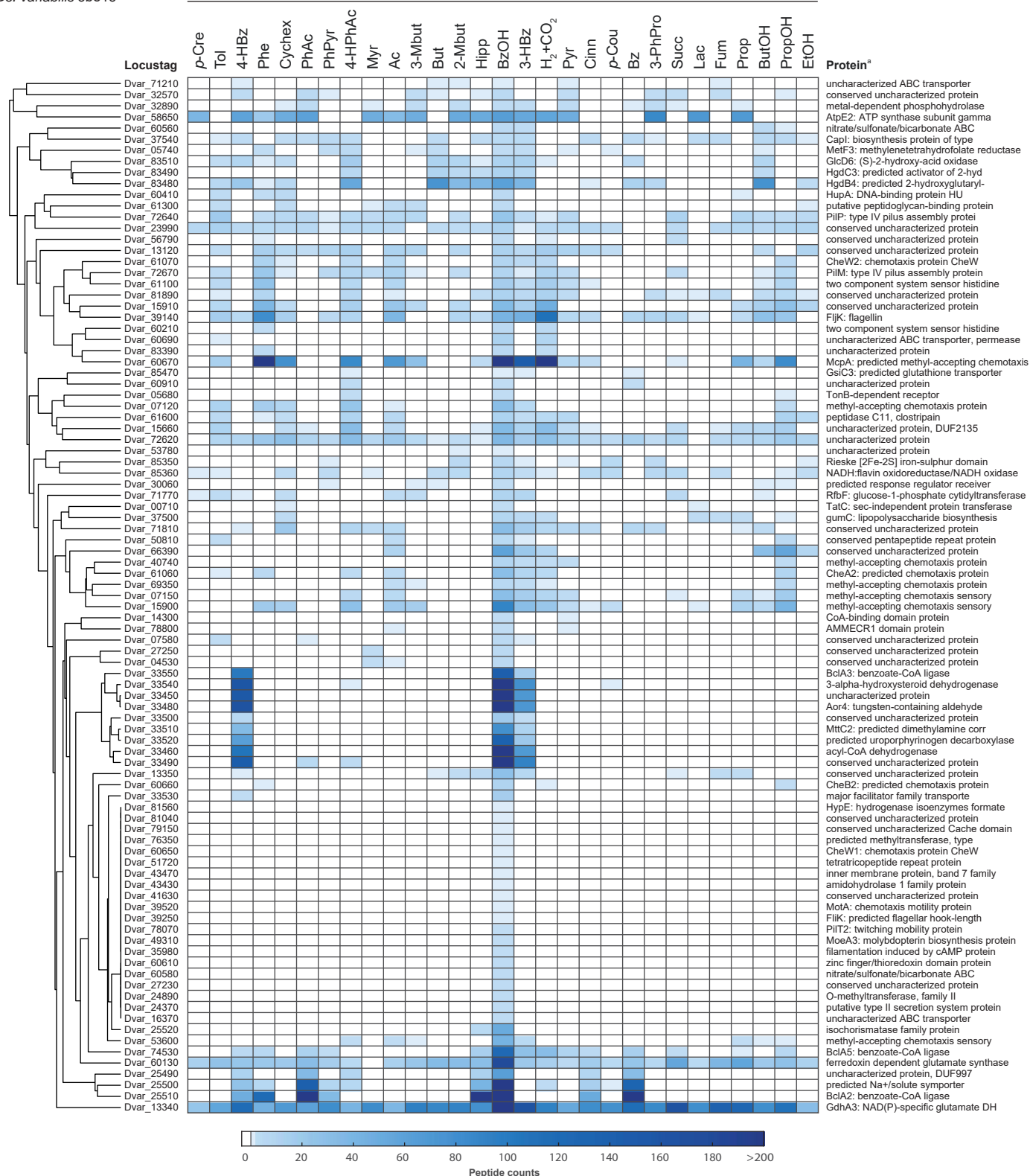


**Fig. S40: Detailed view on abundances of proteins forming a sub-cluster in the global clustering depicted in Fig. S6.** The global clustering is based on standardized protein abundances of all detected proteins of *Ds. variabilis* 3be13 across the 29 studied substrate adaptation conditions.

<sup>a</sup> Full description of protein functions are available in the genome annotation under accession CP159846.



Cluster 16

Ds. variabilis 3be13

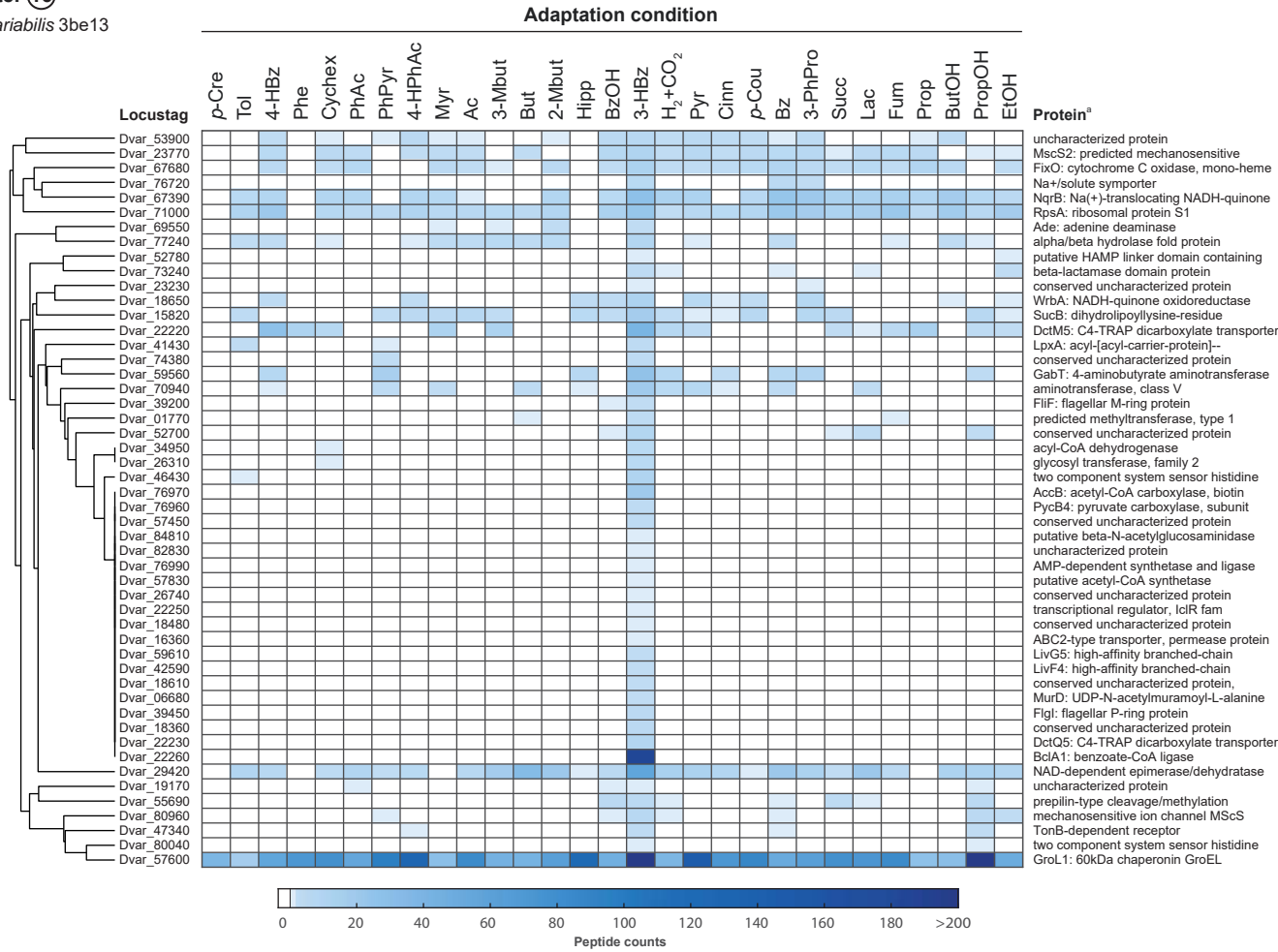


**Fig. S41: Detailed view on abundances of proteins forming a sub-cluster in the global clustering depicted in Fig. S6.** The global clustering is based on standardized protein abundances of all detected proteins of *Ds. variabilis* 3be13 across the 29 studied substrate adaptation conditions.

<sup>a</sup> Full description of protein functions are available in the genome annotation under accession CP159846.



## Cluster 17

Ds. variabilis 3be13

## Adaptation condition

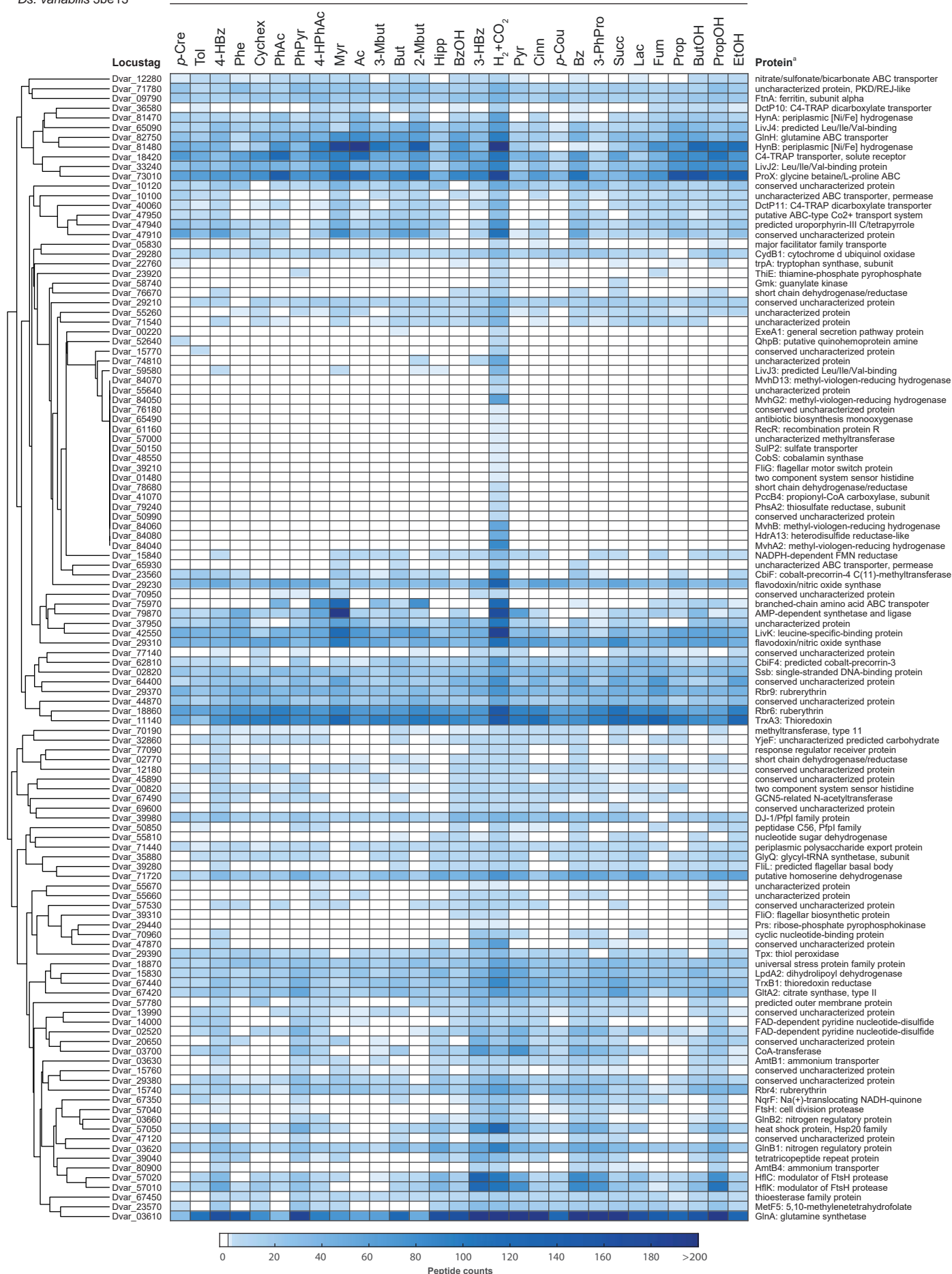


**Fig. S42: Detailed view on abundances of proteins forming a sub-cluster in the global clustering depicted in Fig. S6.** The global clustering is based on standardized protein abundances of all detected proteins of *Ds. variabilis* 3be13 across the 29 studied substrate adaptation conditions.

<sup>a</sup> Full description of protein functions are available in the genome annotation under accession CP159846.

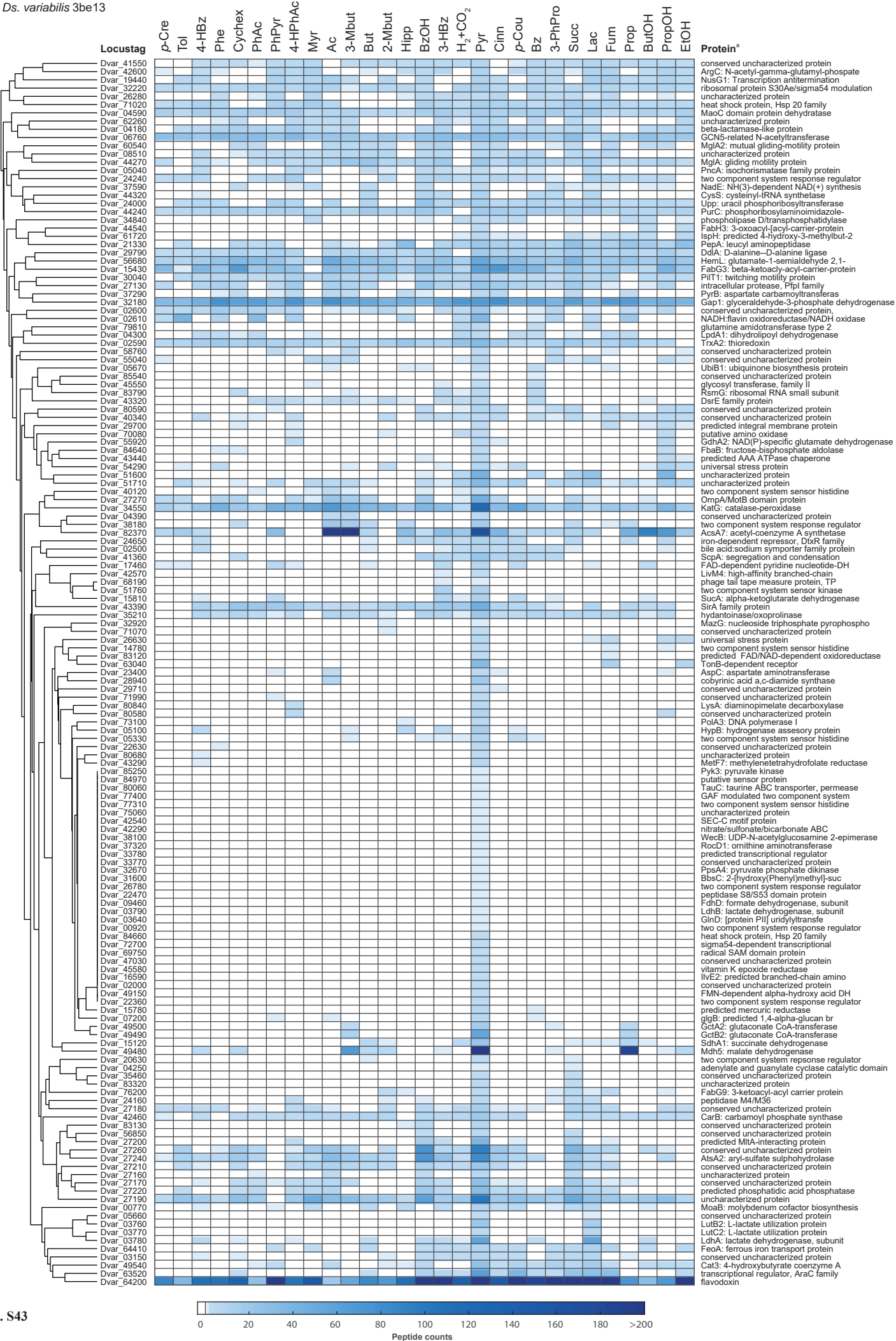
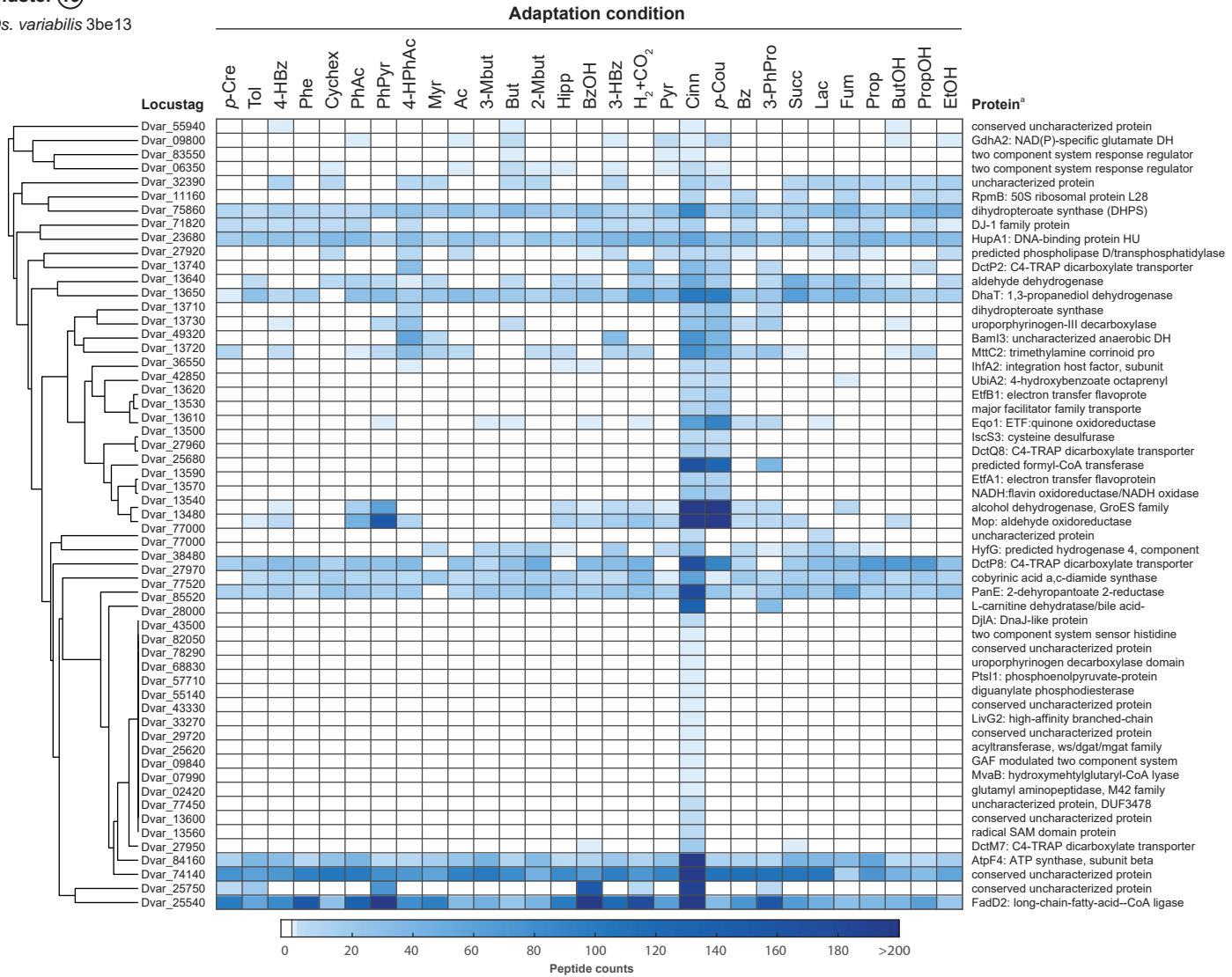


Fig. S43

Cluster 19

*Ds. variabilis* 3be13



**Fig. S44: Detailed view on abundances of proteins forming a sub-cluster in the global clustering depicted in Fig. S6.** The global clustering is based on standardized protein abundances of all detected proteins of *Ds. variabilis* 3be13 across the 29 studied substrate adaptation conditions.  
<sup>a</sup> Full description of protein functions are available in the genome annotation under accession CP159846.

Cluster 20

Ds. variabilis 3be13

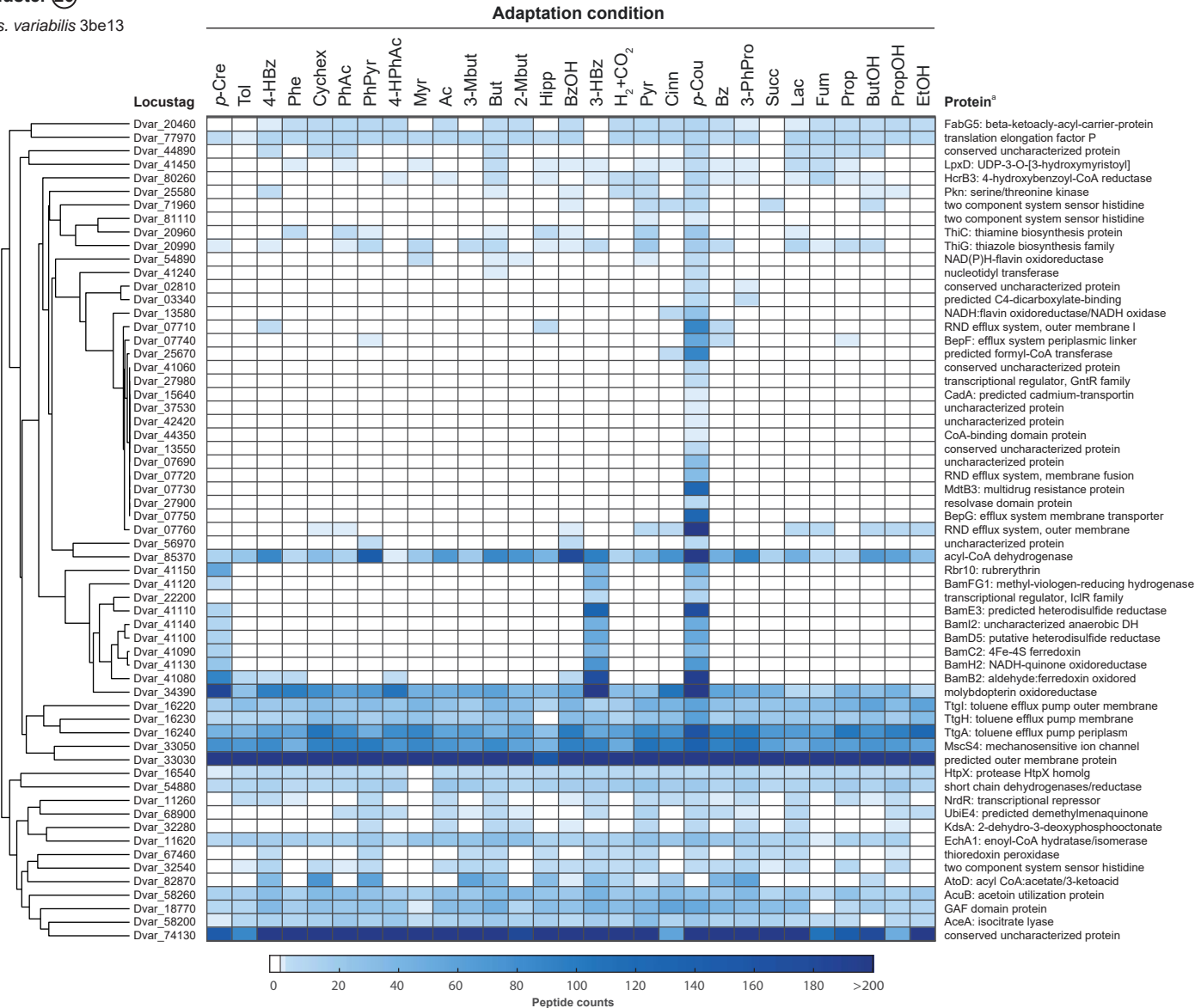


**Fig. S45: Detailed view on abundances of proteins forming a sub-cluster in the global clustering depicted in Fig. S6.** The global clustering is based on standardized protein abundances of all detected proteins of *Ds. variabilis* 3be13 across the 29 studied substrate adaptation conditions.

<sup>a</sup> Full description of protein functions are available in the genome annotation under accession CP159846.

Cluster 21

*Ds. variabilis* 3be13

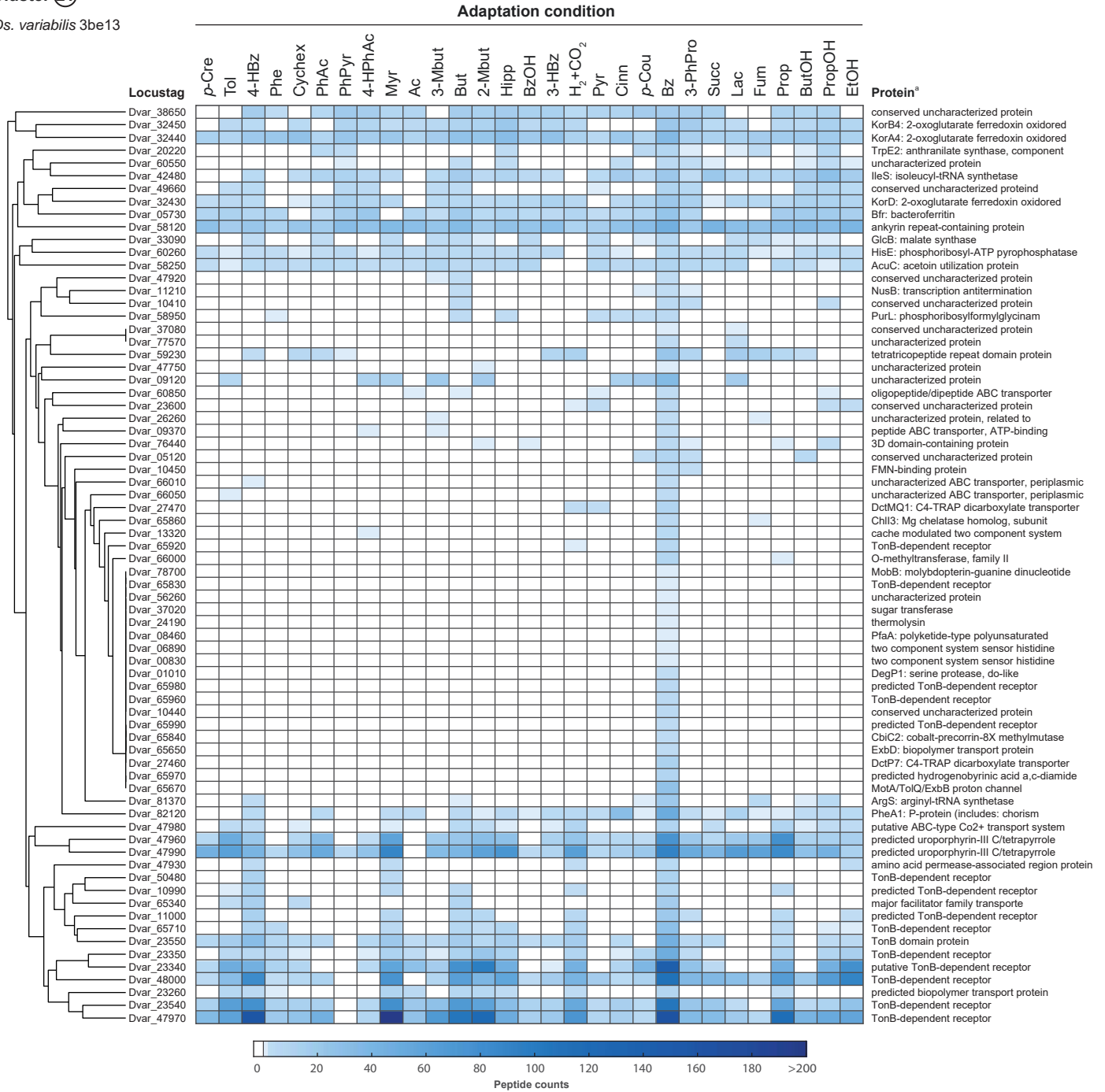


**Fig. S46: Detailed view on abundances of proteins forming a sub-cluster in the global clustering depicted in Fig. S6.** The global clustering is based on standardized protein abundances of all detected proteins of *Ds. variabilis* 3be13 across the 29 studied substrate adaptation conditions.

<sup>a</sup> Full description of protein functions are available in the genome annotation under accession CP159846.

Cluster 22

Ds. variabilis 3be13

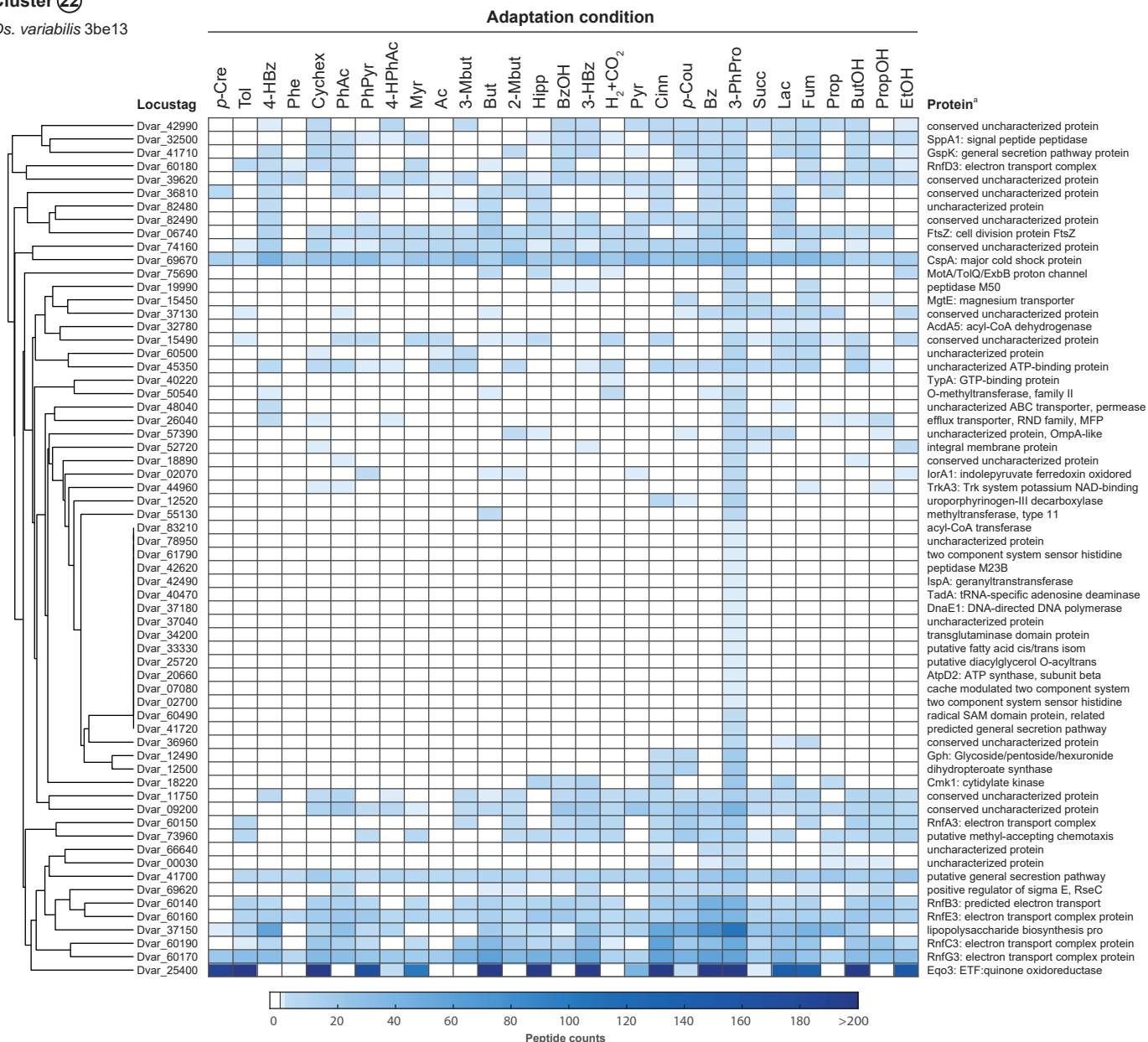
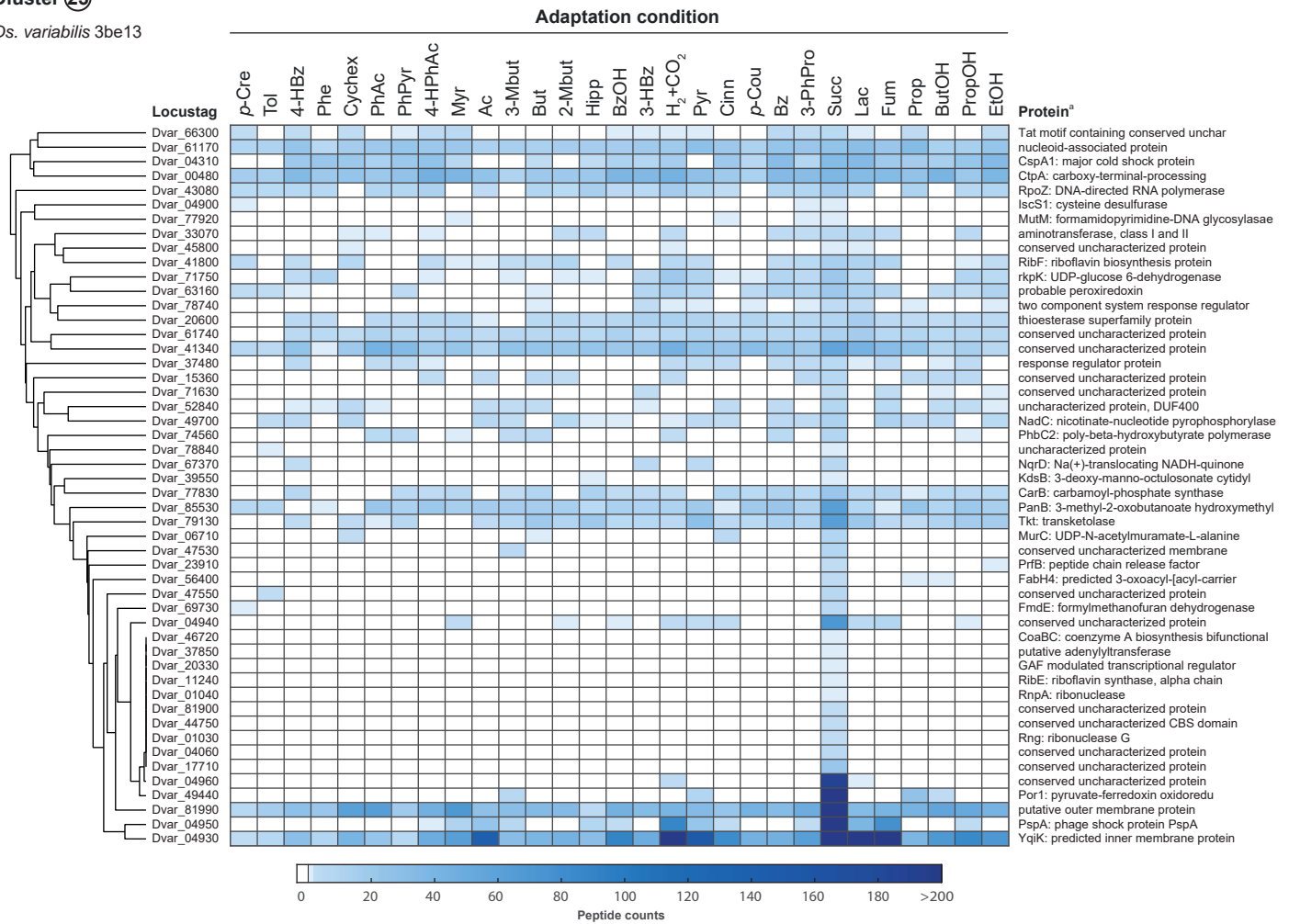


Fig. S47: Detailed view on abundances of proteins forming a sub-cluster in the global clustering depicted in Fig. S6. The global clustering is based on standardized protein abundances of all detected proteins of *Ds. variabilis* 3be13 across the 29 studied substrate adaptation conditions.

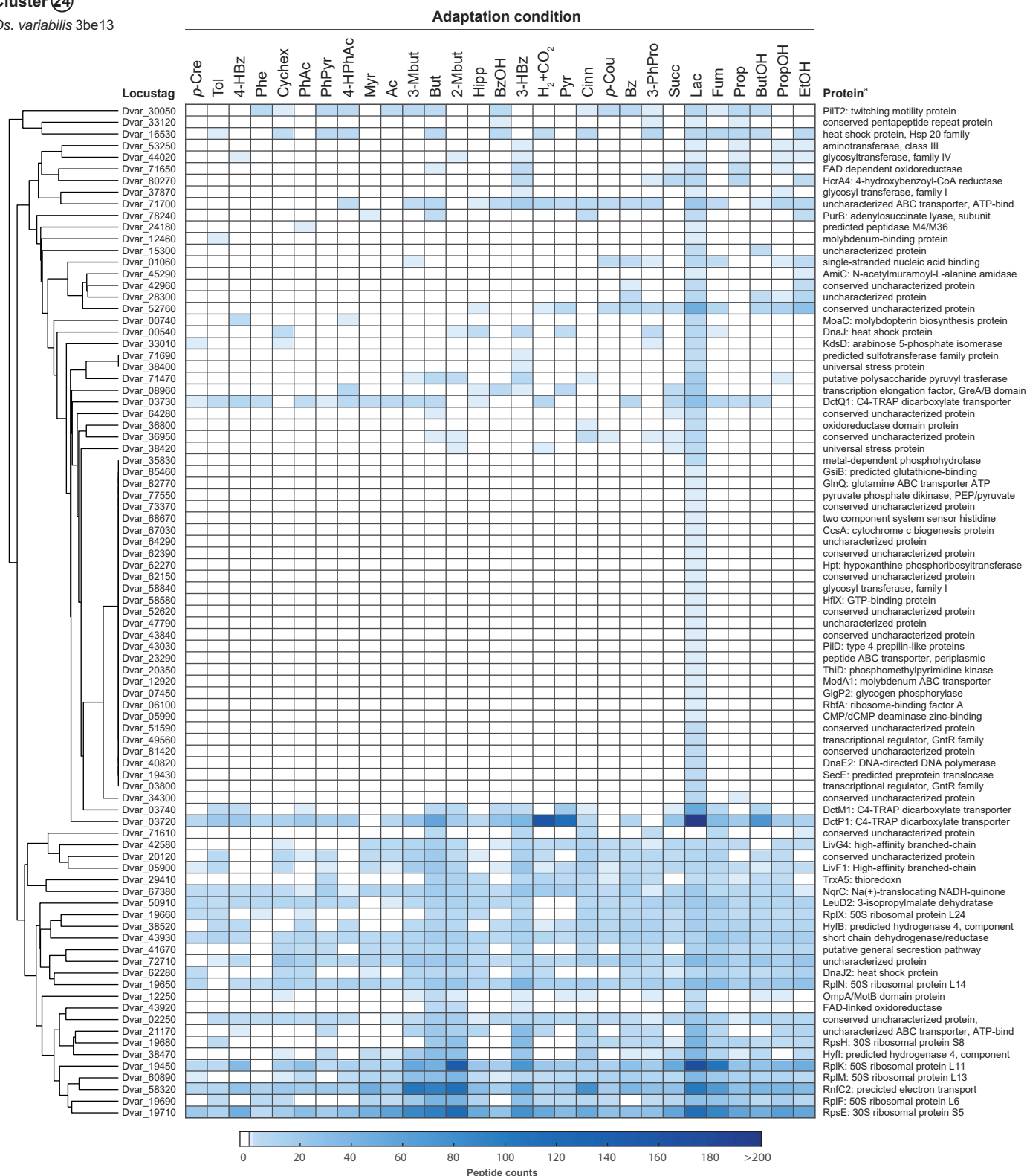
<sup>a</sup> Full description of protein functions are available in the genome annotation under accession CP159846.





**Fig. S48: Detailed view on abundances of proteins forming a sub-cluster in the global clustering depicted in Fig. S6.** The global clustering is based on standardized protein abundances of all detected proteins of *Ds. variabilis* 3be13 across the 29 studied substrate adaptation conditions.

<sup>a</sup> Full description of protein functions are available in the genome annotation under accession CP159846.





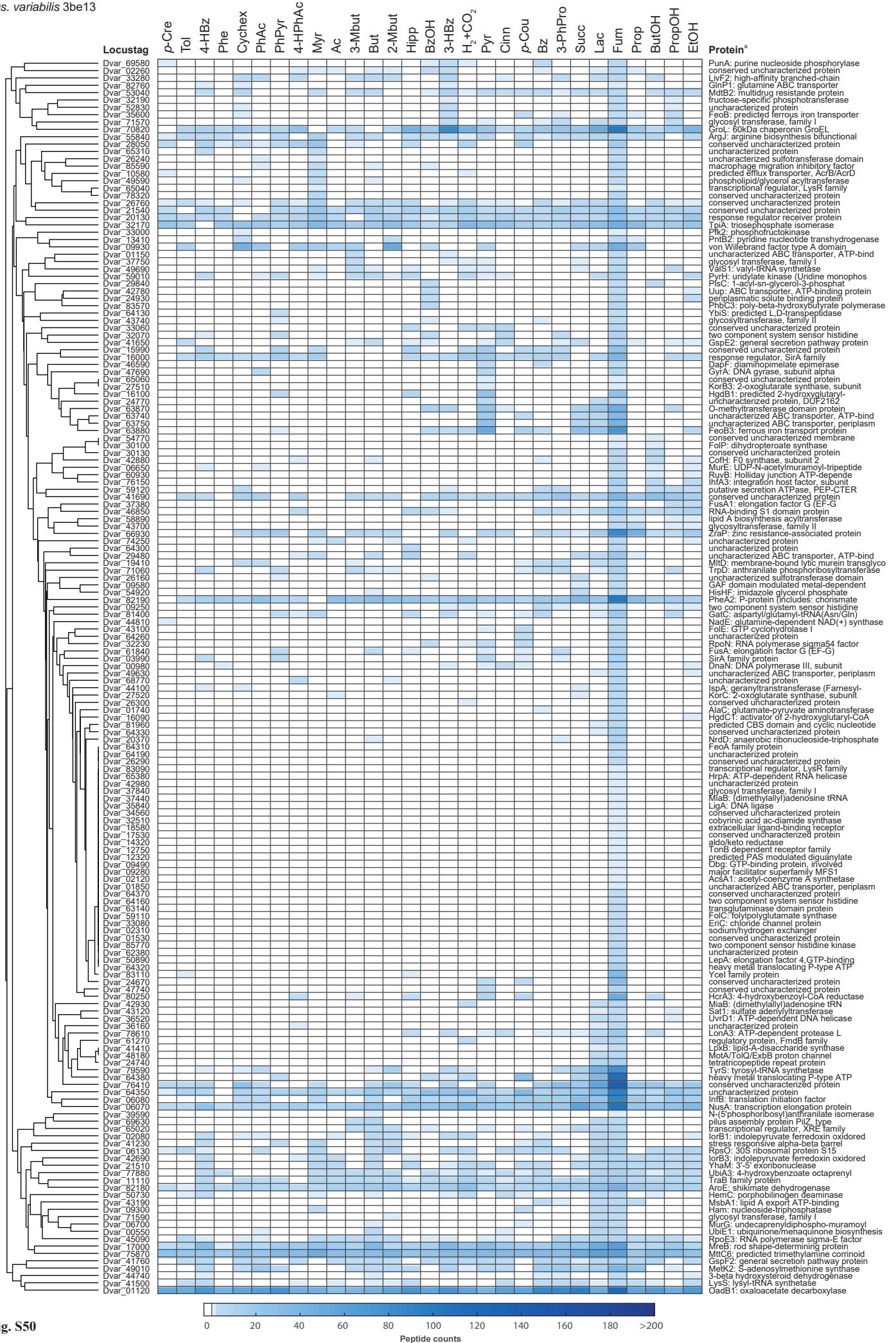
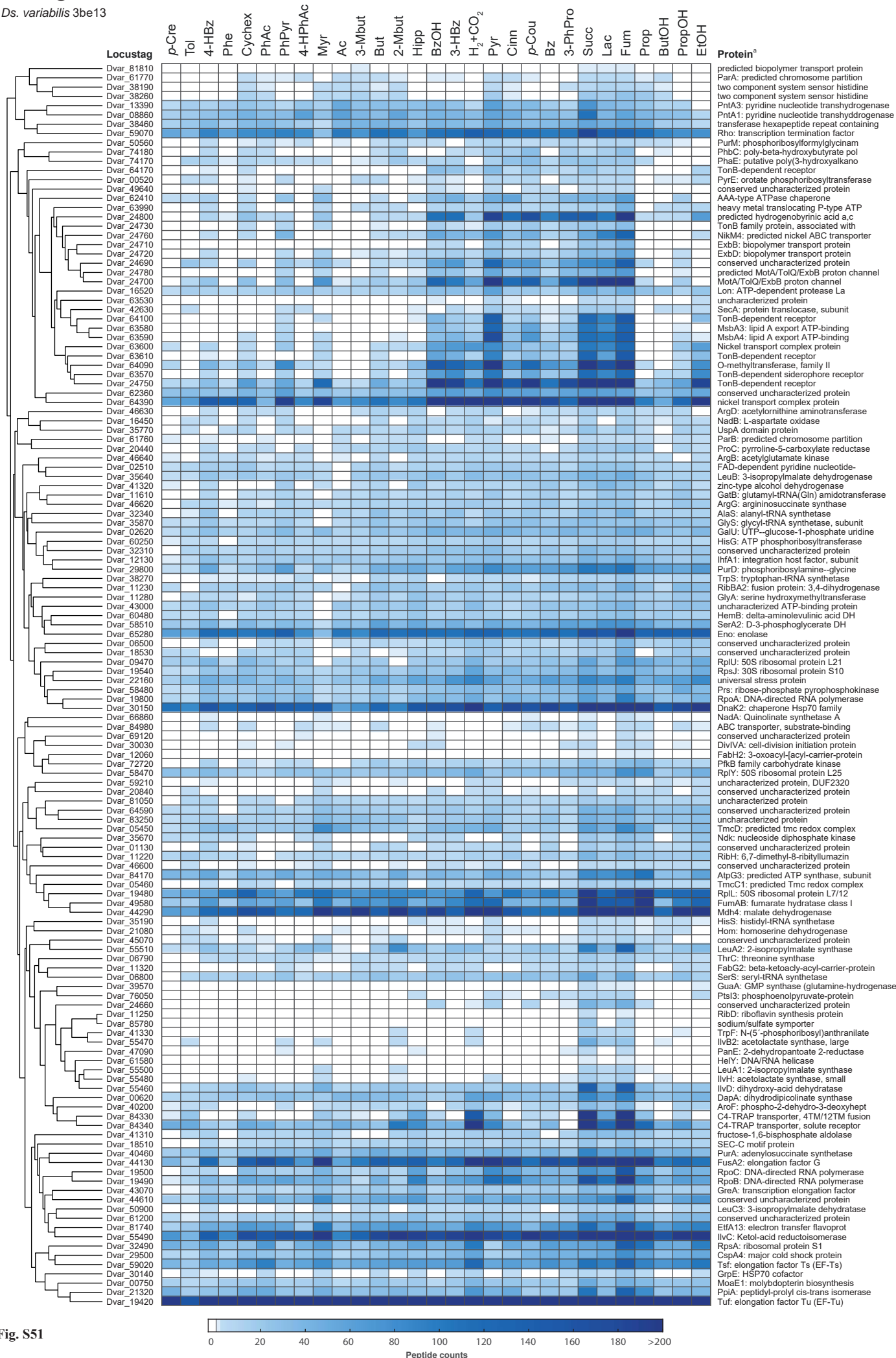
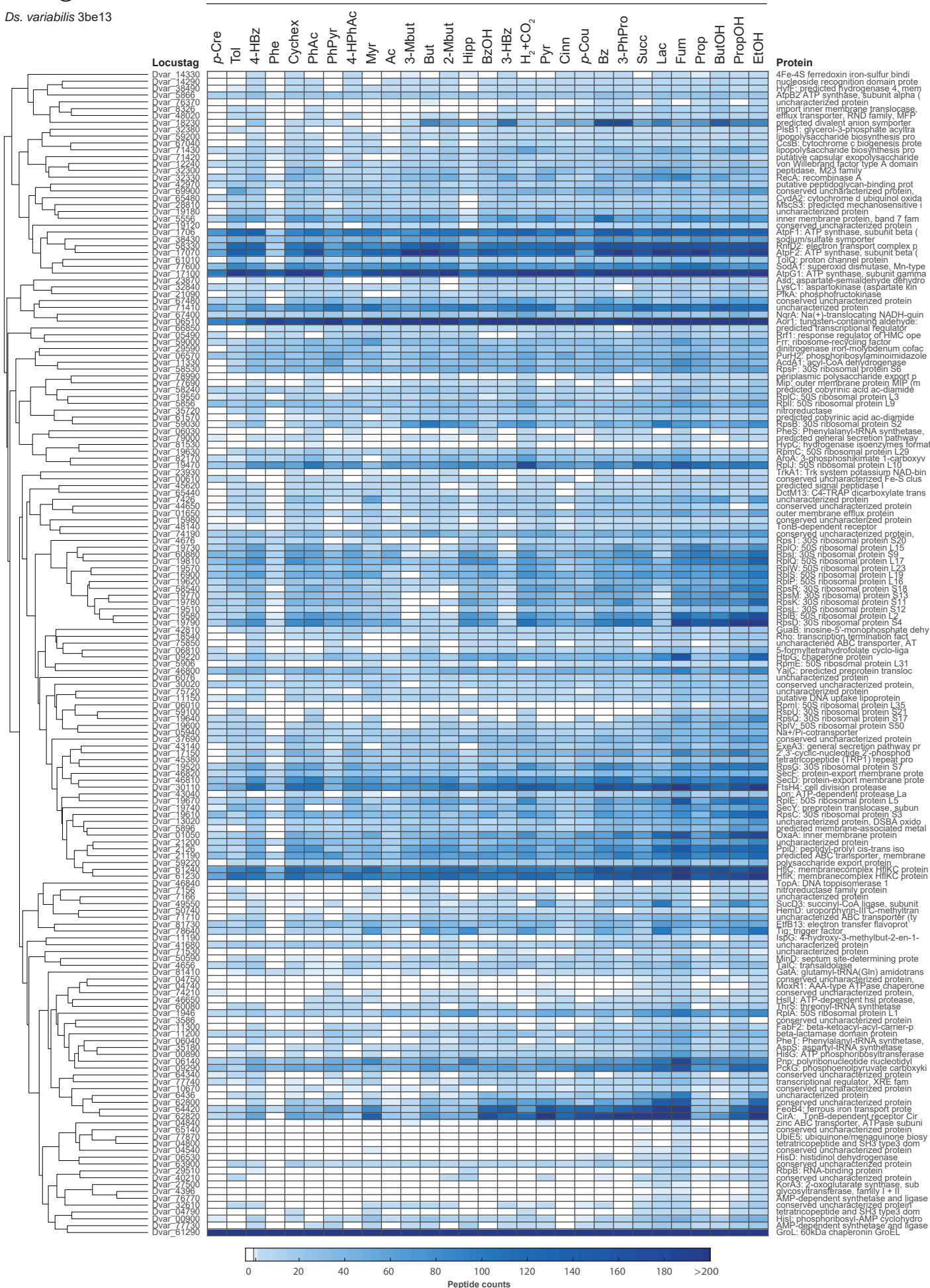


Fig. S50





**Fig. S52: Detailed view on abundances of proteins forming a sub-cluster in the global clustering depicted in Fig. S6.** The global clustering is based on standardized protein abundances of all detected proteins of *Ds. variabilis* 3be13 across the 29 studied substrate adaptation conditions.

<sup>a</sup> Full description of protein functions are available in the genome annotation under accession CP159846.



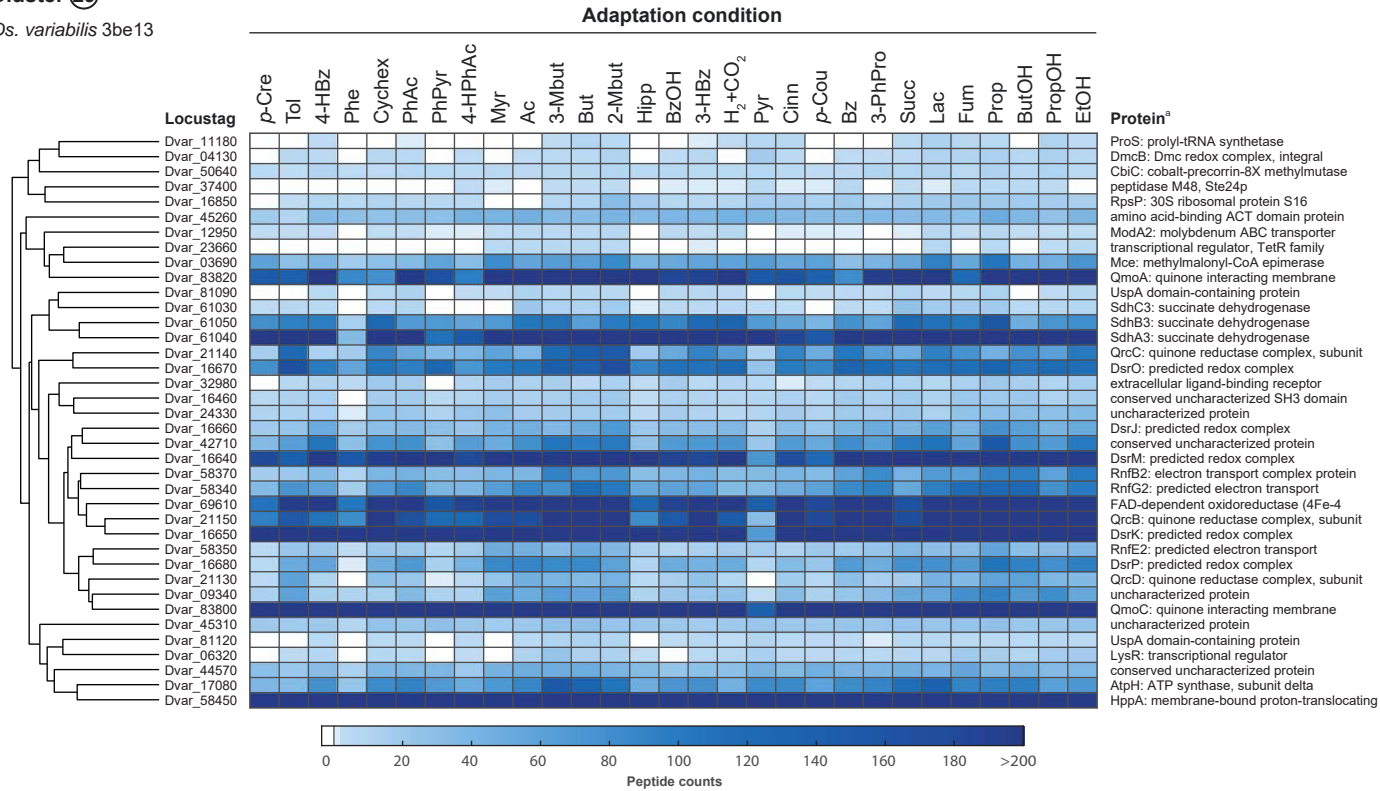
**Fig. S53: Detailed view on abundances of proteins forming a sub-cluster in the global clustering depicted in Fig. S6.** The global clustering is based on standardized protein abundances of all detected proteins of *Ds. variabilis* 3be13 across the 29 studied substrate adaptation conditions.

<sup>a</sup> Full description of protein functions are available in the genome annotation under accession CP159846.



Cluster 29

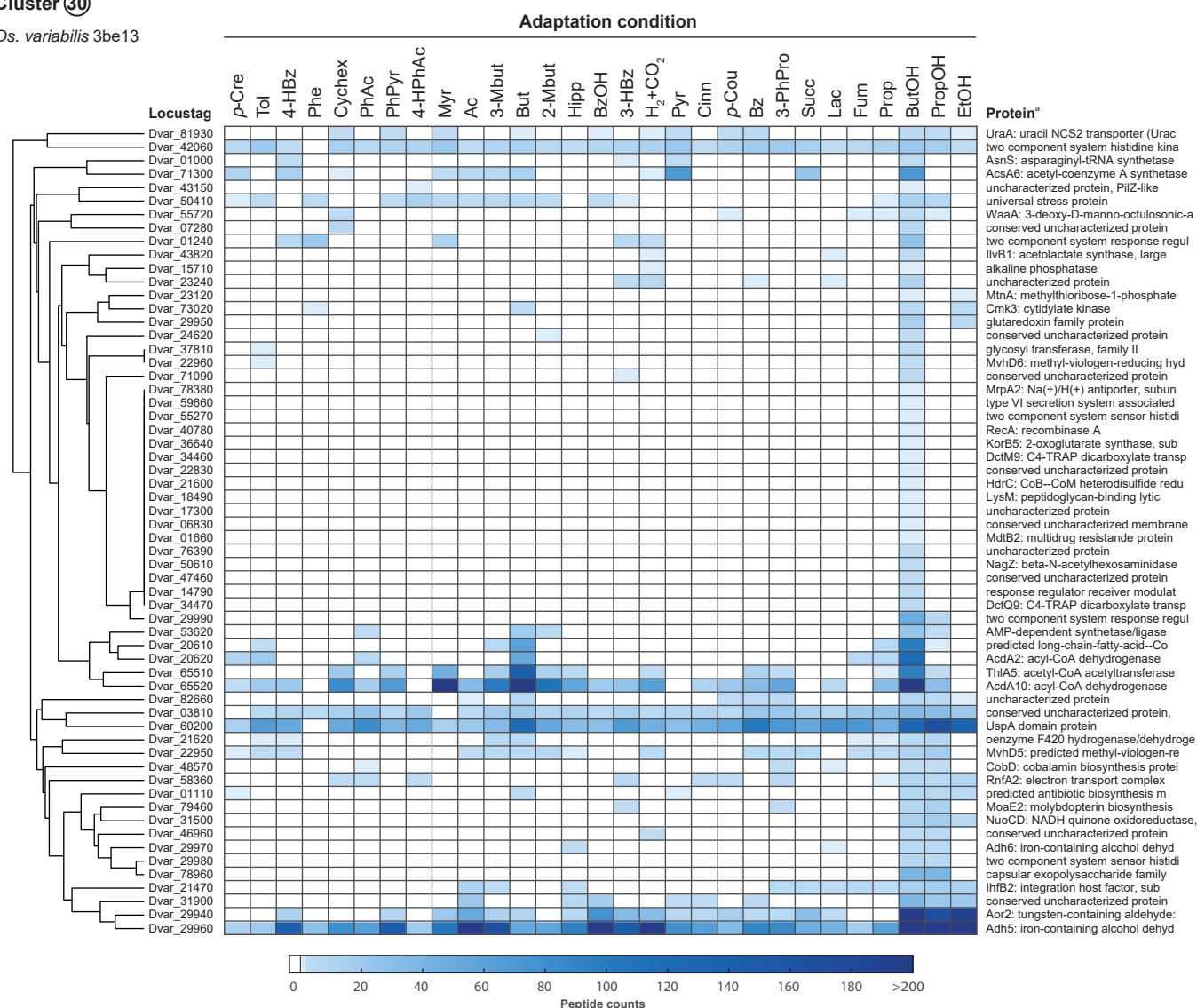
Ds. variabilis 3be13



**Fig. S54: Detailed view on abundances of proteins forming a sub-cluster in the global clustering depicted in Fig. S6.** The global clustering is based on standardized protein abundances of all detected proteins of *Ds. variabilis* 3be13 across the 29 studied substrate adaptation conditions.

<sup>a</sup> Full description of protein functions are available in the genome annotation under accession CP159846.

## Cluster 30

*Ds. variabilis* 3be13

**Fig. S55: Detailed view on abundances of proteins forming a sub-cluster in the global clustering depicted in Fig. S6.** The global clustering is based on standardized protein abundances of all detected proteins of *Ds. variabilis* 3be13 across the 29 studied substrate adaptation conditions.

<sup>a</sup> Full description of protein functions are available in the genome annotation under accession CP159846.

Cluster 31

*Ds. variabilis* 3be13

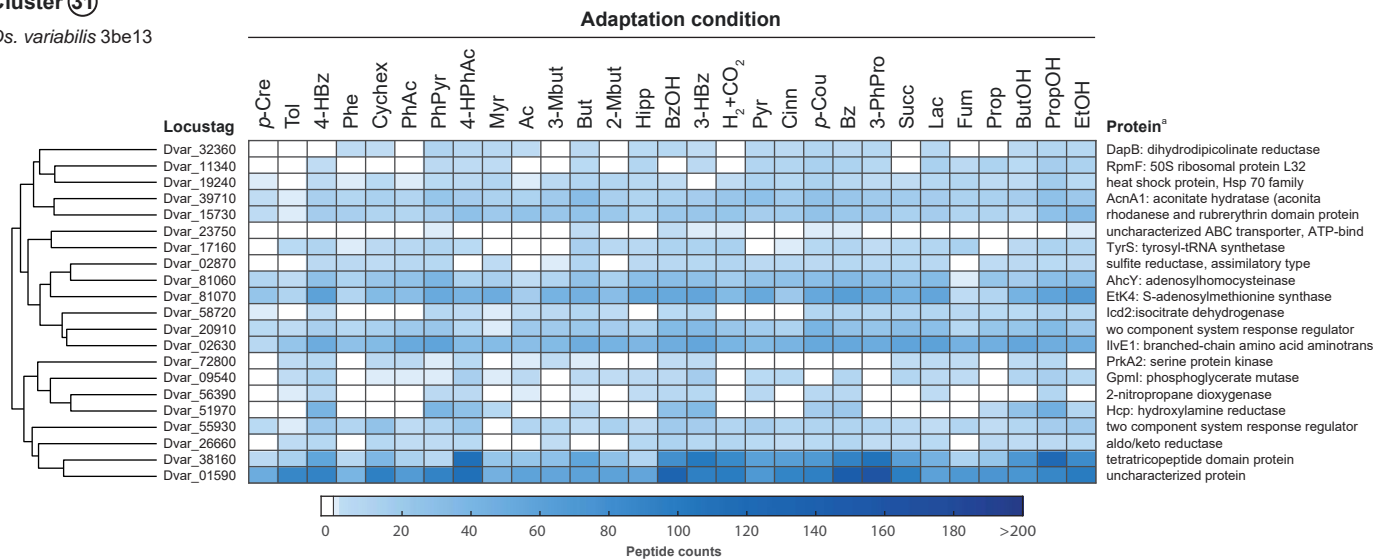


**Fig. S56: Detailed view on abundances of proteins forming a sub-cluster in the global clustering depicted in Fig. S6.** The global clustering is based on standardized protein abundances of all detected proteins of *Ds. variabilis* 3be13 across the 29 studied substrate adaptation conditions.

<sup>a</sup> Full description of protein functions are available in the genome annotation under accession CP159846.

## Adaptation condition

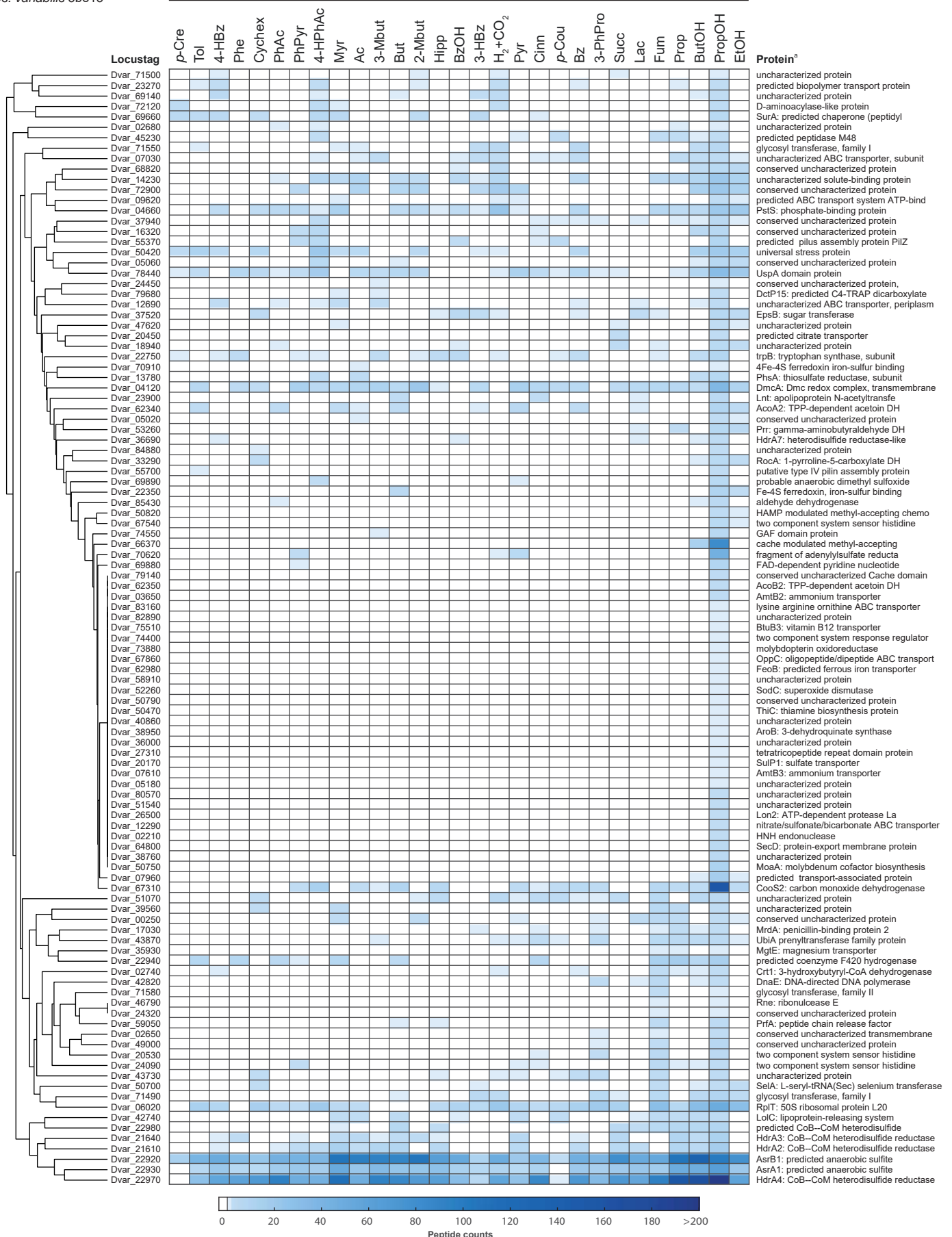


**Fig. S57: Detailed view on abundances of proteins forming a sub-cluster in the global clustering depicted in Fig. S6.** The global clustering is based on standardized protein abundances of all detected proteins of *Ds. variabilis* 3be13 across the 29 studied substrate adaptation conditions.

<sup>a</sup> Full description of protein functions are available in the genome annotation under accession CP159846.



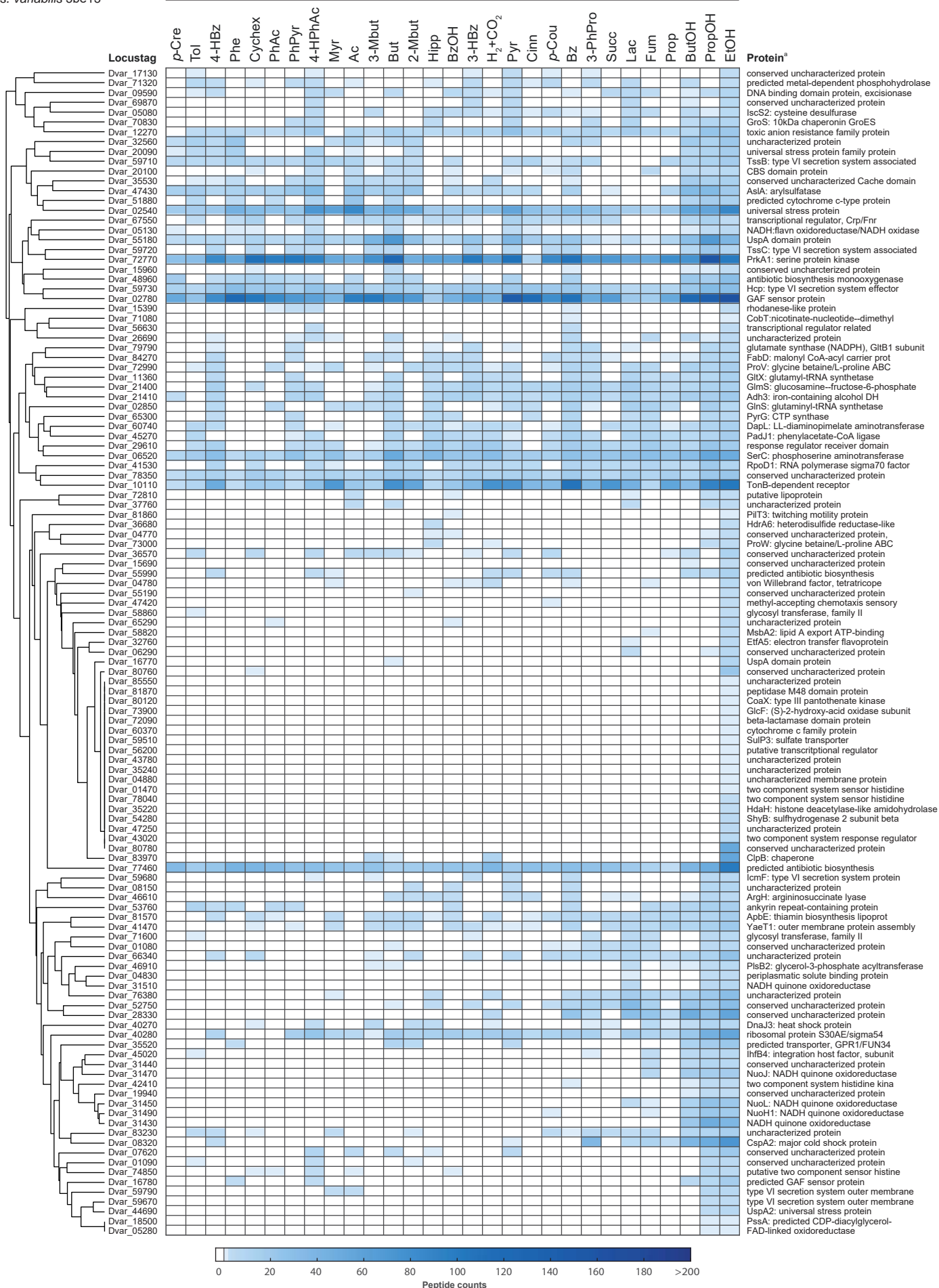


**Fig. S58: Detailed view on abundances of proteins forming a sub-cluster in the global clustering depicted in Fig. S6.** The global clustering is based on standardized protein abundances of all detected proteins of *Ds. variabilis* 3be13 across the 29 studied substrate adaptation conditions.

<sup>a</sup> Full description of protein functions are available in the genome annotation under accession CP159846.

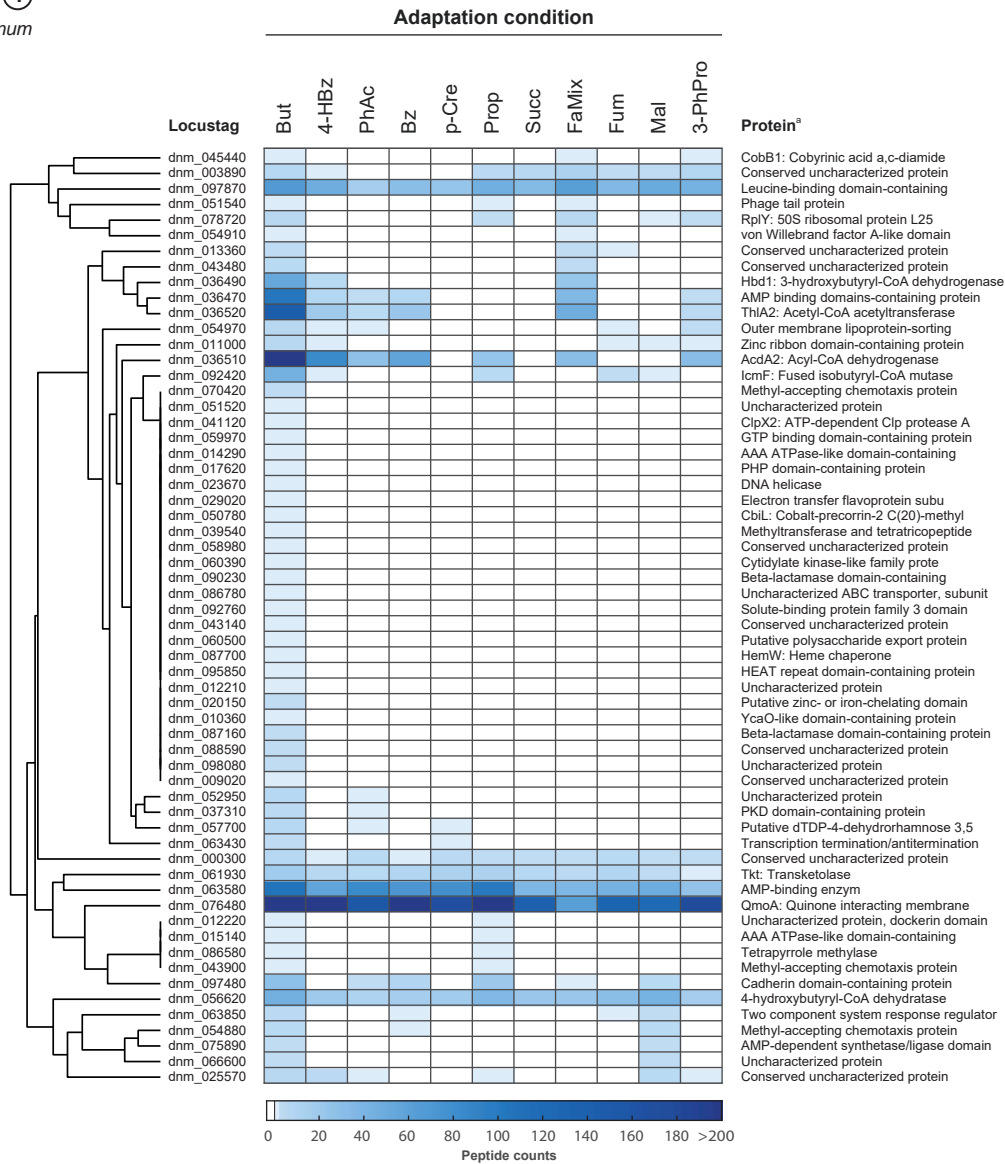


**Fig. S59: Detailed view on abundances of proteins forming a sub-cluster in the global clustering depicted in Fig. S7.** The global clustering is based on standardized protein abundances of all detected proteins of *Dn. magnum* across the 11 studied substrate adaptation conditions.

\* Full description of protein functions are available in the genome annotation under accession CP061800.

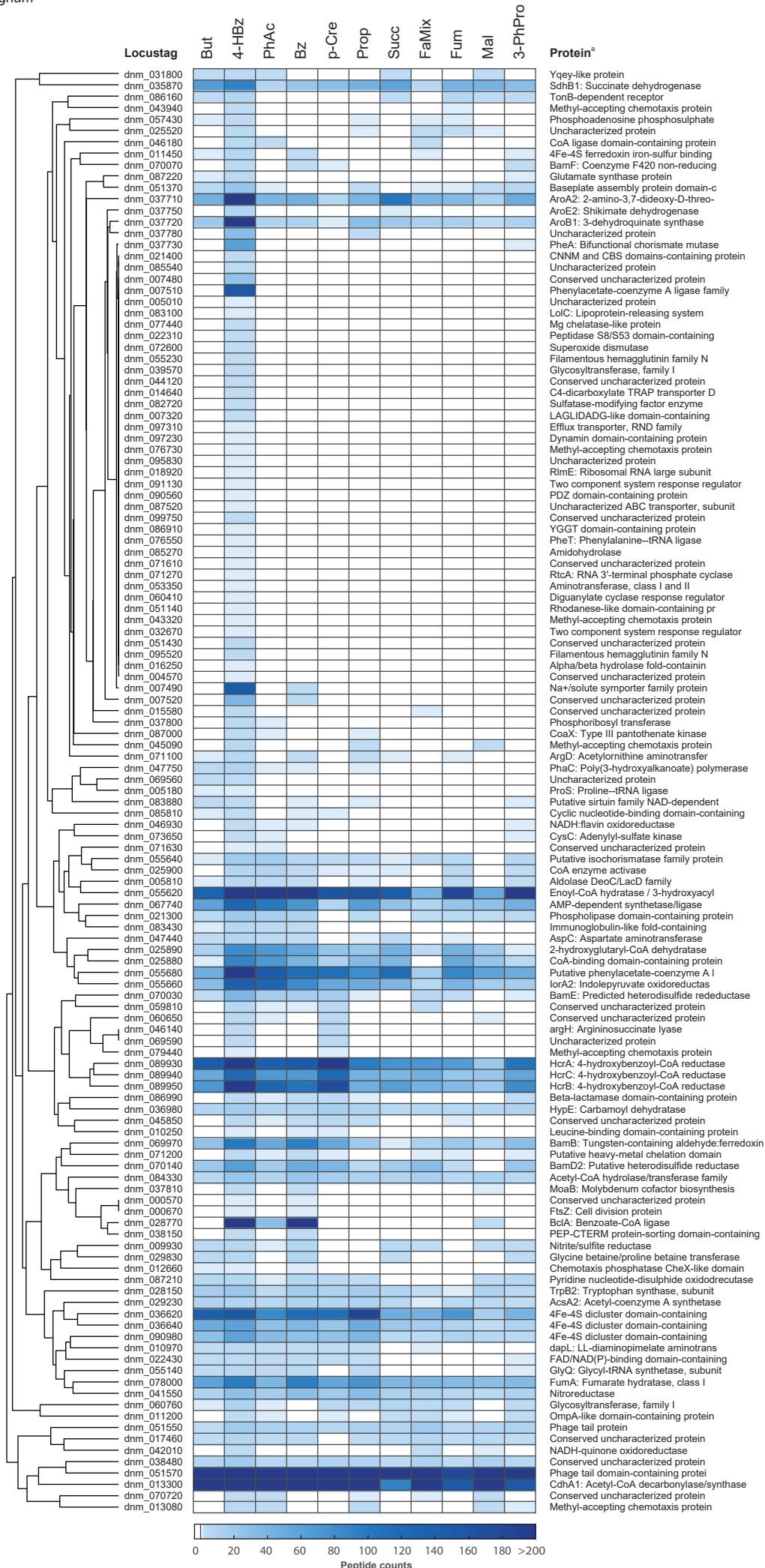


**Fig. S60: Detailed view on abundances of proteins forming a sub-cluster in the global clustering depicted in Fig. S7.** The global clustering is based on standardized protein abundances of all detected proteins of *Dn. magnum* across the 11 studied substrate adaptation conditions.

<sup>a</sup> Full description of protein functions are available in the genome annotation under accession CP061800.

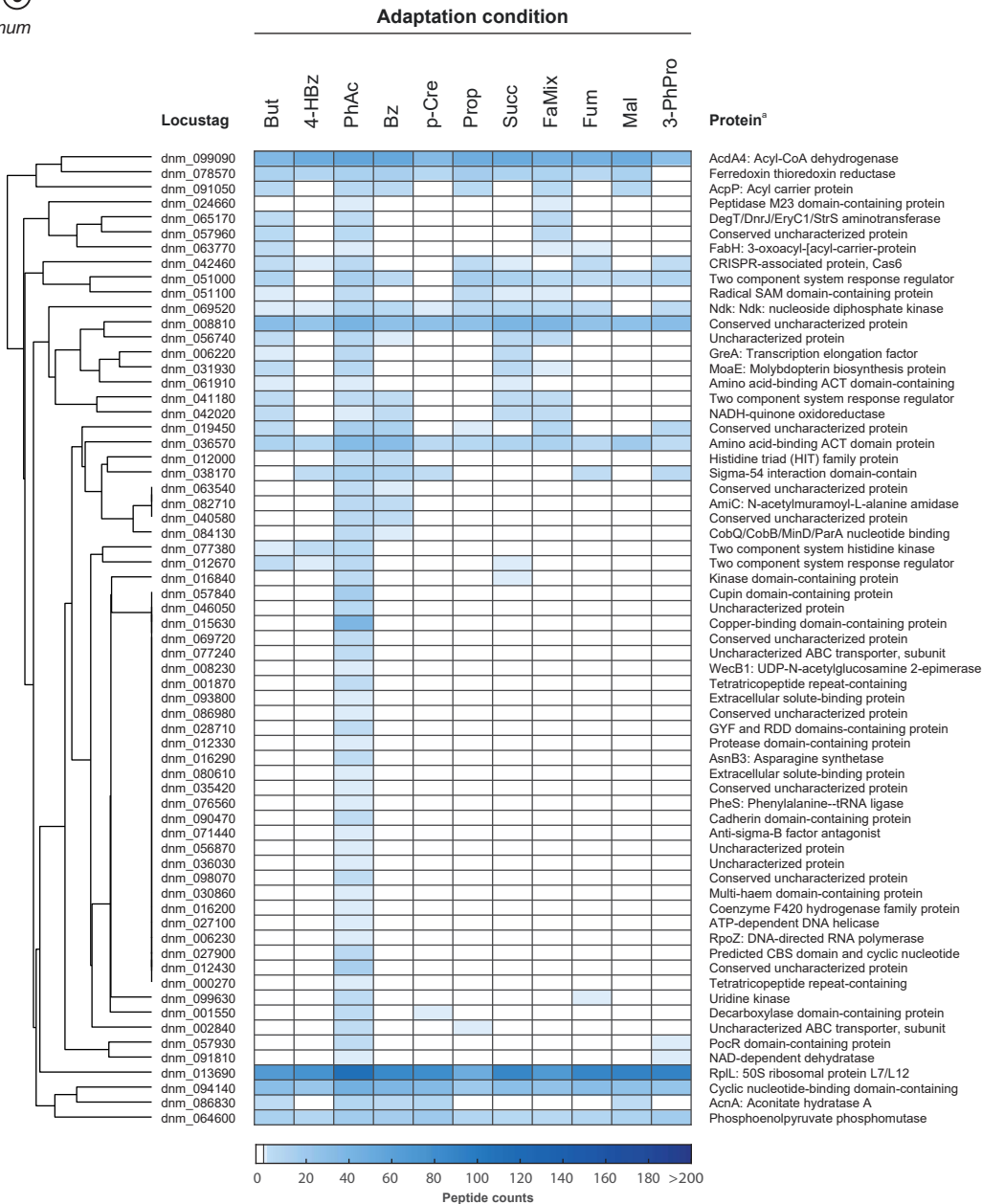


**Fig. S61: Detailed view on abundances of proteins forming a sub-cluster in the global clustering depicted in Fig. S7.** The global clustering is based on standardized protein abundances of all detected proteins of *Dn. magnum* across the 11 studied substrate adaptation conditions.  
<sup>a</sup> Full description of protein functions are available in the genome annotation under accession CP061800.

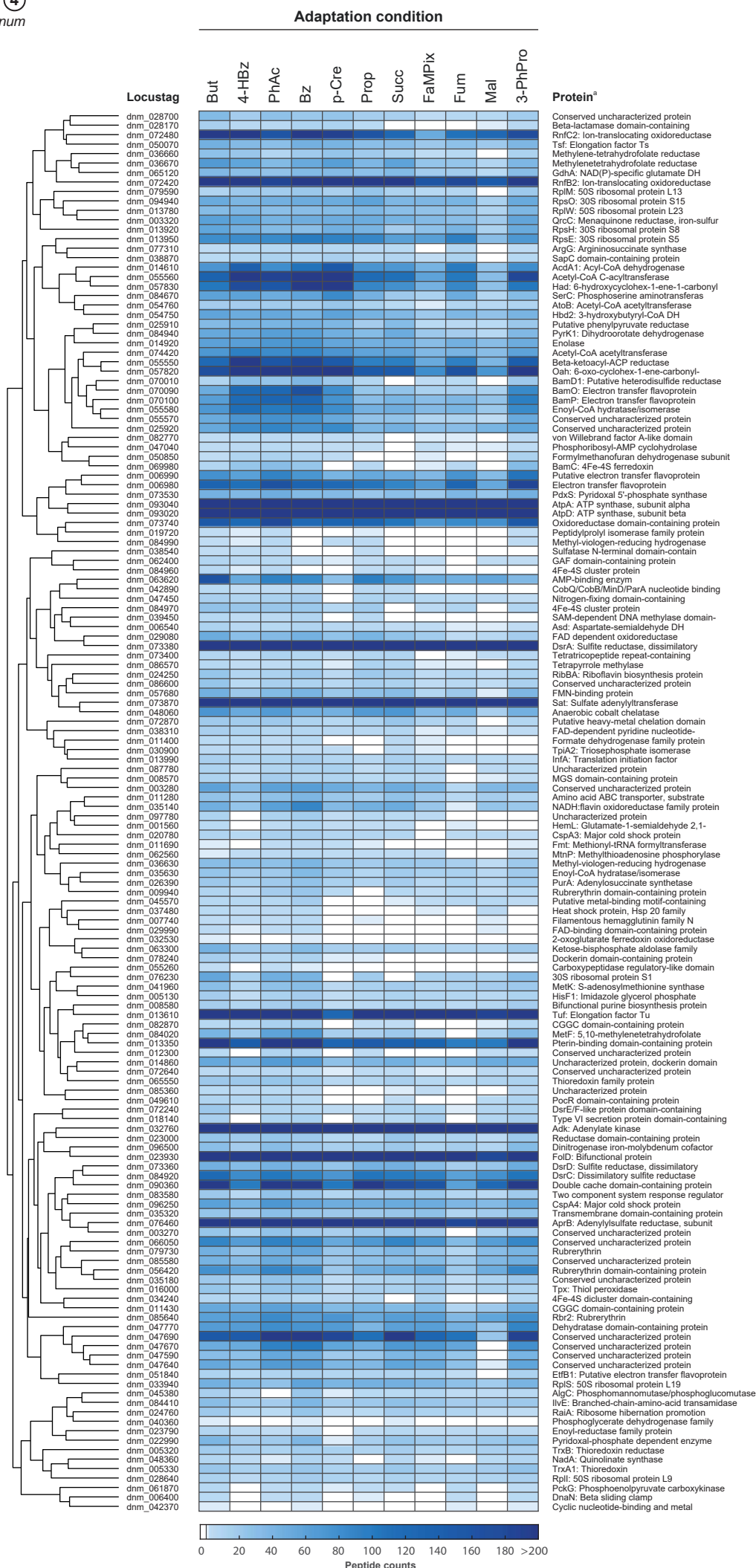


**Fig. S62: Detailed view on abundances of proteins forming a sub-cluster in the global clustering depicted in Fig. S7.** The global clustering is based on standardized protein abundances of all detected proteins of *Dn. magnum* across the 11 studied substrate adaptation conditions.

<sup>a</sup> Full description of protein functions are available in the genome annotation under accession CP061800.



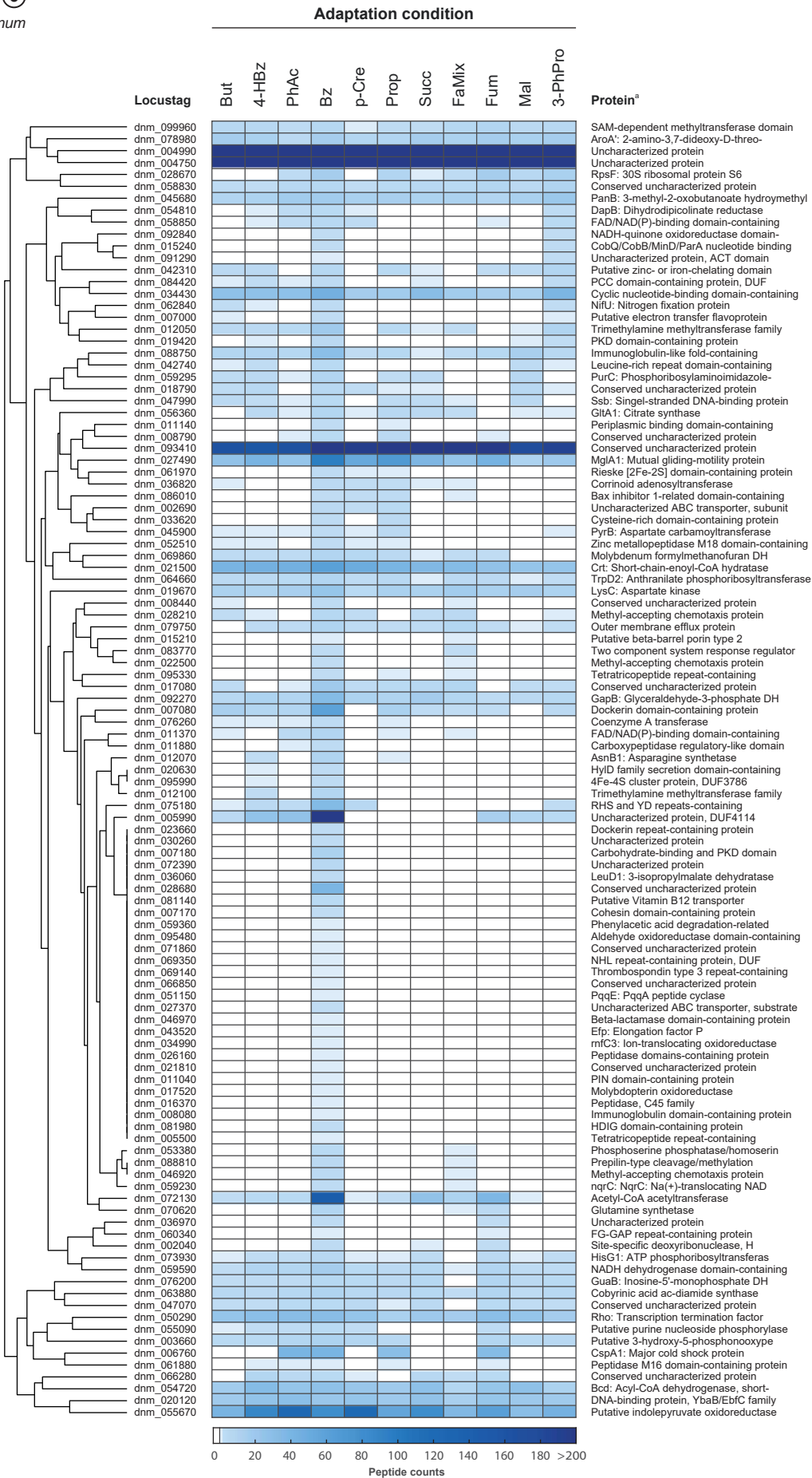


**Fig. S63: Detailed view on abundances of proteins forming a sub-cluster in the global clustering depicted in Fig. S7.** The global clustering is based on standardized protein abundances of all detected proteins of *Dn. magnum* across the 11 studied substrate adaptation conditions.

\* Full description of protein functions are available in the genome annotation under accession CP061800.

## Adaptation condition

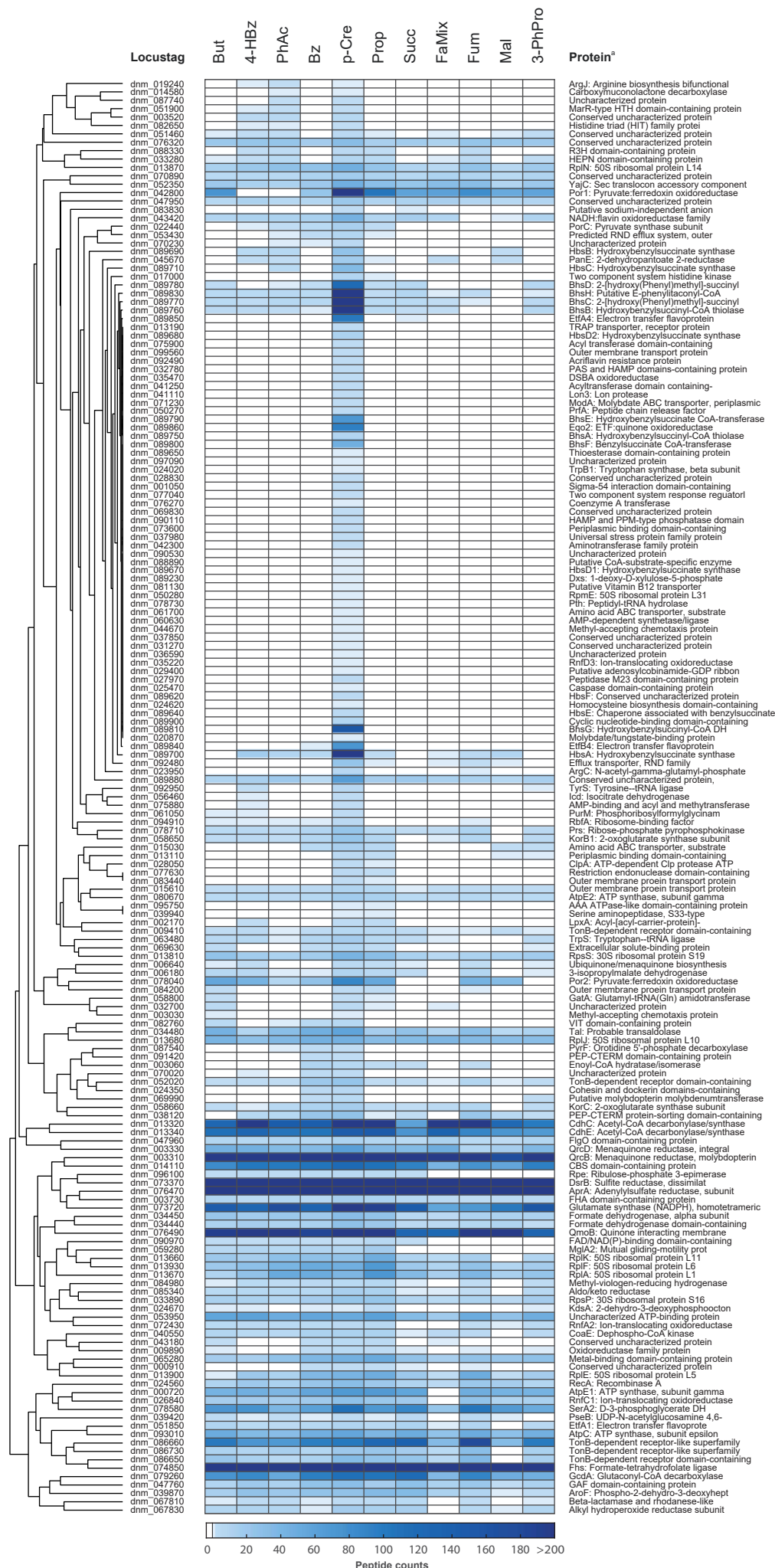


**Fig. S64: Detailed view on abundances of proteins forming a sub-cluster in the global clustering depicted in Fig. S7.** The global clustering is based on standardized protein abundances of all detected proteins of *Dn. magnum* across the 11 studied substrate adaptation conditions.

<sup>a</sup> Full description of protein functions are available in the genome annotation under accession CP061800.

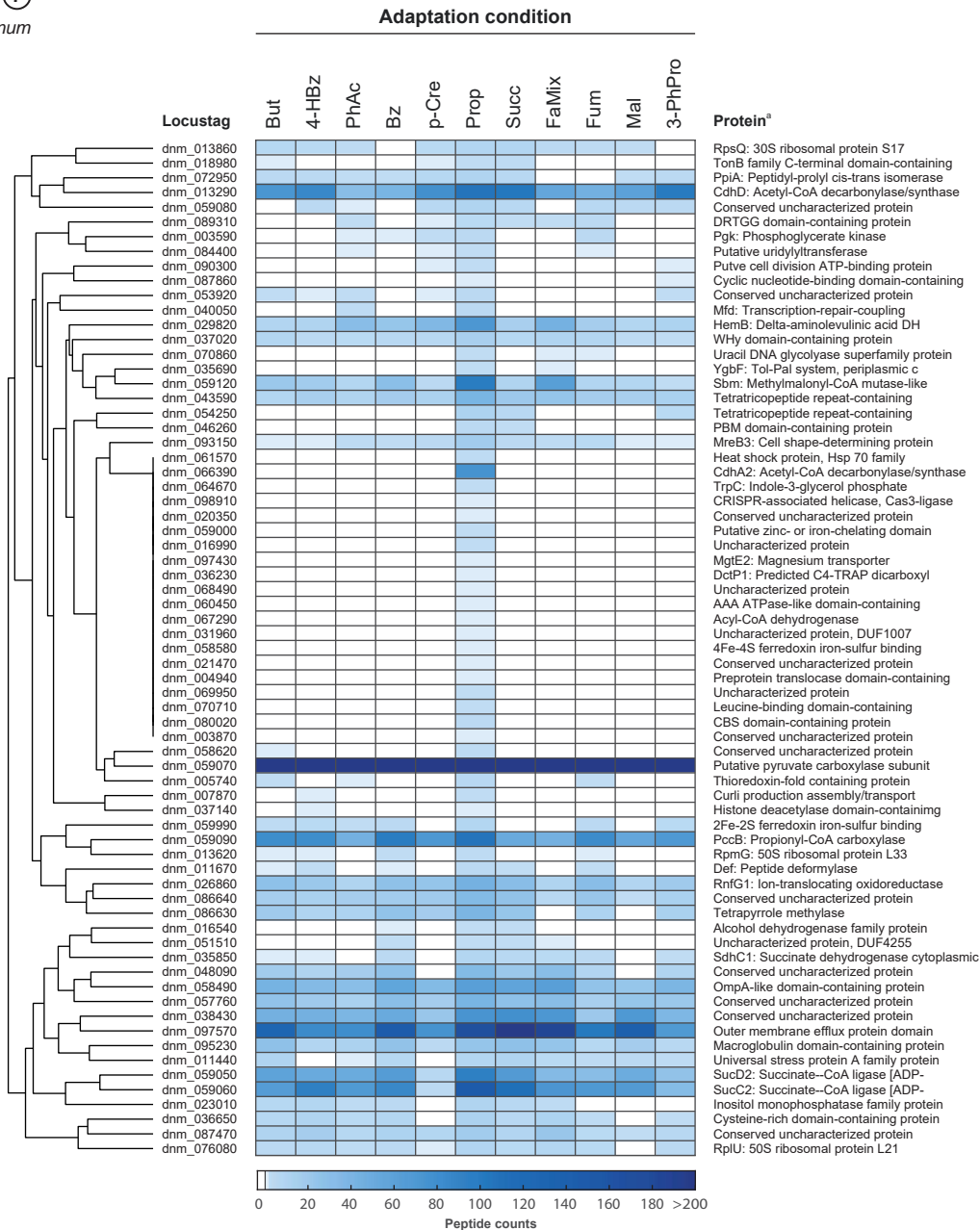


**Fig. S65: Detailed view on abundances of proteins forming a sub-cluster in the global clustering depicted in Fig. S7.** The global clustering is based on standardized protein abundances of all detected proteins of *Dn. magnum* across the 11 studied substrate adaptation conditions.  
<sup>a</sup> Full description of protein functions are available in the genome annotation under accession CP061800.



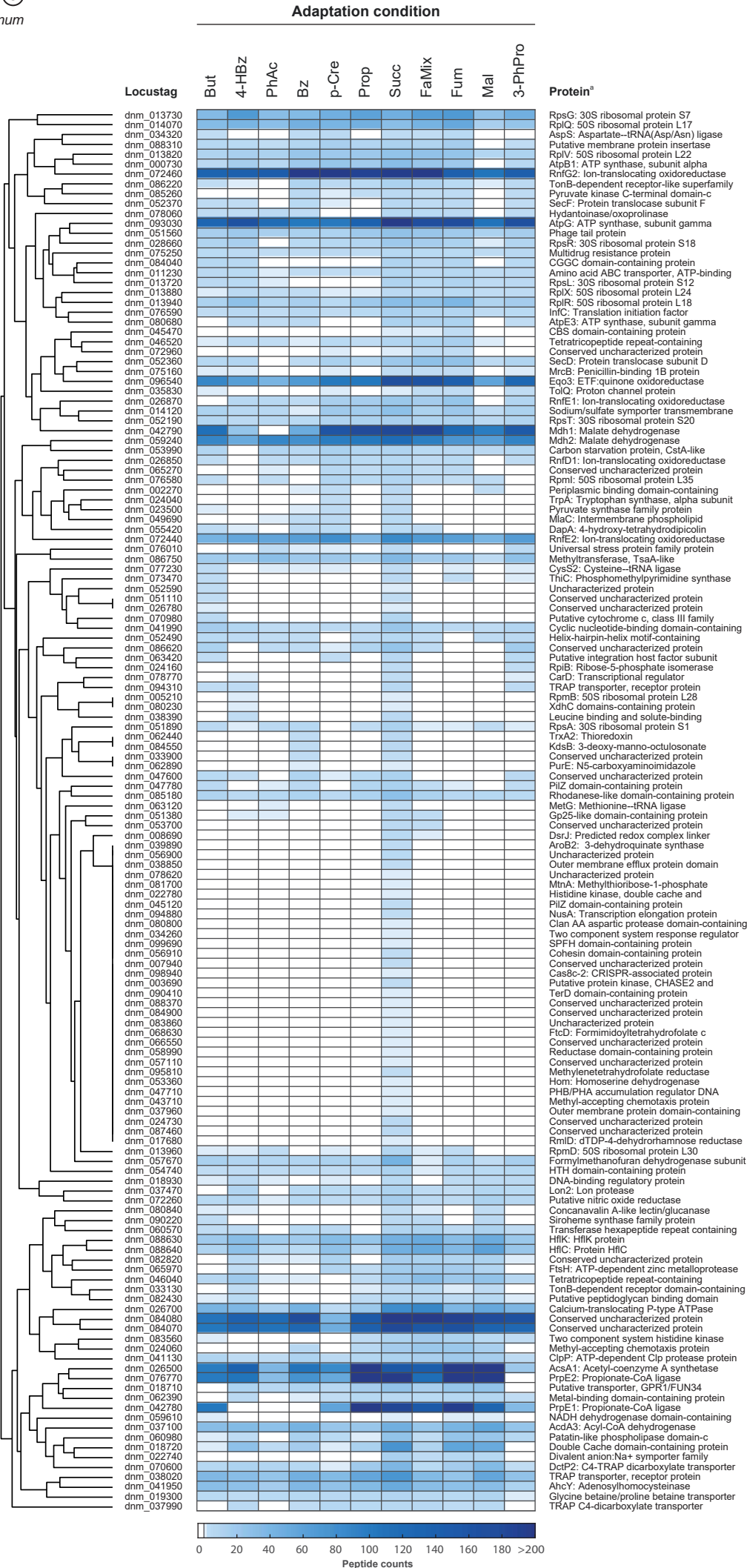


**Fig. S66: Detailed view on abundances of proteins forming a sub-cluster in the global clustering depicted in Fig. S7.** The global clustering is based on standardized protein abundances of all detected proteins of *Dn. magnum* across the 11 studied substrate adaptation conditions.

<sup>a</sup> Full description of protein functions are available in the genome annotation under accession CP061800.

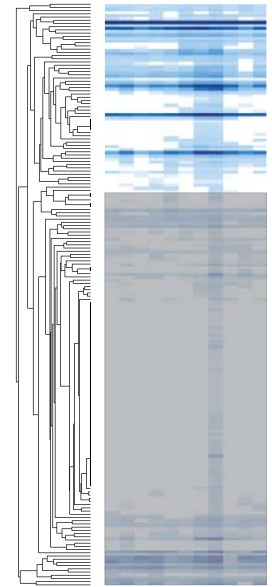
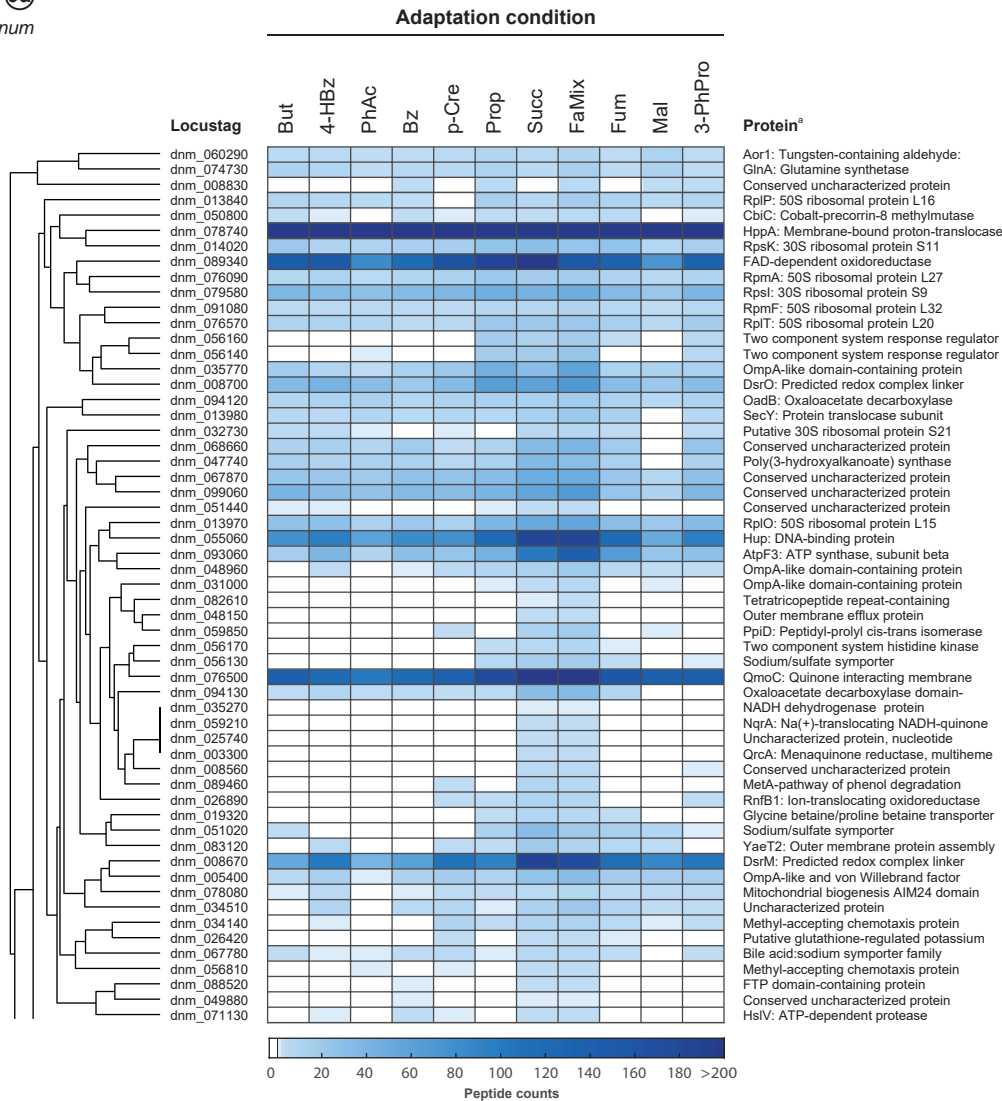


**Fig. S67: Detailed view on abundances of proteins forming a sub-cluster in the global clustering depicted in Fig. S7.** The global clustering is based on standardized protein abundances of all detected proteins of *Dn. magnum* across the 11 studied substrate adaptation conditions.

<sup>a</sup> Full description of protein functions are available in the genome annotation under accession CP061800.

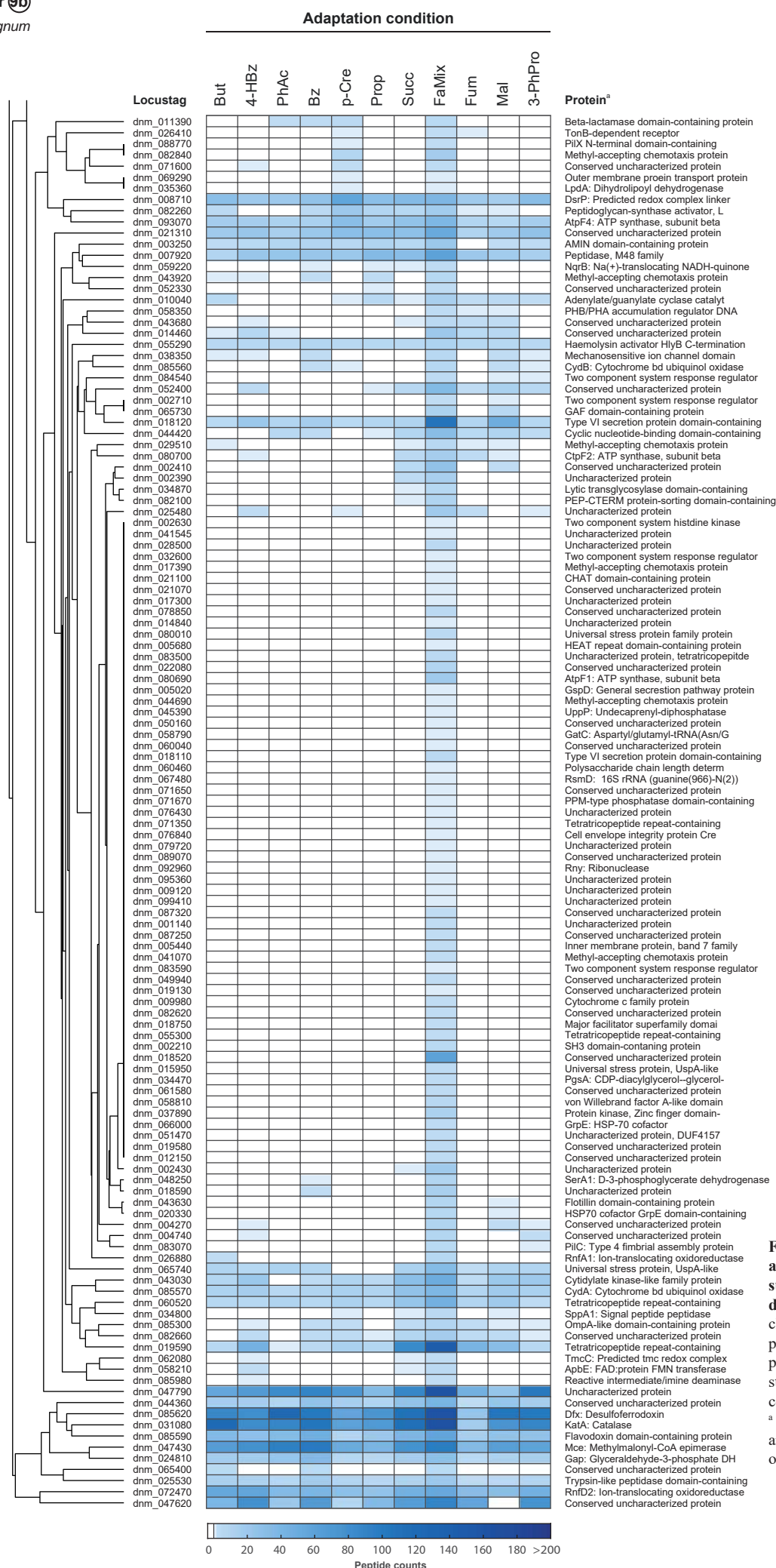


**Fig. S68: Detailed view on abundances of proteins forming a sub-cluster in the global clustering depicted in Fig. S7.** The global clustering is based on standardized protein abundances of all detected proteins of *Dn. magnum* across the 11 studied substrate adaptation conditions.

<sup>a</sup> Full description of protein functions are available in the genome annotation under accession CP061800.

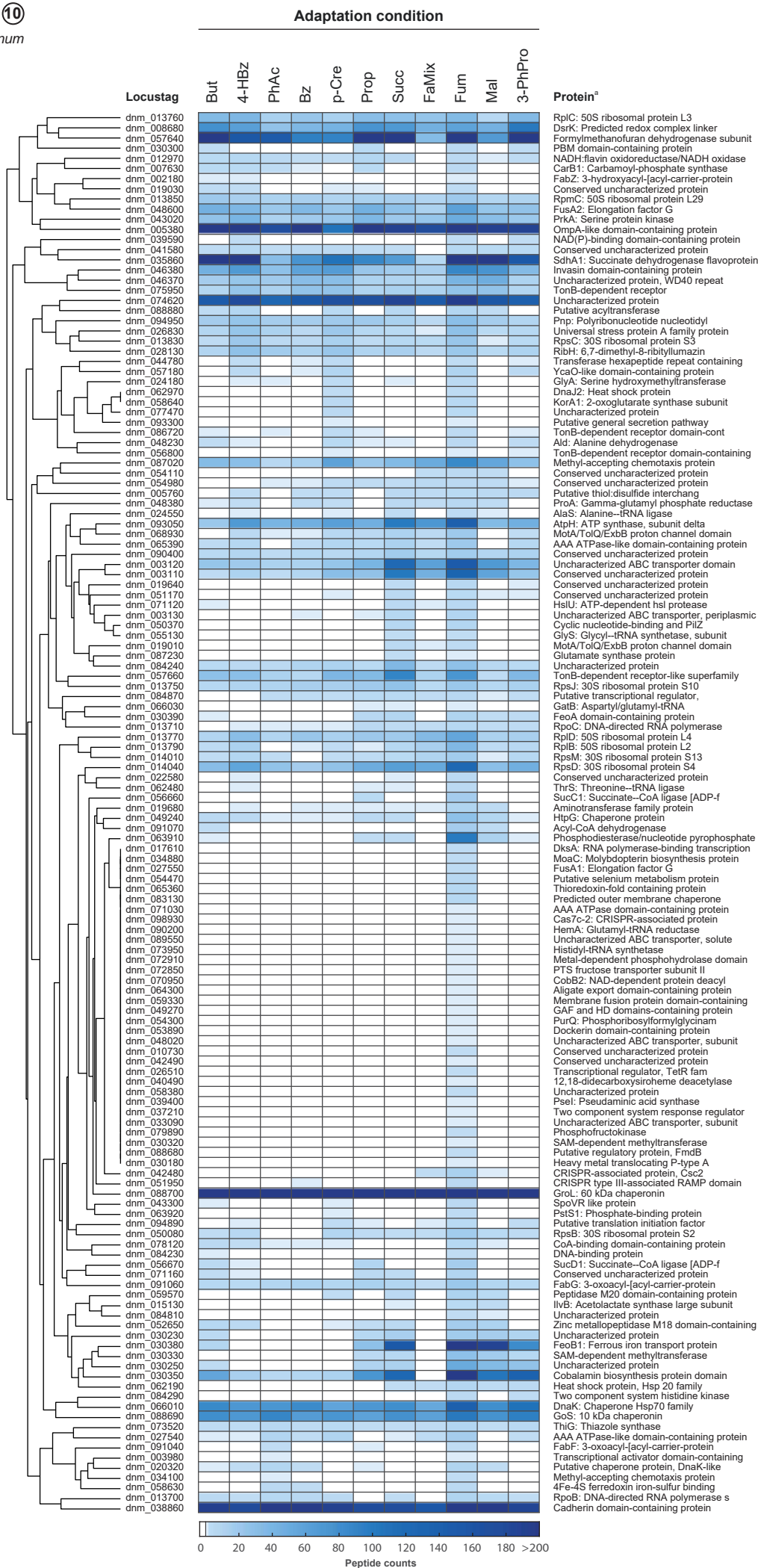


**Fig. S69: Detailed view on abundances of proteins forming a sub-cluster in the global clustering depicted in Fig. S7.** The global clustering is based on standardized protein abundances of all detected proteins of *Dn. magnum* across the 11 studied substrate adaptation conditions.  
<sup>a</sup> Full description of protein functions are available in the genome annotation under accession CP061800.

## Adaptation condition

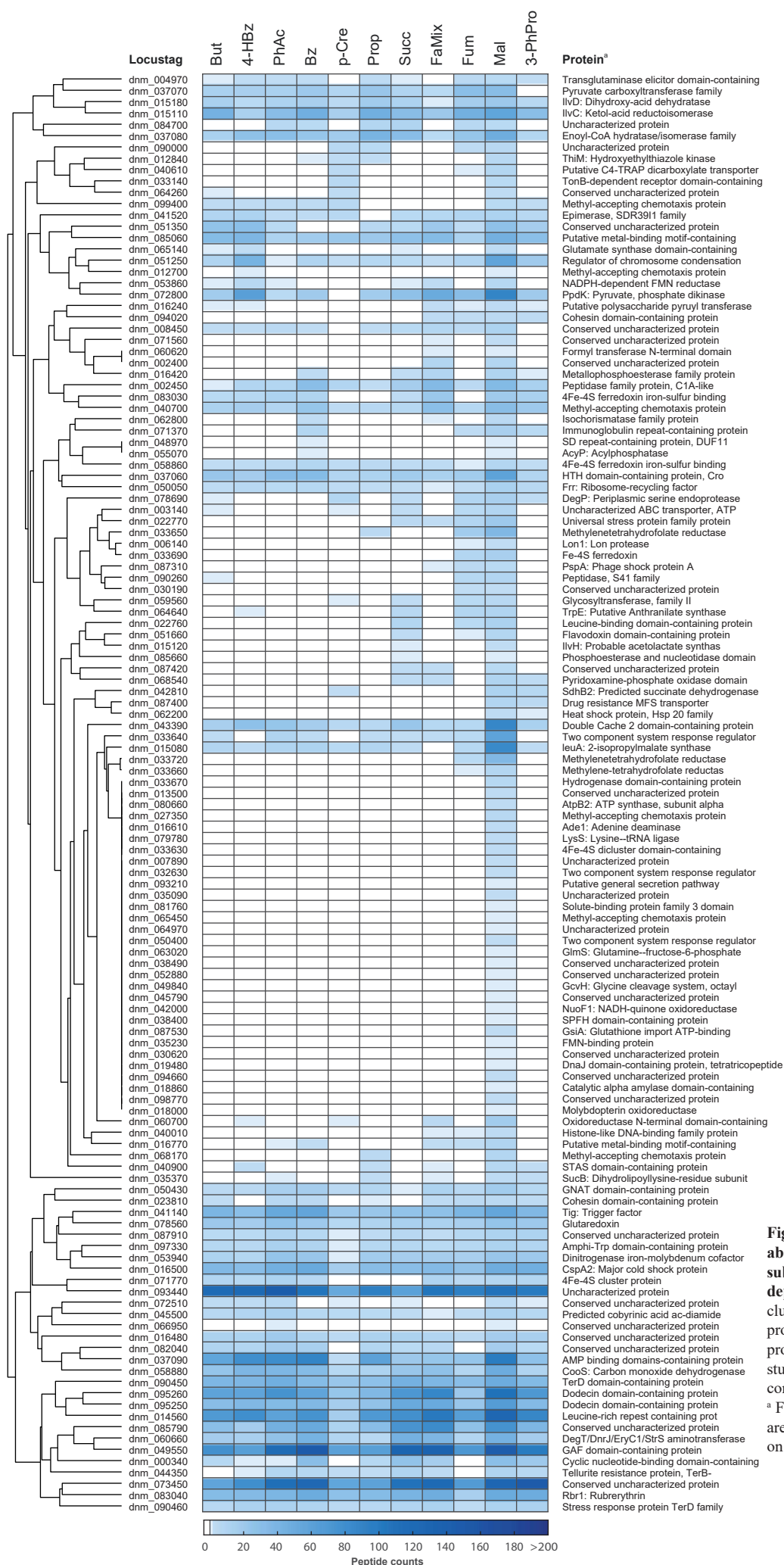


**Fig. S70: Detailed view on abundances of proteins forming a sub-cluster in the global clustering depicted in Fig. S7.** The global clustering is based on standardized protein abundances of all detected proteins of *Dn. magnum* across the 11 studied substrate adaptation conditions.

<sup>a</sup> Full description of protein functions are available in the genome annotation under accession CP061800.



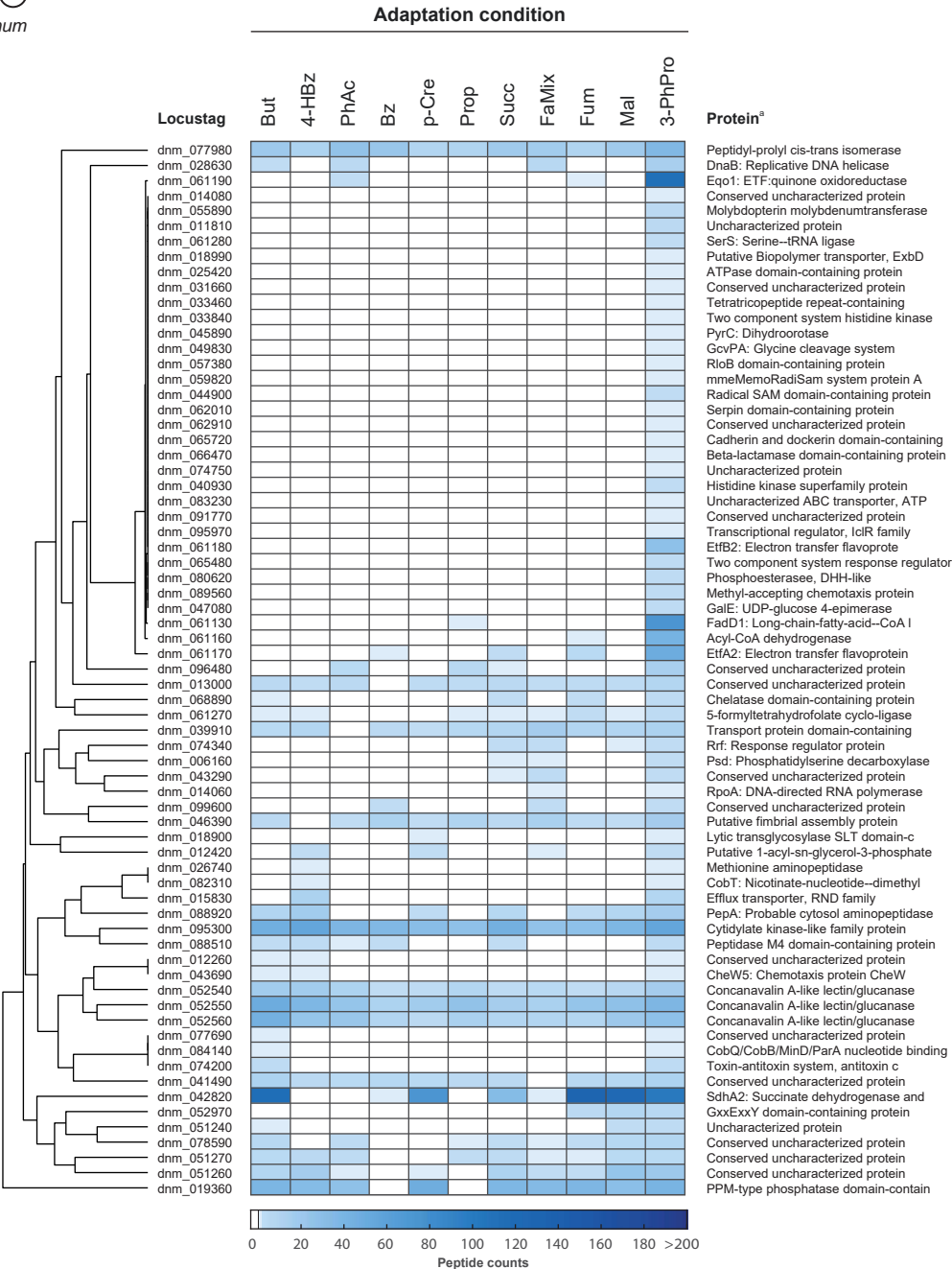


**Fig. S71: Detailed view on abundances of proteins forming a sub-cluster in the global clustering depicted in Fig. S7.** The global clustering is based on standardized protein abundances of all detected proteins of *Dn. magnum* across the 11 studied substrate adaptation conditions.  
<sup>a</sup> Full description of protein functions are available in the genome annotation under accession CP061800.

## Cluster 1

*Dn. limicola*

## Adaptation condition

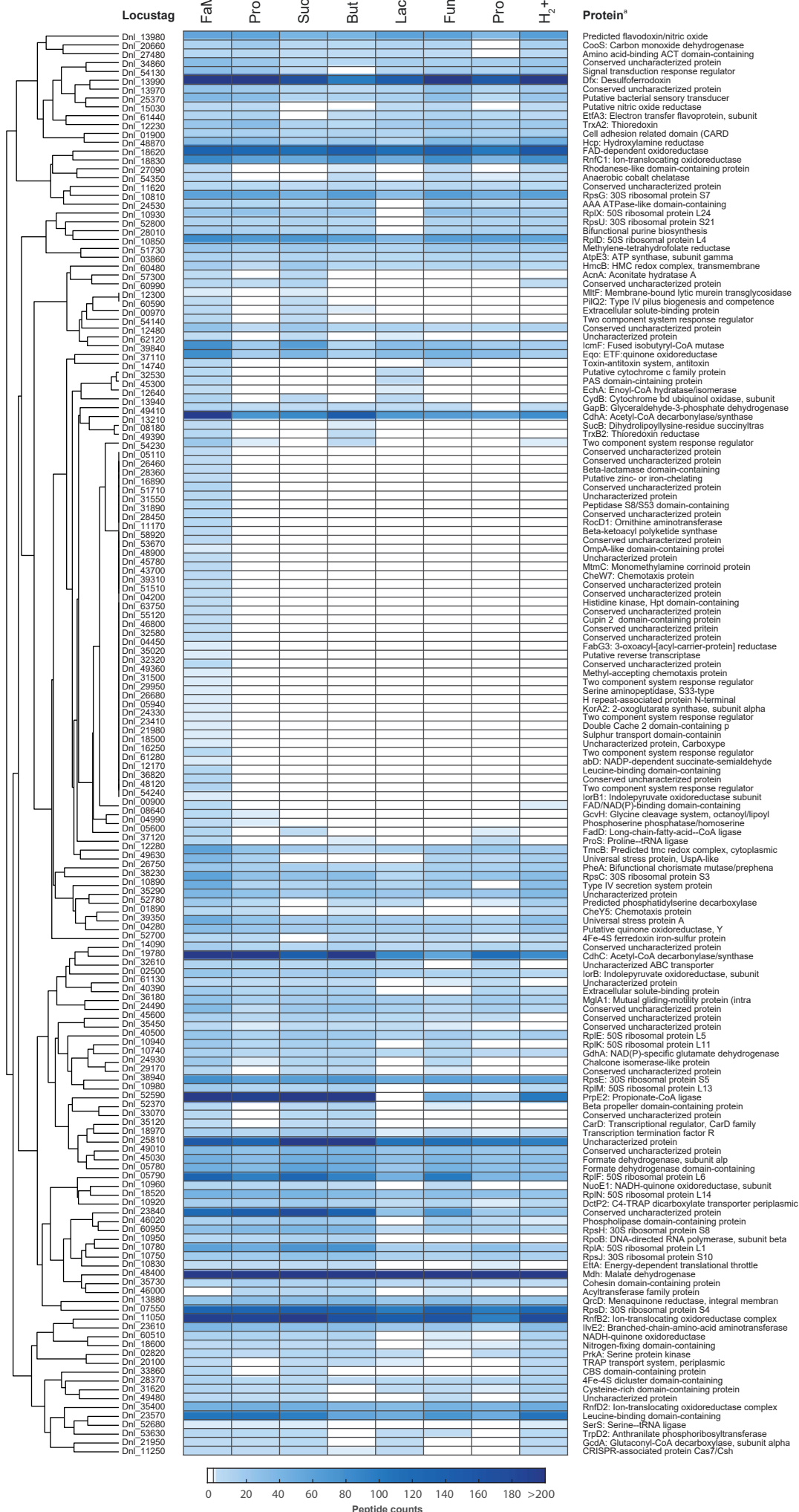
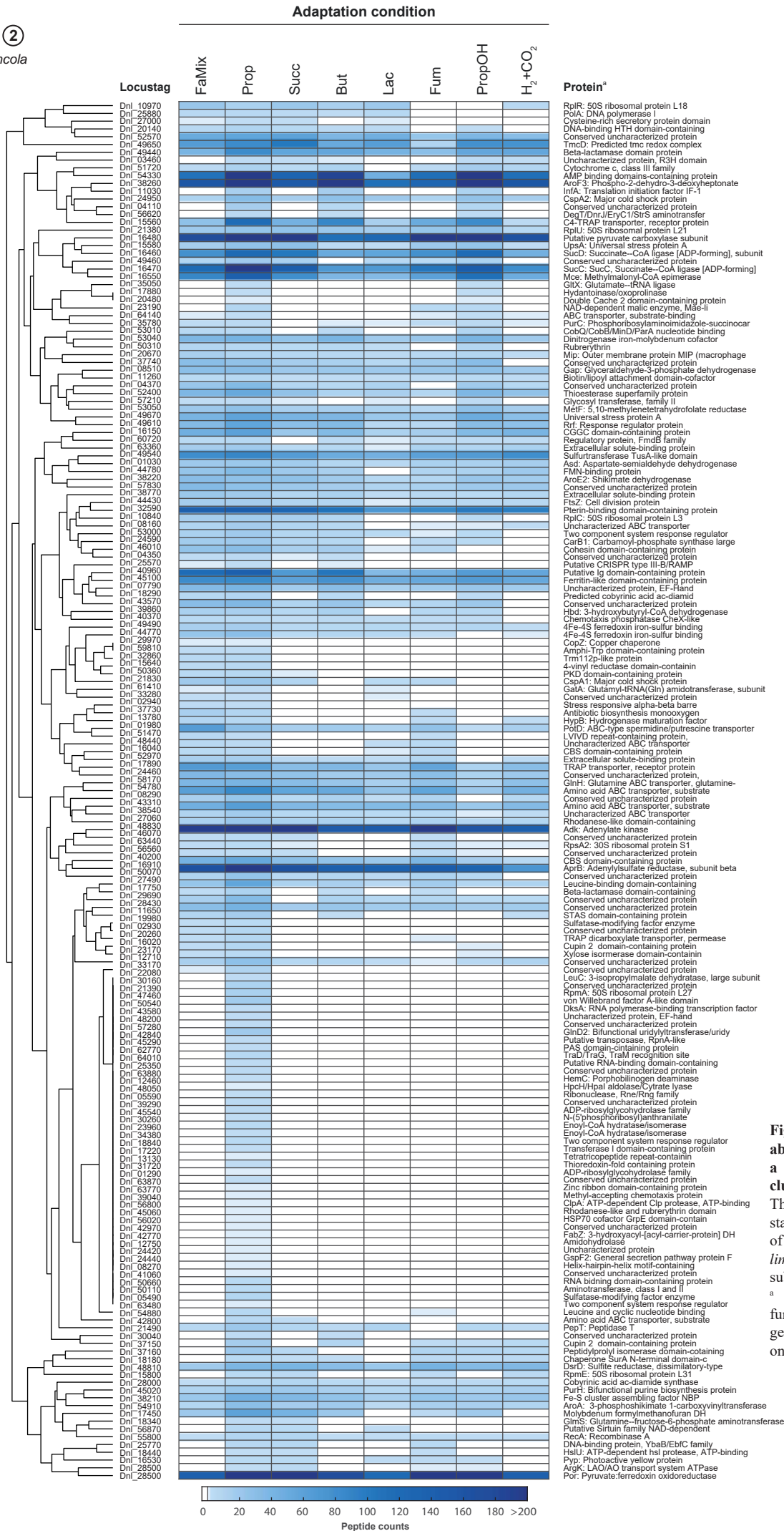


**Fig. S72: Detailed view on abundances of proteins forming a sub-cluster in the global clustering depicted in Fig. S8.** The global clustering is based on standardized protein abundances of all detected proteins of *Dn. limicola* across the 8 studied substrate adaptation conditions.

<sup>a</sup> Full description of protein functions are available in the genome annotation under accession CP061799.





### Cluster 3

*Dn. limicola*

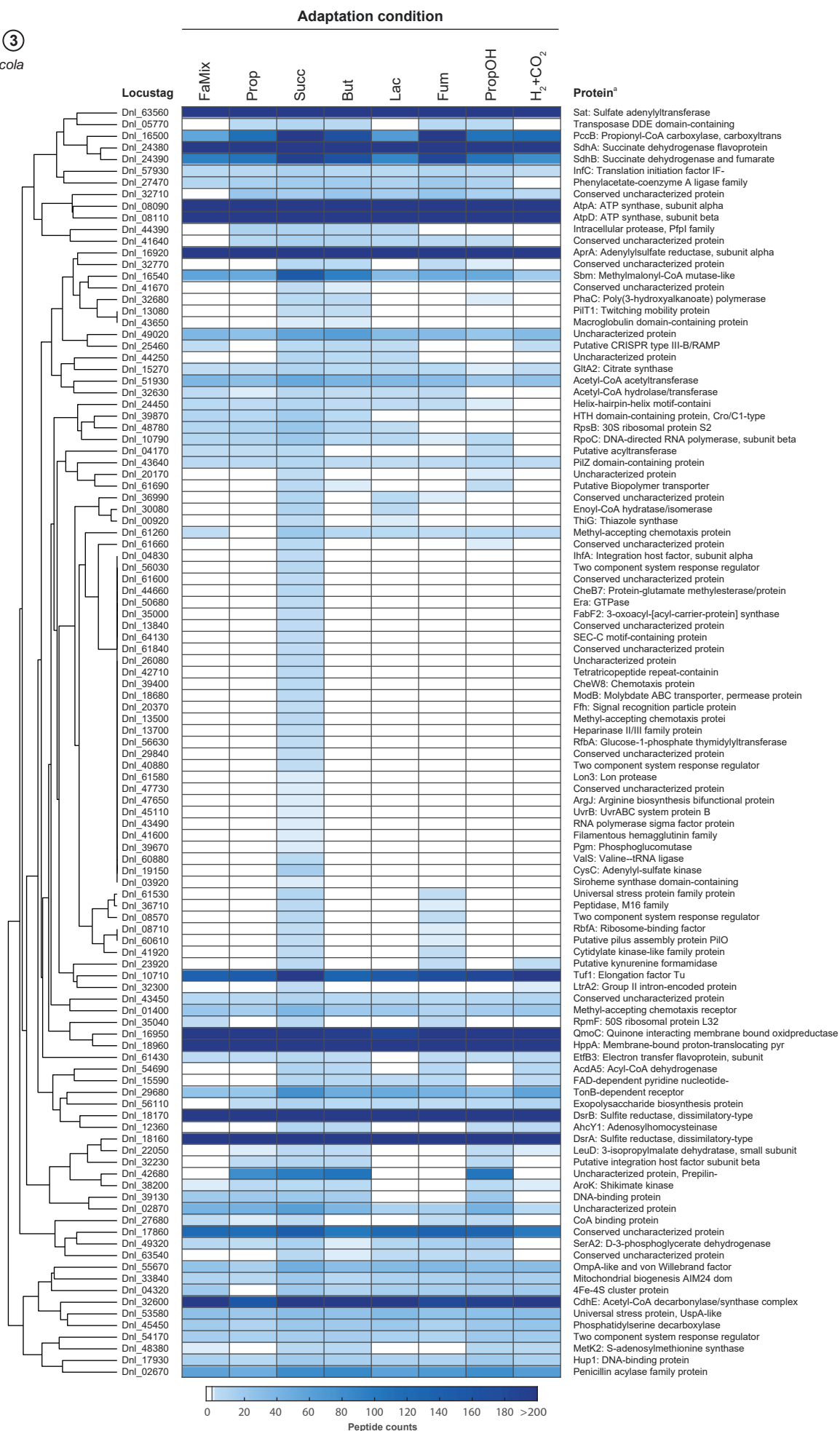


**Fig. S74: Detailed view on abundances of proteins forming a sub-cluster in the global clustering depicted in Fig. S8. The global clustering is based on standardized protein abundances of all detected proteins of *Dn. limicola* across the 8 studied substrate adaptation conditions.**

<sup>a</sup> Full description of protein functions are available in the genome annotation under accession CP061799.

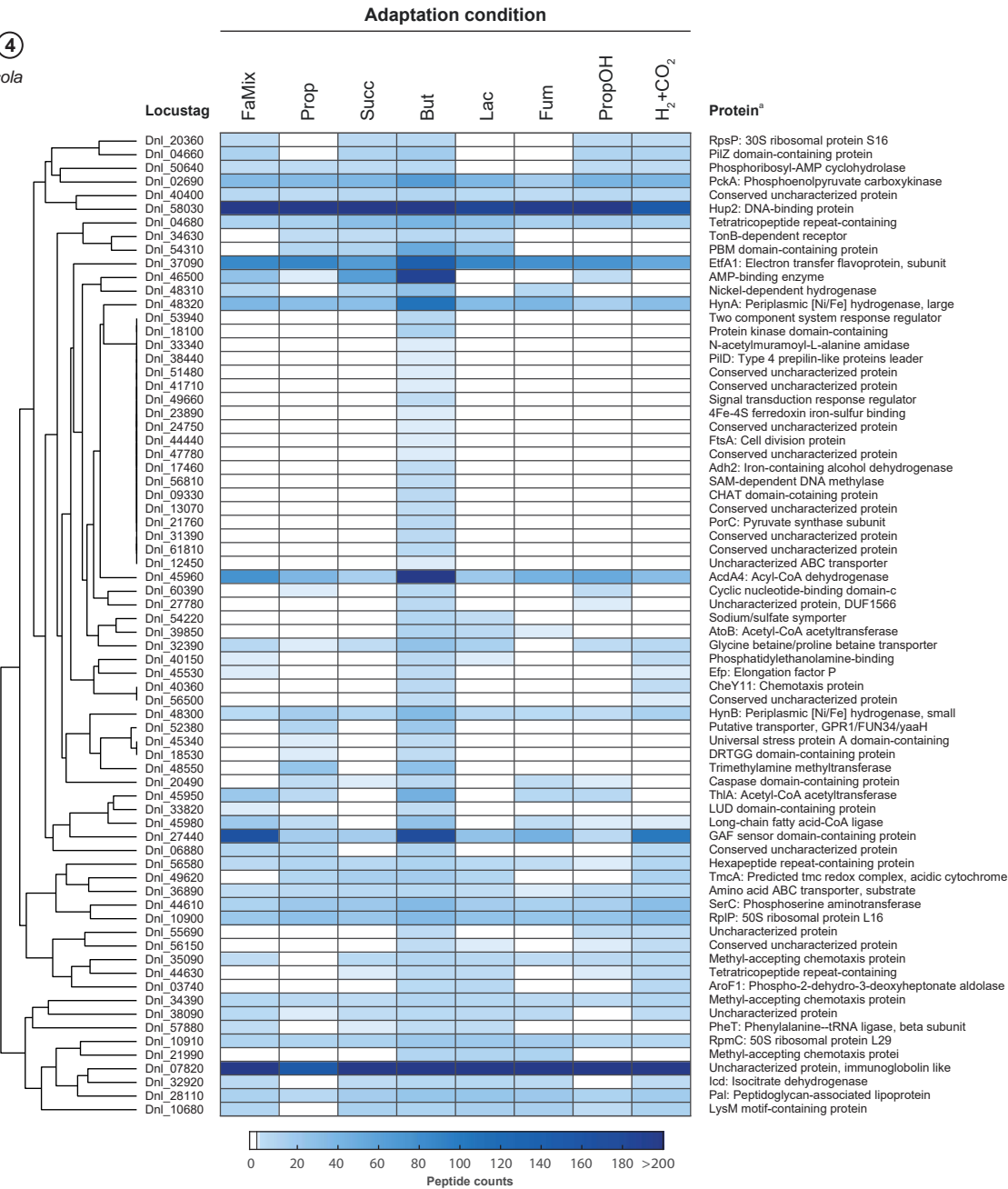


**Fig. S75: Detailed view on abundances of proteins forming a sub-cluster in the global clustering depicted in Fig. S8.** The global clustering is based on standardized protein abundances of all detected proteins of *Dn. limicola* across the 8 studied substrate adaptation conditions.  
<sup>a</sup> Full description of protein functions are available in the genome annotation under accession CP061799.

# Cluster 5a

*Dn. limicola*

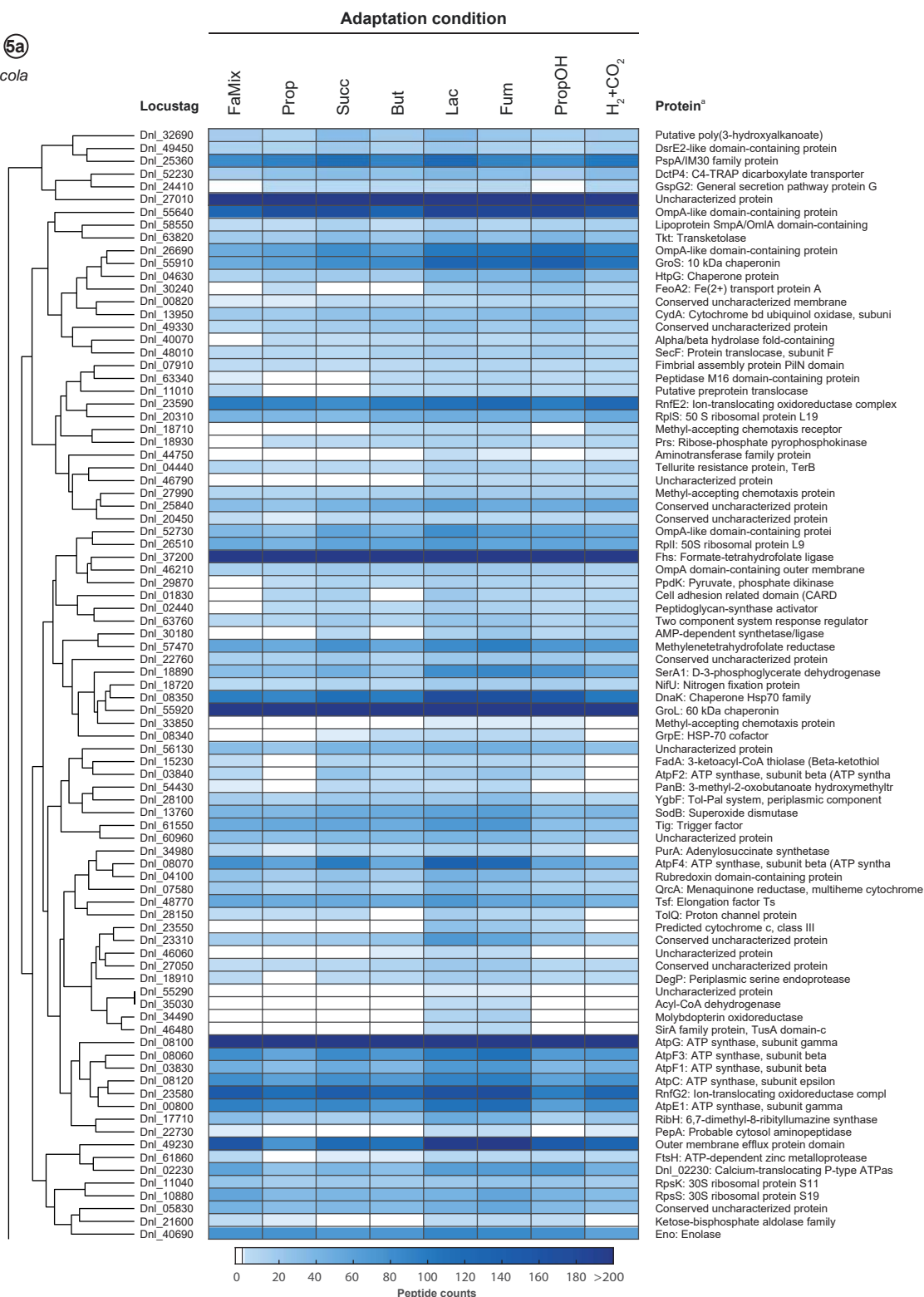


**Fig. S76: Detailed view on abundances of proteins forming a sub-cluster in the global clustering depicted in Fig. S8.** The global clustering is based on standardized protein abundances of all detected proteins of *Dn. limicola* across the 8 studied substrate adaptation conditions.

<sup>a</sup> Full description of protein functions are available in the genome annotation under accession CP061799.

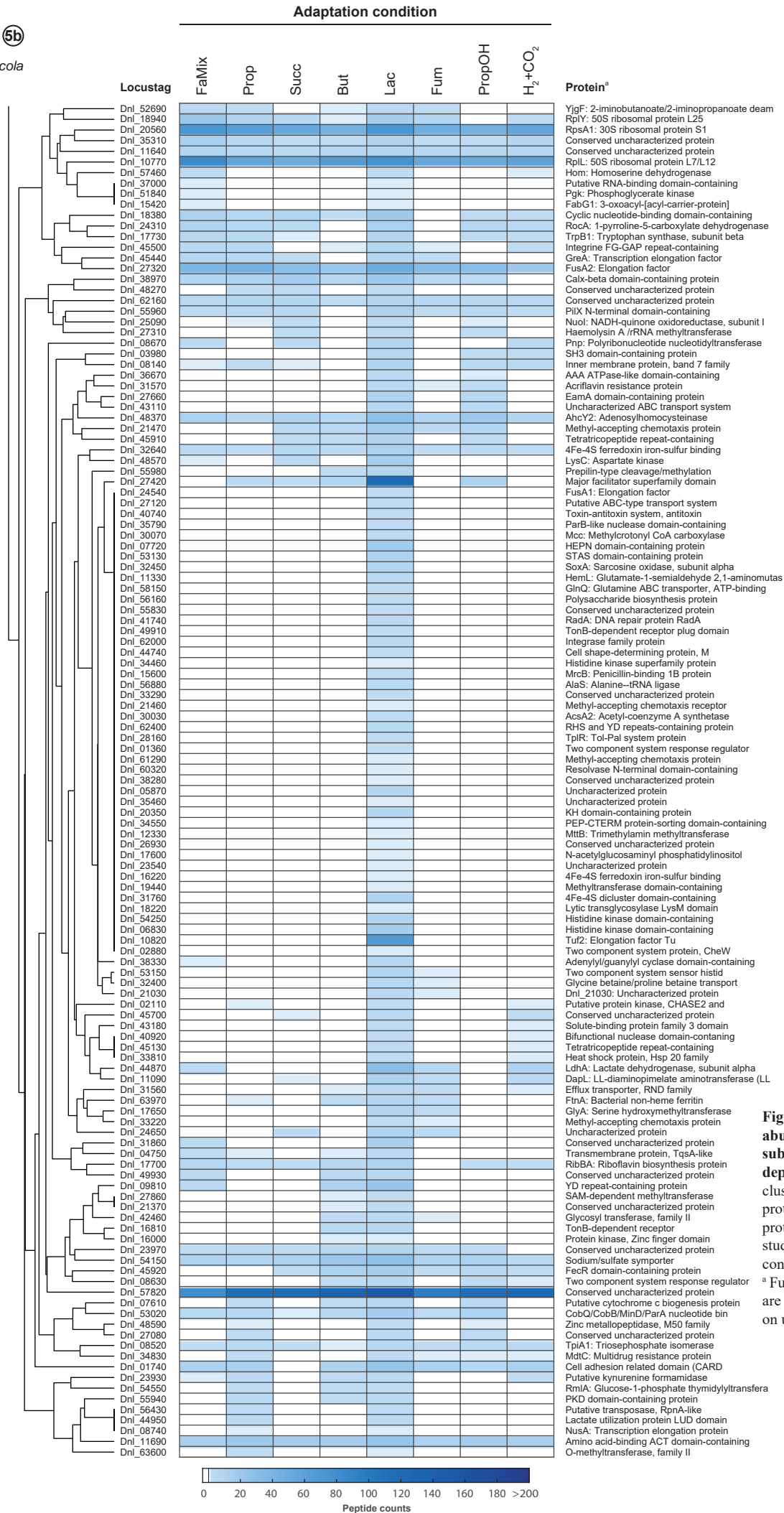


**Fig. S77: Detailed view on abundances of proteins forming a sub-cluster in the global clustering depicted in Fig. S8.** The global clustering is based on standardized protein abundances of all detected proteins of *Dn. limicola* across the 8 studied substrate adaptation conditions.

<sup>a</sup> Full description of protein functions are available in the genome annotation under accession CP061799.

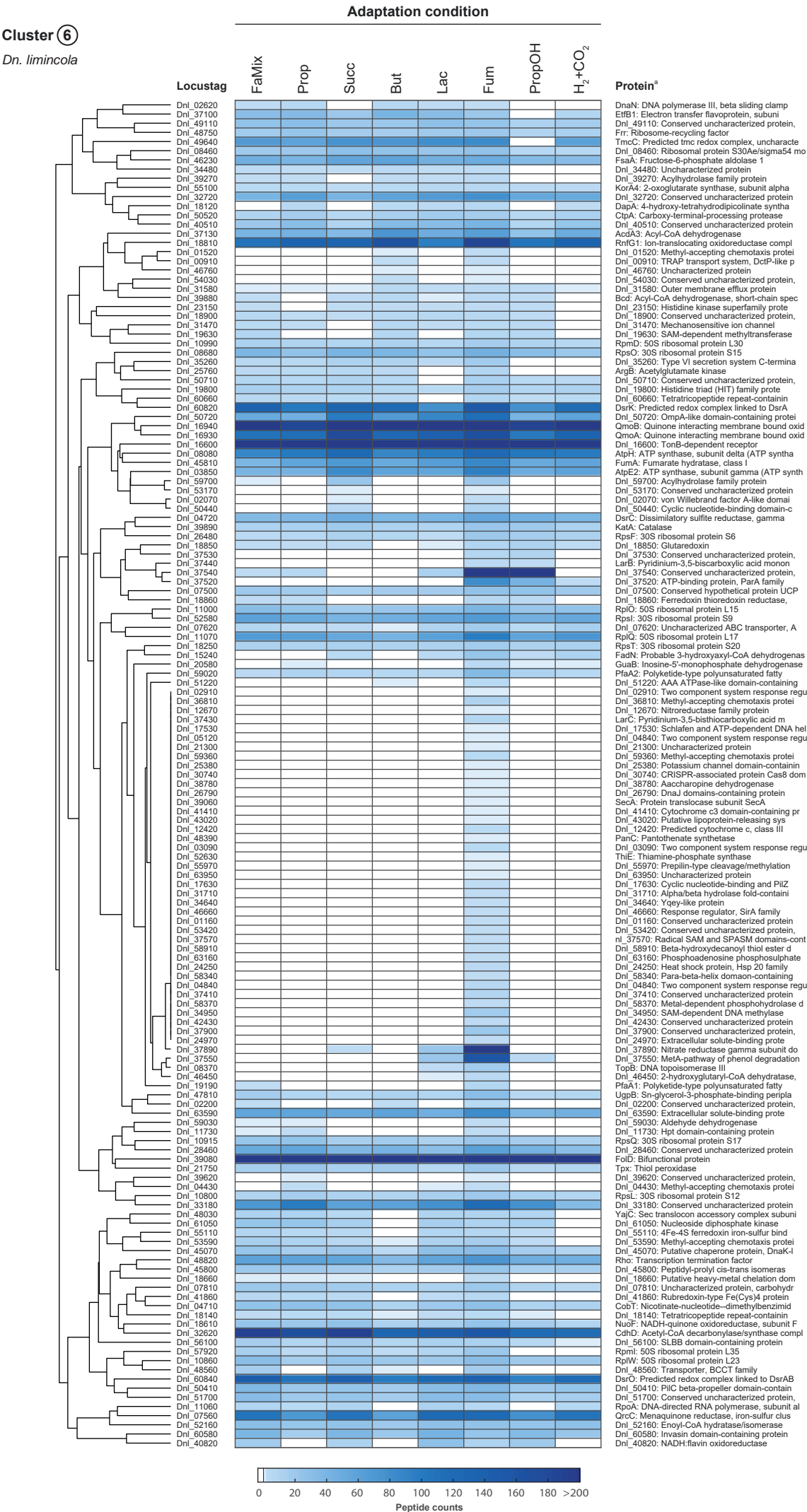


Fig. S78: Detailed view on abundances of proteins forming a sub-cluster in the global clustering depicted in Fig. S8. The global clustering is based on standardized protein abundances of all detected proteins of *Dn. limicola* across the 8 studied substrate adaptation conditions.

<sup>a</sup> Full description of protein functions are available in the genome annotation under accession CP061799.



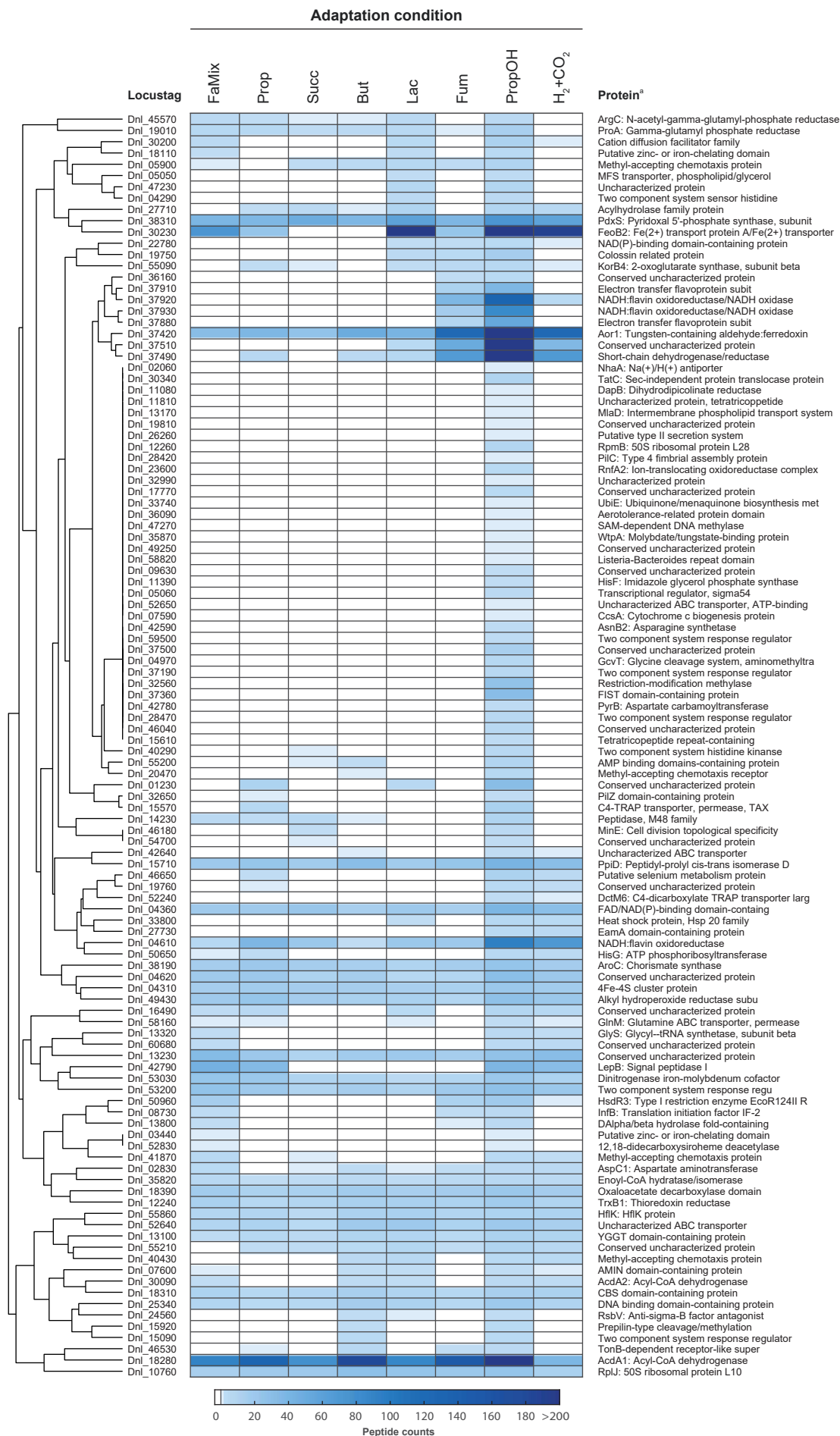
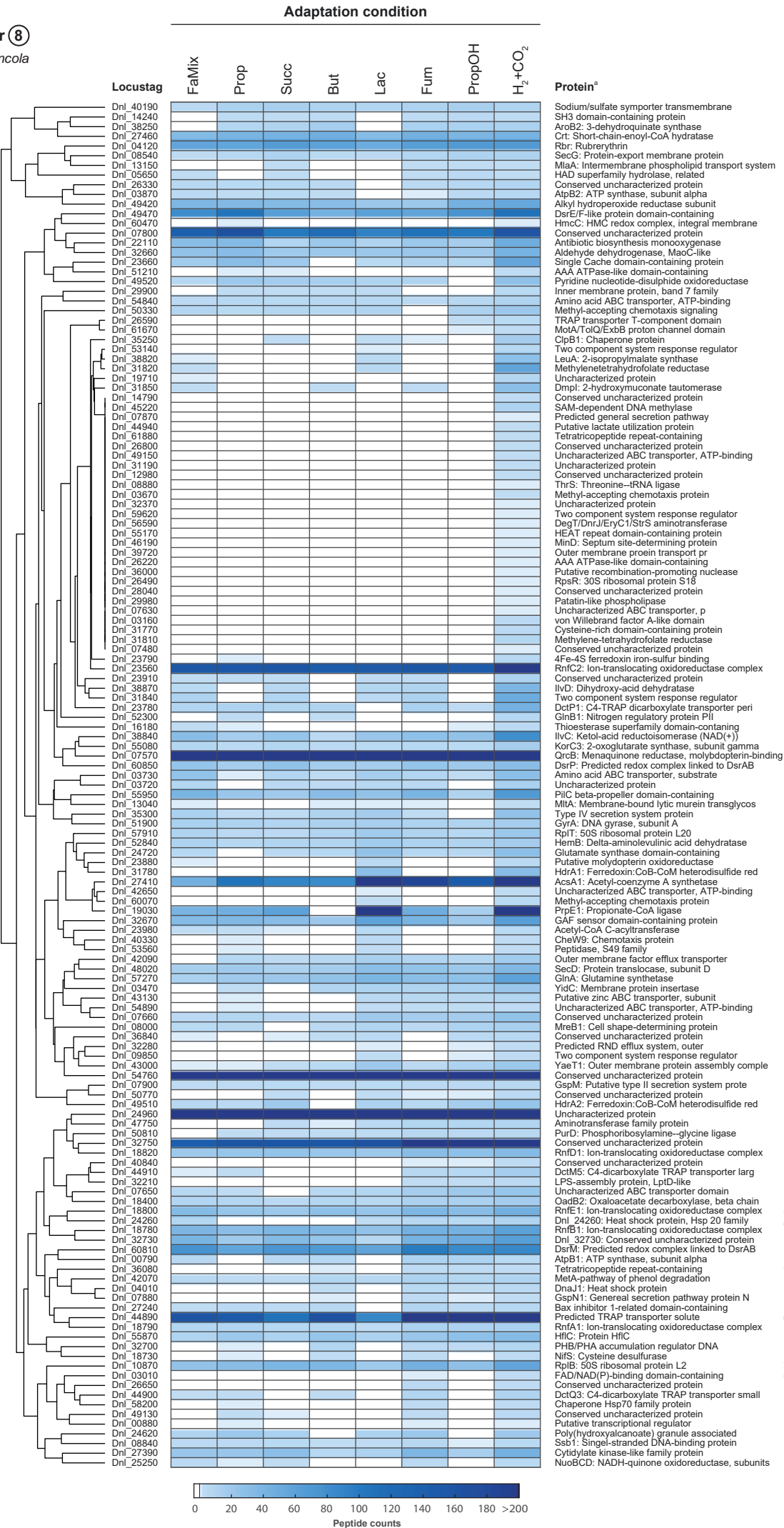


Fig. S79: Detailed view on abundances of proteins forming a sub-cluster in the global clustering depicted in Fig. S8. The global clustering is based on standardized protein abundances of all detected proteins of *Dn. limicola* across the 8 studied substrate adaptation conditions.  
<sup>a</sup> Full description of protein functions are available in the genome annotation under accession CP061799.



**Fig. S80: Detailed view on abundances of proteins forming a sub-cluster in the global clustering depicted in Fig. S8.** The global clustering is based on standardized protein abundances of all detected proteins of *Dn. limicola* across the 8 studied substrate adaptation conditions.  
<sup>a</sup> Full description of protein functions are available in the genome annotation under accession CP061799.



Cluster 1

*Dc. multivorans* 1be1

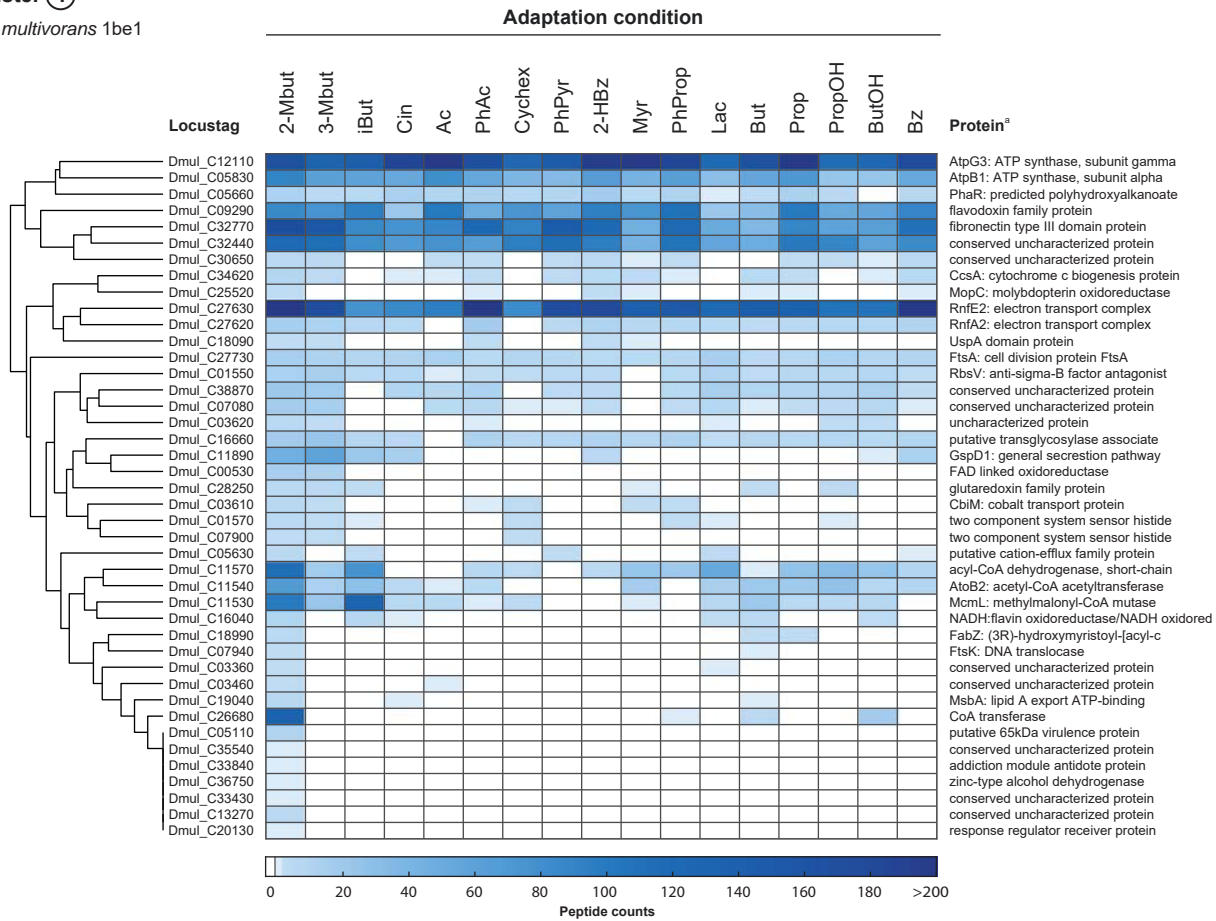


**Fig. S81: Detailed view on abundances of proteins forming a sub-cluster in the global clustering depicted in Fig. S9.** The global clustering is based on standardized protein abundances of all detected proteins of *Dc. multivorans* 1be1 across the 17 studied substrate adaptation conditions.

<sup>a</sup> Full description of protein functions are available in the genome annotation under accession CP015381.

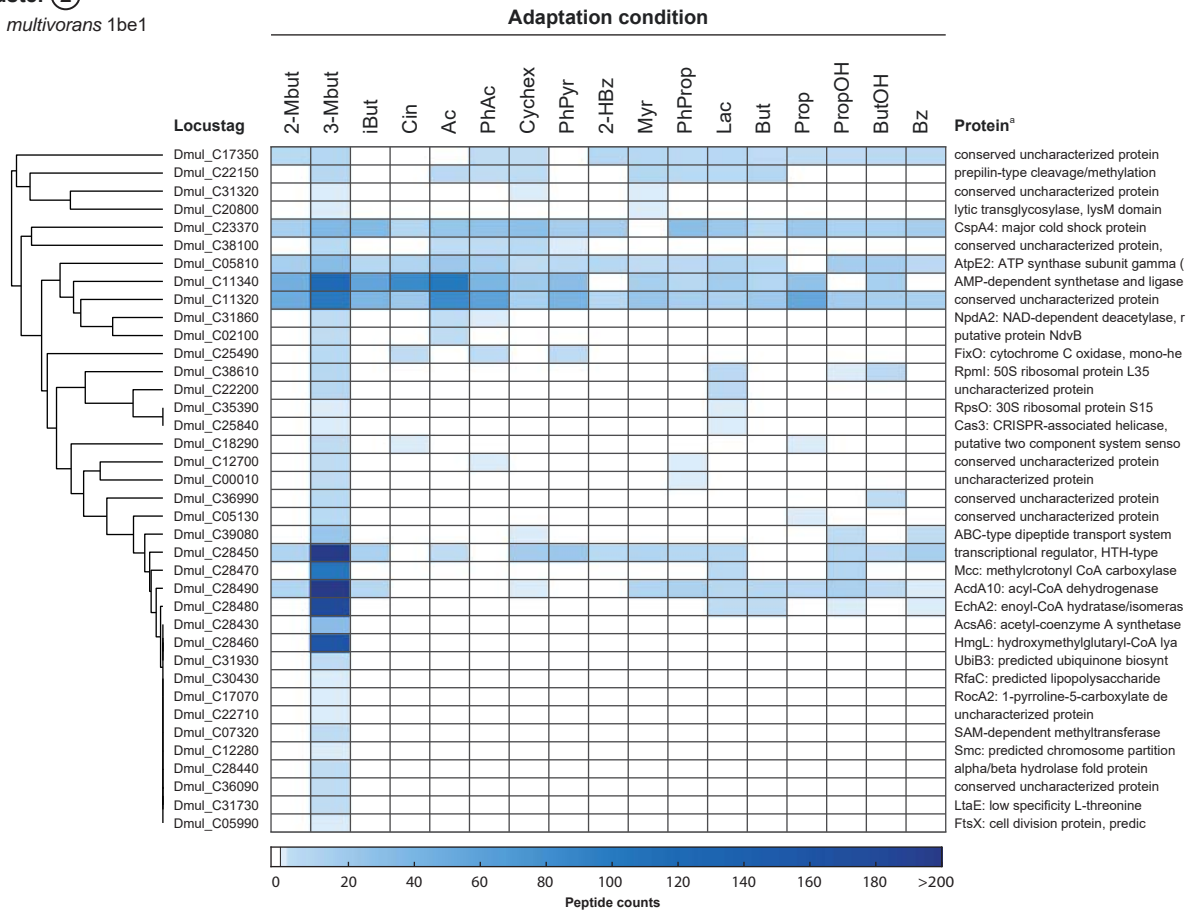


**Fig. S82: Detailed view on abundances of proteins forming a sub-cluster in the global clustering depicted in Fig. S9.** The global clustering is based on standardized protein abundances of all detected proteins of *Dc. multivorans* 1be1 across the 17 studied substrate adaptation conditions.

<sup>a</sup> Full description of protein functions are available in the genome annotation under accession CP015381.

Cluster 3

*Dc. multivorans* 1be1

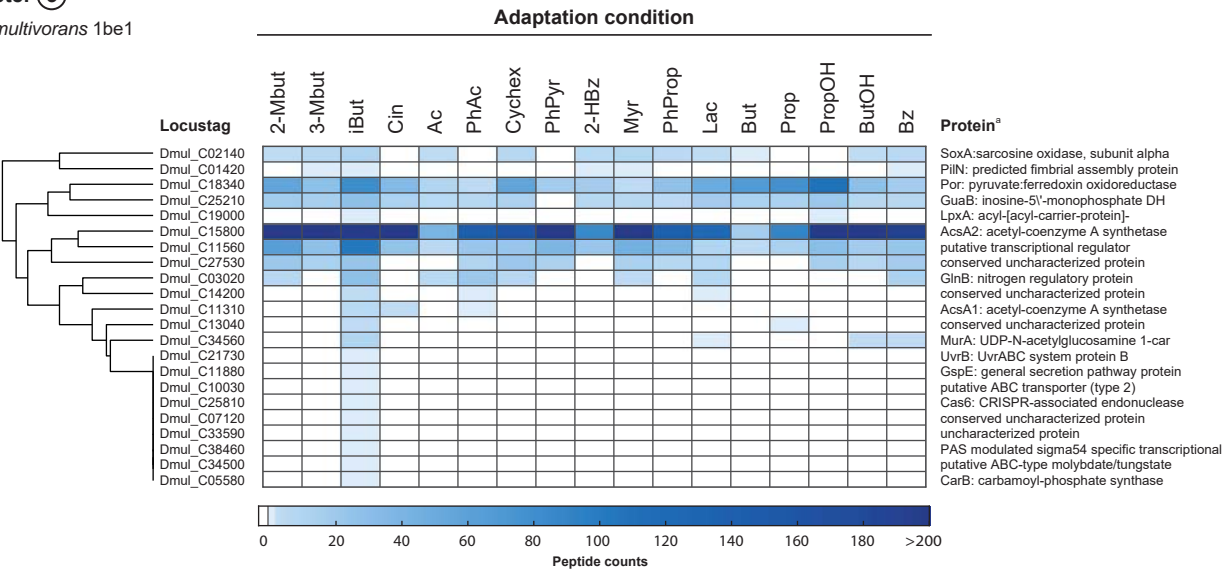


**Fig. S83: Detailed view on abundances of proteins forming a sub-cluster in the global clustering depicted in Fig. S9.** The global clustering is based on standardized protein abundances of all detected proteins of *Dc. multivorans* 1be1 across the 17 studied substrate adaptation conditions.

<sup>a</sup> Full description of protein functions are available in the genome annotation under accession CP015381.

Cluster 4

*Dc. multivorans* 1be1

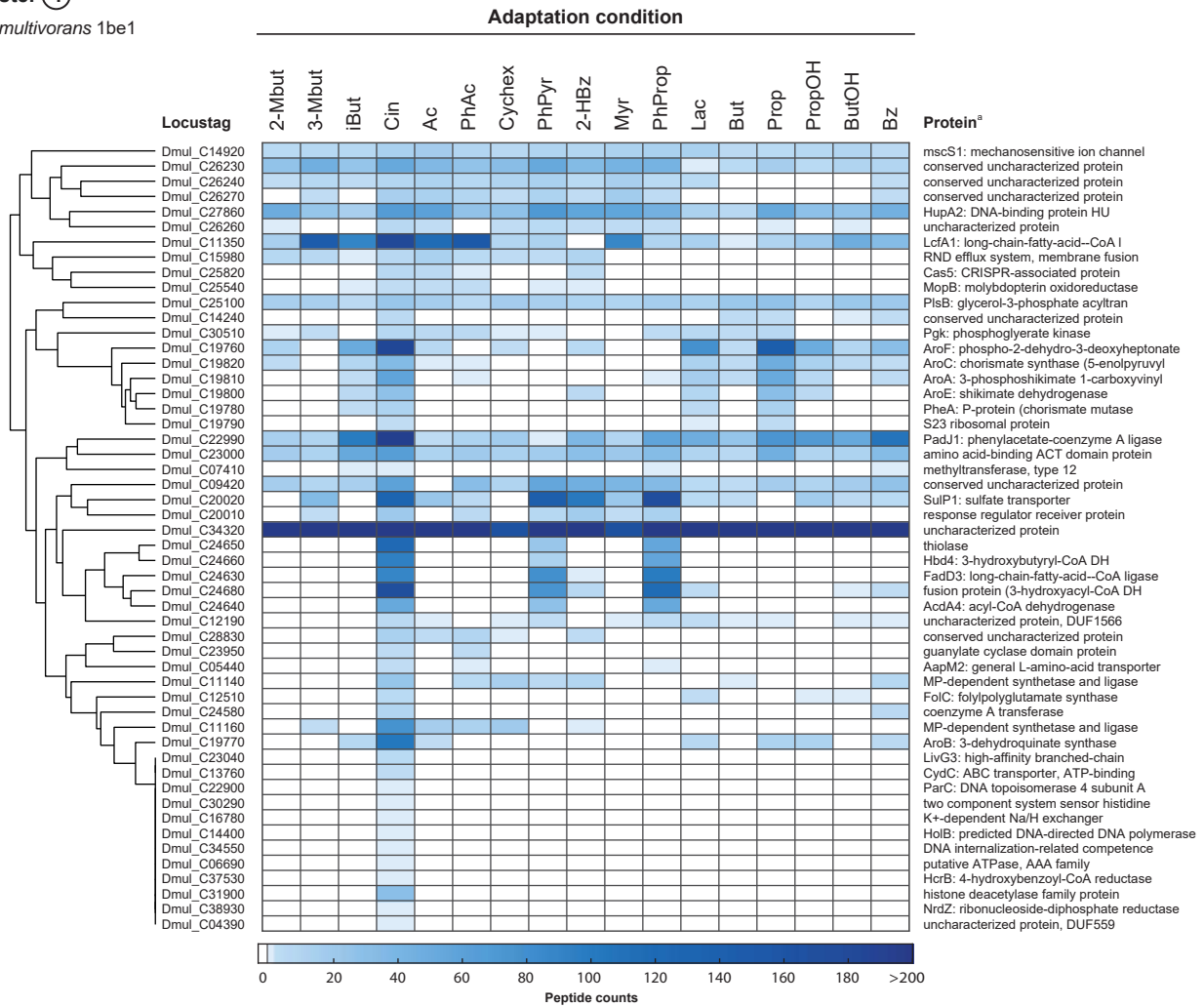


**Fig. S84: Detailed view on abundances of proteins forming a sub-cluster in the global clustering depicted in Fig. S9.** The global clustering is based on standardized protein abundances of all detected proteins of *Dc. multivorans* 1be1 across the 17 studied substrate adaptation conditions.

<sup>a</sup> Full description of protein functions are available in the genome annotation under accession CP015381.

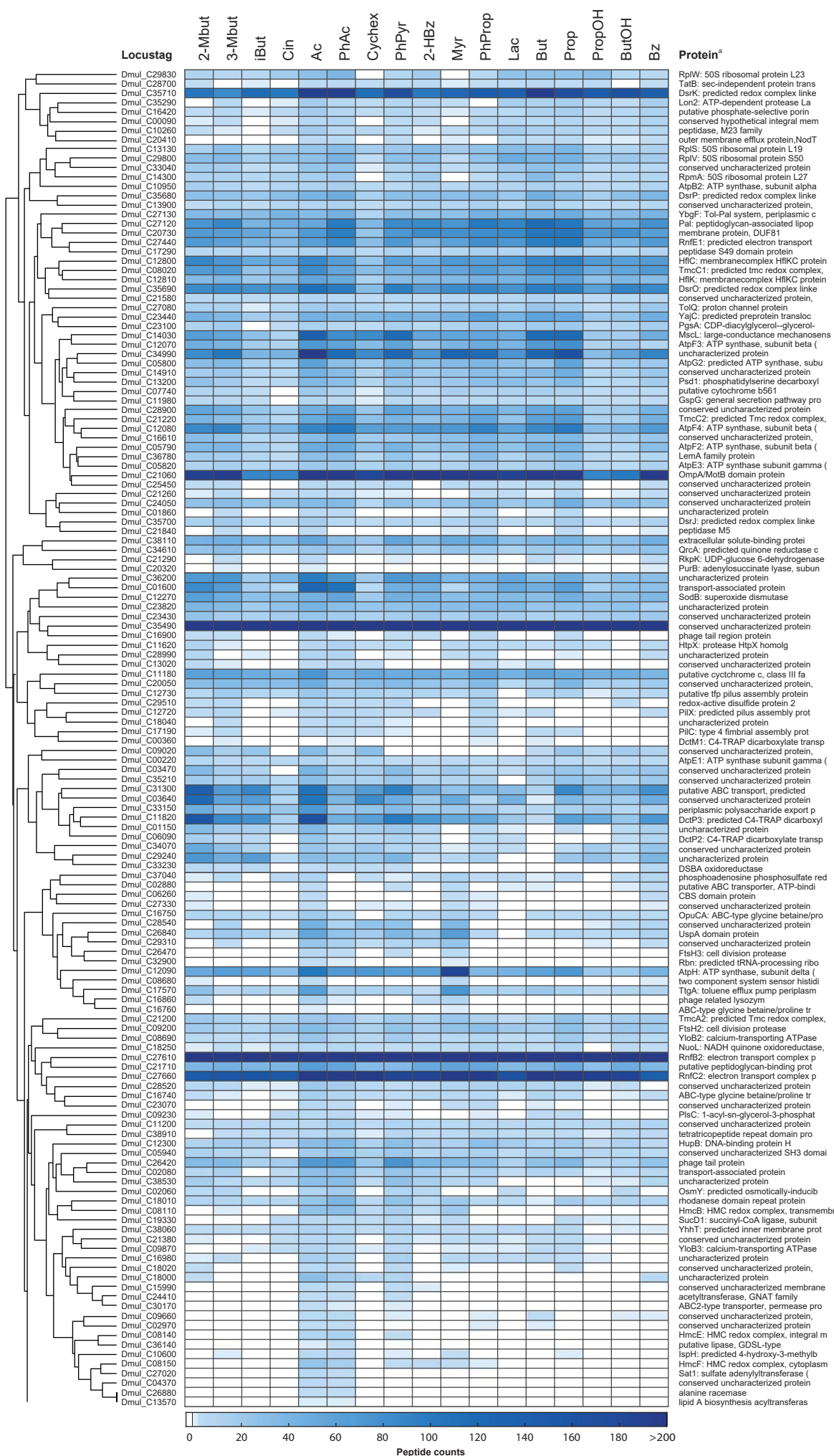


**Fig. S85: Detailed view on abundances of proteins forming a sub-cluster in the global clustering depicted in Fig. S9. The global clustering is based on standardized protein abundances of all detected proteins of *Dc. multivorans* 1be1 across the 17 studied substrate adaptation conditions.**

<sup>a</sup> Full description of protein functions are available in the genome annotation under accession CP015381.

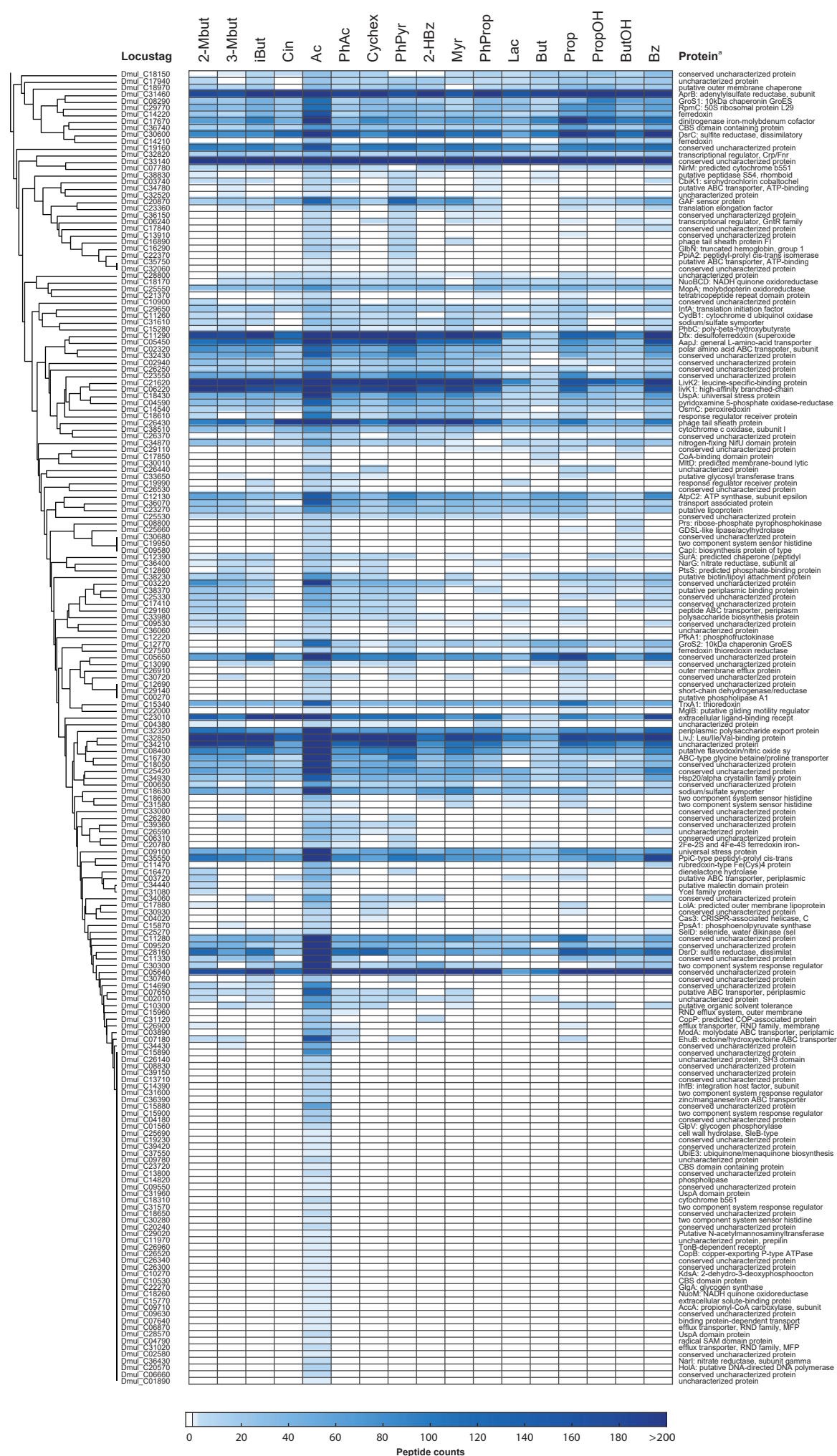


**Fig. S86: Detailed view on abundances of proteins forming a sub-cluster in the global clustering depicted in Fig. S9. The global clustering is based on standardized protein abundances of all detected proteins of *Dc. multivorans* 1be1 across the 17 studied substrate adaptation conditions.**

<sup>a</sup> Full description of protein functions are available in the genome annotation under accession CP015381.



Cluster 6

*Dc. multivorans* 1be1



**Fig. S87: Detailed view on abundances of proteins forming a sub-cluster in the global clustering depicted in Fig. S9.** The global clustering is based on standardized protein abundances of all detected proteins of *Dc. multivorans* 1be1 across the 17 studied substrate adaptation conditions.

<sup>a</sup> Full description of protein functions are available in the genome annotation under accession CP015381.



Cluster 7

*Dc. multivorans* 1be1

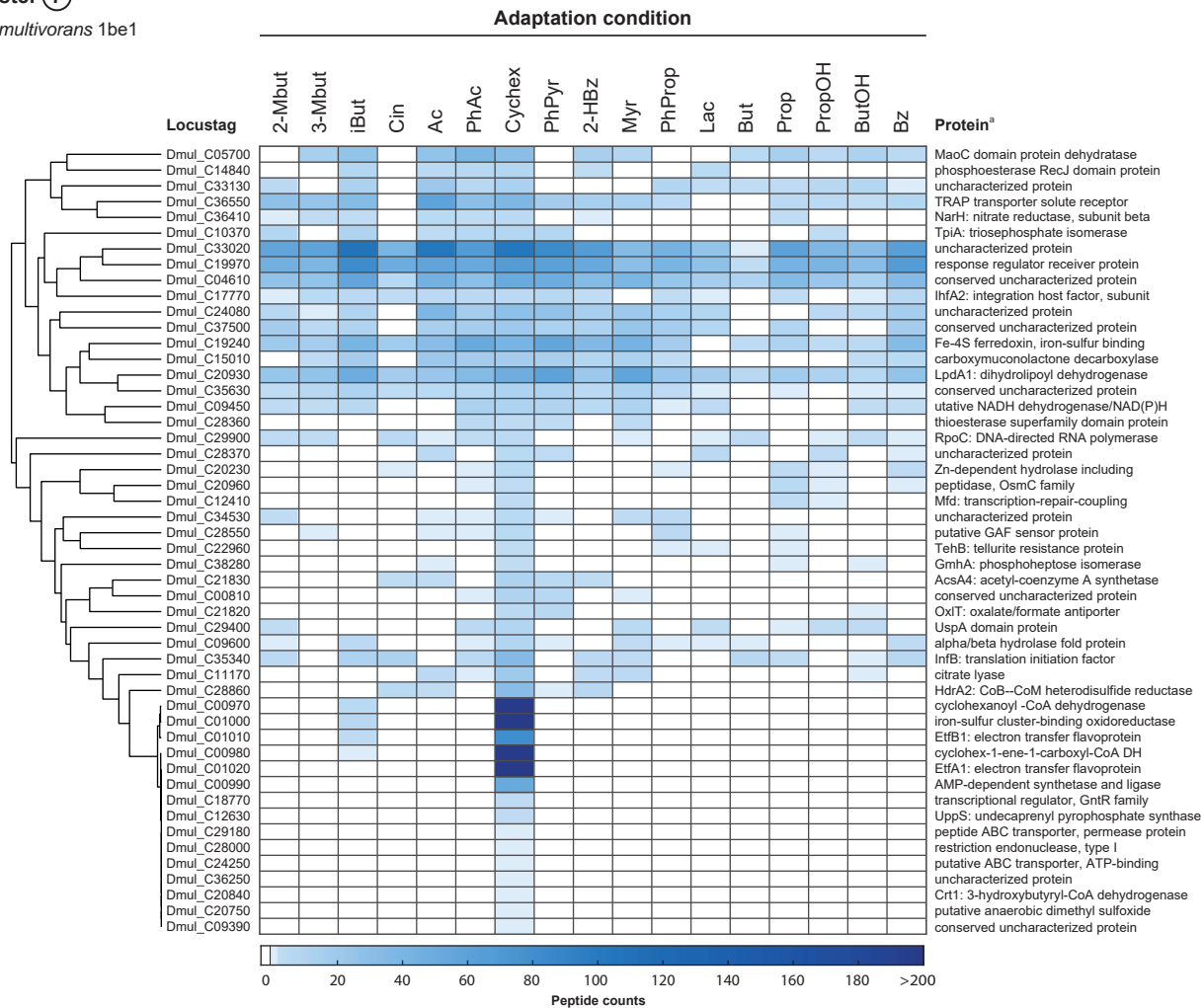
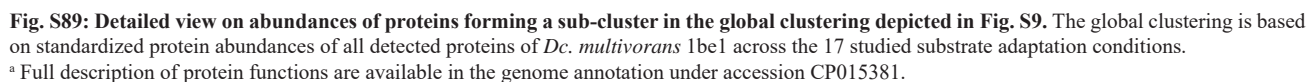


**Fig. S88: Detailed view on abundances of proteins forming a sub-cluster in the global clustering depicted in Fig. S9.** The global clustering is based on standardized protein abundances of all detected proteins of *Dc. multivorans* 1be1 across the 17 studied substrate adaptation conditions.

<sup>a</sup> Full description of protein functions are available in the genome annotation under accession CP015381.

*Dc. multivorans* 1be1



<sup>a</sup> Full description of protein functions are available in the genome annotation under accession CP015381.

Cluster 9

*Dc. multivorans* 1be1

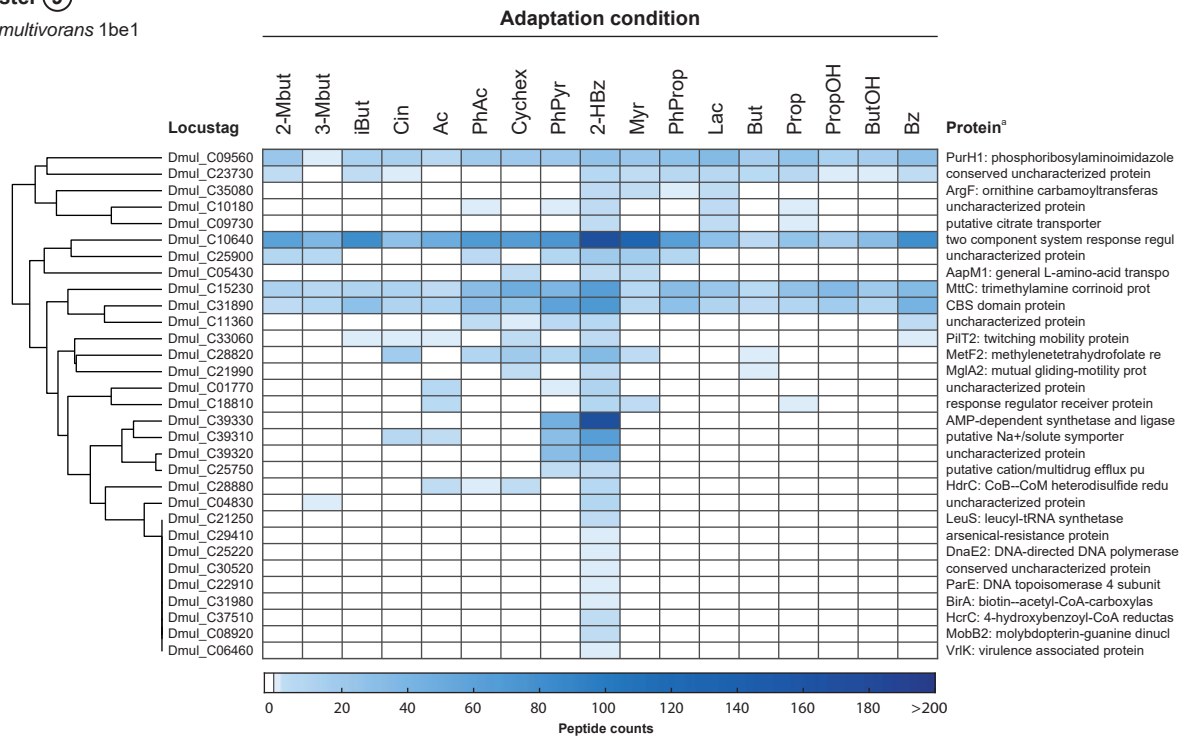


**Fig. S90: Detailed view on abundances of proteins forming a sub-cluster in the global clustering depicted in Fig. S9.** The global clustering is based on standardized protein abundances of all detected proteins of *Dc. multivorans* 1be1 across the 17 studied substrate adaptation conditions.

<sup>a</sup> Full description of protein functions are available in the genome annotation under accession CP015381.

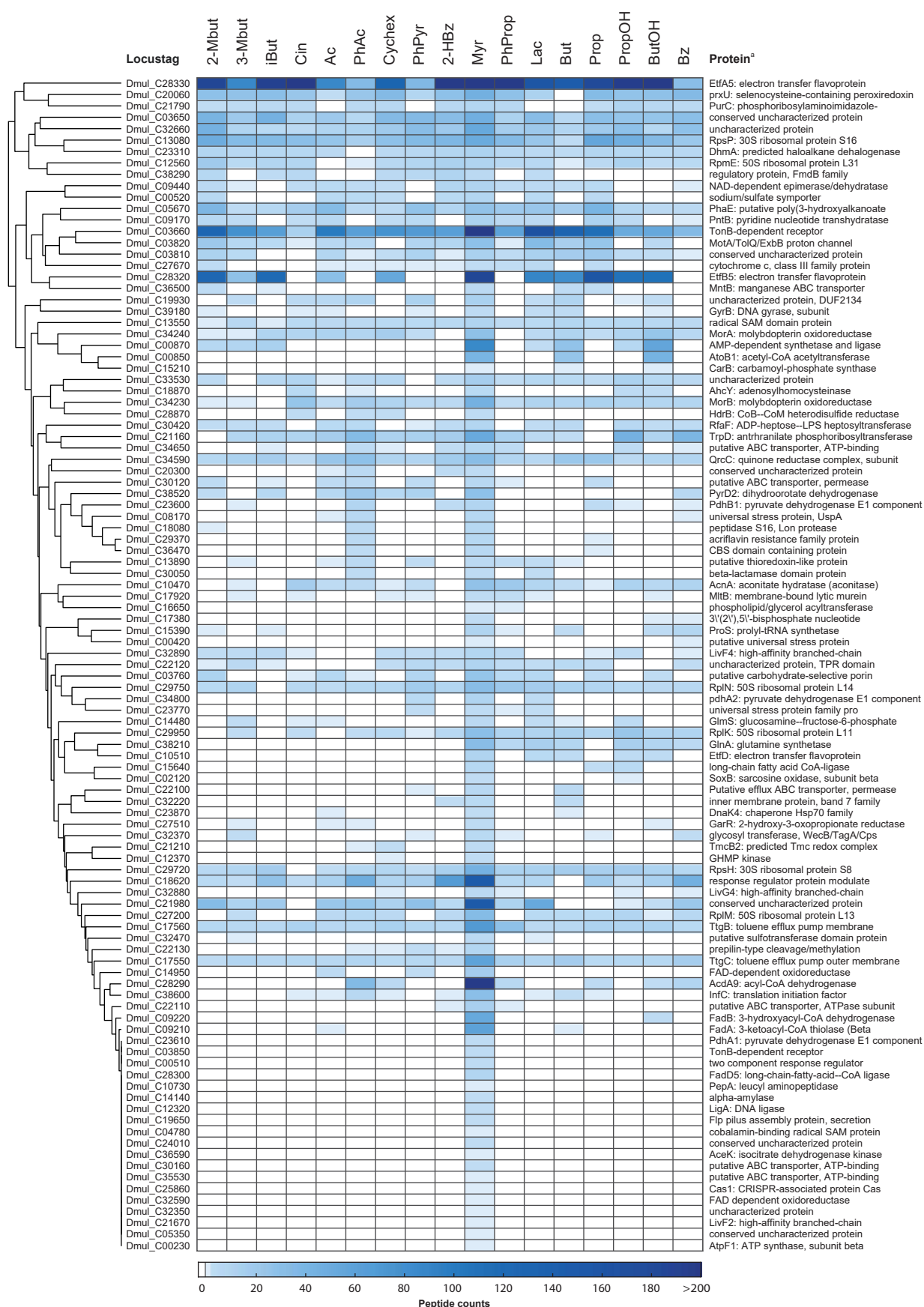


**Fig. S91: Detailed view on abundances of proteins forming a sub-cluster in the global clustering depicted in Fig. S9.** The global clustering is based on standardized protein abundances of all detected proteins of *Dc. multivorans* 1be1 across the 17 studied substrate adaptation conditions.

<sup>a</sup> Full description of protein functions are available in the genome annotation under accession CP015381.

Cluster 11

Dc. multivorans 1be1

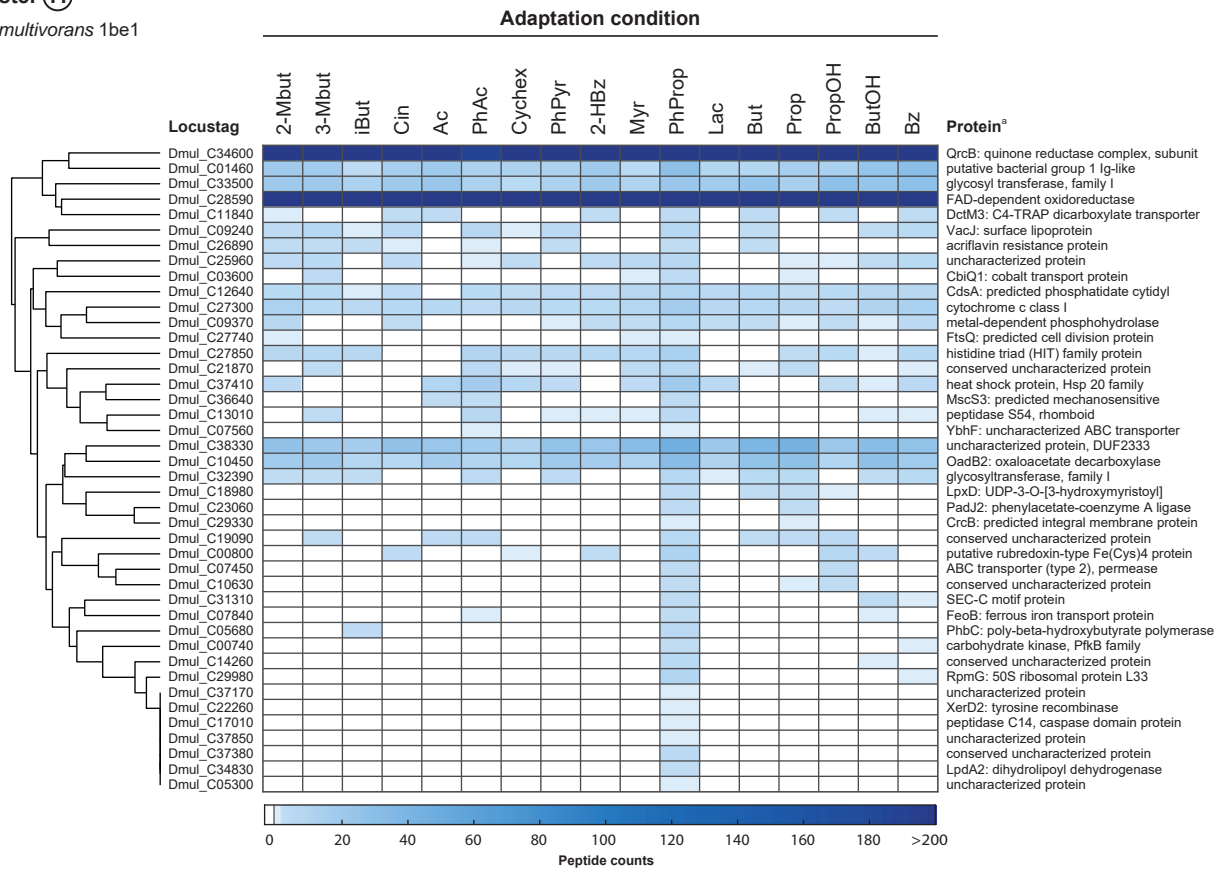


Fig. S92: Detailed view on abundances of proteins forming a sub-cluster in the global clustering depicted in Fig. S9. The global clustering is based on standardized protein abundances of all detected proteins of *Dc. multivorans* 1be1 across the 17 studied substrate adaptation conditions.

<sup>a</sup> Full description of protein functions are available in the genome annotation under accession CP015381.

## Cluster 12

*Dc. multivorans* 1be1

## Adaptation condition

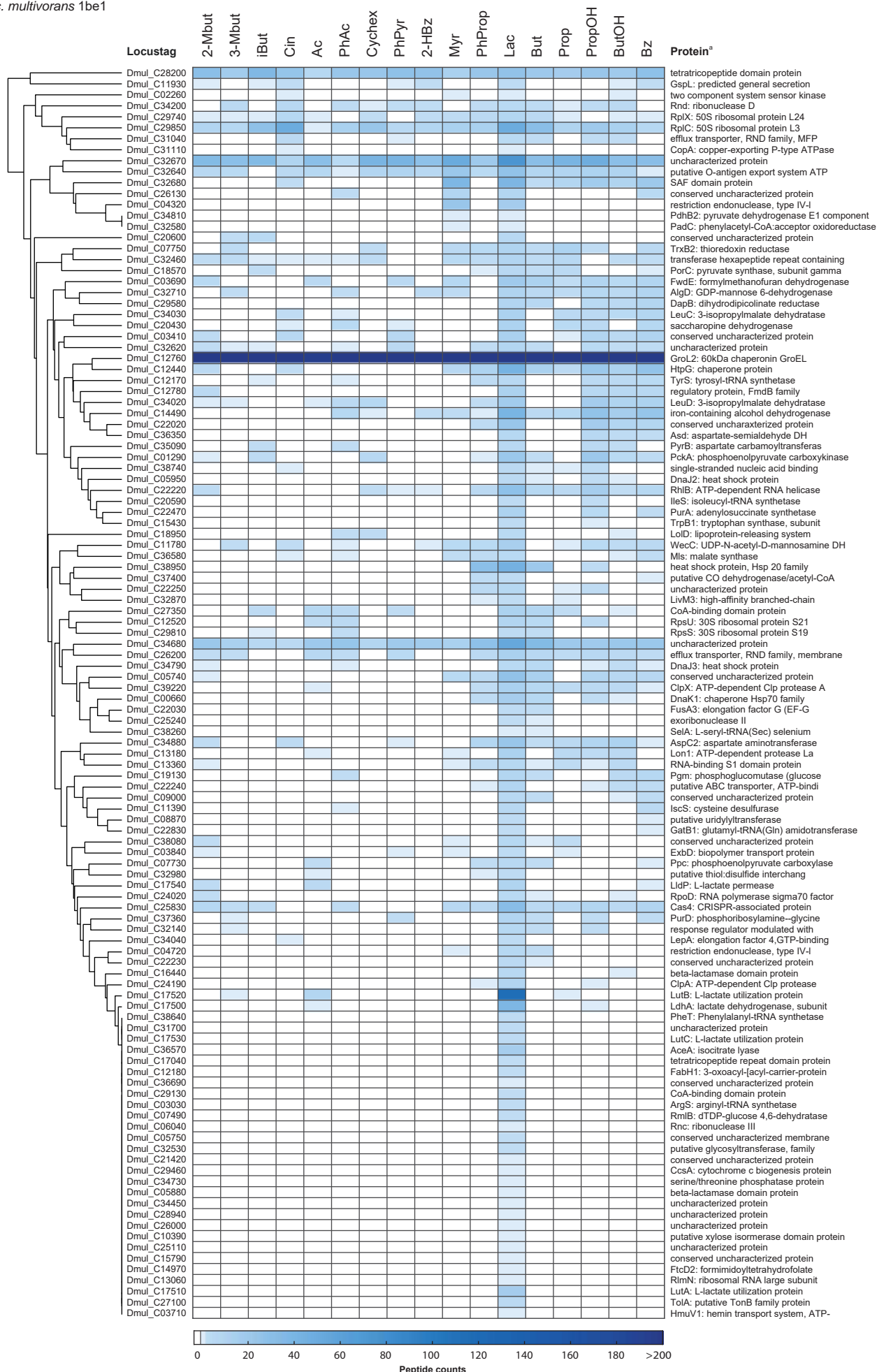


**Fig. S93: Detailed view on abundances of proteins forming a sub-cluster in the global clustering depicted in Fig. S9.** The global clustering is based on standardized protein abundances of all detected proteins of *Dc. multivorans* 1be1 across the 17 studied substrate adaptation conditions.

<sup>a</sup> Full description of protein functions are available in the genome annotation under accession CP015381.

## Cluster 13

*Dc. multivorans* 1be1

## Adaptation condition

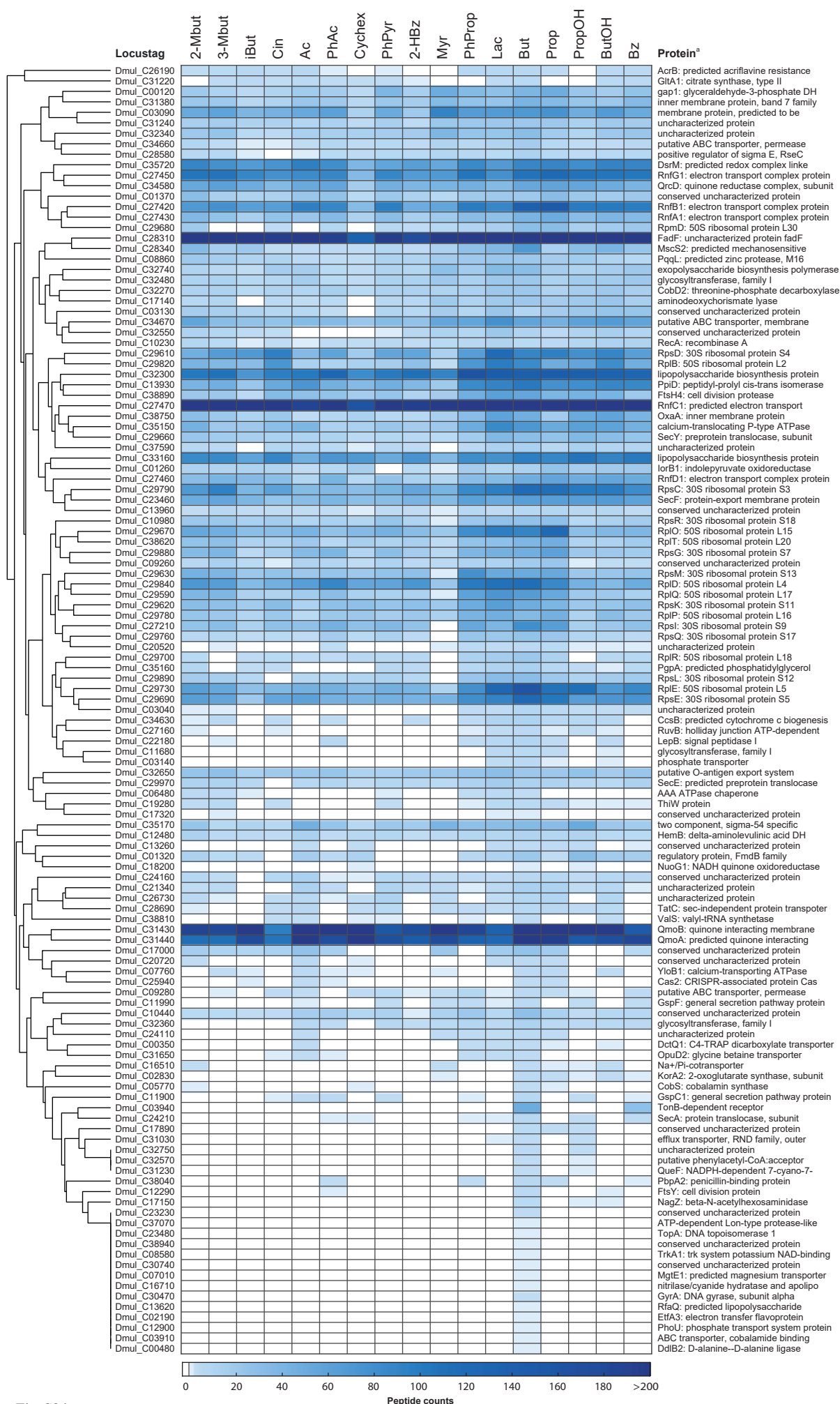


Fig. S94



## Cluster 14

*Dc. multivorans* 1be1

## Adaptation condition



**Fig. S95: Detailed view on abundances of proteins forming a sub-cluster in the global clustering depicted in Fig. S9.** The global clustering is based on standardized protein abundances of all detected proteins of *Dc. multivorans* 1be1 across the 17 studied substrate adaptation conditions.

<sup>a</sup> Full description of protein functions are available in the genome annotation under accession CP015381.

## Cluster 15

Dc. multivorans 1be1

## Adaptation condition

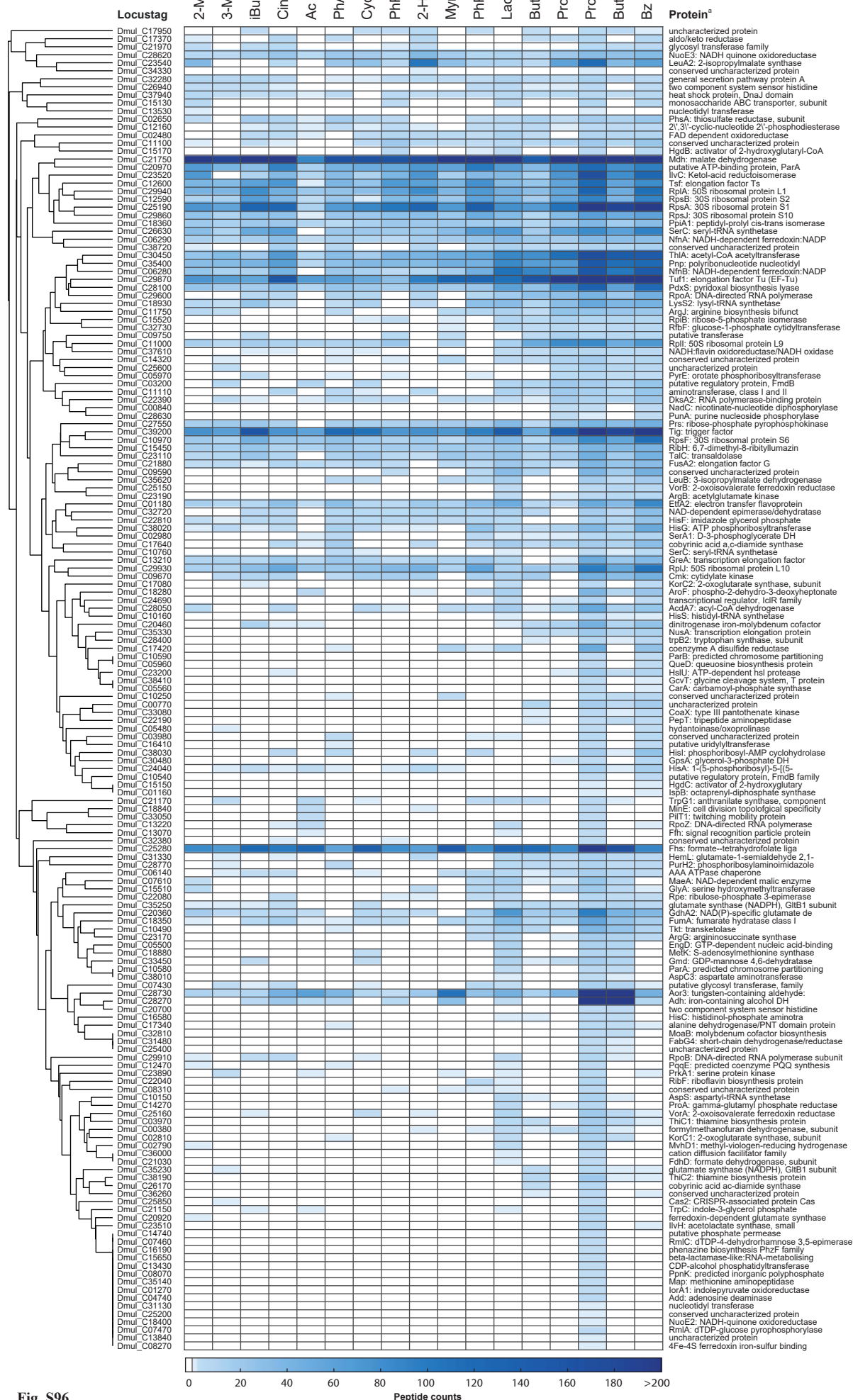
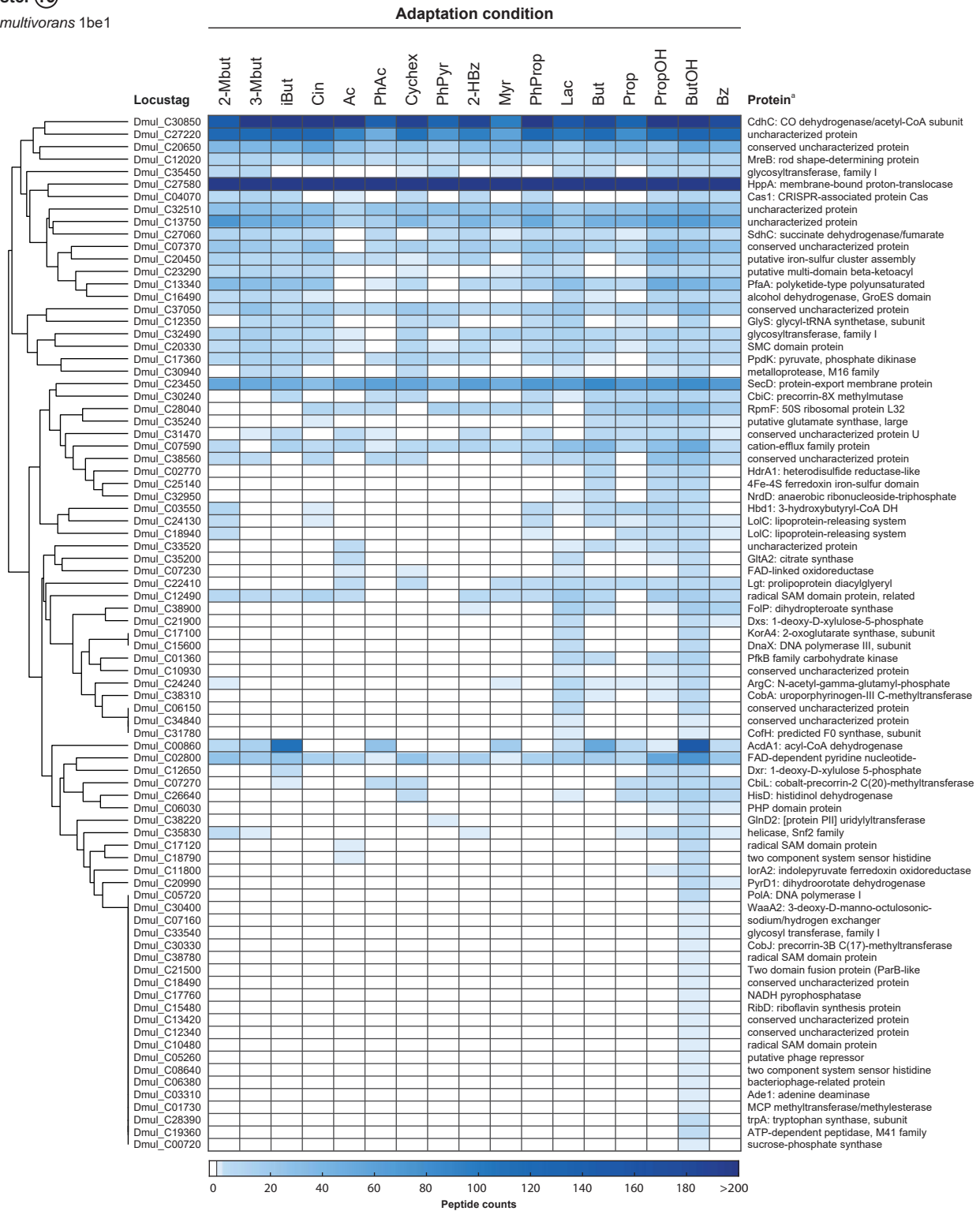


Fig. S96

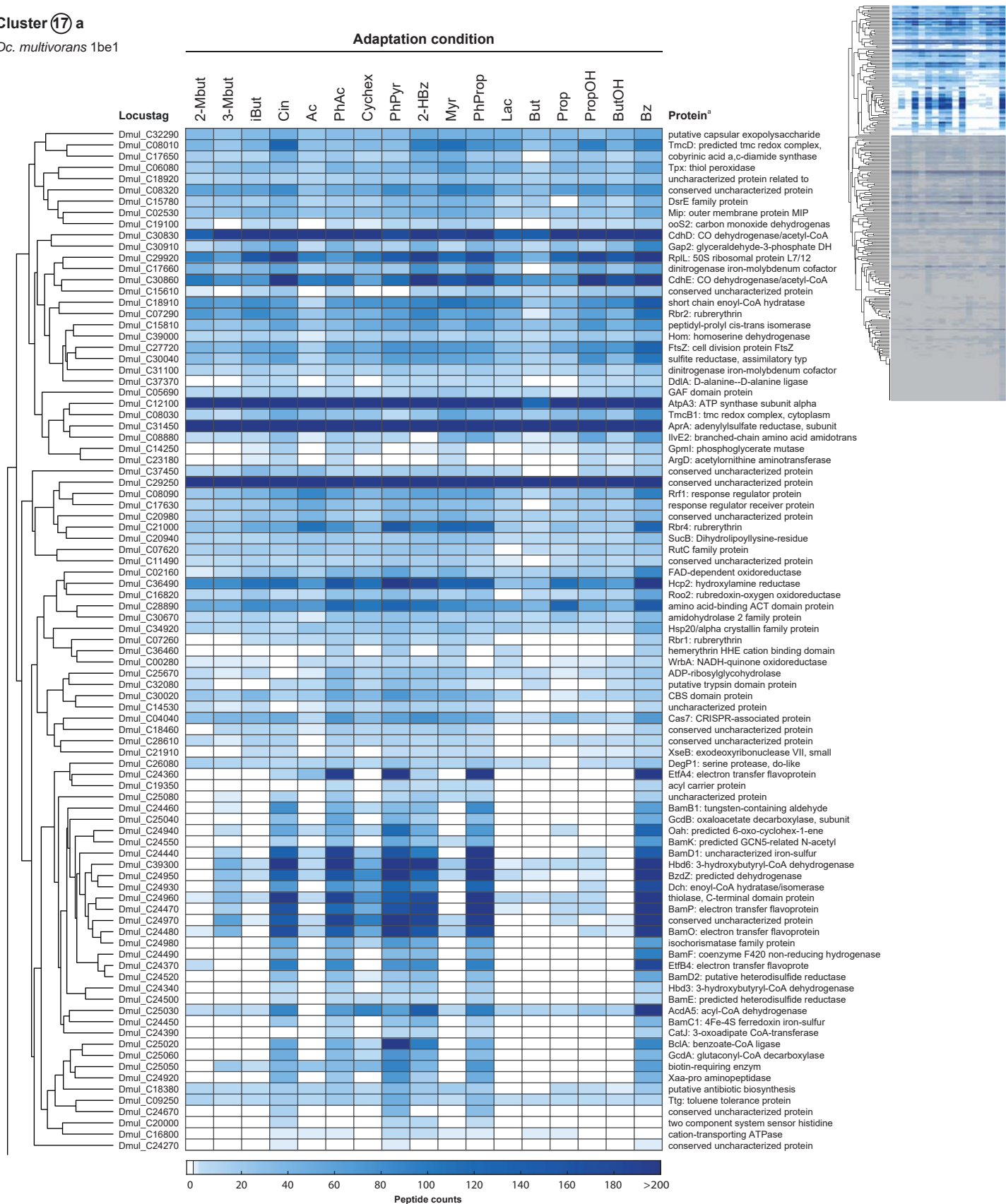
Cluster 16

*Dc. multivorans* 1be1



**Fig. S97: Detailed view on abundances of proteins forming a sub-cluster in the global clustering depicted in Fig. S9.** The global clustering is based on standardized protein abundances of all detected proteins of *Dc. multivorans* 1be1 across the 17 studied substrate adaptation conditions.

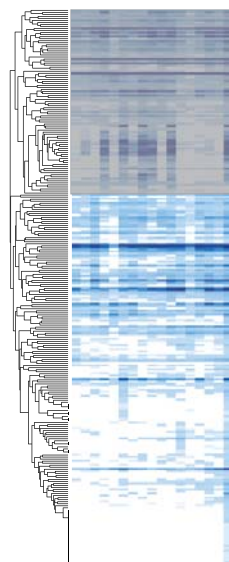
<sup>a</sup> Full description of protein functions are available in the genome annotation under accession CP015381.



**Fig. S98: Detailed view on abundances of proteins forming a sub-cluster in the global clustering depicted in Fig. S9.** The global clustering is based on standardized protein abundances of all detected proteins of *Dc. multivorans* 1be1 across the 17 studied substrate adaptation conditions.

<sup>a</sup> Full description of protein functions are available in the genome annotation under accession CP015381.

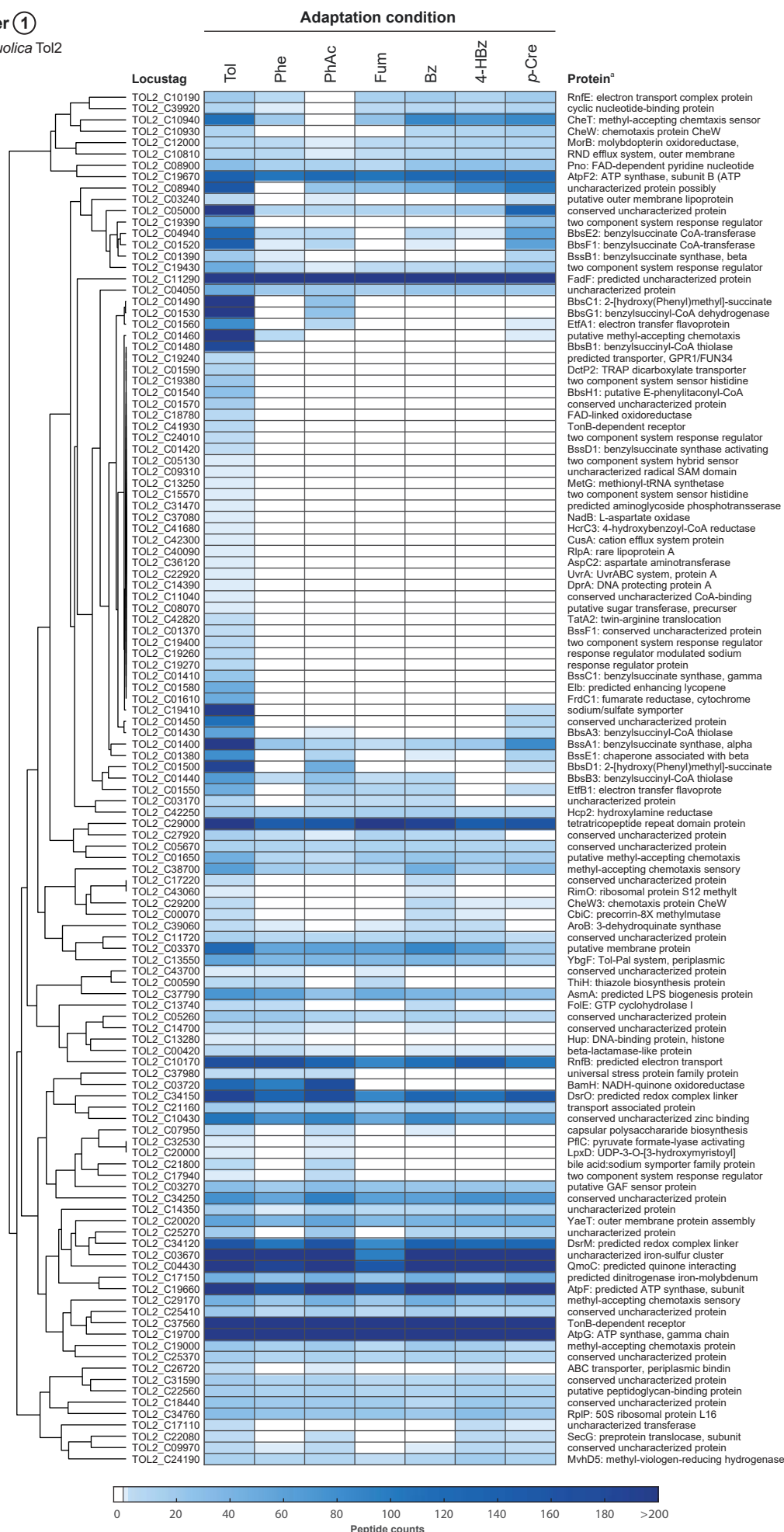




**Fig. S99: Detailed view on abundances of proteins forming a sub-cluster in the global clustering depicted in Fig. S9.** The global clustering is based on standardized protein abundances of all detected proteins of *Dc. multivorans* 1b1 across the 17 studied substrate adaptation conditions.

<sup>a</sup> Full description of protein functions are available in the genome annotation under accession CP015381.

## Cluster ①

*Db. toluolica* Tol2

**Fig. S100: Detailed view on abundances of proteins forming a sub-cluster in the global clustering depicted in Fig. S10.** The global clustering is based on standardized protein abundances of all detected proteins of *Db. toluolica* Tol2 across the 7 studied substrate adaptation conditions.

<sup>a</sup> Full description of protein functions are available in the genome annotation under accession FO203503.



Cluster 2a

Db. toluolica Tol2

Adaptation condition

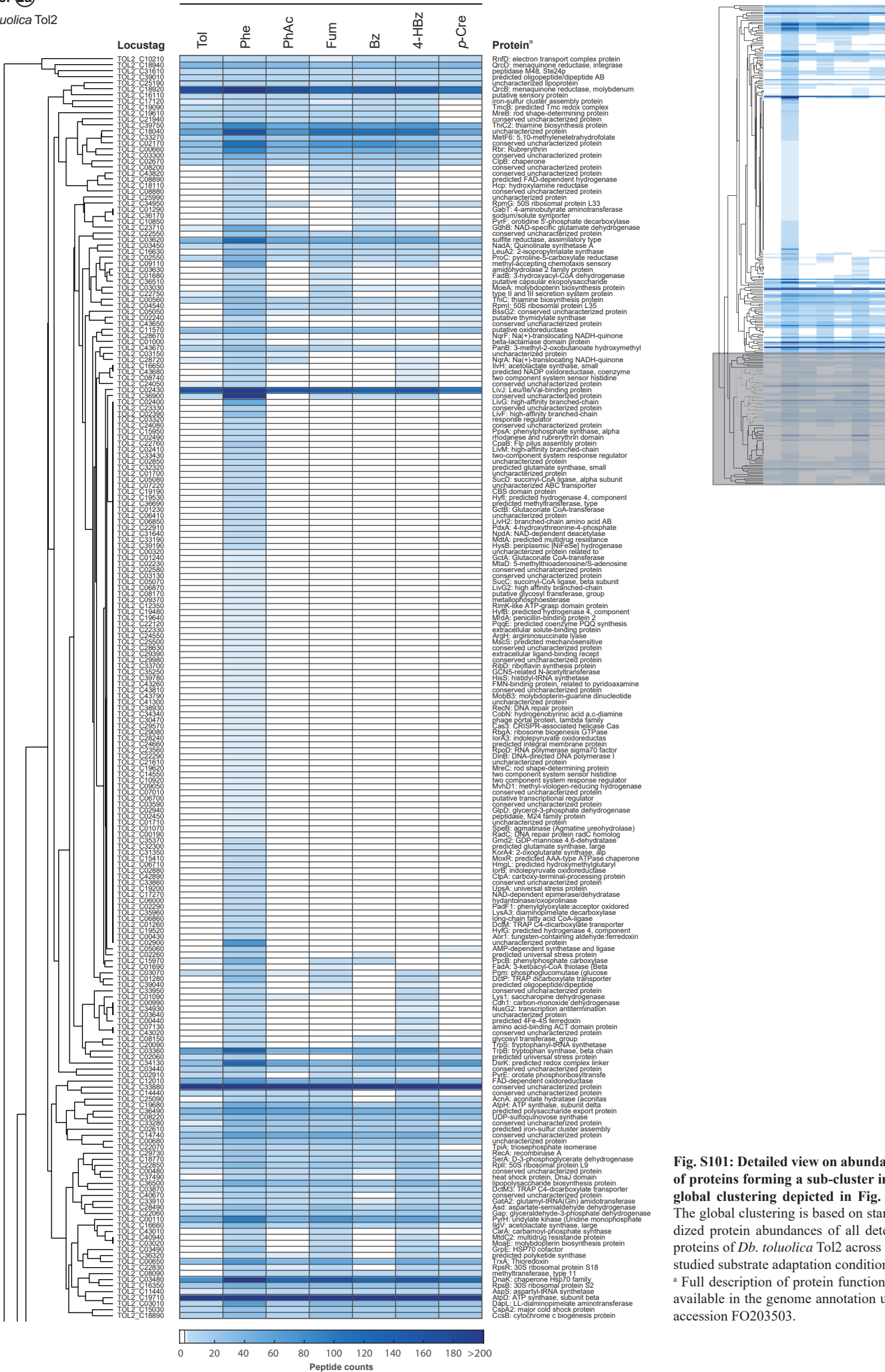
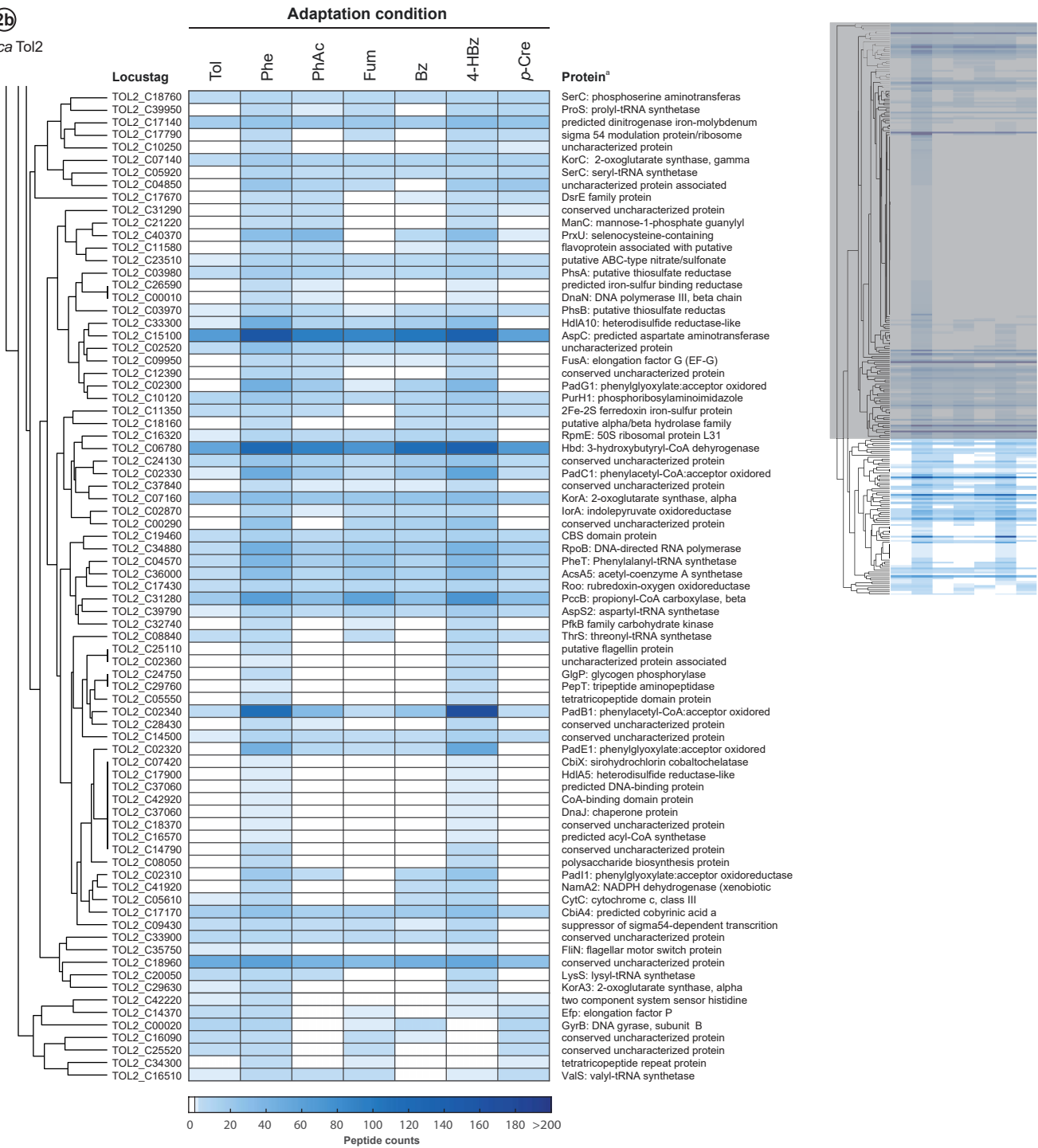
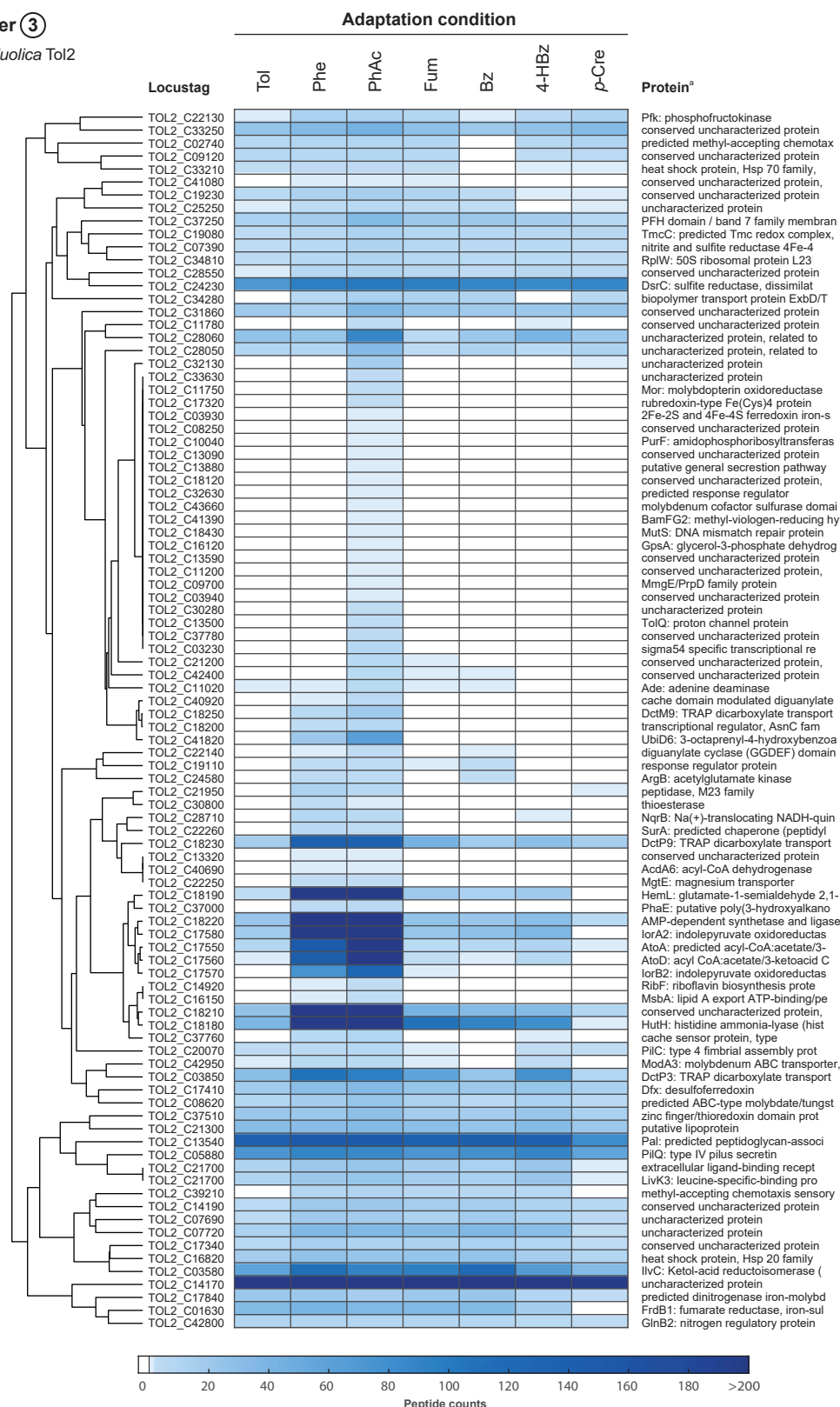


Fig. S101: Detailed view on abundances of proteins forming a sub-cluster in the global clustering depicted in Fig. S10. The global clustering is based on standardized protein abundances of all detected proteins of *Db. toluolica* Tol2 across the 7 studied substrate adaptation conditions. <sup>a</sup> Full description of protein functions are available in the genome annotation under accession FO203503.



# Cluster ③

*Db. toluolica* Tol2



**Fig. S103: Detailed view on abundances of proteins forming a sub-cluster in the global clustering depicted in Fig. S10.** The global clustering is based on standardized protein abundances of all detected proteins of *Db. toluolica* Tol2 across the 7 studied substrate adaptation conditions.

<sup>a</sup> Full description of protein functions are available in the genome annotation under accession FO203503.

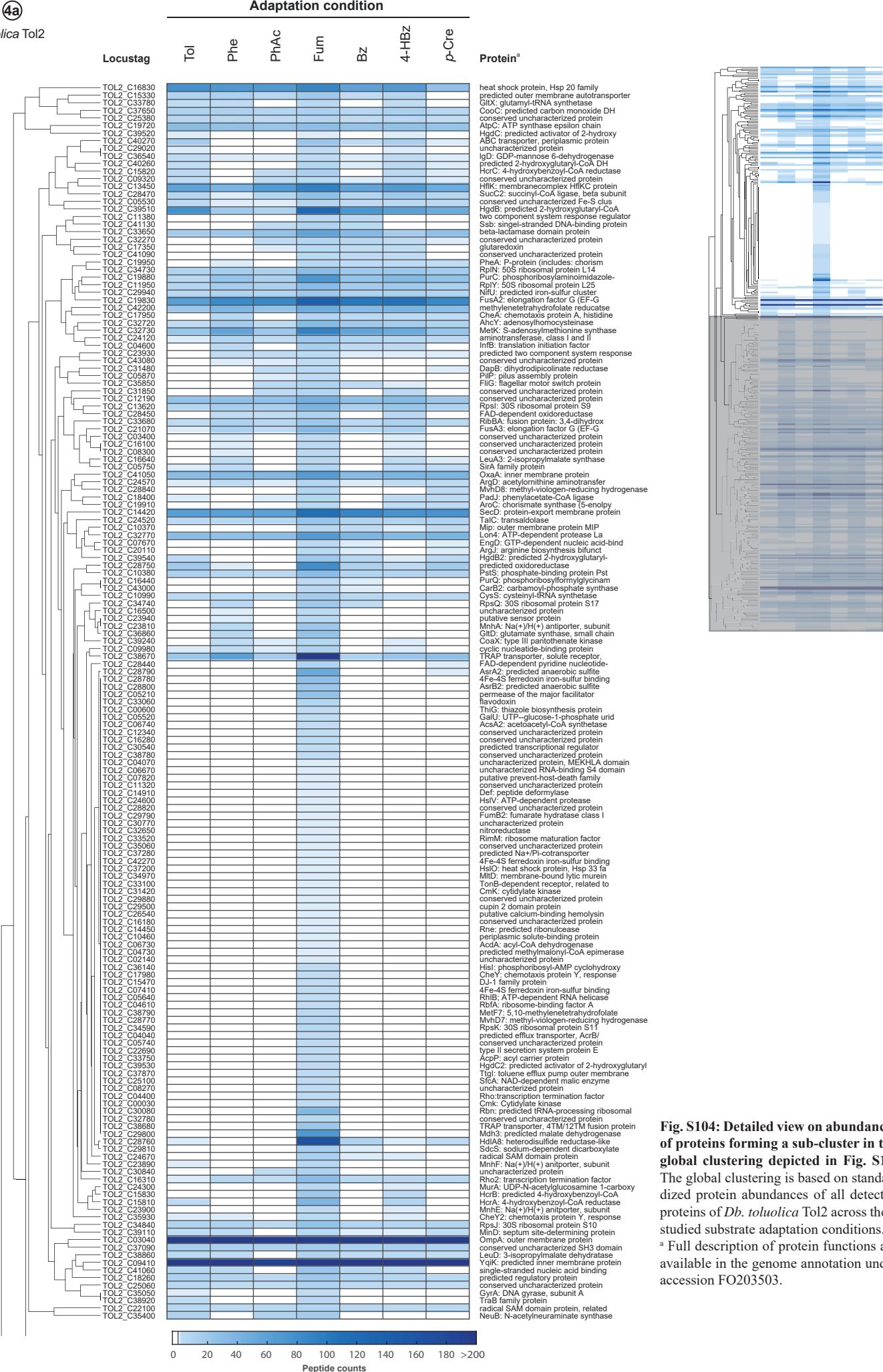
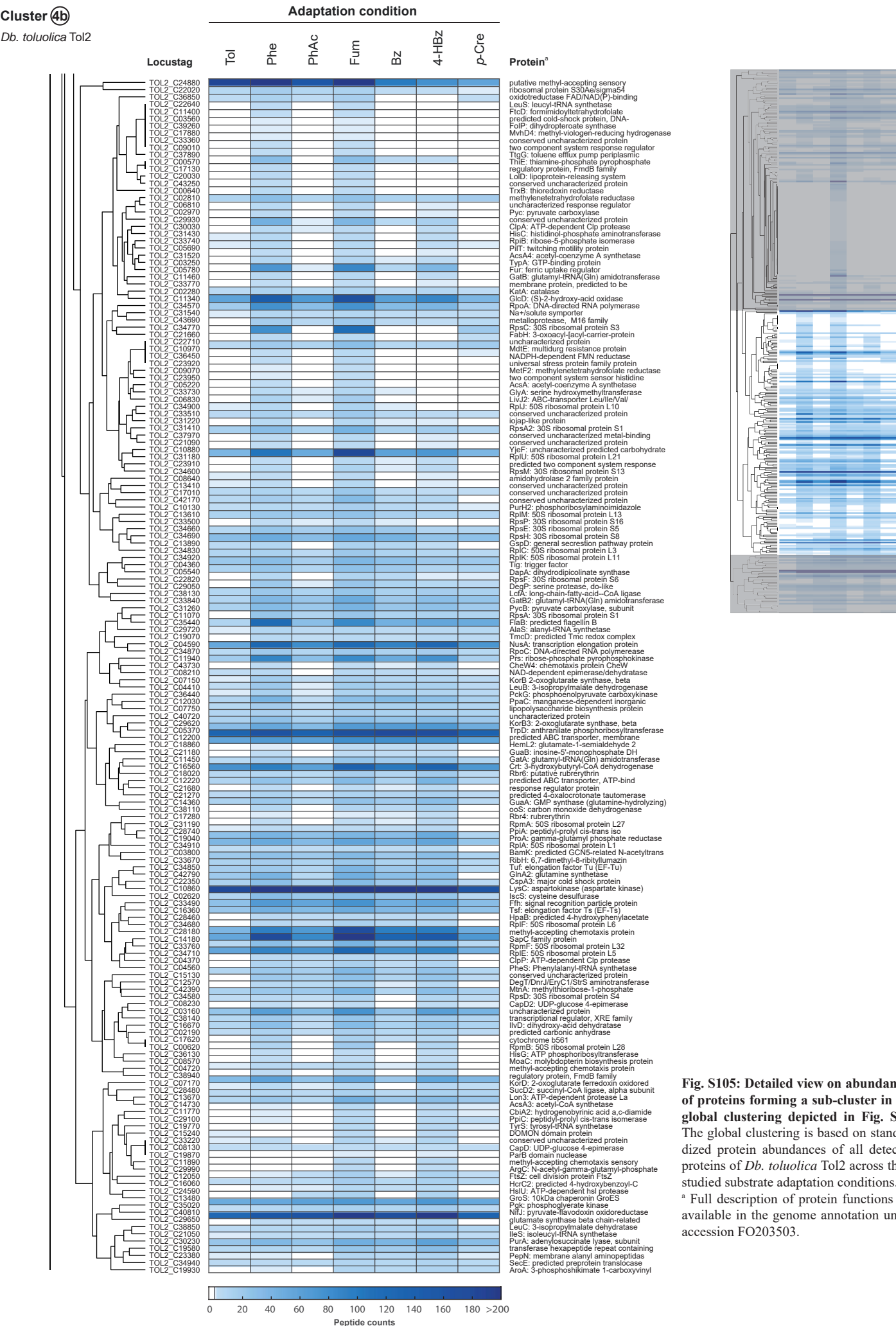
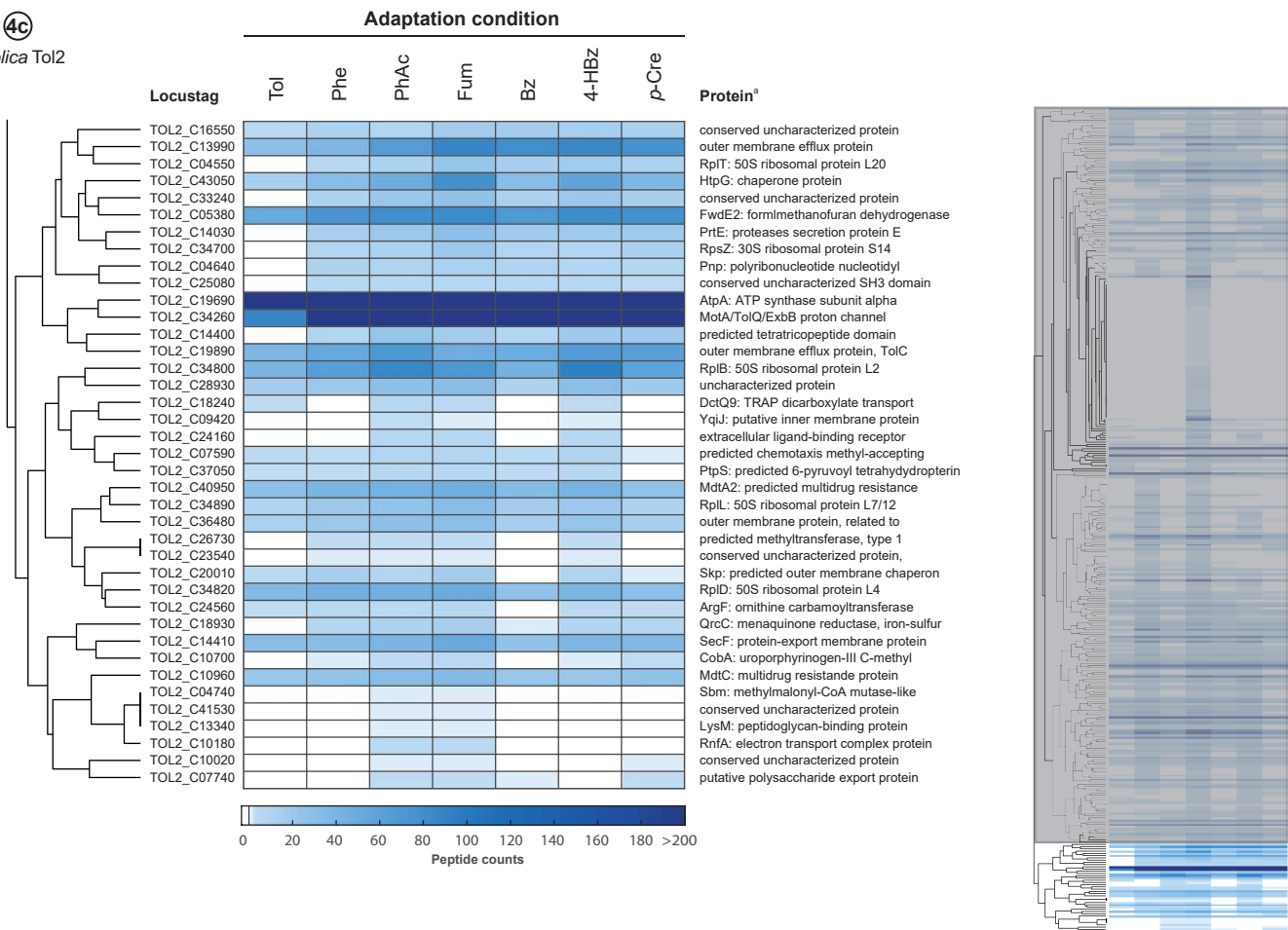


Fig. S104: Detailed view on abundances of proteins forming a sub-cluster in the global clustering depicted in Fig. S10. The global clustering is based on standardized protein abundances of all detected proteins of *Db. toluolica* Tol2 across the 7 studied substrate adaptation conditions. <sup>a</sup> Full description of protein functions are available in the genome annotation under accession FO203503.







**Fig. S106: Detailed view on abundances of proteins forming a sub-cluster in the global clustering depicted in Fig. S10.** The global clustering is based on standardized protein abundances of all detected proteins of *Db. toluolica* Tol2 across the 7 studied substrate adaptation conditions.

<sup>a</sup> Full description of protein functions are available in the genome annotation under accession FO203503.



## Cluster 5

Db. toluolica Tol2

## Adaptation condition

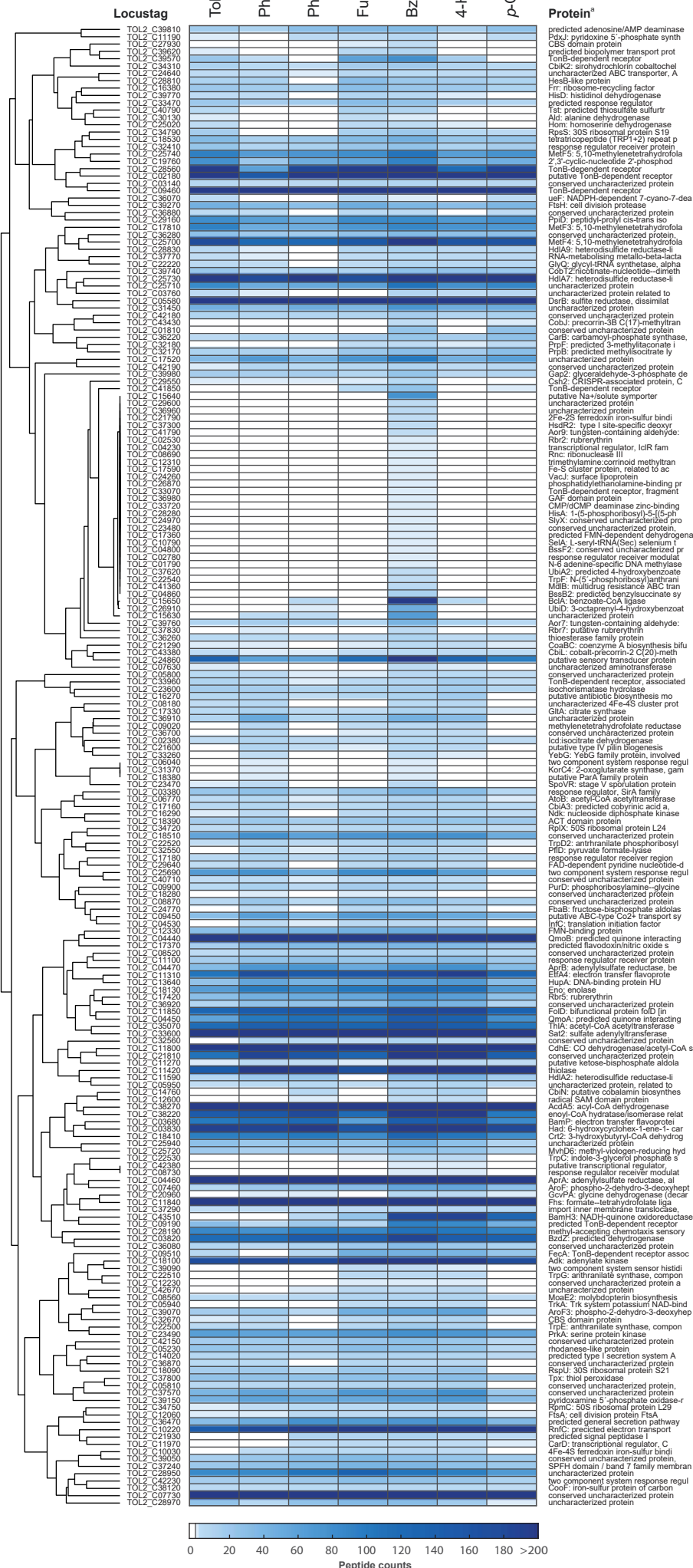


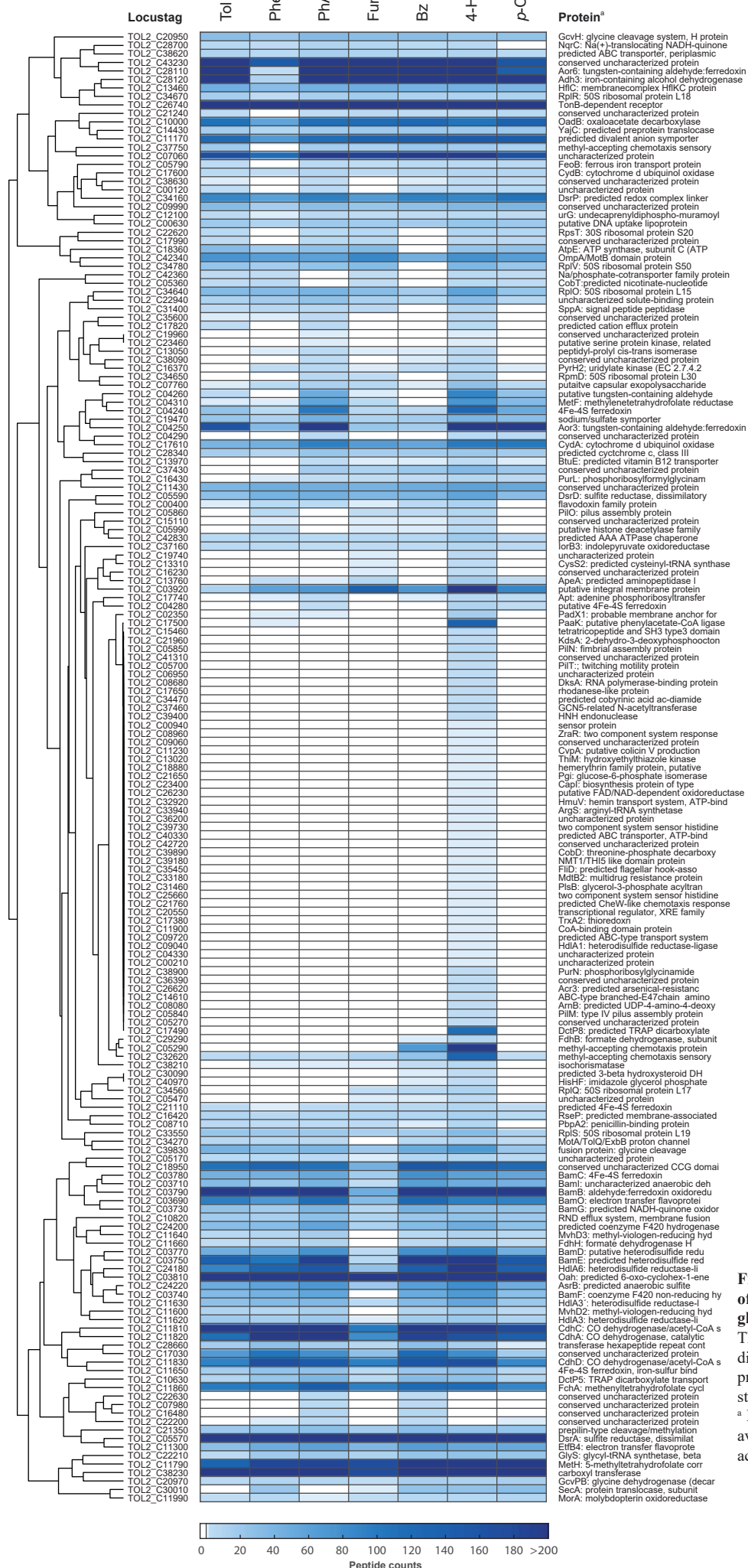
**Fig. S107: Detailed view on abundances of proteins forming a sub-cluster in the global clustering depicted in Fig. S10.** The global clustering is based on standardized protein abundances of all detected proteins of *Db. toluolica* Tol2 across the 7 studied substrate adaptation conditions.

<sup>a</sup> Full description of protein functions are available in the genome annotation under accession FO203503.

## Cluster 6

Db. toluolica Tol2

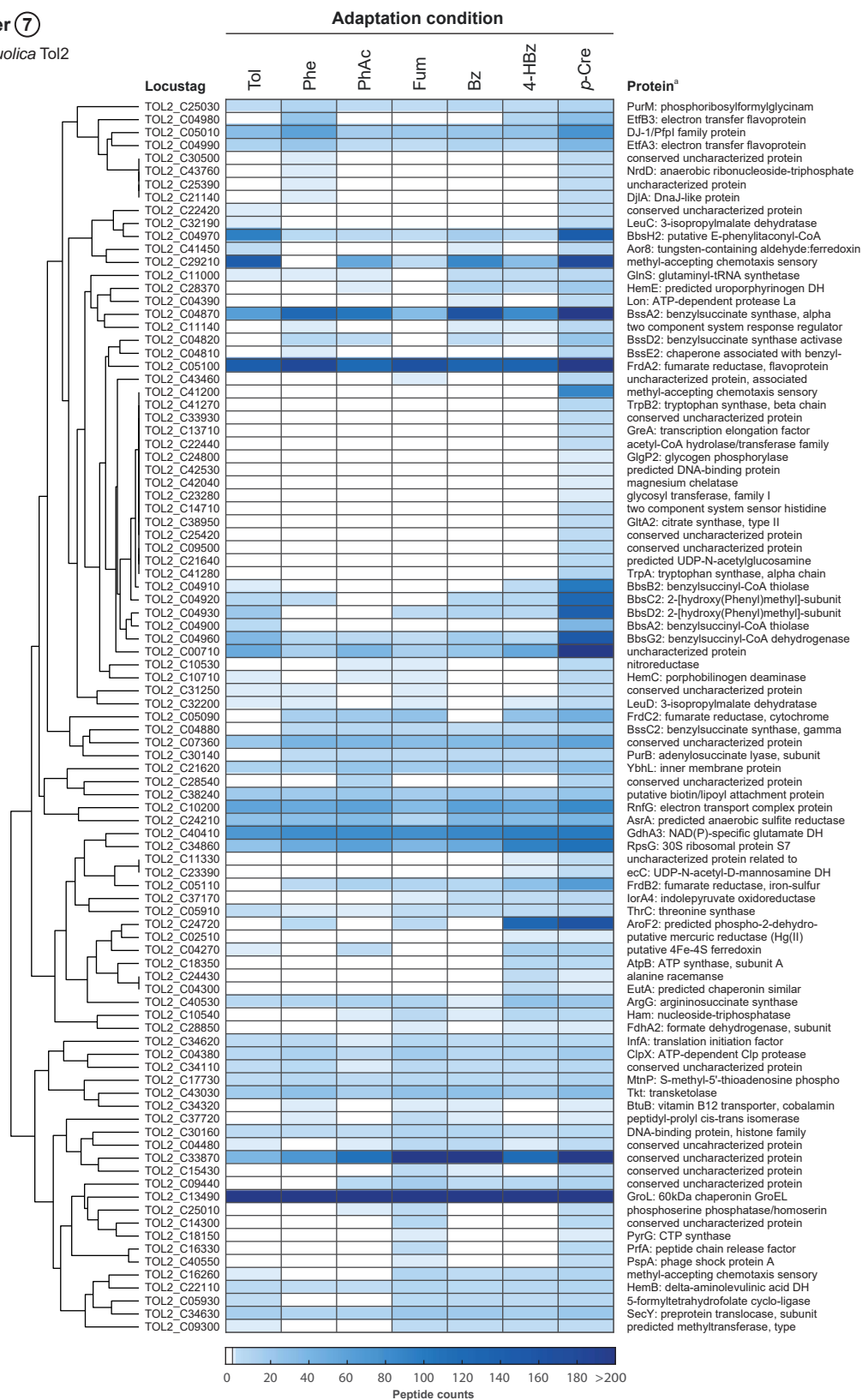
## Adaptation condition



**Fig. S108: Detailed view on abundances of proteins forming a sub-cluster in the global clustering depicted in Fig. S10.** The global clustering is based on standardized protein abundances of all detected proteins of *Db. toluolica* Tol2 across the 7 studied substrate adaptation conditions.

<sup>a</sup> Full description of protein functions are available in the genome annotation under accession FO203503.

## Cluster 7

*Db. toluolica* Tol2

**Fig. S109: Detailed view on abundances of proteins forming a sub-cluster in the global clustering depicted in Fig. S10.** The global clustering is based on standardized protein abundances of all detected proteins of *Db. toluolica* Tol2 across the 7 studied substrate adaptation conditions.

<sup>a</sup> Full description of protein functions are available in the genome annotation under accession FO203503.

# Cluster ①

*Dt. autotrophicum* HRM2

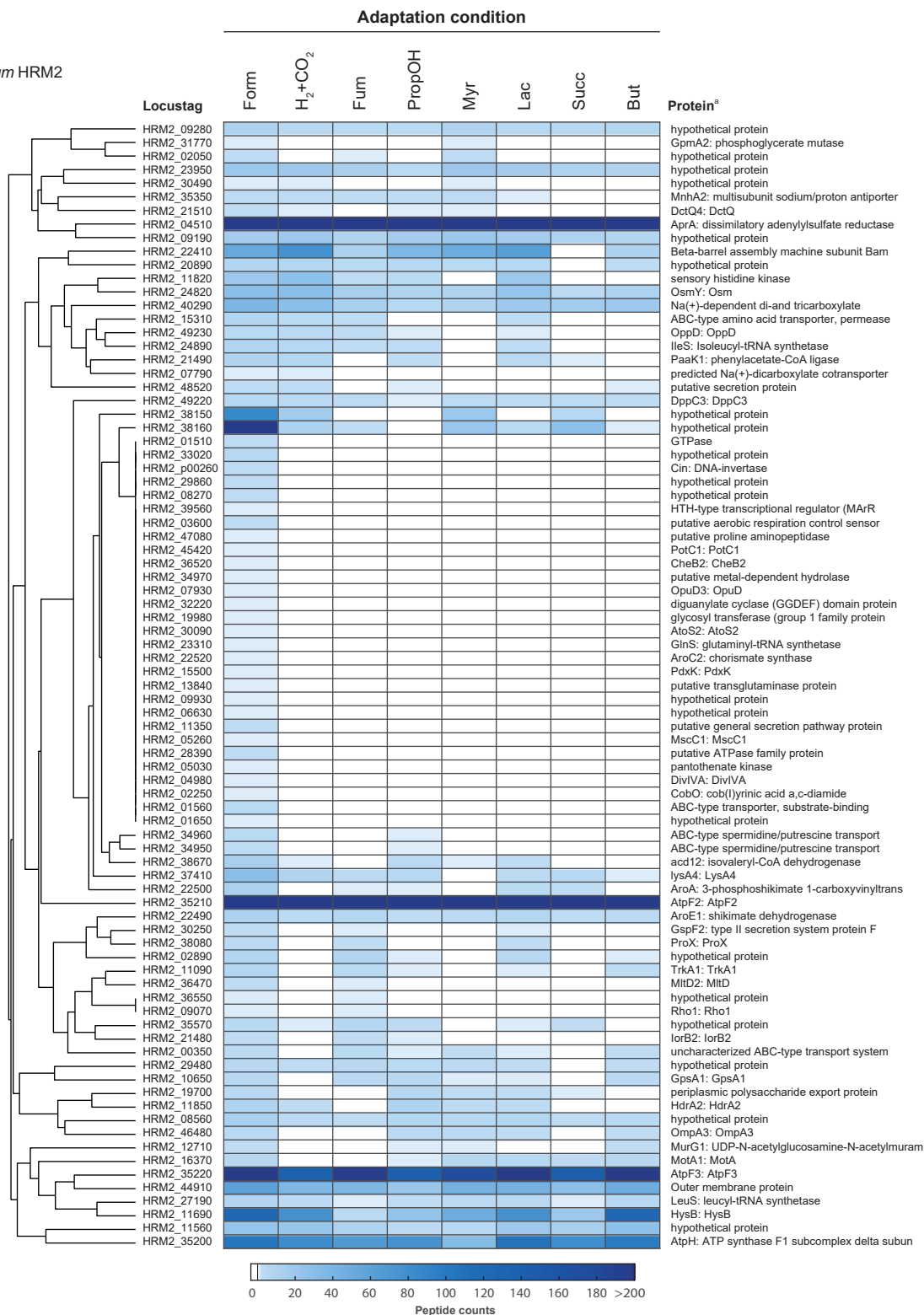
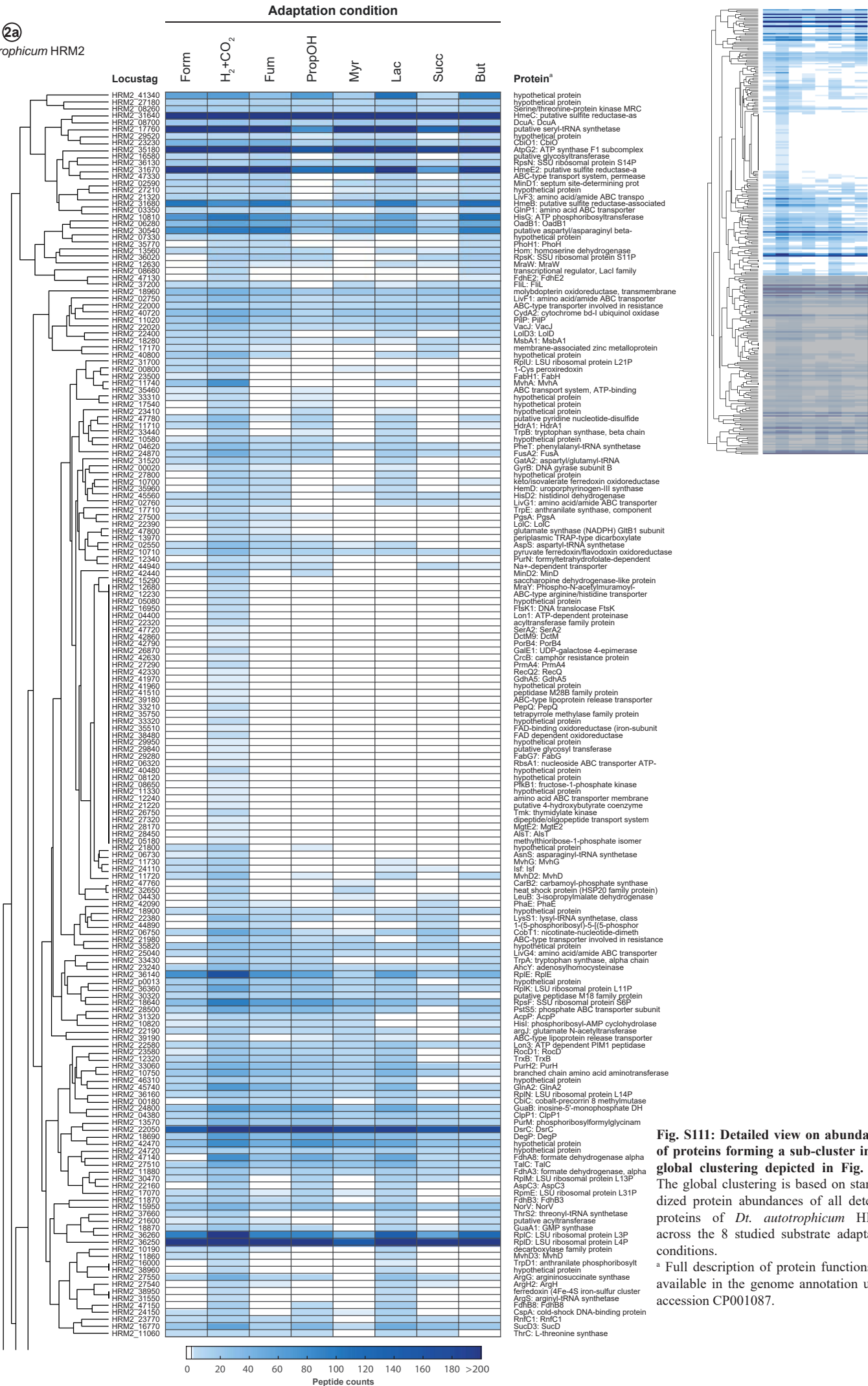


**Fig. S110: Detailed view on abundances of proteins forming a sub-cluster in the global clustering depicted in Fig. S11.** The global clustering is based on standardized protein abundances of all detected proteins of *Dt. autotrophicum* HRM2 across the 8 studied substrate adaptation conditions.

<sup>a</sup> Full description of protein functions are available in the genome annotation under accession CP001087.

Cluster 2a  
*Dt. autotrophicum* HRM2





Cluster 2b

*Dt. autotrophicum* HRM2

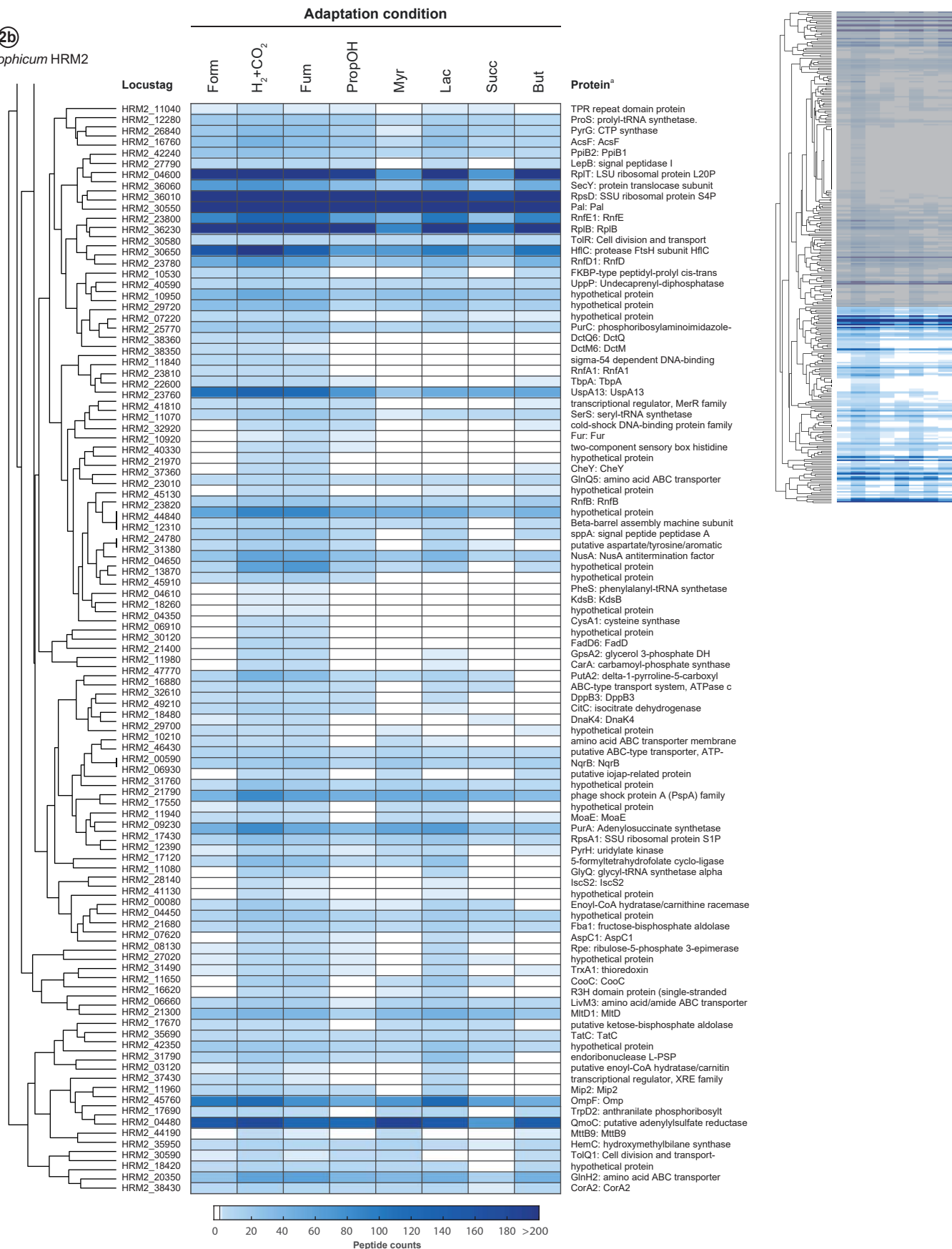


**Fig. S112: Detailed view on abundances of proteins forming a sub-cluster in the global clustering depicted in Fig. S11.** The global clustering is based on standardized protein abundances of all detected proteins of *Dt. autotrophicum* HRM2 across the 8 studied substrate adaptation conditions.

<sup>a</sup> Full description of protein functions are available in the genome annotation under accession CP001087.



Cluster 3  
*Dt. autotrophicum* HRM2

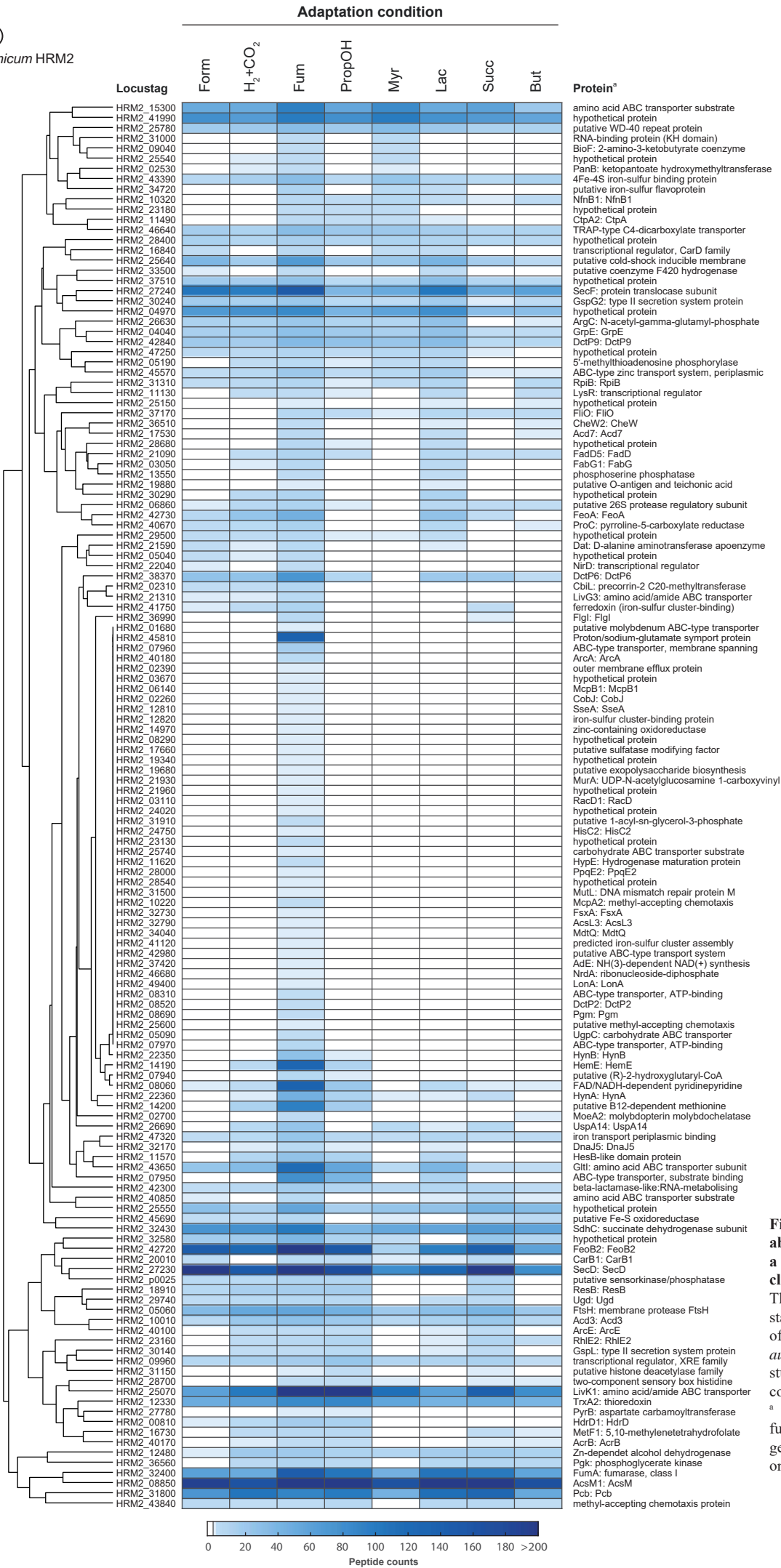


Fig. S113: Detailed view on abundances of proteins forming a sub-cluster in the global clustering depicted in Fig. S11. The global clustering is based on standardized protein abundances of all detected proteins of *Dt. autotrophicum* HRM2 across the 8 studied substrate adaptation conditions.

\* Full description of protein functions are available in the genome annotation under accession CP001087.

## Cluster 4a

*Dt. autotrophicum* HRM2

## Adaptation condition

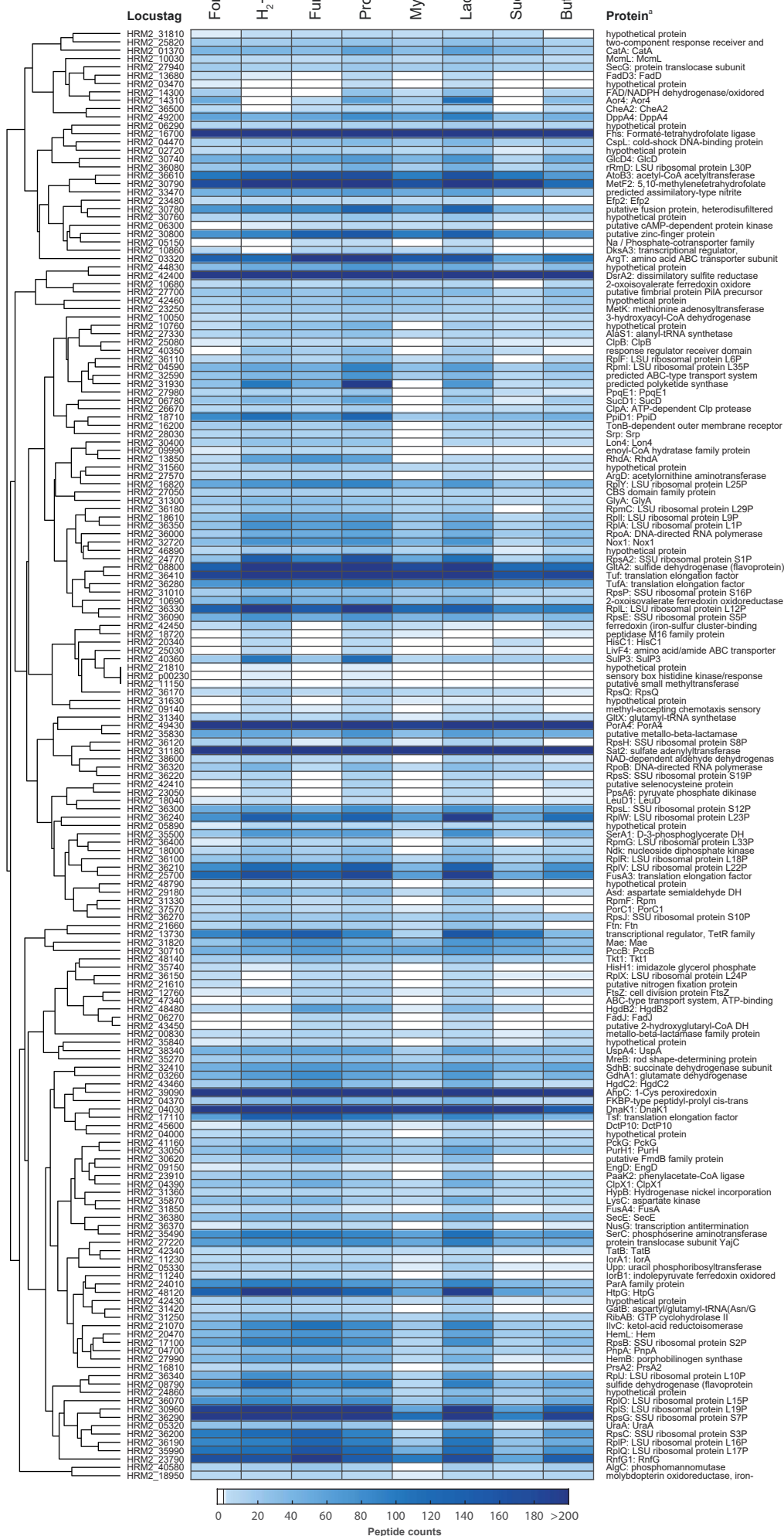


**Fig. S114: Detailed view on abundances of proteins forming a sub-cluster in the global clustering depicted in Fig. S11.** The global clustering is based on standardized protein abundances of all detected proteins of *Dt. autotrophicum* HRM2 across the 8 studied substrate adaptation conditions.

<sup>a</sup> Full description of protein functions are available in the genome annotation under accession CP001087.

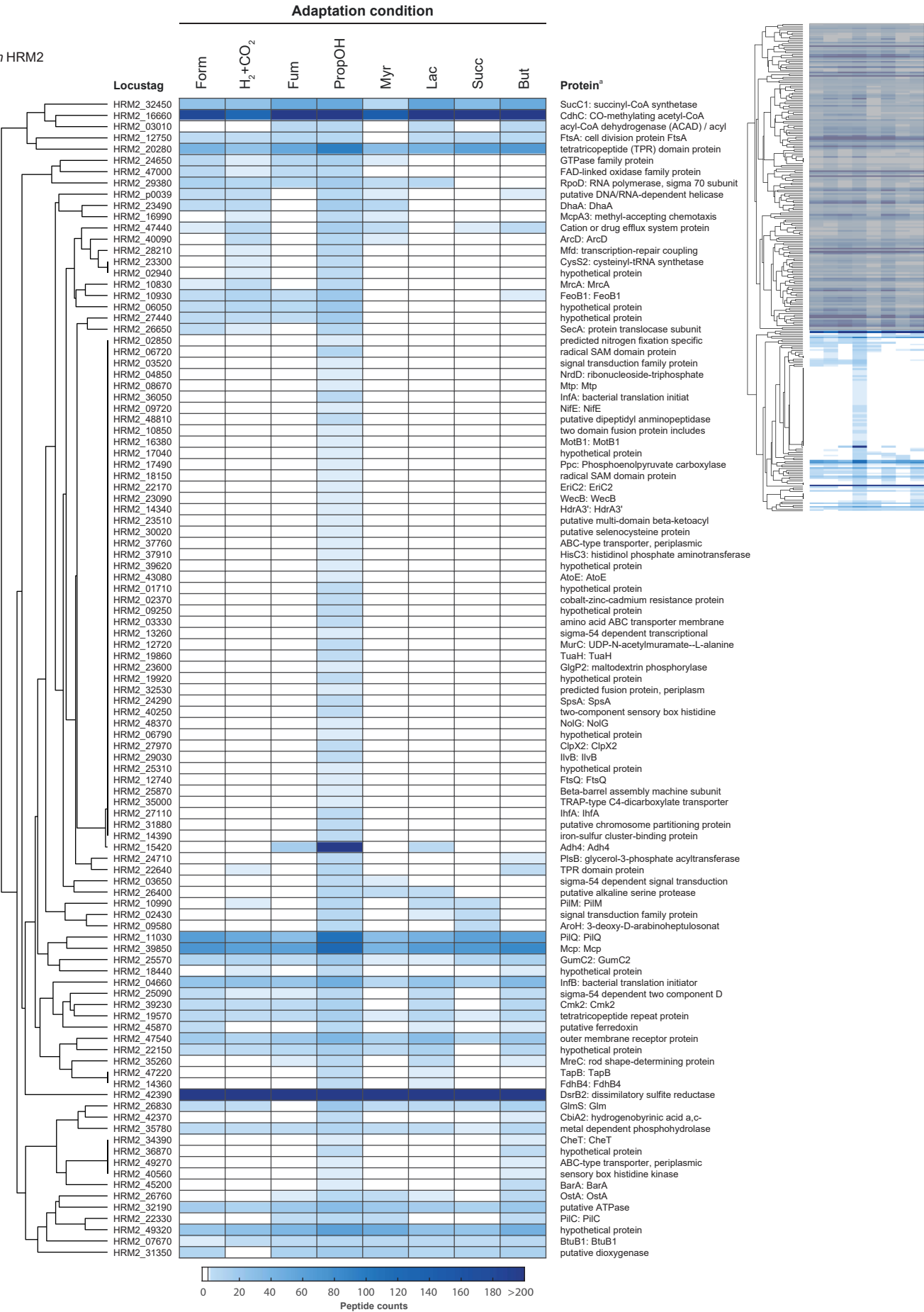
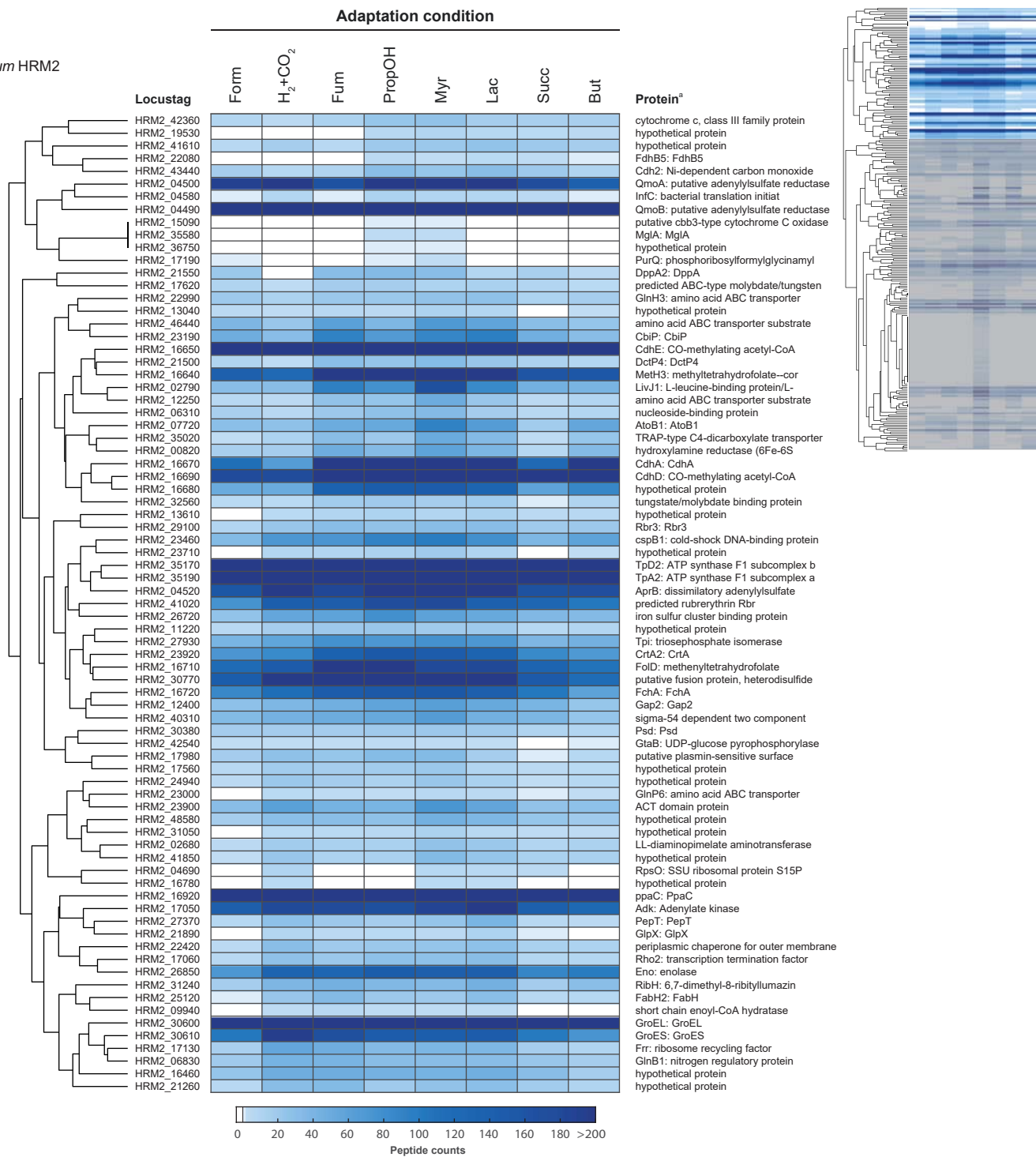


Fig. S115: Detailed view on abundances of proteins forming a sub-cluster in the global clustering depicted in Fig. S11. The global clustering is based on standardized protein abundances of all detected proteins of *Dt. autotrophicum* HRM2 across the 8 studied substrate adaptation conditions.

<sup>a</sup> Full description of protein functions are available in the genome annotation under accession CP001087.

Cluster ⑤  
*Dt. autotrophicum* HRM2



**Fig. S116:** Detailed view on abundances of proteins forming a sub-cluster in the global clustering depicted in Fig. S11. The global clustering is based on standardized protein abundances of all detected proteins of *Dt. autotrophicum* HRM2 across the 8 studied substrate adaptation conditions.  
<sup>a</sup> Full description of protein functions are available in the genome annotation under accession CP001087.

Cluster 5

Dt. autotrophicum HRM2

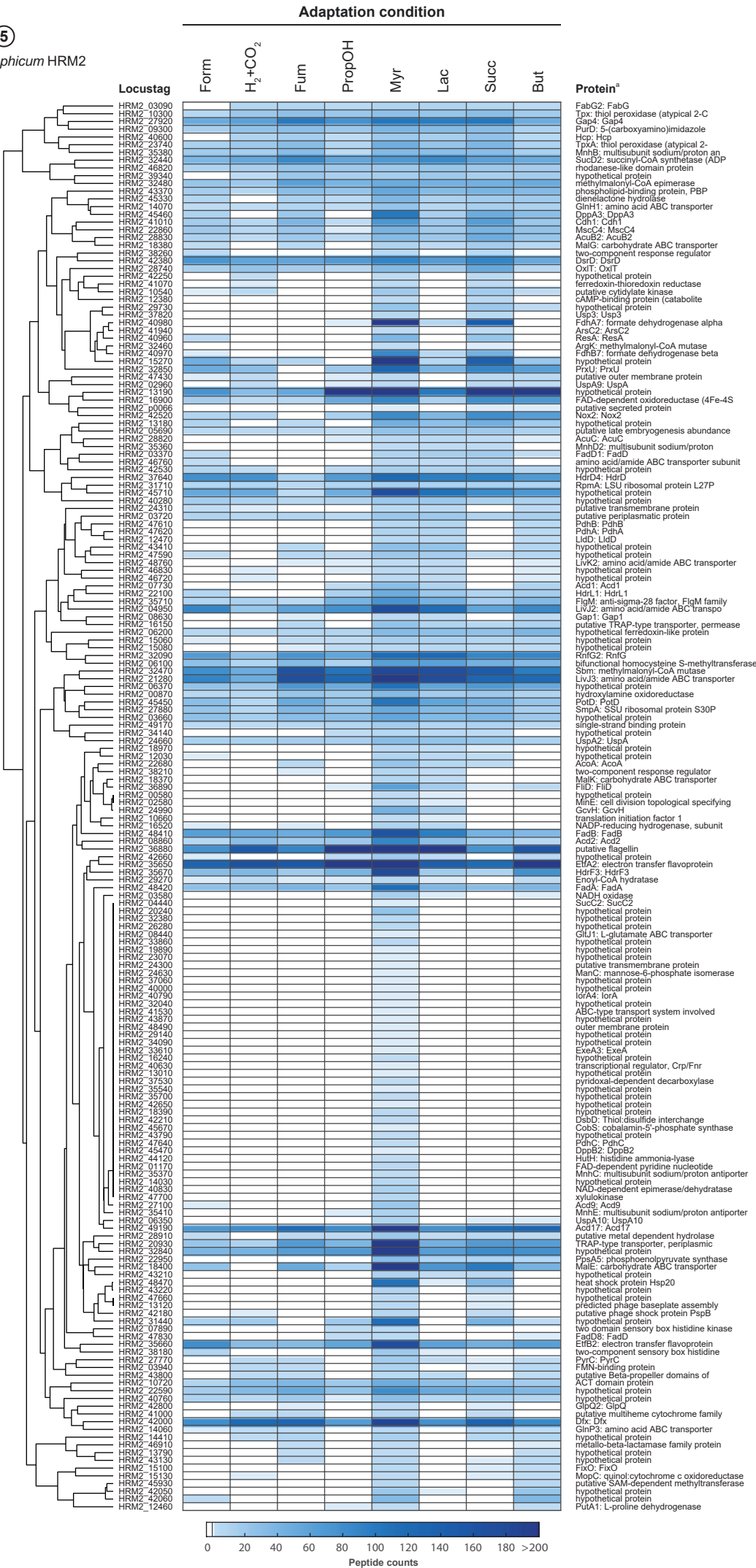


Fig. S117: Detailed view on abundances of proteins forming a sub-cluster in the global clustering depicted in Fig. S11. The global clustering is based on standardized protein abundances of all detected proteins of *Dt. autotrophicum* HRM2 across the 8 studied substrate adaptation conditions. <sup>a</sup> Full description of protein functions are available in the genome annotation under accession CP001087..



## Cluster 6

*Dt. autotrophicum* HRM2

## Adaptation condition

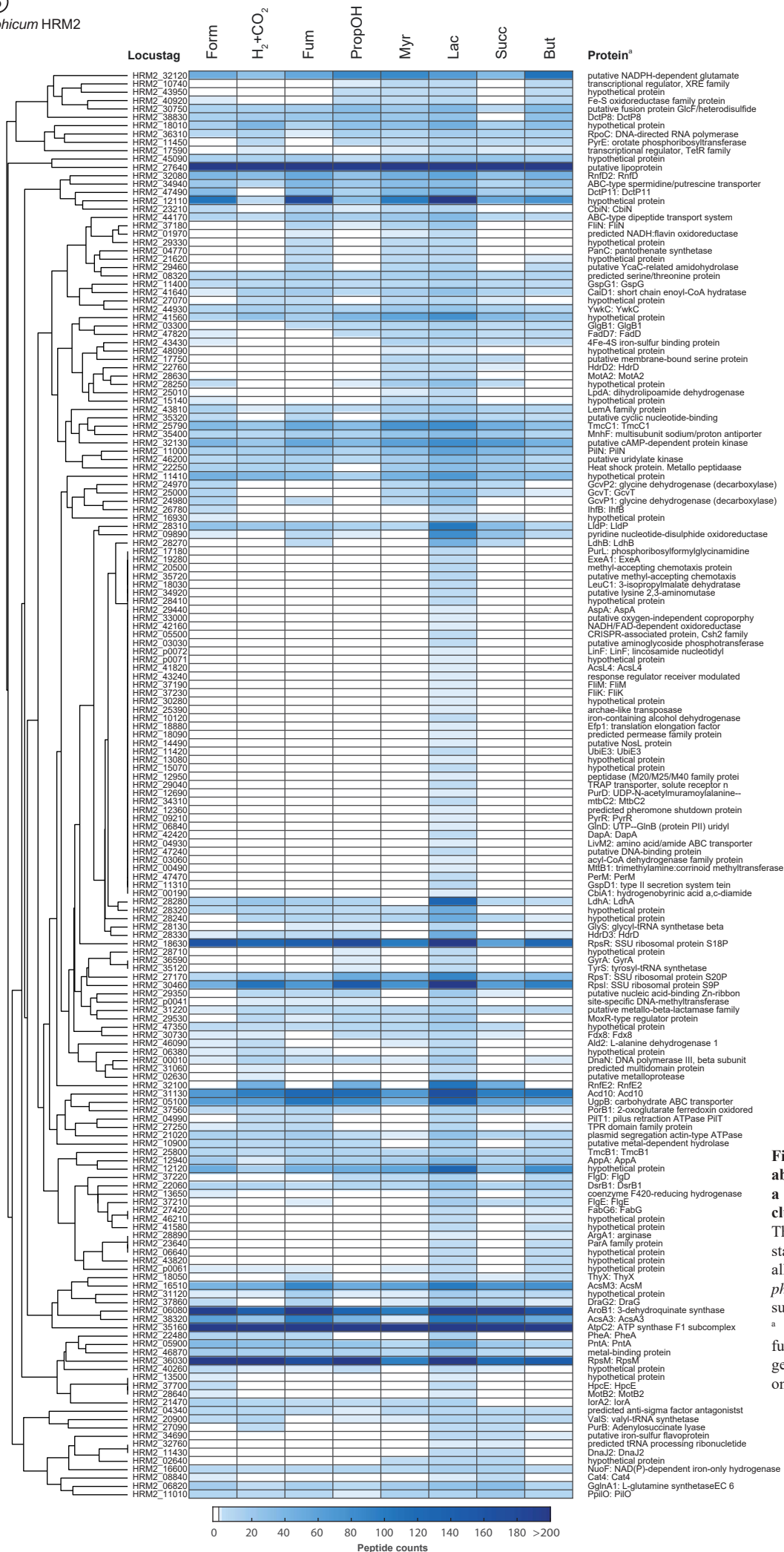


**Fig. S118: Detailed view on abundances of proteins forming a sub-cluster in the global clustering depicted in Fig. S11.** The global clustering is based on standardized protein abundances of all detected proteins of *Dt. autotrophicum* HRM2 across the 8 studied substrate adaptation conditions.

\* Full description of protein functions are available in the genome annotation under accession CP001087.



Cluster 7

Dt. autotrophicum HRM2

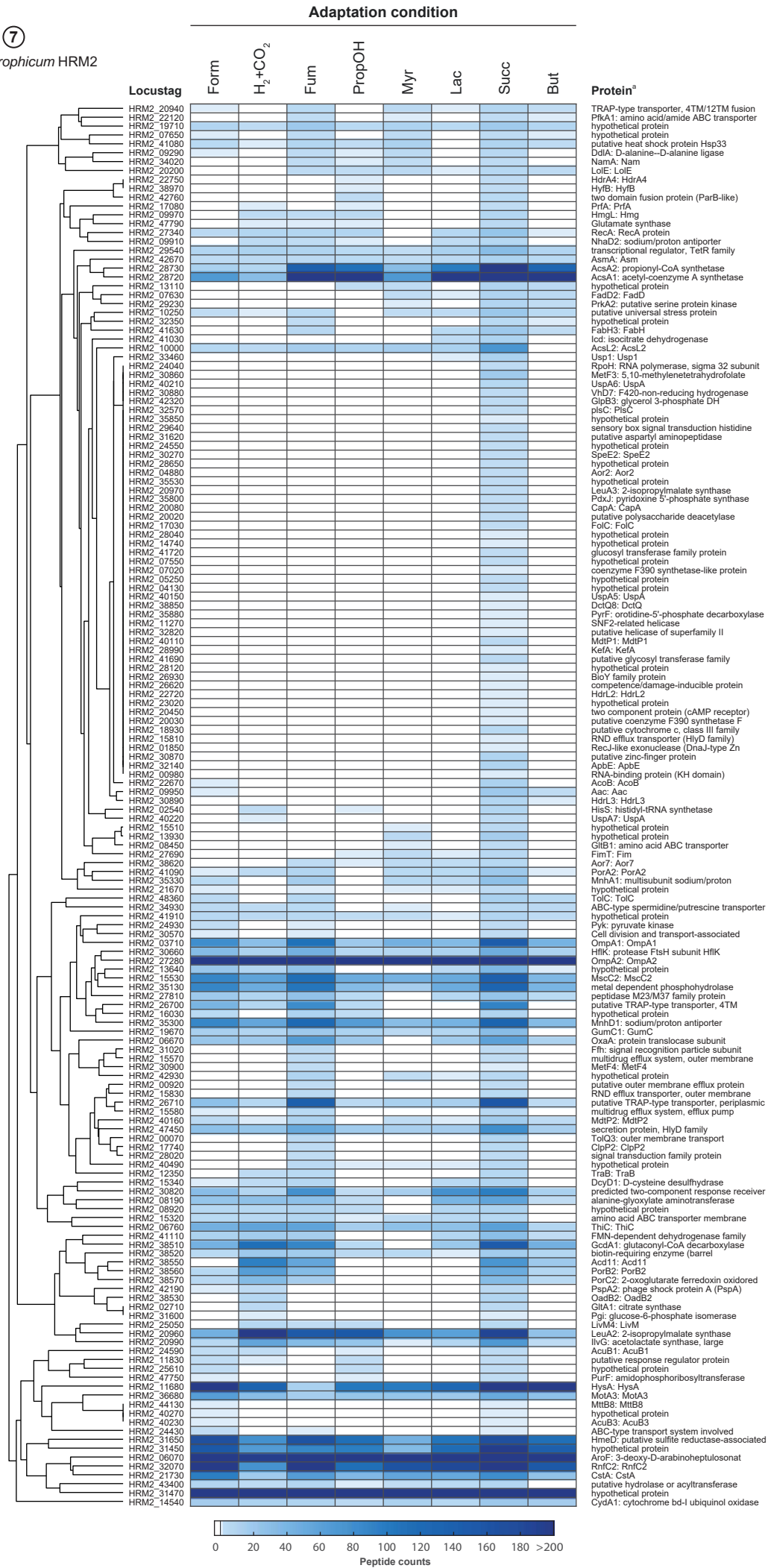
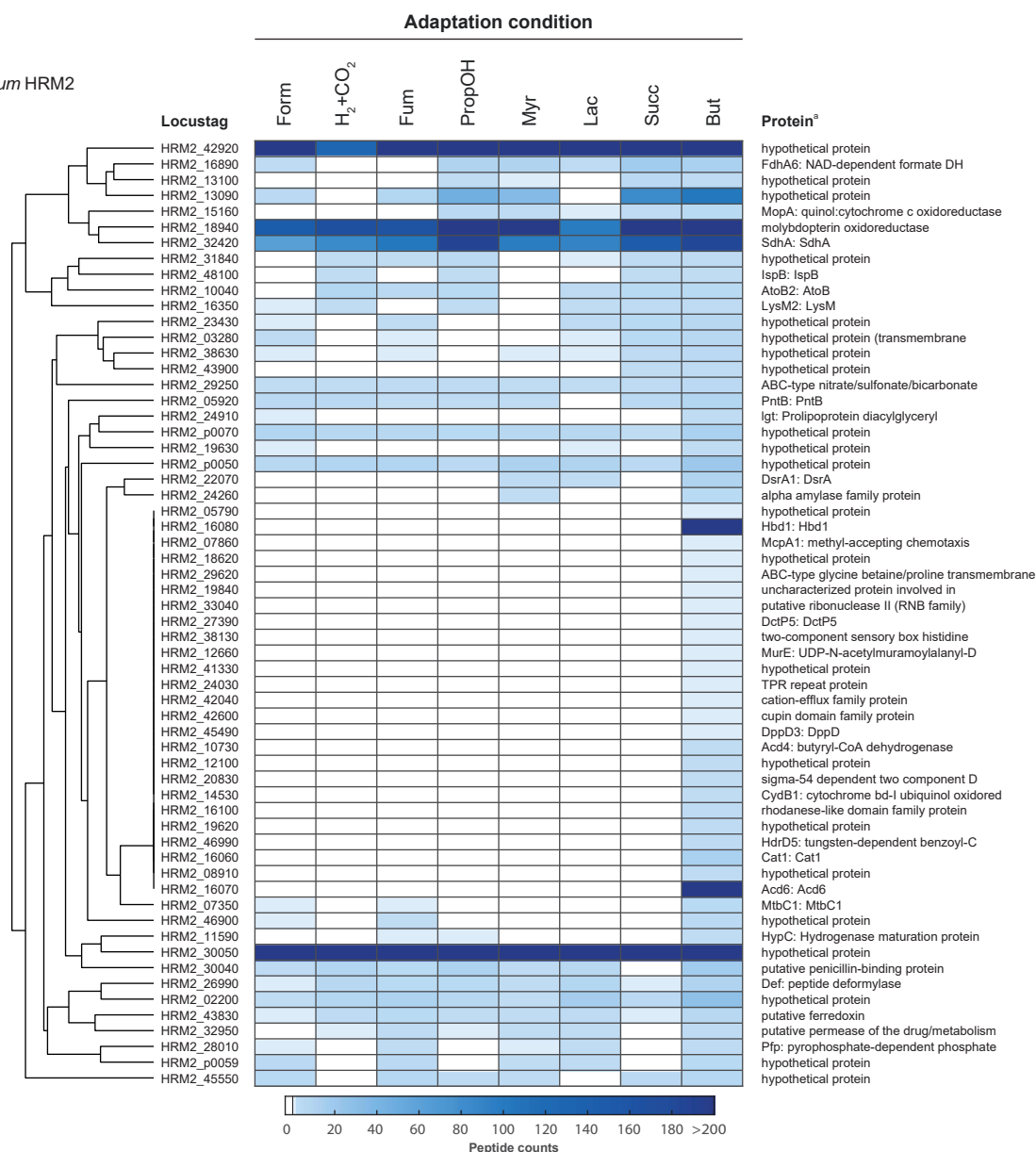


Fig. S119: Detailed view on abundances of proteins forming a sub-cluster in the global clustering depicted in Fig. S11. The global clustering is based on standardized protein abundances of all detected proteins of *Dt. autotrophicum* HRM2 across the 8 studied substrate adaptation conditions.

<sup>a</sup> Full description of protein functions are available in the genome annotation under accession CP001087.

# Cluster 8

*Dt. autotrophicum* HRM2



**Fig. S120: Detailed view on abundances of proteins forming a sub-cluster in the global clustering depicted in Fig. S11.** The global clustering is based on standardized protein abundances of all detected proteins of *Dt. autotrophicum* HRM2 across the 8 studied substrate adaptation conditions.

<sup>a</sup> Full description of protein functions are available in the genome annotation under accession CP001087.

## Supplementary Tables

**Table S1** Biogeography, habitats, and diversity of isolated strains belonging to *Desulfosarcina*, *Desulfococcus*, *Desulfobacula*, *Desulfobacterium* and *Desulfonema*.

Strain	Sample			Genome	
	Type	Location	Reference	Status	Reference
<i>Desulfosarcina</i> (9 isolated strains, 5 Species, 5 Genomes)					
<i>Ds. widdelii</i>					
PP31	Petroleum contaminated Marine shelf sediment	Shuaiba, Kuwait	(112)	complete	(113)
<i>Ds. ovata</i> subs. <i>Sediminis</i>					
28bB2T	Marine shelf sediment	Tokyo Bay, Japan	(114)	complete	(113)
oXyS1	Waterphase of an Oiltank	Wilhelmshaven, Germany	(115)	complete	(113)
<i>Desulfosarcina</i> sp.					
SD1	Mangrove sediment	Mtoni mangrove forest at Mzinga creek, Dar-es- Salaam, Tanzania	(116)	complete	(118)
BuS5	Marine hydrocarbon seep	Guaymas Basin, Gulf of California	(117)		
CME1	Estuarine sediment	Kysing Fjord, Norsminde, Denmark	(119)		
<i>Ds. alkanivorans</i>					
PL12	Petroleum contaminated Marine shelf sediment	Shuaiba, Kuwait	(120)	complete	(113)
<i>Ds. variabilis</i>					
3be13	Marine shelf sediment	Montpellier, France	(68)		
<i>Ds. cetonica</i>					
480	Oil recovery water	Aspheron Peninsula, Aserbaidshan	(121)		
<i>Desulfococcus</i> (4 isolated strains, 2 Species, 1 Genome)					
<i>Ds. multivorans</i>					
1be1	Marine shelf sediment	Montpellier, France	(68)	complete	(28)
<i>Ds. biacutus</i>					
KMRActS	Anaerobic digestor sludge	Marburg, Germany	(122)		
<i>Desulfococcus</i> sp.					
Hy5	Marine sediment	Rio marin, venice, Italy	(123)		
WHC	Intertidal sediment	Wilhelmshaven, Germany	(124)		
<i>Desulfobacula</i> (2 isolated strains, 2 Species, 2 Genomes)					
<i>Db. tuluolica</i>					
Tol2	Marine shelf sediment	Eel Pond, Falmouth, USA	(125)	complete	(27)
<i>Db. phenolica</i>					
Ph01	Marine sediment	Rio marin, venice, Italy	(126)	draft	(127)

**Table S1** continued

Strain	Sample			Genome	
	Type	Location	Reference	Status	Reference
<i>Desulfobacterium</i> (13 isolated strains, 4 Species, 1 Genome)					
<i>Dt. autotrophicum</i>					
HRM2	Marine sediment	Rio marin, Venice, Italy	(128)	complete	(129)
<i>Dt. catecholicum</i>					
NZva20	Marine shelf sediment	Delaware Bay, Nelson, New Zealand	(130)		
<i>Dt. indolicum</i>					
InO4	Marine sediment	Rio marin, Venice, Italy	(131)		
<i>Dt. niacini</i>					
NAV-1	Marine sediment	Rio marin, Venice, Italy	(132)		
<i>Dt. sp.</i>					
AK1	Estuarine sediment	New York-New Jersey Harbor estuary, USA	(133)		
LSv25	Marine shelf sediment	Hornsund, Svalbard, Norway	(134)		
BSv41	Marine shelf sediment	Van Mijenfjord, Svalbard, Norway	(135)		
mAB1	Saltmarsh/Marine sediment	Étang du Prévost	(135)		
W3A	Marine shelf sediment	Chesapeake Bay, Virginia, USA	(136)		
X2	Marine shelf sediment	Chesapeake Bay, Virginia, USA	(136)		
Cat2	Marine shelf sediment	North Sea coast, Germany	(123)		
HRM4	Marine sediment	Rio marin, Venice, Italy	(128)		
HRM6	Marine sediment	Rio marin, Venice, Italy	(128)		
<i>Desulfonema</i> (4 isolated strains, 3 Species, 1 Genome)					
<i>Dn. ishimotonii</i>					
Tokyo 01	Marine shelf sediment	Tokyo Bay, Japan	(137)	complete	(138)
Jade 02	Intertidal sediment	Jadebusen, Germany	(137)		
<i>Dn. limicola</i>					
5ac10	Intertidal sediment	Jadebusen, Germany	(139, 140)		(29)
<i>Dn. magnum</i>					
4be13	Marine shelf sediment	Étang du Prévost	(139, 140)		(29)

**Table S2** Biogeography and habitats of phylotypes affiliating with the *Desulfococcus/Desulfosarcina* cluster.

Sample type	Method	Sample location	Reference
Estuarine sediment	16S-rRNA and <i>dsrB</i> sequencing	Yangtze Estuary, China	(141)
Marine shelf sediment	16S-rRNA gene amplicon sequencing	Cape Lookout Bight, North Carolina, USA	(142)
Settling ponds and wetland sediment	16S-rRNA sequencing	Pennsylvania, USA	(143)
Seeding sludge	16S-rRNA sequencing	Hongkong, China	(144)
Marine shelf sediment	16S-rRNA sequencing	Jansand, Germany; Courseulles-sur-Mer, Mont St. Michel, France	(145)
Estuarine to marin bay waters	16S-rRNA and <i>dsrAB</i> sequencing	Adour estuary, France	(146)
Saltmarsh sediment	16S-rRNA and <i>dsrB</i> sequencing	Yancheng Nature Reserve, China	(147)
Wetland	16S-rRNA sequencing	North Dakota, USA	(148)
Marine shelf sediment	16S-rRNA sequencing	Ría de Vigo, Spain	(149)
Saline lake reservoir	16S-rRNA, FISH, PLFA	Lake Grevelingen, The Netherlands	(150)
Hypersaline lake/marine shelf sediment	16S-rRNA sequencing	Great salt lake, Utah, USA	(151)
Coid grain surfaces of marine and Terrestrial spots	16S-rRNA sequencing	Pigeon Cay, The Bahamas	(152)
Sublake/ lake/ freshwater reservoir	16S-rRNA sequencing, EL-FAME	Maojiabu and Xilihu, Hangzhou, China	(153)
Uranium contaminated aquifer	16S-rRNA and <i>dsrA</i> sequencing	Oak ridge, Tennessee, USA	(154)
Marine shelf sediment	AAMG	Rabigh coast, Saudi-Arabia	(155)
Meromictic lake	16S-rRNA sequencing	Lake Cadagno, Swiss Alps	(156)
Marine shelf sediment	16S-cDNA sequencing	Mira channel, Portugal	(157)
Rhizospheres from seagrasses	16S-rRNA gene amplicon sequencing	Culatra Island, Faro, Portugal	(158)
Methane seep/deep sea sediment	16S-rRNA and <i>aprA</i> sequencing, FISH-NanoSIMS	Southern ridge, California, USA; Mound 12, Costa rica	(159)
Methane seep/deep sea sediment	16S-rRNA, FISH/CARD-FISH, BONCAT	Santa monica Basin, California, USA; Hydrate ridge, Gulf of Mexico	(160)
Saline lake reservoir	16S-rRNA and <i>aprA</i> sequencing	Lake Grevelingen, The Netherlands	(161)
Subtropical freshwater reservoirs	16S-rRNA pyro-sequencing	Queensland, Australia	(162)
Deep sea sediment; shelf sediment	16S-rRNA pyro-sequencing	Skagerrak; Bothnian bay, Baltic/north sea	(163)
Marsh/estuarine sediment	<i>dsrAB</i> , RFLP	Shanyutan, China	(164)
Mangrove wetland	16S-rRNA sequencing	Jimei district, Xiamen City, China	(165)
Deep sea sediment	16S-rRNA sequencing	Gulf of Mexico	(166)
Hydrothermal sediment	16S-rRNA, CARD-FISH	Guaymas Basin, Gulf of California, Mexico	(167)
Oil contaminated desert soils	16S-rRNA, ARISA	north of Oman	(168)
Crude oil contaminated marsh	Metagenomic analysis	Bay Jimmy, Louisiana, USA	(169)
Mangrove soil	<i>dsrB</i> , DGGE	Red sea coast, Jeddah, Saudi-Arabia	(170)
Deep sea sediment/cold seep	16S-rRNA, ARISA	Sonora Margin, Guaymas Basin, Gulf of California, Mexico	(171)
Landfill	16S-rRNA sequencing	Jinjianpu landfill, China	(172)
Salt marh sediment	16S-rRNA sequencing	Bayou La Batre, Alabama, USA	(173)
Marine watercolumn	16S-rRNA, <i>dsrB</i> , DGGE	Gdansk Bay, Baltic Sea	(174)
Intertidal mudflat	16S rRNA gene-Illumina Miseq sequencing	Sansha bay, Fuan, China	(175)
Marine shield sediment	16S-rRNA, <i>dsrB</i> sequencing, SIP	Aarhus Bugt, Denmark	(176)
Hydrothermal vent system	16S-rRNA, <i>dsrB</i> , FISH, CSLM	Central Bay, Prony, New Caledonia	(177)
Coastal seawater	16S-rRNA sequencing	Key West, Florida, USA	(178)
Intertidal mangrove zone	16S-rRNA sequencing	Lim Chu Kang, Singapore	(179)
Landfill	16S-rRNA gene pyrosequencing	Laohukeng, ShenZhen, China	(180)
Marine shelf sediment	16S-rRNA gene pyrosequencing	Busan New Port, North Port, South Korea	(181)
Rice paddy soils	16S-rRNA sequencing	Guiyang city, China	(182)
Oil Sands Composite Tailings Deposit	16S-rRNA sequencing, PFLA	Kingfisher CT deposit, Canada	(183)
Coastal microbial mat	16S-rRNA sequencing	Shark bay, Australia	(184)
Petroleum-hydrocarbon-contaminated Marine sediment	16S-rRNA sequencing	Hong-Kong, China	(185)
Petroleum reservoir	16S-rRNA, <i>dsrB</i> , FLASH	Xinjiang Luliang Oil Field, China	(186)
Hydrothermal, metalliferous Marine sediments	masD/assA amino sequences	Chowder Hill, Juan de Fuca Ridge	(187)
Salt marsh sediment	16S-rRNA, T-RFLP, SIP	Talbert salt marsh, California, USA	(188)
Sea cucumber gut	16S-rRNA gene pyrosequencing	Quingdao, China	(189)
Coastal wetland	16S-rRNA sequencing	Magnolia/Talbert marsh, California, USA	(190)
Eutrophic, meromictic lake	16S-rRNA/ <i>aprA</i> , CARD-FISH	Lake Harutori, Hokkaido, Japan	(191)
Deep sea sediment	16S-rRNA, TEFAP	Eastern Mediterranean Levantine Basin	(192)
Boreal acid sulphate soil	CARD-FISH, EL/NEL-PLFA	AS soil near Helsinki, Finland	(193)

**Table S2** continued

Sample type	Method	Sample location	Reference
Cold seep/deep sea sediment	16S-rDNA, FISH	Sonora Margin, Guaymas Basin, Gulf of California, Mexico	(171)
Saline solis from barren land	16S-rRNA, <i>apsA</i> sequencing	Arabian Sea coast, Gujarat, India	(194)
Marine shelf sediment/deepsurface fluid	SSU rRNA sequencing	Juan de Fuca Ridge	(195)
Seep sediment/deep sea sediment	FISH-nanoSIMS	Mound 12, Costa Rica	(196)
Seep sediment/deep sea sediment	CARD-FISH, SIP	Amon mud volcano, Nile deep-sea in the mediterranean sea	(197)
Pond in a pyrite mine	16S-rRNA sequencing	Rudawy Janowickie Mountains, Poland	(198)
Marine shelf sediment	SSU-rRNA sequencing and lipid sequence via HPLC, FLEC	Highborne Cay, The Bahamas	(199)
Marine shelf sediment	16S-rRNA pyrosequencing	Port of Aveiro, Atlantic coast, Portugal	(200)
Seep sediment/deep sea sediment	16S-rRNA, nanoSIMS	Hydrate ridge, Gulf of Mexico	(201)
Estuarine sediment	16S-rRNA, DGGE	Colne estuary, Essex, UK	(202)
Natural corrosion deposits from marine Steel structures	16S-rRNA, <i>dsrB</i> , DGGE	carbon steel sheet piles of a European harbor	(203)
Marine oil fields	<i>dsrB</i> , DHPLC, DGGE	MOB11, Brazil; MOB12A/B, USA	(204)
Deep-sea methane seeps	16S-rRNA, ARISA, CARD-FISH	Wairarapa Takahae, New Zealand	(205)
Mesotrophic and oligotrophic lake	<i>aprA</i> sequencing	Lake Biwa; Lake Okotanpe, Japan	(206)
Hydrothermal sediment	16S-rRNA, CARD-FISH	Yonaguni Knoll IV, southern Okinawa Trough	(24)
Seep sediment/deep sea sediment	16S-rRNA, GC-MS	Cinarcik Basin, Marmara Sea	(207)
Estuarine microbial mat	SSU-rRNA sequencing	Elkhorn Slough estuary, California, USA	(208)
Tidal flat area	16S-rRNA, DGGE	Spiekeroog Island, Germany	(209)
Hydrocarbon seep/deep sea sediment	16S-rRNA, CARD-FISH	Gulf of Mexico	(210)
River water/sediment	16S-rRNA sequencing	Taif River, Taif, Saudi Arabia	(211)
Deep sea mud volcano	CARD-FISH	Isis mud volcano, Mediterranean Sea	(212)
Paddy field	16S-rRNA sequencing	Fukutsu, Japan	(213)
Intertidal mudflat, mangrove sediment	16S-rRNA sequencing	Mai Po Ramsar wetland, Hong-Kong	(214)
Hydrothermal deep sea sediment	16S-rRNA, FISH	Chowder Hill hydrothermal vent field, Juan de Fuca ridge	(215)
Hg enriched river sediment	16S-rRNA sequencing	South River, Virginia, USA	(216)
Marine shelf sediment	16S-rRNA, DGGE	Porto Marghera, Venice, Italy	(217)
River/estuarine sediment	<i>dsrB</i> , DGGE	Danshuei River estuary, Taiwan	(218)
Cold mineral spring	16S-rRNA, <i>dsrB</i> , oligonucleotide hybridization	Ust'Kachka resort, Russia	(219)
Polluted microbial mat	16S-rRNA, slot-blot hybridization	Wadi Gaza, Gaza Strip, Palestine	(220)
Marine microbial mat	16S-rRNA sequencing	Island Schiermonnikoog, The Netherlands	(221)
Submarine spring	16S-rRNA sequencing	Jewish Sink, Gulf of Mexico	(222)
Seep sediment/deep sea sediment	16S-rRNA, CARD-FISH	Nile Deep Sea Fan, Mediterranean Sea	(223)
Coal oil point seep	<i>dsrAB</i> sequencing	Tonya Seep, California, USA	(224)
Deep sea sediment	16S-rRNA, DGGE	Nyegga G11 pockmark, Offcoast Norway	(225)
Haloalkaline lake	16S-rRNA, ARDRA	Lake Elmenteita, Kenya	(226)
Hydrothermal deep sea sediment	16S-rRNA, CARD-FISH	Logatchev hydrothermal field, north Atlantic Ocean	(227)
Meromictic lake	16S-rRNA, CARD-FISH	Lake Cadagno, Alps, Switzerland	(228)
Methane seep/deep sea sediment	16S-rRNA, DGGE, CARD-FISH	Basin off Sumatra, Indian Ocean	(229)
Deep sea sediment	<i>dsrA</i> , <i>aprA</i> sequencing	Black Sea	(230)
Marine oxygen-minimum-zone	16S-rRNA, <i>dsr</i> , <i>apr</i> sequencing	Off the Chilean Coast	(5)
Shallow marine hydrothermal sediment	16S-rRNA, <i>dsrAB</i> , RFLP	Nea Kameni Island, Greece	(231)
Spring water	16S-rRNA sequencing	Zodletone Spring, Oklahoma, USA	(232)
Deep sea/methane seep sediment	16S-rRNA, FISH/CARD-FISH	Hydrate ridge, Gulf of Mexico	(233)
Marine shelf sediment	16S-rDNA, DGGE	Emerald Basin, Halifax Harbour, Canada	(234)
Intertidal sediment	16S-rRNA, <i>dsrAB</i> , <i>aprA</i> , FISH	Wadden Sea, Germany	(235)
Marine shelf sediment	16S-rRNA, FISH	Cabreara national Park, Balearic Islands	(236)
Deep sea sediment	16S-rRNA, <i>dsrAB</i> , FISH	Santa barbara Basin, California, USA	(237)
Hydrocarbon polluted estuarine sediment	16S-rRNA, <i>dsrAB</i> sequencing, PLFA	Pearl river Estuary, China	(238)
Hypersaline brine pool/deep sea	16S-rRNA, <i>dsrAB</i> , sequencing	Gulf of Mexico	(239)
Cold seep/deep sea sediment	16S-rRNA sequencing	Larsen B area, Weddell, Antarktika	(240)
Cave sediment	16S-rRNA, DGGE	Altamira cave, Spain	(241)
Anoxic tidal fjord	SSU-rRNA, RFLP	Nitinat Lake, British Columbia, Canada	(242)
Estuarine intertidal flat	16S-rRNA, Mag-SIP	Oosterschelde Estuary, The Netherlands	(243)
Deep sea sediment	16S-rRNA, <i>dsrAB</i> , DGGE	Green Canyon Region, Gulf of Mexico	(244)



**Table S2** continued

Sample type	Method	Sample location	Reference
Petroleum polluted marine sediment	16S-rRNA, <i>dsrAB</i> sequencing	Boston harbor, Massachusetts, USA	(245)
Deep sea sediment	16S-rRNA sequencing	Mid-Chilean Margin, Chile	(246)
Riversediment	16S-rRNA, T-RFLP	River Lahn, Marburg, Germany	(247)
Marine shelf sediment	16S-rRNA, probe hybridization	Étang de Berre, France	(248)
Estuarine sediment	16S-rRNA, T-RFLP	Hayle estuary, Fal estuary, Kingsbridge estuary, Cornwall and Devon, South West England, UK	(249)
Deep sea microbial mat/sediment	16S-rRNA, FISH/CARD-FISH	Nile Deep Sea fan, Mediterranean Sea	(250)
Shelf sediment/microbial mat	16S-rRNA, CARD-FISH, FAME	Gullfaks, Tommeliten, North Sea	(251)
Deep sea microbial mat/sediment	16S-rRNA, CARD-FISH	GHOSTDABS Field, Black Sea	(252)
Riversediment	16S-rRNA, <i>dsrB</i> , DGGE, PFLA	Meuse, Rhine, Overijsselse Vech, The Netherlands	(253)
Cold seep/deep sea sediment	16S-rRNA, CARD-FISH	Gulf of Mexico	(254)
Marine oligochaetes	16S-rRNA, <i>dsrAB</i> , <i>aprA</i> , FISH	Island of Elba, Mediterranean Sea, Italy	(255)
Lakesediment	16S-rRNA, FISH	Lake Aha, China	(256)
Hypersaline pond	16S-rRNA, nanoSIMS, CARD-FISH	Exportadora De Sal, Baja California Sur, Mexico	(257)
Marine shelf sediment	16S-rRNA, DGGE	Paletta Creek, California, USA	(258)
Cold seep/deep sea sediment	16S-rRNA sequencing	Kazan mud volcano, Mediterranean Sea	(259)
Extremely hypersaline lake sediment	16S-rRNA, <i>dsrAB</i> , RFLP	Great salt lake, Utah, USA	(260)
Cold seep/deep sea sediment	16S-rRNA, FISH	Mosby Mud Volcano, Norwegian-Barents-Spitzbergen continental margin	(261)
Estuarine/riversediment	<i>dsrA</i> sequencing	River Colne Estuary, Essex, UK	(262)
Microbial mat, calcified deep sea reef	16S-rRNA, CARD-FISH	Crimean Peninsula, Black Sea	(263)
Deep sea sediment	16S-rRNA, T-RFLP, DGGE, PLFA	Skagerrak, Denmark	(264)
Deep sea sediment	16S-rRNA, DGGE	Benguela Upwelling System, Namibia	(265)
Saltmarsh	16S-rRNA, FISH	Little Sippewissett salt marsh, Massachusetts, USA	(266)
Hydrocarbon polluted shelf sediment	16S-rRNA, RISA	Canal viell cove, France	(267)
Anoxic watercolumn	16S-rRNA, <i>dsrA</i> sequencing	Western central Basin, Black Sea	(268)
Intertidal soil and intertidal mudflat	16S-rRNA, <i>dsrAB</i> , DGGE	River Rhine, Rozenburg, The Netherlands	(269)
Meromictic lake sediment/water	<i>dsrA</i> sequencing	Lake Suigetsu, Fukui, Japan	(270)
Mud volcano, deep sea sediment	16S-rRNA, RFLP	Northern GoM Slope, Gulf of Mexico	(271)
Intertidal sediment	16S-rRNA, FISH, ARDRA	Wadden Sea, south of Sylt, North Sea	(272)
Riverwater/sediment	FISH	Dresden-Ubigau, Coswig, Hitzacker, River Elbe, Germany	(273)
Shelf sediment/deep sea sediment	16S-rRNA, FISH	Black Sea	(274)
Deepsea carbonate crust	16S-rRNA sequencing	Napoli mud Volcano, Mediterranean Sea	(275)
Meromictic lake	16S-rRNA, FISH	Gek-Gel Lake, Azerbaijan	(276)
Meromictic lake	<i>dsrA</i> sequencing	Partly saline Lake Suigetsu, Fukui, Japan	(277)
Deep sea sediment/microbial mat	16S-rRNA, T-RFLP, HPLC-APCI-MS	Sagami Trough, Japan	(278)
Deep sea sediment/microbial mat	16S-rRNA, <i>dsrAB</i> sequencing	Green Canyon, Gulf of Mexico	(279)
Deep sea sediment and carbonate crust	16S-rDNA, GC-IRMS	Mud Vulcanos, Gulf of Cadiz	(280)
Lake sediment	16S-rRNA, <i>dsrAB</i> , DGGE	brakish lake Ogawara, Japan	(281)
Deep sea sediment/microbial mat	16S-rRNA sequencing, T-RFLP	Offshore Hokkaido Island, Japan Sea	(282)
Deep sea sediment and carbonate crust	16S-rRNA, FISH	Dniepr Canyon, Black Sea	(283)
Meromictic lake	16S-rRNA, <i>dsrAB</i> , <i>apsA</i> , RFLP	Hypersaline Mono Lake, California, USA	(284)
Intertidal sediment	FISH, FAME	Spiekeroog Island, North Sea, Germany	(285)
Gutless oligochaete <i>O. crassitunicatus</i>	16S-rRNA, FISH	Pacific Ocean, Peru Margin	(286)
Intertidal sediment	16S-rRNA, FISH, CARD-FISH	Dangast/Jadebay, Wadden Sea, Germany	(16)
Deep sea microbial mat	16S-rRNA sequencing	Milano mud Volcano, Mediterranean Sea	(287)
Deep sea microbial reef structure	16S-rRNA, FISH, slot-blot hybridization	Black Sea	(288)
Marine shelf sediment	FISH	Eckernförde Bay, Baltic Sea, Germany	(289)
HM polluted marine shelf sediment	16S-rRNA, DGGE, FISH	Sørfjord, Norway	(290)
Saltmarsh	<i>dsrAB</i> , DGGE	Plum Island, Massachusetts, USA	(291)
Eutrophic lake	FISH, CARD-FISH	Lake Plußsee, Rathjensdorf, Germany	(292)
Mesopelagic oxygen minimum zone	16S-rRNA, CARD-FISH	Arabian Sea, 400 km western of India	(293)
Eutrophic lake	16S-rRNA sequencing	Lake Kasumigaura, Japan	(294)
Floodplain lake	16S-rRNA, dot-blot hybridization	La Granja, Beni River Subbasin, Bolivia	(295)
Cold seep/deep sea sediment	16S-rRNA, CARD-FISH	Gulf of Mexico	(296)

Table S2 continued

Sample type	Method	Sample location	Reference
Deep sea sediment/microbial mat	16S-rRNA, FISH	Hydrate ridge, Oregon, USA; Cremean area, Black Sea	(297)
Seep sediment/deep sea sediment	SSU-rRNA sequencing	Monterey Bay, California, USA	(298)
Marine shelf sediment	CARD-FISH, GC-IRMS	Tommeliten Seepage Area, North Sea	(299)
deep sea microbial mat/carbonate crust	16S-rRNA, FISH	Lower Crimean Shelf, Black Sea	(300)
Methane seep/deep sea sediment	16S-rRNA sequencing	Ryukyu arc, off Ishigaki Island, Japan	(301)
Intertidal sediment	16S-rRNA, FISH, CARD-FISH	Janssand, Spiekeroog Island, Germany	(22)
Saltmarsh	16S-rRNA sequencing	Plum Island, Massachusetts, USA	(302)
Meromictic lake	16S-rDNA, DGGE	Lake Kaiike, Kamikoshiki Island, Japan	(303)
Deep sea black smoker chimney	<i>dsrAB</i> sequencing	Kairei Field, Indian Ocean	(304)
Estuarine intertidal mudflat	16S-rRNA, DNA-DNA-hybridization, DGGE	North Inlet Estuary, South Carolina, USA	(305)
Deep sea sediment	16S-rRNA, FISH, FISH-SIMS	Eel River Basin, California, USA	(306)
Shelf, deep sea sediment	16S-rRNA, DGGE, PLFA	George V Basin, Mertz Drift, North Mertz Drift, O'Briens Bay, Burton Lake, Vestfold Hills, Eastern Antarctica	(307)
Monomictic lake	SSU-rRNA, probe hybridization	Lake Biwa, Japan	(308)
Marine shelf sediment	16S-rRNA, DNA-DNA-hybridization	Signy Island, Antarctica	(309)
Deep sea sediment	16S-rDNA sequencing	George V Basin, Eastern Antarctica	(310)
Cold seep/deep sea sediment	16S-rRNA, T-RFLP	Japan Trench	(311)
Intertidal sediment	16S-rRNA, DGGE, PLFA, FISH	Dangast/Jadebay, Wadden Sea, Germany	(15)
Hydrothermal deep sea sediment	16S-rRNA sequencing	Guaymas Basin, Gulf of California, Mexico	(312)
Marine shelf sediment	16S-rRNA, DGGE	Tokyo Bay, Japan	(313)
Cyanobacterial mat, hypersaline lake	16S-rRNA, <i>dsrAB</i> , probe hybridization	Solar Lake, Sinai, Egypt	(314)
Deep sea sediment/microbial mat	16S-rDNA, FISH	Eel River Basin, Santa Babara Basin, USA	(315)
<i>O. algarvensis</i> , gutless oligochaete	16S-rRNA, FISH	Capo di San Andrea, Elba, Italy	(61)
Saltmarsh	16S-rRNA, probe hybridization	Savannah, Georgia, USA	(316)
Flooded rice roots/wetland sediment	SSU-rRNA, T-RFLP, dot-blot hybridization	Rice Research Institute, Vercelli, Italy	(317)
Seep sediment/deep sea sediment	FISH-SIMS	Eel River Basin, Santa Babara Basin, USA	(318)
Saltmarsh	16S-rRNA, probe hybridization	Savannah, Georgia, USA	(319)
Seep sediment/deep sea sediment	16S-rRNA, FISH	Hydrate ridge, Oregon, USA	(320)
Meromictic lakes	16S-rDNA, RFLP	Vestfold Hills, Eastern Antarctica	(321)
Marine shelf sediment	16S-rDNA sequencing	d'Arcachon, South-West France	(322)
Marine shelf sediment	16S-rRNA, FISH, slot-blot hybridization	Smeerenburgfjorden; Svalbard; Magdalenefjorden; Raudfjorden; Hornsund, Svalbard Arctic Ocean	(323)
Saltmarsh	16S-rRNA, slot-blot hybridization	Brunswick, Georgia, USA	(324)
Marine shelf sediment	16S-rDNA, dot-blot hybridization, ARDRA	Hornsund, Svalbard, Arctic Ocean	(325)
Marine shelf sediment	16S-rRNA, probe hybridization	Baltic Sea/North Sea, Aarhus, Denmark	(326)
Post-glacial freshwater sediments	16S-rRNA sequencing	North Basin of Windermere, England	(327)
Marine snow aggregates	16S-rRNA, RFLP	Gulf of Trieste, Aurisina, Italy	(328)
PCB polluted shelf sediment	16S-rDNA, RFLP	Baltimore Harbor, Maryland, USA	(329)
Marine shelf sediment	16S-rRNA, probe hybridization	Santa Rosa Sound, Florida, USA	(330)
Seep sediment/deep sea sediment	16S-rRNA, RFLP	Guaymas Basin, Gulf of California, Mexico	(331)
Saltmarsh	16S-rDNA, probe hybridization	Chapman's Marsh, New Hampshire, USA	(332)
Contaminated shelf sediment	16S-rDNA sequencing	Off Bainbridge Island, Puget Sound, USA	(333)
Marine shelf sediment	16S-rRNA, probe hybridization	Santa Rosa Sound, Florida, USA	(334)
Marine shelf sediment	16S-rRNA, probe hybridization	Santa Rosa Sound, Florida, USA	(335)
Hypersaline pond	16S-rRNA, probe hybridization	Exportadora De Sal, Baja California Sur, Mexico	(336)
Marine shelf sediment	SSU-rRNA sequencing	New England, USA	(337)
Marine deep sea/shelf sediment	16S-rRNA, <i>dsrB</i> sequencing	Skagerrak; Lillebælt, Baltic Sea	(338)
HM polluted shelf sediment	metagenomic shotgun sequencing	Centre Island; Che Lei Pai; Port Island; Tung Ping Chau, Tolo Harbour, China	(339)
Manrgove sediment	16S-rRNA, metagenomic sequencing	Mangroves at Yunxiao, China	(340)
Marine shelf sediment	16S-rRNA sequencing	Van Keulenfjorden, Svalbard	(341)
Marine lake sediment	16S-rRNA, FISH	Scharendijke Basin, marine Lake Grevelingen southwestern part of the Netherlands	(342)

**Table S2** continued

Sample type	Method	Sample location	Reference
Intertidal flat	16S-rRNA, Illumina MiSeq	Eastern Beibu Gulf, China	(343)
Lake sediment	<i>dsrAB</i> , DGGE	Ghantasila Island, Chilika Lake, India	(344)
Hydrocarbon seep/deep sea sediment	metagenomic shotgun sequencing, 16S-rRNA, CARD-FISH	Green Canyon, Gulf of Mexico	(345)
Marine arctic deep sea sediment	16S-rRNA, FISH	Storfjordrenna, Svalbard	(23)
Deep sea sediment	16S-rRNA, metagenomic shotgun sequencing, CARD-FISH	Håkon Mosby mud Volcano, Norwegian- Barents-Spitzbergen Continental Margin	(346)
Marine shelf sediment	16S-rRNA, RFLP, Metagenomic shotgun sequencing	Northern Gulf of Mexico, near the Mississippi Delta	(347)
Deagras rhizosphere, shelf sediment	16S-rRNA sequencing	Off shore of Hobie Island, Florida, USA	(348)
Deep sea sediment	16S-rRNA sequencing	southwest of Oki Trough, Sea of Japan	(349)

**Table S3** Biogeography and habitats of phylotypes affiliating with the genus *Desulfobacula*.

Sample type	Method	Sample location	Reference
Lake water/lake sediment	<i>hgcA</i> , 16S-rRNA, metagenomic analysis	lake manganika;	(350)
Oily deep sea sediment	16S rRNA and metagenomic sequencing	lake McQuade, USA	(351)
Deep sea sediment	16S-rRNA sequencing	Chapopote; Campeche Knolls in the Gulf of Mexico	(352)
Deep sea wood fall	16S-rRNA, ARISA	Kryos Basin, Eastern Mediterranean Sea	(353)
Intertidal sediment	16S-rRNA sequencing	Central Province, Eastern Mediterranean Sea	(354)
Marine shelf sediment	16S-rRNA, MasD, CARD-FISH	Janssand, German Wadden Sea	(355)
Methane seep/deep sea sediment	16S-rRNA, FISH-nanoSIMS	Caspian Sea	(159)
Marine shelf sediment	16S-rRNA sequencing	Eel River Basin, southern Ridge	(356)
Marine water column	<i>dsrB</i> , DGGE	Thuwal Seeps, Saudi Arabia	(174)
Marine shelf sediment	16S-rRNA, <i>assA</i> , <i>bssA</i> sequencing	Gdansk Bay, Baltic Sea	(357)
Deep sea sediment/microbial mat	IPL, 16S-rRNA sequencing	Chesapeake Bay, Virginia, USA	(358)
Saltmarsh	16S-rRNA sequencing	Japan Trench	(190)
Deep groundwater	16S-rDNA pyrosequencing	Magnolia Marsh, Georgia, USA	(359)
Hydrocarbon seep/deep sea sediment	TEFAP 454 pyrosequencing	ONK-PVA6, ONKALO, Finland	(192)
Oil polluted marine shelf sediment	16S-rRNA, Genome sequencing	Acre location, Mediterranean Sea	(360)
Intertidal sediment	<i>dsrA</i> , 16S-rRNA sequencing	Taeon, Republic of Korea	(361)
Hydrocarbon seep/deep sea sediment	16S-rRNA, FISH-nanoSIMS	Adour estuary, French Coast	(201)
Deep sea sediment	16S-rRNA, DGGE, CARD-FISH	Hydrate Ridge, Gulf of Mexico	(362)
Estuarine sediment	16S-rRNA, <i>dsrAB</i> , DGGE	Continental Slope off Namibia	(202)
Sulfidic spring	16S-rRNA, FISH, SR-FTIR	Colne Estuary, Essex, UK	(363)
Cold seep/deep sea sediment	16S-rRNA, ARISA, CARD-FISH	Mühlbacher Schwefelquelle, Germany	(205)
		Omakere Ridge; Wairarapa Takahae, Hikurangi Continental Margin, New Zealand	
Marine shelf sediment	16S-rRNA, T-RFLP	Gulf of Finland, Baltic Sea	(364)
Contaminated marine shelf sediment	<i>bamA</i> , FISH	Sanban-ze, Tokyo Bay, Japan	(114)
Marine shelf sediment	16S-rRNA, T-RFLP	Western Gulf of Finland	(365)
Coal oil point seep	454 sequencing, <i>dsrAB</i>	Tonya Seep, California, USA	(224)
Aquifer	16S-rRNA, T-RFLP	Testfeld Süd, Germany	(366)
Aquifer	16S-rRNA, ARDRA, T-RFLP	Saxony-Anhalt, Germany	(367)
Cold seep/deep sea sediment	16S-rRNA, FISH	Håkon Mosby mud Volcano, Norwegian-Barents-Spitzbergen Continental Margin	(261)
Meromictic Lake	16S-rRNA, probe hybridization	Lake Cadagno, Switzerland	(368)
Deep sea sediment	16S-rDNA sequencing	Antarctic Continental shelf	(310)
Deep sea sediment	16S-rRNA, <i>dsrAB</i> sequencing	Area, Mertz Glacier Polynya	(369)
Hypersaline pond	16S-rDNA, RFLP, dot-blot-hybridization	Everest Mound, Guaymas basin, Gulf of California, Mexico	(370)
Marine shelf sediment	16S-rRNA, DNA-DNA-hybridization	Etang de Faraman, Salin-de-Giraud salterns, France	(309)
Marine shelf sediment	16S-rRNA sequencing	Shallow Bay, Signy Island, Antarctica	(323)
Deep sea sediment	16S-rRNA sequencing	Hornsund, Svalbard Arctic Ocean	(331)
		Guaymas Basin, Gulf of California, Mexico	

**Table S4** Biogeography and habitats of phylotypes affiliating with the genus *Desulfobacterium*.

Sample type	Method	Sample location	Reference
Mangrove sediment	16S-rRNA, metagenomic sequencing	Yunxiao, China	(340)
Perennially frozen lake	16S-rRNA sequencing	Tarn Flat Area, Northern Victoria Land	(371)
Marine shelf sediment	SSU-rRNA, RFLP	Northern Gulf of Mexico	(347)
Marine shelf sediment	16S-rRNA, <i>dsrB</i> , DGGE	Chersonesus (Blue) Bay, Black Sea	(372)
Hypersaline pond	Metagenomic sequencing	Lagunita, Churince lake, Mexico	(373)
Eutrophic lake	16S-rRNA, DGGE	Lake Vechten, The Netherlands	(374)
Deep sea sediment	16S-rRNA, CARD-FISH-raman	Smeerenburgfjorden, Svalbard	(375)
Marine shelf sediment	16S-rRNA sequencing	San Francisco bay, California, USA	(376)
Hydrothermal sediment	16S-rRNA, DGGE	Bahía de Banderas, Nayarit, Mexico	(377)
Oil field	16S-rRNA, <i>dsrB</i> , ARDRA	Xinjiang Oil Field, Dongying, China	(378)
Deep sea hydrothermal field	16S-rRNA, <i>dsr</i> (amino sequence) sequencing, metagenomic analysis	Pacmanus and Desmos hydrothermal fields, Manus Basin, Papua New Guinea	(379)
Organically/HM polluted shelf sediment	16S-rRNA sequencing	Sfax city, Tunisia	(380)
Saline enclosed reservoir	16S-rRNA sequencing, PLFA-SIP	Lake Grevelingen, The Netherlands	(150)
Methan seep/deep sea sediment	16S-rRNA, FISH-nanoSIMS	Eel River Basin, California, USA	(159)
Deep sea hydrothermal field	16S-rRNA pyrosequencing	Mat Mound, Guaymas Basin, Gulf of California	(381)
Deep sea sediment	16S-rRNA pyrosequencing	Skagerrak, Denmark	(163)
Deep sea hydrothermal field	16S-rRNA, CARD-FISH	Guaymas Basin, Gulf of California, Mexico	(167)
Deep sea hydrothermal field	16S-rRNA sequencing	Bastille Chimney, Juan de Fuca Ridge	(382)
Deep sea sediment	16S-rRNA, BONCAT, FISH, CARD-FISH	Santa Monica Basin, California; Hydrate Ridge, Oregon, USA	(160)
Methan seep/deep sea sediment	16S-rRNA, T-RFLP	Hydrate Ridge, Cascadia convergent Margin; Eel River Basin, California, USA	(383)
Intertidal sediment	<i>dsrAB</i> , T-RFLP	AberBenoît, Treglonoua Basin, France	(384)
Marine shelf sediment	16S-rRNA, DGGE	Eckernförde Bay, Germany	(385)
Deep sea sediment/microbial mat	IPL, 16S-rRNA sequencing	Japan Trench	(358)
Saltmarsh	16S-rRNA sequencing	Magnolia/Talbert marsh, California, USA	(190)
Deep sea sediment	16S-rRNA, SIP, CARD-FISH	Amon Mud Volcano, Nile deep Sea Fan	(197)
Paddy soil	<i>dsrAB</i> , T-RFLP	Wanshan Hg mining Area, China	(386)
Deep groundwater	16S-rDNA pyrosequencing	ONK-PVA6, ONKALO, Finland	(359)
Wetland	16S-rRNA sequencing	Luoshijiang Wetland, China	(387)
Lake sediment	<i>dsrAB</i> , <i>aprA</i> sequencing	Subglacial Lake Whillans, Antarktika	(388)
Deep sea hydrothermal field	16S-rRNA, <i>dsrAB</i> , FISH	Mat Mound, Guaymas Basin, Gulf of California	(389)
Estuarine sediment	16S-rRNA, <i>dsrAB</i> , DGGE	Colne estuary, Essex, UK	(202)
Marine shelf sediment	16S-rRNA, T-RFLP	Gulf of Finland, Baltic Sea	(364)
Intertidal sediment	16S-rRNA sequencing	Coast of the Genkai Sea, Japan	(213)
Lake water and sediment	<i>aprA</i> , 16S-rRNA sequencing	Lake Pavin, France	(390)
Deep sea sediment	<i>aprA</i> and <i>dsrA</i> sequencing	Peru Margin; Black sea	(230)
Coal oil point seep	454 sequencing, <i>dsrAB</i>	Tonya Seep, California, USA	(224)
Marine shelf sediment	<i>aprA</i> , DGGE	Tirez lagoon, Iberian region of La Mancha	(391)
Marine shelf sediment	16S-rRNA, <i>dsrAB</i> , RFLP	Nea Kameni Island, Santorini, Greece	(231)
Aquifer	16S-rRNA, T-RFLP	Testfeld Süd, Germany	(366)
Aquifer	16S-rRNA, T-RFLP	Testfeld Süd, Germany	(392)
Cold seep/deep sea sediment	16S-rRNA sequencing	Larsen B, western Weddell, Antarktika	(240)
Aquifer	16S-rRNA, DGGE	Mikkeli, Finland	(393)
PCB-enriched marine shelf sediment	16S-rRNA, <i>dsrAB</i> sequencing	Boston Harbor, Massachusetts, USA	(245)
Contaminated marine shelf sediment	16S-rDNA, DGGE	Paletta Creek, San Diego Bay, USA	(258)
Deep sea sediment	16S-rRNA, DGGE	Benguela upwelling System, Namibia	(265)
Deep-sea hypersaline anoxic lake	16S-crDNA sequencing	Lake Uruana, Eastern Mediterranean	(394)
Meromictic lake	16S-rRNA, FISH	Gel Lake, Azerbaijan	(276)
Meromictic lake	16S-rRNA, DGGE	Lake Kaiike, Kamikoshiki Island, Japan	(395)
Meromictic lake	16S-rRNA, probe hybridization	Lake Cadagno, Switzerland	(368)
Marine shelf sediment	16S-rDNA, RFLP	Thermaikos Gulf, Eastern mediterranean Sea	(396)
Saltmarsh and estuarine/limnic sediment	16S-rRNA, probe hybridization	Colne estuary, Essex, UK	(397)
Deep sea sediment	16S-rRNA, <i>dsrAB</i> sequencing	Everest Mound, Guaymas basin, Gulf of California, Mexico	(369)
Lake sediment	SSU-rRNA sequencing	Lake Biwa, Japan	(308)

**Table S4** continued

Sample type	Method	Sample location	Reference
Estuarine sediment	16S-rRNA probe hybridization	Colne estuary, Essex, UK	(398)
Estuarine sediment	16S-rRNA probe hybridization	Colne estuary, Essex, UK	(399)
River sediment	16S-rRNA probe hybridization	Tama river, Tokyo, Japan	(400)
Saltmarsh	16S-rRNA probe hybridization	Skidaway River, Savannah, USA	(324)
Marine shelf sediment	16S-rRNA, slot-blot hybridization	Smeerenburgfjorden, Svalbard, Antarctica	(323)
Saltmarsh	16S-rDNA, dot-blot hybridization	Canary Creek Marsh, Delaware, USA	(401)
Meromictic lake	16S-rRNA, probe-hybridization	Lake Kizaki, Japan	(402)
Cold seep/deep sea sediment	16S-rDNA, RFLP	Japan Trench	(403)
Deep sea sediment	16S-rRNA, RFLP	Guaymas Basin, Gulf of California, Mexico	(331)
Fjord water	16S-rRNA, in-situ hybridization	Mariager Fjord, Denmark	(404)



**Table S5** Biogeography and habitats of phylotypes affiliating with the genus *Desulfonema*.

Sample type	Method	Sample location	Reference
Lake sediment	16S-rRNA, metagenomic sequencing	Cock Soda Lake, Altai, Russia	(405)
Marine shelf sediment	16S-rDNA sequencing	Salines de la Trinitat, Tarragona, Spain	(406)
Microbial mat (Lake)	16S-rRNA, metagenomic sequencing	Lake Huron, Michigan, USA	(407)
Methane seep/deep sea sediment	16S-rRNA, T-RFLP	Eel River Basin, California, USA	(383)
Deep sea hydrothermal vent system	SSU-rRNA, 454 tag sequencing	Main Endeavour Field, Juan de Fuca Ridge	(408)
Estuarine sediment	16S-rRNA, dsrAB, DGGE	Colne estuary, Essex, UK	(202)
Marine shelf sediment	16S-rRNA, T-RFLP	Aarhus Bay, Denmark	(409)
River sediment	16S-rRNA sequencing	Clinch River, Oak ridge, Tennessee, USA	(410)
Microflorae of moss pillars	16S-rRNA sequencing	Hotoke-Ike Lake, Skarvsnes, Antartica	(411)
Cold mineral spring	16S-rRNA sequencing	Ust' Kachka Resort, Russia	(219)
Deep sea sediment	16S-rRNA, DGGE, ARDRA	Northern Bering Sea	(412)
Microbial mat (Cave)	16S-rRNA, FISH, RFLP	Lower Kane Cave, USA	(413)
Marine macrobial mat	16S-rRNA, FISH	Chilean Continental shelf	(414)
Microbial mat (hypersaline pond)	16S-rRNA, CARD-FISH, NanoSIMS	Exportadora De Sal, Baja California Sur, Mexico	(257)
Coastal saline pond	16S-rRNA, T-RFLP	saltern of Salins-de-Giraud, Camargue, France	(415)
Methane seep/deep sea sediment	16S-rRNA, Magneto-FISH, CARD-FISH	Eel River Basin, California, USA	(416)
Lake sediment	16S-rRNA, FISH	Lake Aha, China	(256)
Biofilm (Cave)	16S-rRNA, FISH	Grotta Sulfurea, Italy	(417)
Deep sea sediment	16S-rDNA, RFLP	Florida Escarpment, Gulf of Mexico	(418)
Floodplain lake	16S-rRNA, dot-blot-hybridization	La Granja, Beni River Subbasin, Bolivia	(295)
Meromictic lake	16S-rRNA, DGGE	Lake Kaiike, Kamikoshiki Island, Japan	(395)
Intertidal sediment	16S-rRNA, DGGE, FISH	Jadebusen, Dangast, Germany	(15)
Cyanobacterial mat/ hypersaline lake sediment	16S-rRNA, dsrAB, probe hybridization	Solar Lake, Sinai, Egypt	(314)
Flooded rice roots/sediment	16S-rRNA, T-RFLP	Rice Research Institute, Vercelli, Italy	
Marine shelf sediment	16S-rDNA sequencing	Bassin d'Arcachon, South-West France	(322)
Marine shelf sediment	16S-rRNA, FISH, slot-blot hybridization	Smeerenburgfjorden, Svalbard, Antarctica	(323)
Cyanobacterial mat/ hypersaline lake	16S-rRNA, probe hybridization	Solar Lake, Sinai, Egypt	(419)
PCB polluted shelf sediment	16S-rRNA, RFLP	Baltimore Harbor, Maryland, USA	(329)
Intertidal sediment	16S-rRNA, FISH	Dangast, Germany	(420)
Cyanobacterial mat/ hypersaline lake	16S-rRNA, DGGE	Solar Lake, Sinai, Egypt	(421)

**Table S6:** Properties of genome-sequenced members of the *Desulfobacteraceae*. Only completely genome-sequenced members are shown. Strains selected for proteogenomic analysis in our laboratory are highlighted.

Property	<i>Desulfosarcina variabilis</i> 3be13	<i>Desulfosarcina alkanivorans</i> PL12	<i>Desulfosarcina ovata</i> 28b2T	<i>Desulfosarcina ovata</i> oXyS1	<i>Desulfosarcina widei</i> !!! PP31	<i>Desulfonema magnum</i>	<i>Desulfonema limicola</i>	<i>Desulfococcus multivorans</i> 1bet1	<i>Desulfococcus Hxd3</i>	<i>Desulfatibacillum alkenivorans</i> AK-01	<i>Desulfobacula toluolica</i> To12	<i>Desulfobacterium autotrophicum</i> HRM2
<b>PHYSIOLOGICAL CHARACTERISTICS</b>												
<b>Organic substrates</b>												
Aliphatic hydrocarbons	–	C <sub>6</sub> , C <sub>10</sub>	–	–	–	–	–	–	C <sub>12</sub> – C <sub>20</sub>	C <sub>13</sub> – C <sub>18</sub>	–	–
Aromatic hydrocarbons	–	n.d.	1	3	1	–	–	–	–	–	1	–
Fatty acids	≤C <sub>14</sub> <sup>a,b</sup>	n.d.	n.d.	<C <sub>4</sub>	<C <sub>4</sub>	≤C <sub>10</sub> <sup>a</sup>	≤C <sub>14</sub> <sup>a</sup>	<C <sub>14</sub> <sup>a,b</sup>	C <sub>4</sub> – C <sub>18</sub>	<C <sub>16</sub>	<C <sub>4</sub>	<C <sub>16</sub> <sup>a</sup>
Other aliphatic compounds	8	8	n.d.	8	7	5	4	6	–	3 <sup>c</sup>	8	8
Other aromatic compounds	13	–	n.d.	4	1	5	–	7	–	–	7	–
<b>Electron acceptors</b>												
Sulfate	+	+	+	+	+	+	+	+	+	+	+	+
Sulfite	+	+	n.d.	n.d.	–	–	+	+	+	+	+	–
Thiosulfate	+	+	n.d.	n.d.	+	–	+	+	+	+	+	+
<b>Autotrophy</b>	–	+	n.d.	n.d.	+	–	+	–	–	+	–	+
<b>Syntrophy</b>	–	+	n.d.	n.d.	n.d.	n.d.	n.d.	–	n.d.	+	–	+
<b>Morphology</b>	oval, sarcina	oval, sarcina	oval, sarcina	oval, sarcina	oval, sarcina	filaments	filaments	spherical	spherical	rod-shaped	oval	oval
<b>Isolation habitat</b>	–O <sub>2</sub> marine sediment	–O <sub>2</sub> marine sediment	–O <sub>2</sub> marine sediment	Seawater in oil tank	–O <sub>2</sub> marine sediment	–O <sub>2</sub> marine sediment	–O <sub>2</sub> marine sediment	Sewage digester	Seawater in oil tank	–O <sub>2</sub> estuary sediment	–O <sub>2</sub> marine sediment	–O <sub>2</sub> marine sediment
<b>GENOME FEATURES</b>												
Size (bp)	9,639,276	7,324,708	8,413,530	7,630,248	7,297,718	8,027,777	6,908,045	4,455,399	3,944,167	6,517,073	5,197,905	5,652,035
G+C content (mol %)	51.3	56.6	53.9	53.9	54.0	44.8	38.5	56.8	56.2	54.5	41.4	48.8
rRNA operons	2	6	6	6	6	1	2	3	1	2	4	6
tRNAs	58	50	52	55	54	68	61	54	47	56	48	50
Coding sequences (CDS)	8,579	6,234	6,493	6,493	6,518	9,970	6,207	3,942	3,267	5,296	4,375	4,947
Coding (%) <sup>d</sup>	86	86	86	86	86	87	90	87	88	87	87	88
Average CDS size (bp) <sup>d</sup>	960	954	971	973	923	700	1,001	986	1,066	1,080	1,031	1,017
Assigned function <sup>d</sup>	5,422	2,890	2,542	2,893	3,103	4,015	3,929	2,684	2,333	3,971	3,221	3,477
Conserved unknown <sup>d</sup>	1,423	3,344 <sup>e</sup>	3,951 <sup>e</sup>	3,600 <sup>e</sup>	3,415 <sup>e</sup>	1,121	1,173	663	405	381	654	551
Unknown <sup>d</sup>	1,724	–	2 (136,16)	–	–	4,834	1,105	595	529	944	500	873
Plasmids (size in kbp)	–	–	2 (136,16)	–	–	–	–	–	–	–	–	1 (63)
Phage	1	n.d.	1 <sup>f</sup>	2 <sup>f</sup>	6 <sup>f</sup>	2	1	–	–	–	1	1
CRISPR	3	1	4	4	–	20	8	6	2	1	3	1
Mobile elements <sup>d</sup>	147	71	148	109	81	351	703	45	18	79	163	98
Accession number	CP159846	AP021874	AP021876	AP021879	AP021875	CP061800	CP061799	CP015381	CP000859	CP001322	FO203503	CP001087
Reference(s)	This study, (68)	(120, 433)	(114)	(115)	(114)	(29, 68)	(29, 68)	(28)	(68, 423)	(424, 425)	(27, 125)	(128, 129)

<sup>a</sup> including branched-chain fatty acids, <sup>b</sup> including cyclohexane carboxylate, <sup>c</sup> only poorly utilized, <sup>d</sup> data extracted from respective Genbank files, <sup>e</sup> no differentiation between unknown/conserved unknown, <sup>f</sup> incomplete, n.d. not described

**Table S7:** Properties of selected, genome-sequenced sulfate reducing bacteria not belonging to the *Desulfobacteraceae*.

Property	H <sub>2</sub> /CO <sub>2</sub>	Aliphatic compounds	Aromatic compounds	Size (bp)	G+C content (mol %)	Coding sequences (CDS)	Mobile elements <sup>d</sup>	Isolation habitat	Accession	Reference
<i>Dfm. tiedjei</i> DSM6799	+	+	+	6,500,104	49.0	5,494	59	Sewage sludge	CP003360	(25)
<i>Sb. fumaroxidans</i> MPOB	+	+	+	4,990,251	59.0	4,064	64	Methanogenic granular sludge	CP000478	(426)
<i>Dbm. acetoxidans</i> DSM11109	–	+	–	3,282,536	51.1	2,866	10	Anaerobic granular sludge	CP002629	(427)
<i>Dbu. oralis</i> HOT041	–	+	–	2,774,417	59.8	2,395	64	Oral subgingival	CP021255	(428)
<i>Dca. sulfexigens</i> DSM10523	+	–	–	4,023,512	45.4	2,794	26	Tidal flat sediment	CP003985	(429)
<i>Dl. psychrophila</i> LSv54	+	+	–	3,523,383	46.8	3,115	25	Marine sediment	CR52287	(430)
<i>Gb. sulfurreducens</i> PCA	+	+	–	3,814,139	60.9	3,466	28	Ditch surface sediment	AE017180	(431)
<i>Da. baarsii</i> DSM2075	+	+	–	3,655,731	65.7	3,303	5	Ditch mud	CP002085	(432)
<i>Dm. baculatum</i> X	+	+	–	3,942,657	58.6	3,494	19	Water-saturated manganese carbonate ore	CP001629	(433)
<i>Dh. retbaense</i> HR100	+	+	–	2,909,567	57.3	2,552	25	Surface sediment	CP001734	(434)
<i>Dv. gigas</i> DSM1382	+	+	–	3,693,899	63.4	3,273	18	Water pond	CP006585	(435)
<i>Dv. salexigens</i> DSM2638	+	+	–	4,289,847	47.1	3,807	11	Sling mud	CP001649	
<i>Dv. alaskensis</i> G20	+	+	–	3,730,232	57.8	3,258	45	Oil well corrosion site	CP000112	(436)
<i>Dv. vulgaris</i> Hildenborough	+	+	–	3,570,858	63.2	3,395	28	Wealden clay	AE017285	(437)
<i>Dv. desulfuricans</i> MB	+	+	–	2,873,437	58.1	2,382	21	Rumen, sheep	CP001358	

**Table S8:** Relative share of protein abundance per KEGG pathway category of averaged peptide counts for total protein (TP) and constitutively formed proteins (CP) per *Desulfobacteraceae* member. Abbreviations: Dbt, *Desulfobacula toluolica* Tol2; Dcm, *Desulfococcus multivorans* 1be1; *Desulfonema limicola*; Dnm, *Desulfonema magnum*; Dsv, *Desulfosarcina variabilis* 3be13; Dta, *Desulfobacterium autotrophicum* HRM2.

KEGG Pathway	Dbt		Dcm		Dnl		Dnm		Dsv		Dta	
	TP	CP	TP	CP	TP	CP	TP	CP	TP	CP	TP	CP
1-01 Carbohydrate metabolism	16.6	16.0	16.7	15.0	20.7	20.0	20.0	16.9	19.1	16.3	16.7	16.1
1-02 Energy metabolism	25.3	26.2	35.9	41.4	42.3	43.6	35.9	38.0	32.2	38.8	31.9	33.7
1-03 Lipid metabolism	2.1	2.1	1.8	0.9	0.5	0.4	1.4	1.3	2.3	1.5	2.4	1.9
1-04 Nucleotide metabolism	2.3	2.3	1.8	1.7	2.7	2.5	4.1	4.6	3.0	3.5	2.4	2.5
1-05 Amino acid metabolism	12.4	12.8	8.3	5.8	5.0	4.8	8.7	8.7	9.4	7.7	8.2	7.4
1-06 Metabolism of other amino acids	1.5	1.7	0.9	0.8	2.7	2.9	1.9	2.1	1.4	1.6	1.7	1.8
1-07 Glycan biosynthesis and metabolism	0.1	0.0	0.7	0.6	0.3	0.3	0.2	0.2	0.2	0.1	0.2	0.2
1-08 Metabolism of cofactors and vitamins	4.4	4.3	3.4	3.5	5.4	5.7	5.7	6.1	5.1	5.8	3.8	4.0
1-09 Metabolism of terpenoids and polyketides	2.2	2.3	1.1	0.8	0.6	0.5	0.9	0.8	1.1	0.4	0.8	0.8
1-10 Biosynthesis of other secondary metabolites	3.8	4.0	0.9	0.8	2.5	2.7	1.7	1.9	1.3	1.2	1.3	1.4
1-11 Xenobiotics biodegradation and metabolism	9.6	9.5	5.0	3.5	3.5	3.5	6.9	7.0	7.1	5.5	5.1	4.6
1-12 Chemical structure transformation maps	0.0	0.0	0.0	0.0	0.0	0.0	0.0	0.0	0.0	0.0	0.0	0.0
2-01 Transcription	0.1	0.1	0.0	0.0	0.0	0.0	0.0	0.0	0.2	0.2	0.1	0.1
2-02- Translation	2.0	1.8	4.1	4.1	3.2	3.2	2.4	2.5	2.9	2.3	6.6	7.0
2-03 Folding sorting and degradation	3.6	3.8	4.2	4.8	4.1	4.3	2.4	2.7	4.7	5.6	6.7	7.2
2-04 Replication and repair	0.1	0.0	0.8	1.0	0.4	0.4	0.3	0.3	0.3	0.3	0.3	0.2
2-05 Chromosome	0.0	0.0	0.0	0.0	0.0	0.0	0.0	0.0	0.0	0.0	0.0	0.0
2-06 Information processing in viruses	0.0	0.0	0.0	0.0	0.0	0.0	0.0	0.0	0.0	0.0	0.0	0.0
3-01 Membrane transport	1.6	1.6	3.8	4.1	1.0	0.8	0.5	0.4	1.9	1.8	2.8	2.5
3-02 Signal transduction	5.6	5.0	2.6	2.4	1.9	1.6	3.0	2.8	3.5	3.2	3.6	3.5
3-03 Signaling molecules and interaction	0.0	0.0	0.0	0.0	0.0	0.0	0.0	0.0	0.0	0.0	0.0	0.0
4-01 Transport and catabolism	0.2	0.2	0.3	0.3	0.2	0.2	0.4	0.4	0.4	0.4	0.1	0.0
4-02 Cell growth and death	0.4	0.4	0.8	0.6	0.5	0.5	0.3	0.2	1.0	1.1	1.3	1.2
4-03 Cellular community-eukaryotes	0.0	0.0	0.0	0.0	0.0	0.0	0.0	0.0	0.0	0.0	0.0	0.0
4-04 Cellular community-prokaryote	3.7	4.0	5.6	6.4	1.9	1.6	2.5	2.2	2.7	2.4	2.9	2.8
4-05 Cell motility	2.5	2.0	1.1	1.4	0.6	0.5	1.0	0.9	0.4	0.3	1.1	1.1

**Table S9:** Number of transport systems (TS), Transporter proteins (TP) and identified transporter proteins (ID) per studied *Desulfobacteraceae* member as inferred from TCDB. Abbreviations: Dbt, *Desulfobacula toluolica* Tol2; Dem, *Desulfococcus multivorans* 1bel; *Desulfonema limiticola*; Dnm, *Desulfonema magnum*; Dsv, *Desulfosarcina variabilis* 3bel3; Dta, *Desulfobacterium autotrophicum* HRM2.

Subclass	Dbt			Dem			Dnl			Dnm			Dsv			Dta		
	TS	TP	ID	TS	TP	ID	TS	TP	ID	TS	TP	ID	TS	TP	ID	TS	TP	ID
<b>1.A</b> Alpha-type channel	28	37	10	31	33	15	38	41	7	41	44	10	36	43	30	32	39	17
<b>1.B</b> Beta-barrel Porins	52	66	21	21	21	17	42	43	14	53	57	21	53	53	29	32	33	18
<b>1.C</b> Pore-forming toxins	2	2	1	3	3	1	3	3	2	2	2	1	4	5	2	4	4	1
<b>1.E</b> Holins	1	1	0	3	3	1	1	1	0	1	1	0	2	2	0	2	2	0
<b>1.P</b> Non-envelope Virus Penetration Complex	1	3	1	0	0	0	0	0	0	0	0	0	0	0	0	0	0	0
<b>2.A</b> Porters (uniporters, symporters, antiporters)	17 4	23 8	52	124 4	17 4	69	95 7	11 7	27	103 7	13 7	27	180 6	22 6	76	195 9	25 9	56
<b>2.C</b> Ion-gradient-driven energizers	4	10	3	3	9	8	2	5	2	1	7	2	5	8	6	2	5	3
<b>3.A</b> P-P-bond-hydrolysis-driven transporters	71	20	50	80	21	11	56	16	77	57	17	48	115	37	16	113	34	93
<b>3.B</b> Decarboxylation-driven transporters	1	2	2	0	0	0	1	4	3	1	3	3	1	3	0	2	6	3
<b>3.D</b> Oxidoreduction-driven transporters	12	63	24	9	53	34	8	42	33	6	30	14	15	86	56	12	47	25
<b>4.A</b> Phosphotransfer-driven Group Translocators (PTS)	0	0	0	0	0	0	0	0	0	0	0	0	0	0	0	2	2	9
<b>4.C</b> Acyl-CoA ligase-coupled transporters	25	25	2	28	28	1	22	22	2	31	31	2	4	4	2	27	27	4
<b>4.D</b> Polysaccharide synthase/exporters	0	0	0	5	5	0	4	4	0	6	6	0	8	8	4	6	6	0
<b>4.F</b> Choline/Ethanolamine Phosphotransferase	2	2	0	3	3	2	2	2	0	3	3	1	2	2	0	1	1	1
<b>4.H</b> Lysylphosphatidylglycerol Synthase/Flippases	0	0	0	0	0	0	0	0	0	0	0	0	0	0	0	1	1	0
<b>5.A</b> Transmembrane 2-electron transfer carriers	11	30	7	7	17	9	5	10	4	2	2	4	9	18	7	7	15	5
<b>5.B</b> Transmembrane 1-electron transfer carriers	6	19	9	3	21	14	4	18	12	3	7	5	5	12	10	8	16	8
<b>8.A</b> Auxiliary transport proteins	31	36	17	20	22	8	26	26	3	32	34	6	26	27	14	27	30	19
<b>8.B</b> Ribosomally synthesized toxins/agonists that target channels and carriers	1	1	0	0	0	0	0	0	0	1	1	0	0	0	0	1	1	1
<b>9.A</b> Transporters of unknown biochemical mechanisms	11	16	8	3	4	5	6	7	5	7	9	4	11	17	12	9	11	6
<b>9.B</b> Putative transport proteins	10 6	10 7	21	48	48	23	69	71	18	69	77	10	89	92	34	65	67	19
Total	53 9	86 3	22 8	391	66 0	32 3	384	58 4	20 9	419	62 1	15 8	565	97 9	44 5	548	91 5	28 8

**Table S10** Diversity profiles extracted from the MAGs of the studied sites. The ten most abundant orders are displayed.

Sample Location	Order	Rank	No. detections	Median % contribution
<b>Benguela upwelling</b>				
	Totals	0	6,340	0.0
	Unknown	1	1,730	26.1
	BSN033	2	816	13.0
	Betaproteobacteriales	3	746	4.1
	Aerophobales	4	433	6.2
	<b>Desulfobacteriales</b>	<b>5</b>	<b>350</b>	<b>4.9</b>
	UBA10834	6	273	3.0
	B26-1	7	237	2.3
	DHVEG-1	8	231	2.1
	Marinisomatales	9	231	3.6
	UBA7937	10	218	2.8
<b>Black Sea</b>				
	Totals	0	12,972	0.0
	Unknown	1	2,247	16.4
	Aminicenantales	2	1,380	11.2
	C00003060	3	1,018	7.5
	SM23-42	4	643	4.5
	UBA10834	5	619	4.4
	GIF9	6	572	4.2
	Pirellulales	7	566	4.1
	<b>Desulfobacteriales</b>	<b>8</b>	<b>549</b>	<b>4.5</b>
	Anaerolineales	9	501	3.3
	UBA7967	10	499	2.9
<b>Guaymas Basin</b>				
	Totals	0	163,948	0.0
	Unknown	1	141,807	86.5
	<b>Desulfobacteriales</b>	<b>2</b>	<b>6,097</b>	<b>3.9</b>
	Methanosarcinales	3	2,885	1.5
	Archaeoglobales	4	2,627	1.6
	Anaerolineales	5	1,886	1.1
	Candidatus			
	Altarchaeales	6	1,693	0.6
	Thermoplasmatales	7	876	0.3
	Candidatus			
	Cloacimonadales	8	852	0.4
	Thermotogales	9	819	0.5
	Desulfurococcales	10	787	0.3
<b>Gulf of Kutch</b>				
	Totals	0	56,819	0.0
	Unknown	1	48,312	85.7
	Nitrospinales	2	2,327	2.5
	Pseudomonadales	3	1,397	1.8
	Desulfuromonadales	4	1,207	2.2
	Balneolales	5	960	1.5
	<b>Desulfobacteriales</b>	<b>6</b>	<b>908</b>	<b>1.6</b>
	Xanthomonadales	7	692	1.2
	Nitrosopumilales	8	475	0.1
	Woeseiales	9	281	0.5
	Verrucomicrobiales	10	260	0.3
	Bin61	10	323	5.3



**Table S10** Continued

Sample Location	Order	Rank	No. detections	Median % contribution
<b>Pacific Ocean off the coast of California</b>				
Totals		0	5,777	0.0
	UBA5794	1	924	14.3
	<b>Desulfobacterales</b>	<b>2</b>	<b>628</b>	<b>10.2</b>
	Polyangiales	3	509	7.7
	Ectothiorhodospirales	4	459	8.1
	Rhizobiales	5	457	6.4
	Kiloniellales	6	395	6.3
	Pseudomonadales	7	387	3.1
	HK1	8	372	5.7
	BM002	9	347	5.2
<b>South China Sea</b>				
Totals		0	185,496	0.0
	Unknown	1	117,656	61.4
	<b>Desulfobacterales</b>	<b>2</b>	<b>12,013</b>	<b>6.4</b>
	Bacteroidales	3	8,630	4.5
	Anaerolineales	4	5,476	2.8
	Desulfobulbales	5	3,859	2.2
	Methylococcales	6	2,664	1.6
	Spirochaetales	7	2,613	1.2
	Thermoplasmatales	8	2,602	1.1
	Thiotrichales	9	2,443	1.5
	Methanosarcinales	10	2,040	0.9
<b>Sumatra upwelling</b>				
Totals		0	5,292	0.0
	Unknown	1	1,285	25.1
	<b>Desulfobacterales</b>	<b>2</b>	<b>1,067</b>	<b>20.0</b>
	C00003060	3	572	11.0
	UBA2258	4	484	8.2
	Betaproteobacteriales	5	408	3.0
	Rhizobiales	6	391	2.8
	Aminicenantales	7	381	6.6
	Aerophobales	8	180	2.4
	SG8-4	9	143	2.3
	Dehalococcoidales	10	116	0.6
<b>Challenger Deep</b>				
Totals		0	101,997	0.0
	Unknown	1	99,227	97.8
	Myxococcales	2	2,770	2.2

## Supplementary References

Supplementary material references are provided in a separate Excel file: "Auxiliary Reference List.xlsx".

## Legends for data S1 and S2

**Data S1:** Constitutive proteins of the six proteomically studied Desulfobacteraceae members.

**Data S2:** Compiled results of the metagenomics analyses.